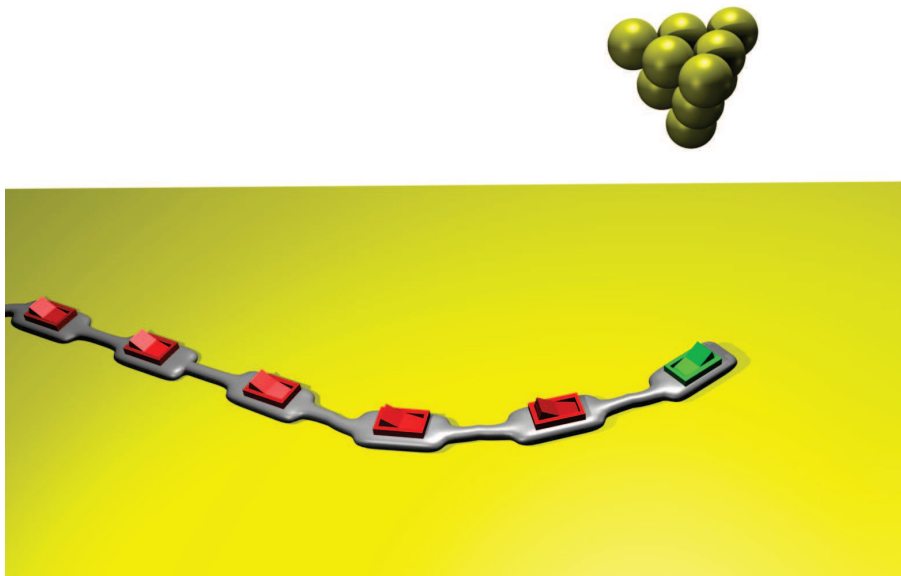


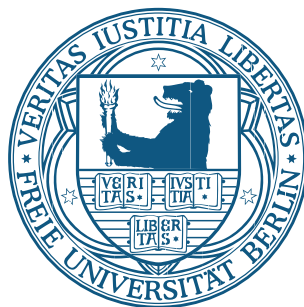
# Covalent Molecular Architectures and Dithienylethene Switches on Metal Surfaces – a Scanning Tunneling Microscopy Study



Leif Lafferentz

Im Fachbereich Physik der Freien Universität Berlin eingereichte Dissertation

Mai 2013





Diese Arbeit entstand in der Arbeitsgruppe von Dr. Leonhard Grill am Fachbereich der Freien Universität Berlin und am Fritz-Haber-Institut der Max-Planck-Gesellschaft.

Berlin, Mai 2013

Termin der Disputation: 8. Juli 2013

Erstgutachter: Priv.-Doz. Dr. L. Grill

Zweitgutachter: Prof. Dr. W. Kuch



## Abstract

The subject of this work is the study of molecular structures on gold surfaces at the single-molecule level with scanning tunneling microscopy (STM). The focus lies on one- and two-dimensional covalently coupled structures. A method for their formation has been devised only recently, therefore their properties as well as the coupling process are in need of investigation. These networks possess promising characteristics, among them the stability required for inclusion into a device.

One-dimensional oligo-terfluorene chains can serve as a prototype for molecular wires, whose most important characteristic is their electric conductance. To facilitate its measurement, a novel configuration is realized, in which individual chains are partly decoupled from the gold surface in a horizontal geometry. This is facilitated by the introduction of thin layers of insulating material, i.e. sodium chloride. It is shown that the polymerization of the terfluorenes can be performed in the presence of the NaCl. On the other hand, the crystalline growth of the insulating islands can be continued next to the polymer chains. The decoupled configuration is realized by manipulation with the STM tip and on a preparative route. Tunneling spectroscopy along individual chains reveals their partial decoupling, i.e. that of the segments that are adsorbed on top of the insulator, whereas the rest of the same chain shows the spectrum typically observed on the gold surface.

Furthermore, to increase the control of the coupling process a novel approach was implemented that facilitates a hierarchical polymerization procedure. To that end, porphyrin building blocks equipped with different substituents were employed to realize the stepwise supply of reactive sites. The entire process was monitored by variable-temperature STM from the intact monomers, via chain intermediates, to the final 2D network structures. The prearrangement of the chain intermediates by a self-templating effect on Au(111) and by the interaction with the corrugated Au(100) surface were found to lead to enhanced network regularity, which is a major challenge for covalent coupling due to its non-reversibility. The process was furthermore employed for the formation of copolymers made of porphyrin and terfluorene building blocks. Due to the controlled provision of reactive sites, the resulting network structures are characterized by a high degree of selectivity.

Molecular switches offer the exciting prospect to control the flow of electrical signals through a network. Dithienylethenes (DTE) are promising candidates as conductance switches, because the ring-opening/-closing isomerization has a strong influence on the HOMO-LUMO gap of these molecules. In this study, different derivatives of DTE have been investigated on Au(111) as monomeric units. Subsequently, coupling into both homo- and also co-polymeric structures was performed, which constitutes the first demonstration of the inclusion of such functional units in a covalent structure at a surface. By means of tunneling spectroscopy the state of the units could be unambiguously determined. Thus, it was found that the molecules are in the ring-open form upon evaporation. It was shown that reversible isomerization of the DTE units inside the chains can be induced by application of bias pulses from the STM tip. Finally, the chains are used to form single-molecule junctions between STM tip and sample to perform conductance measurements. These indicate that switching is possible in this configuration and corroborate the expected dependence of the conductance on the state of the switch.

## Kurzfassung

Das Ziel dieser Arbeit ist die Erforschung von molekularen Strukturen an Gold-Oberflächen unter Ultrahochvakuum. Die experimentelle Methode ist die Rastertunnelmikroskopie, die die Abbildung und Untersuchung von einzelnen Molekülen erlaubt. Der Fokus liegt auf ein- und zwei-dimensionalen kovalenten Strukturen.

Eindimensionale Oligo-Terfluoren-Ketten sind ein Prototyp eines molekularen Drahtes. Dessen wichtigste Eigenschaft ist die elektrische Leitfähigkeit. Um deren Messung zu ermöglichen, wurde eine neue Konfiguration entwickelt, in der einzelne Ketten in einer horizontalen Geometrie teilweise von der Gold-Oberfläche entkoppelt werden. Dazu werden dünne Isolatorschichten aus Natriumchlorid auf der Au(111)-Oberfläche gewachsen. Die entkoppelte Konfiguration wird zum einen mithilfe von Manipulation mit der STM Spitze erreicht und zum anderen durch eine präparative Prozedur. Die Aufnahme von Tunnel-Spektren entlang einer solchen Kette zeigt ihre teilweise elektronische Entkopplung, genauer gesagt die des Segments auf dem Isolator, wohingegen der Rest der Kette die Signatur aufweist, die typisch für die Adsorption auf Gold ist.

Weiterhin ist die Untersuchung und Weiterentwicklung der 2D-beschränkten Polymerisierung Gegenstand dieser Arbeit. Zur Steigerung der Kontrolle des Verknüpfungsprozesses wurde ein neuer, hierarchischer Ansatz verfolgt. Dazu wurden Porphyrin-Bausteine mit verschiedenen Substituenten eingesetzt. Es konnte gezeigt werden, dass sich damit eine schrittweise Aktivierung und Bindung ermöglichen lässt. Mithilfe von variabel-Temperatur-STM konnte der gesamte Prozess von den Monomeren, über eindimensionale Zwischenprodukte, bis hin zu zweidimensionalen Netzwerken verfolgt werden. Dabei wurde beobachtet, dass die Anordnung der Zwischenprodukte zu einer Verbesserung der Regelmässigkeit der Netzwerke führt, auf Au(111) durch einen Auto-Templat-Effekt, auf einer strukturierten Au(100)-Probe zusätzlich durch die Wechselwirkung mit der Oberfläche. Eine solche Steigerung der Regelmässigkeit ist eine zentrale Herausforderung für die zweidimensionale Polymerisierung, weil der Prozess nicht reversibel ist und keine Reparatur von Defekten erlaubt. Der schrittweise Prozess wurde weiterhin für die Produktion von Copolymeren eingesetzt. Aufgrund der kontrollierten Aktivierung der Bausteine ließen sich die Verknüpfungen mit einem hohen Grad an Selektivität durchführen.

Der Einsatz von molekularen Schaltern für die Steuerung von Signalen in einem Netzwerk ist eine vielversprechende Perspektive. Dithienylethene (DTE) sind aussichtsreiche Kandidaten, denn ihre Isomerisierung basierend auf einer Ring-Öffnung/Schluss-Reaktion führt zu einer Änderung des HOMO-LUMO-*gaps* und der damit verbundenen Leitfähigkeit. In dieser Arbeit wurden verschiedene DTE-Derivate auf Au(111) als einzelne Bausteine untersucht. Weiterhin wurden die Monomere erfolgreich zu Homo- und Copolymeren verknüpft, was die erste Demonstration vom Einbau solcher funktionaler Einheiten in kovalente Netzwerke an Oberflächen darstellt. Der Schaltzustand der einzelnen Einheiten ließ sich durch Tunnel-Spektroskopie eindeutig bestimmen. Aus den Spektren konnte geschlossen werden, dass sich die DTE-Einheiten nach der Deposition in der ring-offenen Form befinden. Es konnte gezeigt werden, dass sich die Einheiten gezielt und reversibel durch den Einsatz von Spannungs-Pulsen von der STM-Spitze schalten lassen. Weiterhin wurden Gold-Molekül-Gold-Kontakte mit einzelnen Oligo-DTE-Ketten hergestellt, die Hinweise darauf liefern, dass Schalten in dieser Konfiguration möglich ist und dass die Leitfähigkeit der Moleküle den erwarteten Zusammenhang mit dem Schaltzustand aufweist.

# Contents

Motivation	8
<b>1 Introduction to scanning tunneling microscopy (STM)</b>	<b>10</b>
1.1 Theoretical description of the tunneling process . . . . .	11
1.2 Tunneling spectroscopy . . . . .	15
1.3 Manipulation by STM . . . . .	18
1.3.1 Lateral manipulation . . . . .	19
1.3.2 Vertical manipulation . . . . .	20
1.4 Experimental setup . . . . .	23
1.4.1 STM Scanner and sample holder . . . . .	23
1.4.2 UHV chamber and cryostat . . . . .	24
1.4.3 Electronics and user interface . . . . .	27
1.5 Substrates: Au(111) and Au(100) . . . . .	28
1.6 Molecules . . . . .	31
<b>2 Molecular wires connecting metallic and insulating surface areas</b>	<b>34</b>
2.1 Introduction . . . . .	34
2.1.1 Pulling of molecular wires . . . . .	38
2.1.2 Decoupling molecules from the surface . . . . .	41
2.2 Preparation of wires both adsorbed to NaCl and gold . . . . .	43
2.3 Electronic decoupling and conductance measurement . . . . .	48
2.4 Theoretical polymer length distribution . . . . .	53
2.4.1 Length distribution of polyfluorene chains on Au(111) . . . . .	54
2.5 Conclusion . . . . .	58

<b>3</b>	<b>Covalent linking using a hierarchical approach</b>	<b>60</b>
3.1	Introduction . . . . .	60
3.2	Hierarchical growth - experimental results . . . . .	70
3.2.1	Thermal desorption spectroscopy . . . . .	78
3.2.2	Network size . . . . .	79
3.2.3	Substrate-directed growth . . . . .	83
3.2.4	Formation of co-polymers . . . . .	86
3.3	Conclusion . . . . .	89
<b>4</b>	<b>Polymerization and isomerization of dithienylethene</b>	<b>92</b>
4.1	Introduction to molecular switches . . . . .	92
4.1.1	Diarylethene molecular switches . . . . .	98
4.2	Characterization of diarylethene monomers on Au(111) . . . . .	103
4.2.1	Open-ring brominated DTE . . . . .	105
4.2.2	Closed-ring brominated DTE . . . . .	108
4.2.3	DTE with fluorene . . . . .	109
4.3	Polymerization of dithienylethene . . . . .	113
4.3.1	Structures made from Br <sub>2</sub> DTE . . . . .	113
4.3.2	Oligomeric chains made from I <sub>2</sub> DTE . . . . .	115
4.3.3	Oligomeric chains made from TM-I <sub>2</sub> DTE . . . . .	119
4.4	Manipulation of oligo-DTE . . . . .	124
4.5	Conclusion . . . . .	135
	<b>Conclusion and Outlook</b>	<b>136</b>
	<b>List of presentations</b>	<b>140</b>

## Motivation

The focus of this work are molecular structures at metal surfaces studied with scanning tunneling microscopy (STM). While the experiments are strictly concerned with basic research, the underlying theme is that of "molecular electronics" which proposes to employ single molecules as functional units in electronic circuits. It has been suggested that organic molecules performing tasks such as rectification, switching and the transduction of electrical signals might be utilized to complement or even replace silicon-based electronics, as the latter face serious obstacles to sustain the trend in miniaturization required to raise processing speeds, lower energy demands and reduce cost of production. The potential of functional molecules stems from their dimensions in the nanometer scale and the variability of their properties that can be readily modified by implementing changes to their chemical structure. However, while synthetic chemistry has been explored for many decades, the study of molecules at surfaces, especially at the single molecule level, is still a relatively new field. Studies investigating larger functional molecules were performed since about the turn of the century. Thus, many systems consisting of molecules at surfaces are still in need of investigation and understanding.

*Firstly*, a lot of effort has been directed towards the experimental and theoretical study of molecular electrical conductance. In a molecular electronics device, this property would be crucial for the transduction of electrical signals. However, the determination of single-molecule conductance is challenging even for small molecules ( $\sim$  one nanometer) and few studies exist that employ larger molecules that might constitute a molecular wire. *Secondly*, the self-organized assembly of organic molecules at surfaces is a rich field that has been intensely studied, producing a wealth of different and intricate two-dimensional structures. While initially these aggregates were only stabilized by non-covalent bonds, recently the formation of covalently connected networks could be successfully performed. There is an inherent interest in the latter, because only these structures provide the stability that allows their incorporation into a device. However, while in the last years a number of studies concerned with covalent structures were conducted, a strategy to control the network growth for the formation of more complex architectures is still missing. *Thirdly*, as mentioned above, an exciting prospect of the utilization of molecular structures is to equip them with functionality. The role model is nature that employs a host of nano-machines that facilitate tasks such as performing muscle contraction, transporting cargo inside cells and maintaining an electrochemical gradient across membranes. Molecular switches that can be induced to change their properties are an important instance of that category. A switch that can be prompted by an external stimulus to reversibly change its electrical conductance in a controlled manner would be ideally suited as a unit to control the signals in a molecular circuit.

Surface science was revolutionized by the invention of the scanning tunneling microscope (STM) by Gerd Binnig and Heinrich Rohrer in 1981 [1]. For this achievement they were awarded the Nobel prize only five years later, in 1986 [2]. The STM allows the detailed investigation of matter at the nanometer scale and in real space. While the imaging of atomic and molecular structures might be considered to be its most spectacular faculty, it is complemented by the possibility to acquire spectroscopic information locally, unveiling electronic, magnetic and vibrational properties. The structures cannot only be probed, but also actively influenced by the manipulation

capabilities of the STM. This opens the exciting possibility to create *supramolecular* structures from their components and also carry out *intramolecular* modifications, such as performing conformational changes, bonding, dissociation and isomerization. STM can be performed at cryogenic temperatures, at room temperature and elevated temperatures up to several hundred degrees centigrade. Furthermore, it is successfully utilized in vacuum, in ambient conditions and in solution. Considering its capabilities, STM can be regarded as the Swiss army knife of surface science.

The first chapter of this work serves to introduce the basic principles of scanning tunneling microscopy and describe the employed setup. Experimental results are presented in the three following chapters. As they are concerned with different topics, they are each preceded by an introductory section.

The goal of ch. 2 is the electronic characterization of long molecular chains that might serve as wires. To that end, the realization of a novel configuration is attempted, in which the molecule is partly decoupled from the underlying substrate by a thin insulating film. This horizontal setup shall serve as a more stable and controlled approach towards investigation of electrical transport, allowing to perform the length-dependent conductance measurements. In ch. 3 the on-surface polymerization is investigated with the aim to increase the control of the process. To that end, a stepwise procedure is implemented, which proceeds via an interim stage. The intention is to guide the formation of the final structures by exerting an influence on the intermediate products. Furthermore, a functional network will entail different building blocks, for instance wire and switching units, that need to be arranged in a suitable manner. By the stepwise provision of reactive sites it is attempted to facilitate the selective coupling of different precursors into copolymer structures. This method shall serve for the fabrication of more sophisticated architectures that are inaccessible through previously employed one-step processes. Moreover, the integration of functional units into a covalently coupled network has not been demonstrated so far. The realization and characterization of such structures is the subject of ch. 4. Molecular switches are considered to hold great potential as functional units at the nanometer scale. However, most efforts regarding single-molecule switching have been directed towards isomerizations that are not compatible with the rigid incorporation into a covalent network, such as the *cis-trans* isomerization of azobenzenes. Diarylethenes (DAE) on the other hand are a class of molecules that are ideally suited to this task, as their (ring-opening/closing) isomerization is accompanied with only a small conformational change. Moreover, it is reflected in a large modification to the electronic properties, which renders the molecules potential candidates for conductance switching. Despite favorable properties, such as fatigue resistance and thermal stability, studies of DAE at the single-molecule level are rare. The goal of ch. 4 is to connect these molecules into covalent structures and demonstrate their retained functionality.

The three topics, i.e. the formation of network structures connected by covalent bonds that allow efficient charge transport, the inclusion of a conductance switch functional unit therein and the fabrication of an experimental configuration attempting local decoupling and length-dependent conductance measurement are closely related in the context of the underlying theme of molecular electronics and are instrumental on the way to a potential realization of a molecular device such as a molecular electronic circuit.

# 1 Introduction to scanning tunneling microscopy (STM)

The present chapter serves to introduce the experimental method used in this thesis, which is scanning tunneling microscopy (STM). STM offers unique capabilities for the investigation of structures at the nanometer scale, including imaging, local spectroscopy and manipulation. With the STM the physics and chemistry of individual atoms and molecules can be studied, unveiling single-molecule properties which are hidden in averaging methods that deal with ensembles. Furthermore, the molecular behavior is sensitive to the environment, such as the local surface potential and the adsorption to defects and step edges, but also the presence of neighboring adsorbates. In STM, the local environment can be determined and to a certain extent even controlled. The capabilities of STM will be presented here by reference to seminal studies employing STM as well as the ones developing its theoretical foundation.

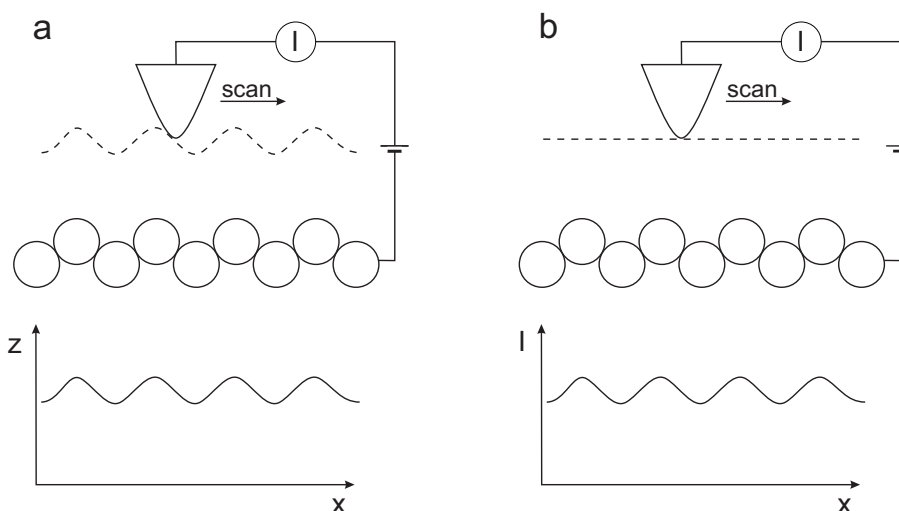


**Figure 1.1:** Sketch of the two main scanning modes in STM, the dashed line indicates the path of the tip, the recorded signal is shown below. (a) Constant current mode: the tip-sample distance is adjusted by a feedback loop to keep  $I_T$  constant. The information is contained in the  $z$  height. (b) Constant height mode: the tip is scanned across a flat surface and the information is contained in the tunneling current.

In STM, two electrodes, an atomically sharp tip and a flat conducting surface, usually the face of a single crystal, are held at a small distance of few atomic diameters in vacuum. Due to the quantum-mechanical tunneling effect, a net current of electrons is transmitted between the tip and the sample if a potential difference is applied. Practical bias voltages lie between millivolts and up to several volts, whereas the resulting tunneling current  $I_T$  is usually in the range of pico- to nanoamperes. The latter is highly sensitive to the separation between the two electrodes as will be discussed in ch. 1.1. This is the basis of the unique spatial resolution offered by STM, which lies in the sub-angstrom length scale. To put this to use, a mechanism to control the lateral and vertical position is required. This is facilitated by attaching one of the electrodes, usually the tip, to piezoelectric actuators ("piezos"), which allow to precisely adjust its position with regard to the other electrode (cf. ch. 1.4). With the help of the piezos the tip is raster scanned across the surface for imaging. The information is contained either in the tunneling current or the  $z$

height signal, depending on which of two scanning modes is employed (cf. Fig. 1.1). In the first, termed constant current mode,  $I_T$  acts as the control signal to regulate the tip-sample distance in a feedback loop. Recording the piezo parameters required to maintain a constant tunneling current yields a map  $z(x,y)$  of the corrugation of the examined area. While these maps are often referred to as topographic, they contain both geometric as well as electronic information, because in addition to the tip-sample separation  $I_T$  depends on the electronic states of the sample. As will be shown in ch. 1.1, in constant current mode the tip follows a surface of constant local density of sample states in a first approximation. Alternatively, in constant height mode the feedback loop is disabled and the tip is scanned across a plane surface. Consequently, the information is contained in the current signal. In this mode the scanning speed is not limited by the finite response time of the feedback loop which allows the observation of dynamic processes, such as surface diffusion. However, because in this mode the tip will not avoid collision with the sample if the latter crosses the scanning grid, this mode requires a sufficiently flat surface area. The images presented in this thesis are recorded in constant current mode unless stated otherwise.

## 1.1 Theoretical description of the tunneling process

The working principle on which the STM is based is tunneling. Tunneling is a transport mechanism that is due to the wave nature of particles and therefore a purely quantum-mechanical effect. The Schrödinger equation possesses solutions in classically forbidden ("barrier") regions, with the consequence that there is a finite probability for a particle to penetrate such barriers and transfer to the other side. Tunneling has been investigated decades before the invention of STM in the 1980s [1]. The development of the concept of tunneling and its experimental verification are among the early achievements of quantum mechanics. Tunneling has been applied to the description of a number of important systems, e.g. the field ionization of atomic hydrogen [3], the field emission from bulk material [4] and numerous types of junctions, in which metal, semiconductors and/or superconductors are separated by a thin barrier consisting of vacuum or dielectric [5]. Consequently, the theoretical models are adapted to different situations and therefore distinguish themselves in several aspects, among them the dimensionality of the junction, the shape of the barrier, the dissipation of energy in the junction and the time dependence [6].

The most facile approach is to treat the tunneling as both elastic and time-independent, the junction as one-dimensional and the barrier as rectangular. (A one-dimensional model is applicable e.g. for early studies employing two-dimensionally uniform junctions made by the oxidation of a metal electrode, followed by the evaporation of a second electrode on top. [7]) The corresponding sketch is shown in Fig. 1.2. To find the solution to this problem, the Schrödinger equation 1 is formulated for the three regions denoted by the roman numerals. While the particle is free ( $V = 0$ ) for regions I and III, its energy is smaller than the potential in region II ( $E < V_0$ ).

$$\left\{ -\frac{\hbar^2}{2m} \left( \frac{\partial}{\partial x} \right)^2 + V(x) \right\} \psi(x) = E \psi(x) \quad (1)$$

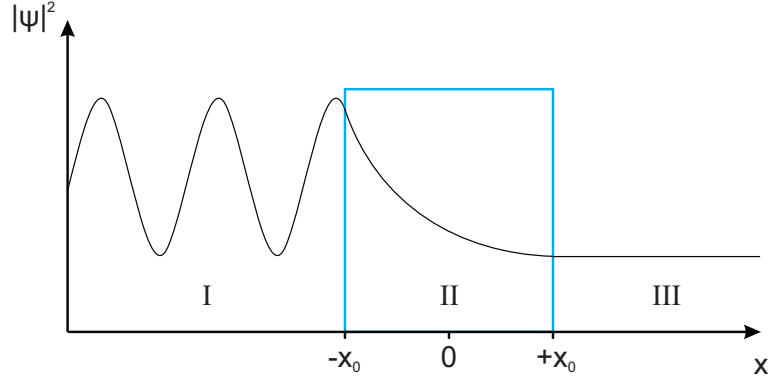


**Figure 1.2:** Sketch of the probability density  $|\psi|^2$ . For  $x < -x_0$   $|\psi|^2$  varies with  $x$  because of interference of the incident and reflected wave. Within the barrier,  $|\psi|^2$  decreases exponentially and stays constant for  $x > +x_0$ .

$$\begin{aligned} \forall x \notin [-x_0, +x_0] : \quad V(x) &= 0 \quad (\text{inside the metal}) \\ \forall x \in [-x_0, +x_0] : \quad V(x) &= V_0 \quad (\text{inside the gap}) \end{aligned}$$

While classically the particle could not penetrate region II and would therefore be reflected by the barrier, quantum mechanically there is a small probability that it arrives and continues in region III. This probability is contained in the transmission coefficient  $T$ , which is the ratio of the transmitted and the incident current density  $T = j_T/j_I$ . To determine  $T$ , the following *ansatz* is made for the solution of three different regions:

$$\psi(x) = \begin{cases} e^{ikx} + \alpha e^{-ikx} & x \leq -x_0 \\ \beta_+ e^{\kappa x} + \beta_- e^{-\kappa x} & -x_0 < x < +x_0 \\ \gamma e^{ikx} & +x_0 \leq x \end{cases} \quad (2)$$

with  $k^2 = 2mE/\hbar^2$  and  $\kappa^2 = 2m(V_0 - E)/\hbar^2$ . The requirement that the wave function and its derivative are continuous at the borders, i.e. at  $\pm x_0$  determines the coefficients ("wave matching"), yielding the following transmission coefficient:

$$T = |\gamma|^2 = \frac{4 \left(\frac{\kappa}{k_0}\right)^2}{4 \left(\frac{\kappa}{k_0}\right)^2 + \left(1 + \left(\frac{\kappa}{k_0}\right)^2\right)^2 \sinh(2\kappa x_0)} \quad (3)$$

In the case of  $\kappa x_0 = \frac{1}{\hbar} \sqrt{2m(V_0 - E)} x_0 \gg 1$ , i.e. a strongly attenuating barrier,  $T$  can be approximated by

$$T \approx \frac{16E(V_0 - E)}{V_0^2} \exp\left(-\frac{4}{\hbar} \sqrt{2m(V_0 - E)} x_0\right) \quad (4)$$

Thus, it is found that the transmission  $T$  and therefore also the tunneling current depends exponentially on the barrier width and also on the square root of the effective barrier height  $\sqrt{2m(V_0 - E)}$ . Estimating the effective barrier height with the work function of gold ( $\approx 4$  eV) leads to an exponential factor of  $\exp\{-4 \times x_0 [\text{\AA}]\}$ . Therefore, a change of the barrier width by one angstrom leads to a change of the transmission by approximately one order of magnitude. This pronounced dependence of the transmission of the barrier width is the basis of the high spatial resolution of STM. With the expression for  $T$  one can describe the current across a junction by taking into account the states that are available for the tunneling. In this way and furthermore allowing an arbitrary barrier shape, Simmons arrived at a general description for the tunneling current [8], albeit still for a one-dimensional system. However, the experimental capabilities of STM are based on the fact that it is three- and not one-dimensional, which requires a corresponding treatment. Furthermore, since the tunneling entails non-stationary states, a time-dependent approach is more suitable than a time-independent one. The prevalent theory describing tunneling in the STM was developed soon after its invention by Tersoff and Hamann [9, 10] based on a treatise by Bardeen [11]. The determination of exact solutions is seldom possible for realistic systems. Therefore, the tunneling current is usually given in the form of first-order time-dependent perturbation theory:

$$I = \frac{2\pi e}{\hbar} \sum_{\mu, \nu} f(E_\mu) [1 - f(E_\nu + eV)] |M_{\mu\nu}|^2 \delta(E_\mu - E_\nu) \quad (5)$$

Therein,  $f(E)$  is the Fermi function,  $V$  the applied bias voltage and  $M_{\mu\nu}$  are the matrix elements between the states  $\psi_\mu$  and  $\psi_\nu$ . For small temperatures (the Fermi function turns into the Heaviside step function) and small bias voltages eq. 5 reduces to:

$$I = \frac{2\pi}{\hbar} e^2 V \sum_{\mu, \nu} |M_{\mu\nu}|^2 \delta(E_\mu - E_F) \delta(E_\nu - E_F) \quad (6)$$

The appearance of the matrix elements is the consequence of formulating a time-dependent solution as the sum of a state that is initially occupied by the electron and a linear combination of states that involve the transfer of the electron to the other electrode and letting the state evolve under the influence of the Hamiltonian describing both tip and sample. While ordinary perturbation theory employs exact solutions of an approximate Hamiltonian, Bardeen's approach utilizes approximate solutions to an exact Hamiltonian. In this method, termed transfer Hamiltonian method, tip and sample states are good solutions only on one side of the junction. In this way, Bardeen expressed the matrix elements through the current density operator in which integration is performed over a surface  $S$  lying completely in the barrier region, separating the two sides:

$$M_{\mu\nu} = \frac{\hbar^2}{2m} \int d\vec{S} \cdot (\psi_\mu^* \nabla \psi_\nu - \psi_\nu \nabla \psi_\mu^*) \quad (7)$$

Tersoff and Hamann applied this expression to the STM geometry [10]. While surface wave

functions of general form could be employed, the precise shape of the tip is generally unknown. Therefore the tip is approximated by a spherical potential well, as sketched in Fig. 1.3, giving rise to radially symmetric (s-wave) tip wave functions.

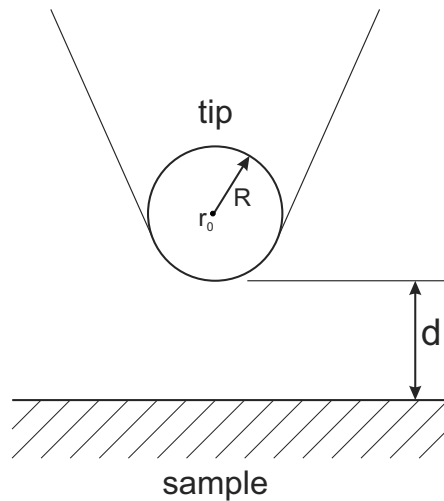


**Figure 1.3:** Sketch of the spherical tip potential used to approximate the tip wave functions, according to Tersoff and Hamann, adapted from [10].

Substituting the matrix elements determined with the help of these wave functions into eq. 5 results in the following result for the tunneling current:

$$I = 32 \pi^3 \hbar^{-1} e^2 V \phi^2 \rho_t(E_F) R^2 \kappa^{-4} e^{2\kappa R} \sum_{\nu} |\psi_{\nu}(\vec{r}_0)|^2 \delta(E_{\nu} - E_F) \quad (8)$$

Therein,  $\rho_t$  is the density of states per unit volume of the tip,  $\phi$  is the work function,  $\kappa = \hbar^{-1} \sqrt{2m\phi}$  and  $R$  and  $\vec{r}_0$  as defined sketched in Fig. 1.3. Since there are only constants before the sum term, the latter determines the distance for a set current value. This allows to assign an interpretation to images recorded with closed feedback loop. Because

$$\rho(\vec{r}, E) = \sum_{\nu} |\psi_{\nu}(\vec{r})|^2 \delta(E_{\nu} - E) \quad (9)$$

is the surface local density of states (LDOS) at energy  $E$  and point  $\vec{r}$ , images recorded in constant current mode represent a contour of constant LDOS at  $E_F$  of the surface. The distance dependence is contained in the sample states as well. The surface wave functions display an exponentially decaying behavior outside the metal: ( $\psi_{\nu}(\vec{r}) \propto e^{-\kappa z}$ ). With the labels in Fig. 1.3 it follows:

$$|\psi_{\nu}(\vec{r}_0)|^2 \propto e^{-2\kappa(d+R)} \quad (10)$$

The tip radius  $R$  cancels in the expression for the current (cf. eq. 8). Therefore the distance dependence is characterized by the following exponential factor:

$$I \propto e^{-2\kappa d} \quad (11)$$

Thus, one arrives at the familiar exponential dependence on the barrier width that was found for the one-dimensional case in eq. 4.

## 1.2 Tunneling spectroscopy

The tunneling current determined by Tersoff and Hamann [10] is based on the approximation of a small applied bias voltage. However, STM allows to apply a bias voltage in a range of several volts which is the basis of tunneling spectroscopy that shall be discussed in the following. While it is usually not possible to choose individual states that appear in the sum of eq. 5, one can select the energy range of participating states via the bias. For the description it is convenient to convert the sum into an energy integral. Due to Fermi's golden rule the energy of the tunneling electrons is preserved, i.e. only tunneling involving states of equal energy have to be considered. Maintaining the limit of small temperature the states in the relevant energy range  $[E_F, E_F + eV]$  are either all occupied or all empty, therefore a sum of the product of Fermi functions over a small energy interval is equivalent to the product of tip and surface density of states at that energy. Furthermore, the tunneling matrix elements are combined into an energy- and bias- dependent transmission factor that reflects the mean transmission probability of the respective states [12]:

$$I \propto \int_0^{eV} \rho_s(E) \rho_t(\pm eV \mp E) T(E, eV) dE \quad (12)$$

The upper (lower) signs apply for the case that the sample is held at a positive (negative) potential with regard to the tip.  $\rho_s$  and  $\rho_t$  are the sample and tip local density of states, measured with respect to the individual Fermi levels. The transmission  $T$  is bias dependent, because the applied voltage determines the combination of states from the two electrodes and influences the shape of the barrier that the electron is subject to during tunneling. It is furthermore dependent on the energy, because the tunneling probability is very sensitive to the effective barrier height, as is reflected in eq. 4. Fig. 1.4 serves to illustrate the tunneling at a finite bias voltage. It shows the density of states of tip and sample for the typical case of a metallic tip and sample. However, while the tip is clean, i.e. characterized by a nearly uniform DOS, the surface electronic states display some structure, as might be expected from molecular adsorbates. If the electrodes are far away and independent of each other (a), they share the vacuum level as a point of reference, with their occupied levels located below their respective work functions. In case of electrical contact (b) the Fermi levels will align and the trapezoidal shape resulting from the connection of the work function levels usually serves as a first approximation of the tunneling barrier [8]. However, an actual tunneling current requires the application of a bias as shown in (c) and (d). In (c) the sample is held at a negative potential with regard to the tip, leading to a rigid upward shift by  $eV$  of the surface electronic states. Therefore, occupied sample states are located opposite to unoccupied tip states, which results in tunneling of the former into the latter. In (d) the roles

are reversed, with the consequence of electrons transmitted from the tip towards the sample. As the electrons at the Fermi energy experience the shallowest effective barrier height, they extend the farthest into the barrier region and therefore possess the biggest transmission probability, which is indicated by length of the horizontal arrows in (c) and (d).

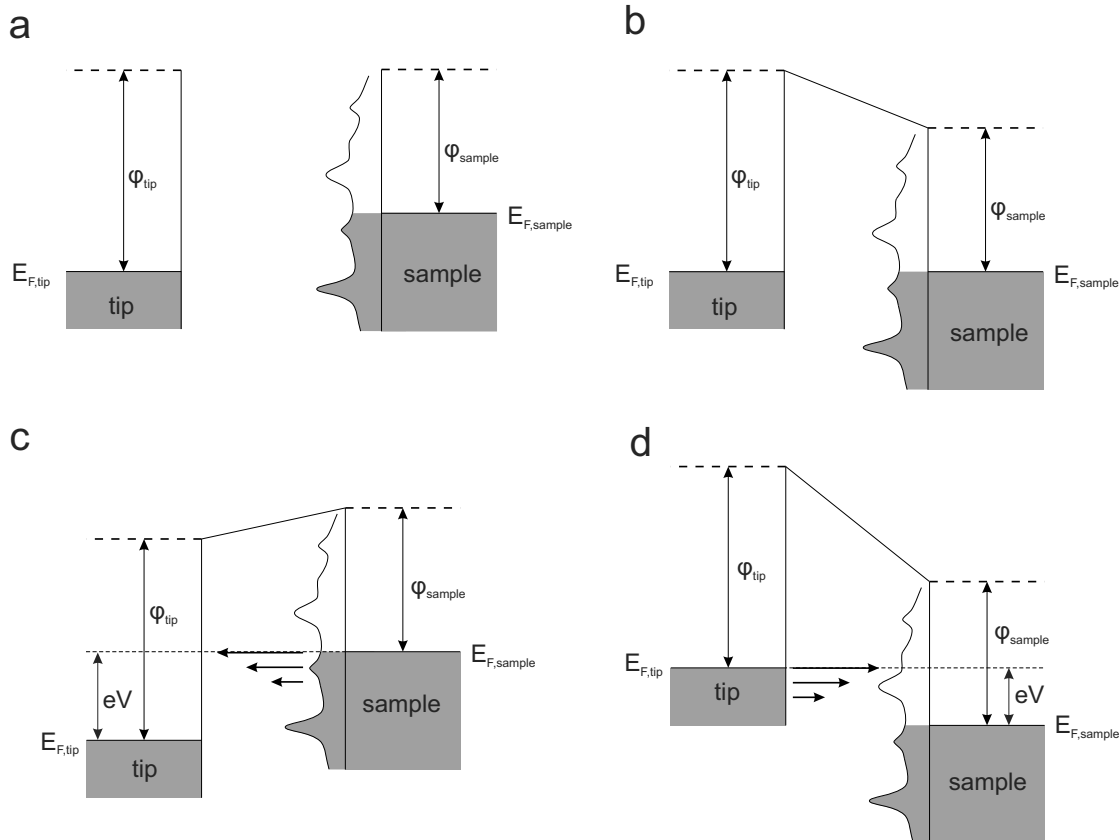


**Figure 1.4:** Energy diagram of tip and sample upon approach and application of a bias voltage. (a) independent electrodes, alignment of the vacuum levels, (b) sample and tip at equilibrium and in electric contact, zero applied bias, (c) negative and (d) positive bias applied to the sample, leading to a rigid shift of the sample energy levels. (Adapted from [12])

Thus, spectroscopy can be performed by changing the bias voltage. However, a variety of techniques exist that differ in the way the measurement is conducted [6]. The most facile method is bias-dependent imaging, in which electronic features are unveiled by scanning the same area at different voltages, either by increasing the bias after each image or by varying it in each point. Upon accessing states unavailable at lower bias the appearance can be modified. Taking molecular adsorbates as an example, changes can become visible in the apparent height and intramolecular features of the structures.

However, as can be seen from eq. 12, all states in the range of  $[E_F, E_F + eV]$  participate in the tunneling (albeit at a different magnitude as pointed out above), which poses a challenge to disentangle the different contributions. To that end, it is worthwhile to inspect the differential conductance, i.e. the first derivative of the current (eq. 12) with regard to the bias:

$$\frac{dI}{dV}(V) \propto \rho_s(eV)\rho_t(0)T(eV, eV) + \int_0^{eV} \rho_s(E)\rho_t(\pm eV \mp E) \frac{dT(E, eV)}{dV} dE \quad (13)$$

The first term is the product of the density of states of tip and sample and the transmission coefficient, whereas the second term reflects the bias dependence of the latter. As the transmission coefficient is assumed to depend on the bias in a smooth and monotonic fashion, and the tip DOS is approximately uniform for a metallic tip, features in  $dI/dV$  can usually be ascribed to the local DOS of the sample at an energy  $eV$  above or below the Fermi level (depending on the polarity). The differential conductance can be measured parallel to the current using a lock-in amplifier. To that end, the bias voltage is superimposed with a sinusoidal modulation, usually of small amplitude ( $\sim 10$  mV) and high frequency (hundreds of Hz). This is applied mostly in two different modalities, for the parallel recording of density of state information during scanning and for the acquisition of spectra in a fixed position. For the former the surface is scanned (either at constant height or constant current) keeping the dc part of the bias constant while the current modulation is extracted by the lock-in amplifier. In the latter, the lateral scanning is interrupted, the feedback loop opened and the bias voltage is swept over the range of interest [13]. In this type of measurement, the information about the electronic states is contained in the current signal. In analogy to the scanning modes depicted in Fig. 1.1, spectroscopy can also be performed in constant current mode. This can be favorable, because while the transmission factor adds only a smooth background to the differential conductance signal, it also gives rise to a considerable increase in the tunneling current at increasing bias. For sensitive samples, such as ones containing organic molecules, it can be necessary to limit the tunneling current to avoid modification by the tip (cf. ch. 1.3). Therefore, instead of the tip-sample distance the tunneling current is kept constant (by closing the feedback loop) while ramping the bias voltage. In this method, called  $z(V)$  spectroscopy [14], the information is contained in the tip-sample distance, which is increased each time new sample states become available to participate in the tunneling.

### 1.3 Manipulation by STM

The STM can be employed not only for imaging and spectroscopy but also to modify the sample. As is the case in imaging and spectroscopy, the great advantage of such tip-induced manipulation lies in the possibility to apply it locally with submolecular resolution. The mechanisms of tip-induced manipulation include strong electric fields [15], excitation by resonantly and/or inelastically tunneled electrons [16–21] and the application of forces upon mechanical contact between the tip and the sample [22–27] - and combinations thereof [28]. The different modes of excitation are characterized by a distinctive behavior that can help to distinguish them. For instance, in inelastic tunneling the electron yield will typically display a threshold that is independent of the bias polarity and that is located at an energy of a vibrational mode of the molecule (of the order of 100 meV). For elastic tunneling on the other hand the threshold is polarity dependent and will coincide with one of the electronic resonances (which usually lie in the range of eV). Finally, a yield independent of the current that flows in the junction is an indication that the electric field is responsible. It has been demonstrated that processes that play an important role in the *physics* of adsorbates on surfaces can be induced with the help of the STM tip, among them molecular diffusion [19, 20, 28, 29], rotation [18, 21, 27] and desorption [16, 17]. For instance, the diffusion of CO molecules on Pd (110) has been investigated by Komeda et al. [19] The molecules perform a one-dimensional random walk along the corrugation lines of the surface that is followed by repeatedly imaging of the line that the molecules is situated in. It was demonstrated that the hopping could be induced by the excitation of a vibrational mode in the molecule by inelastically tunneling electrons. A similar behavior was found by Ohara et al. for the two-dimensional hopping of methylthiolate molecules on Cu(111) [28]. In addition to performing the inelastic excitation, the tip was employed to influence the direction of the hopping through the electric field. (In studies investigating the thermally induced diffusion of adsorbates the situation is usually even reversed and evidence has to be supplied that the presence of the tip does *not* influence the process [30, 31]).

One of the first observations of single-molecule rotation induced by tunneling electrons was made in Ho's group in the study of oxygen molecules on Pt(111) [18]. The molecules are found to alternate between three different orientations upon vibrational excitation that can involve a variable number of electrons depending on the employed bias voltage. But also the rotation of larger molecules was successfully performed, such as the study of Manzano et al. using a hexaphenylbenzene derivative on Au(111) [27]. Once these molecules are mounted on a pinning center, they can be rotated by mechanical contact with the STM tip without inducing translational motion. Probably the most spectacular application of tip-induced manipulation is the controlled displacement of atoms and molecules. The methods for the positioning of atoms and molecules using the STM tip can be roughly divided into two groups, lateral and vertical manipulation. In lateral mode, the adsorbate stays attached to the surface during the procedure, whereas it is picked up from the surface in vertical mode, usually to subsequently be reattached it in a different position.

### 1.3.1 Lateral manipulation

The first demonstration of controlled lateral manipulation was given by Eigler and Schweizer [22]. They used the STM tip to move individual Xe atoms on a Ni(110) surface to arrange them into the IBM logo. In the Rieder group at the FU Berlin, lateral manipulation was extended to small [23, 24] and also bigger molecules [25, 26]. It is based on the same approach that was employed by Eigler and Schweizer for the displacement of Xe atoms, making use of the fact that the interaction between tip and adsorbate depends on their distance. For a manipulable system the interaction at scanning height is sufficiently small that imaging can be performed without causing modifications to the adsorbate. However, if the set point current is raised, the interaction between the tip and sample is increased upon approaching the tip towards the surface. If the bonding between substrate and adsorbate allows it, the latter can be induced to follow the path performed by the tip. During this motion the feedback loop can be open or closed, analogously to the modes depicted in Fig. 1.1.

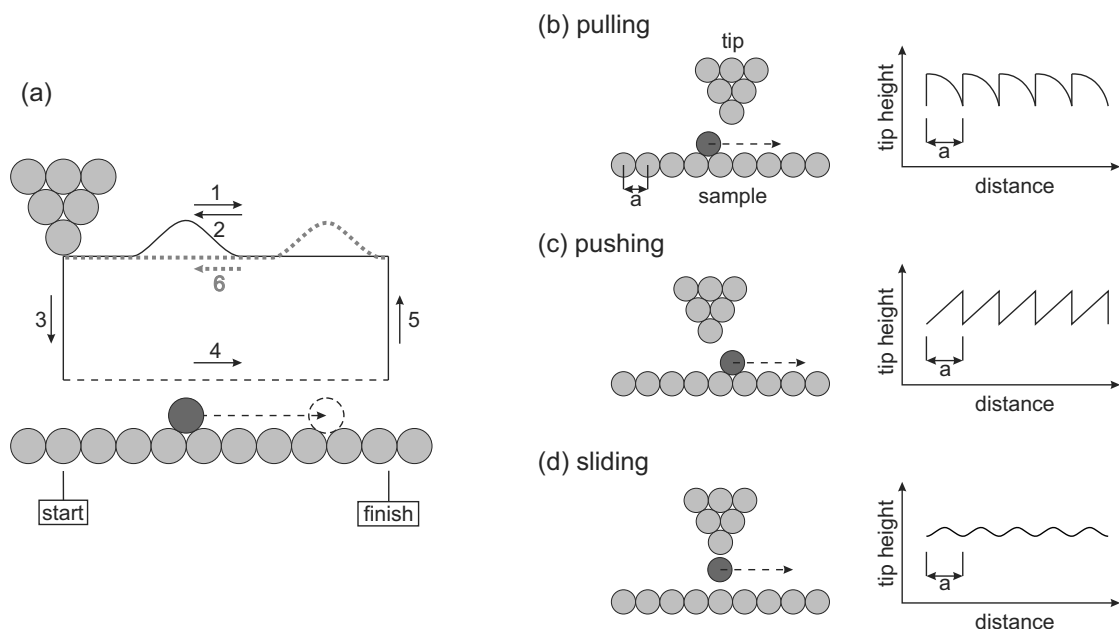


**Figure 1.5:** (a) Sketch of the lateral manipulation procedure. At imaging height (steps 1,2 and 6) the interaction with the tip doesn't perturb the adsorbate (dark gray), whereas it follows the tip at higher set point current (4). In constant current mode, the interaction modality can be inferred from the z height signal as sketched in (b) to (d). The interaction in (b) is attractive, in (c) repulsive and in (d) the molecule moves continuously in the combined potential of tip and surface. (Adapted from [24])

Lateral manipulation is extensively employed in this work for the characterization of adsorbate structures, e.g. to facilitate identification and test the inter- and intramolecular binding strengths. The usual procedure is depicted in Fig. 1.5 (a). First, the tip is scanned forth and back along the designated path across the adsorbate (gray) at imaging parameters (steps 1 and 2). Subsequently, the set point current is increased which prompts the tip to approach the surface (3) and the line is scanned again (4). At this step the tip-sample interaction is strong enough to induce modifications. Afterwards, the tip returns to imaging parameters (5) and the line is scanned once more (6). If the manipulation was successful, the result will be immediately

visible by comparison of sections (2) and (6) in the current signal. Further information about the process can be found in the signal recorded during the manipulation step (4 - dashed line). Meyer et al. could distinguish three different interaction modes [24], as sketched in (b) - (d) for an active feedback loop, i.e. constant current mode in which the information is contained in the  $z$  height signal. Thus, the signal sketched in (b) was associated with an attractive interaction in which the adsorbate follows the tip by hopping from one adsorption site to the next. The process is termed "pulling mode". The signal in (c) on the other hand is characteristic for a repulsive interaction ("pushing mode"), whereas (d) depicts a third case in which the interaction is so strong that the adsorbate moves continuously in the combined potential of tip and surface ("sliding mode"). The correspondence of the periodicity in the  $z$  height signal with the lattice spacing (labeled "a") which allows a facile identification of the adsorption sites along the manipulation path [32, 33] is usually only observed for atoms and small molecules (e.g. CO), whereas the many different adsorption configurations and internal degrees of freedom of larger molecules (such as porphyrin) produce more complicated and less reproducible signals [25]. However, they can also give rise to novel and interesting behavior, such as wheel molecules that could be shown to perform a rolling motion on the weakly corrugated Cu(110) surface [26]. It was demonstrated that the rotation of a molecule around an axis in-plane with the surface could be successfully induced with the STM tip, thus constituting another lateral manipulation mode.

### 1.3.2 Vertical manipulation

In vertical manipulation an atom or molecule is attached to the STM tip and removed from the sample surface to be subsequently reattached in a different location. This can be employed in lieu of lateral manipulation, especially if the translation path includes a prohibitively long distance or the crossing of obstacles such as step edges. The transfer is usually facilitated by bringing the tip so close to the adsorbate that the potential barrier between them vanishes and the particle is located in the combined adsorption well of both tip and sample [34]. In a successful attempt the adsorbate is removed from the surface upon retraction of the tip. This method, termed "transfer-on-contact", does not require the application of a bias voltage or tunneling electrons. However, it has been shown that they can facilitate the process, especially if the tip is not brought into direct contact with the sample and a potential barrier remains. One of the first demonstrations of vertical manipulation was given by Eigler et al. who showed the reversible transfer of a Xe atom between a tip and a Ni(110) surface [35]. In addition to the transfer-on-contact at small bias voltages, the transport could also be induced by the application of bias pulses of appropriate polarity at larger tip heights, which was explained by vibrationally assisted electromigration. As in the case of lateral manipulation, the transfer of adsorbates between STM tip and sample was extended to small molecules in Rieder's group in Berlin. Bartels et al. demonstrated a procedure to reliably pick up single CO molecules and subsequently re-adsorb them on a Cu(111) surface [36]. Both the attachment of a Xe atom and a CO molecule led to an enhancement of the resolution in subsequently recorded images. Thus, in addition to the controlled arrangement of adsorbates on the sample vertical manipulation can also serve to permanently attach an atom or molecule to the tip to modify its properties (the tip is then termed "functionalized"). While

in ch. 1.1 the tip was assumed to be metallic without any pronounced features in the DOS, the presence of the CO renders the contrast chemically sensitive, which allowed the identification of different adsorbates that are hard to distinguish in images recorded with a metallic tip [36]. Similarly, a CO terminated tip led to a modified contrast of pentacene and naphthalocyanine in a study by Gross et al. [37]. Therein, the tunneling through the CO's  $\pi$  orbitals adds p-wave character to the tip, which results in intramolecular resolution that reflects the derivative of the molecular wave function, as described by Chen [38]. However, contributions of a functionalized tip are usually difficult to interpret and the features in the density of states appear in addition to the ones of the adsorbate in spectroscopic measurements. Therefore, great care is taken to keeping a clean metallic tip. The procedure that serves to that end, called "tip forming", again employs a form of vertical manipulation. The tip is indented into the sample to cover it with surface atoms, thus effectively reforming the apex. Albeit performed with less control than the examples cited above, the procedure is nonetheless crucial to maintaining a clean tip that is microscopically sharp, i.e. terminated with a single atom.

Moreover, manipulation with the STM allows to perform surface-confined *chemistry* on individual molecules, such as the breaking and the formation of single covalent bonds [39–44]. One of the earliest examples of single-molecule dissociation on a metal surface was performed in Ho's group [39]. Therein, the intramolecular bond of oxygen molecules adsorbed on Pt(111) is cleaved by tunneling electrons. It is observed that only the molecule directly under the tip is affected while neighboring ones stay intact. This highlights the addressability of the process, which is based on the fact that the tunneling current is confined to a very small region beneath the outermost tip atom. Upon dissociation, the two atoms hop away which causes a sudden increase of the width of the tunneling barrier that is reflected in a drop in the tunneling current (feedback loop disabled during manipulation). In molecules containing more than two atoms the situation is more complex because of the presence of more than one covalent bond that can be excited by the tunneling current. This was demonstrated in a study by Hla et al. who performed dissociation experiments on iodobenzene adsorbed to a Cu(111) surface [44]. It was demonstrated that due to the relative strengths of the bonds inside the molecule the carbon-iodine one can be cleaved selectively, leaving the phenyl intact.

The locally induced formation of a covalent bond on the other hand is a more complicated matter. Suitable reaction partners have to be properly aligned for bonding and maintained that way during excitation. In the light of processes such as diffusion and rotation discussed above this poses a serious challenge. One approach involves the attachment of one of the reactants to the STM tip, i.e. performing vertical manipulation. This method allows to precisely position the reaction partners and to induce bonding by passing a tunneling current through the thus formed junction [40, 42]. However, there are also experiments in which both reactants are adsorbed to the sample surface prior to connection. In a continuation of the above-mentioned study by Hla et al. the same authors proceeded to covalently connect two of the previously formed phenyl radicals [41]. Two molecules were arranged next to each other in their preferential adsorption site at a step edge. Subsequently, the application of tunneling current was used to prompt both the rotation and connection of the phenyl radicals, producing biphenyl. As this reaction is closely related to the on-surface-synthesis approach studied in the present work, it will be revisited

in more detail in ch. 3. Another type of process that can be included with the chemistry of molecular adsorbates is isomerization, which is concerned with intra- rather than intermolecular reactions, such as the ring-opening and closing of diarylethenes. This will be discussed in detail in ch. 4.

## 1.4 Experimental setup

The experimental setup that was mainly employed during this work will be introduced in the present section. To avoid contamination, all operations are performed in an ultrahigh vacuum (UHV) chamber. Therein, the single crystals are carried by sample holders that can be transferred between a preparation chamber and the chamber that contains the STM scanner. The preparation chamber serves for the cleaning of the samples and the deposition of molecules. After preparation, the samples are inserted into the scanner for investigation. The scanner is attached to a cryostat so that both scanner and sample can be cooled to cryogenic temperatures.

### 1.4.1 STM Scanner and sample holder

The STM head is a modified Beetle-Besocke type scanner [45] that was designed and built by G. Meyer [46], together with S. Zöphel and K. Schaeffer [47, 48]. In this design, that is shown in Fig. 1.6, the sample (1) is located beneath the tip (2). The lateral and vertical position of the tip can be adjusted while the sample is static. The tip is attached via the central piezo (3) to a circular disk (4) that is supported by the three outer piezos (5) via sapphire balls. In the employed setup, the bias voltage is applied to the sample, whereas the current is measured on the tip side.

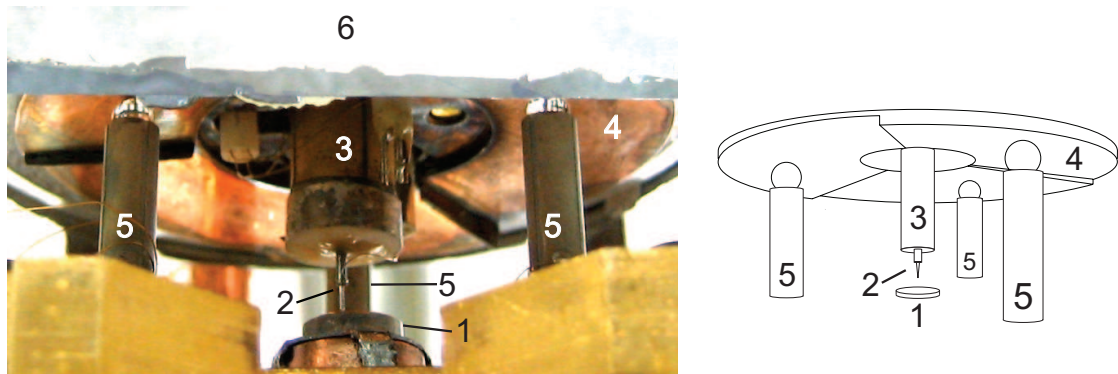


**Figure 1.6:** Photograph and sketch of the employed Beetle-Besocke type scanner head. The sample (1) is located beneath the tip (2) that is attached to the central scanning piezo (3). The central piezo in turn is attached to a copper disk (4) that is supported by three outer piezos (5). The latter are utilized to perform the coarse and fine positioning of the tip with regard to sample (cf. main text). Additionally, the photograph shows the lower edge of a mirror (6) that is used in the sample transfer (not shown in the sketch for better visibility). Photograph copyright by S. Selvanathan.

The three outer piezos can perform a bending motion by the application of suitable signals to their electrode segments. If the motion is slow, the disk will move accordingly and will stay supported in the same positions by the sapphire balls. The (equally slow) discontinuation of the piezo signal will then return the disk into the initial position. However, if the bending takes place too fast for the inert disk to follow, the sapphires will move with respect to it and adopt new supporting positions. By the alternating execution of slow and fast movements the disk (and the tip attached to it) can be translated in what is called "slip-stick-motion". To facilitate approach

and retraction of the tip, the disk is divided in three segments that are all slightly slanted in the same direction, each supported by one of the piezos (cf. the sketch to the right in Fig. 1.6). Therefore, if the disk is induced to perform a rotary motion by bending of the piezos tangentially to it, this will result in a vertical motion of the disk.

The tip employed in this study is made of tungsten and is produced by electrochemical etching of W wire using a membrane of sodium hydroxide solution. Due to repeated contact with the surface ("tip forming", cf. ch. 1.3.2) the apex of the tip is considered to be made of the same material as the sample, i.e. gold in the present work. Due to the possibility to produce clean metallic tips in this way, the exchange of the tip for a new one is only rarely necessary (less than once a year).

To handle the samples the single crystals are attached to sample holders, as shown in Fig. 1.7. Therein, the circular crystal (1) is mounted on top of an equally circular oven (2) that is used to apply the heating for experiments and also for the annealing steps during sample preparation. To allow to monitor the sample temperature, thermocouple wires are attached to it. Sample and heater are electrically isolated from the rest of the sample holder. The latter supplies electrical connections to the sample, both for attachment on the manipulator and inside the STM scanner, which is used for instance for the application of the bias voltage.

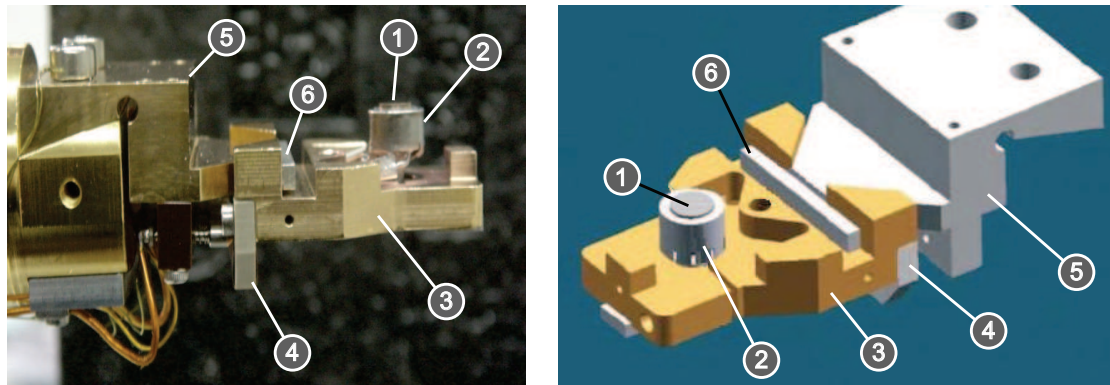


**Figure 1.7:** Photograph and model of the sample holder mounted to the manipulator used for transfer. The single crystal (1) is attached to the button heater (2), which is electrically isolated from the copper body of the sample holder (3). Electrical connections are supplied on the contact pad (4), which are employed both inside the STM and on the manipulator (5). The latter is outfit with a mechanism (6) to pick up the sample holder. Photograph copyright by M. Alemani, model copyright by S. Zöphel.

#### 1.4.2 UHV chamber and cryostat

The entire experimental procedure consisting of sample preparation, sample transfer and investigation in the STM is performed at a pressure of the order of  $10^{-10}$  mbar. Employing unreactive surfaces such as gold under UHV conditions allows the continued measurement for weeks at a time without the need to reprepare the sample due to contamination. The chamber that is shown in Fig. 1.8 consists of two compartments separated by a valve. The part on the left is used for sample preparation and is thus referred to as "prep chamber". It is equipped with a sputter gun

for sample cleaning and a "Kentax" Knudsen cell for molecule deposition. The latter contains four quartz glass crucibles that can be heated independently, which is necessary for the simultaneous evaporation of different types of molecules. The evaporator can be dismantled for refilling without affecting the vacuum in the prep chamber. The molecular flux during evaporation is monitored by means of a quartz crystal microbalance. Furthermore, the prep chamber is outfit with an ionization gauge, a gas inlet for sample treatment, a quadrupole mass spectrometer for rest gas analysis and a storage device that can hold two samples. The sample transfer to and from air is facilitated by a load lock.

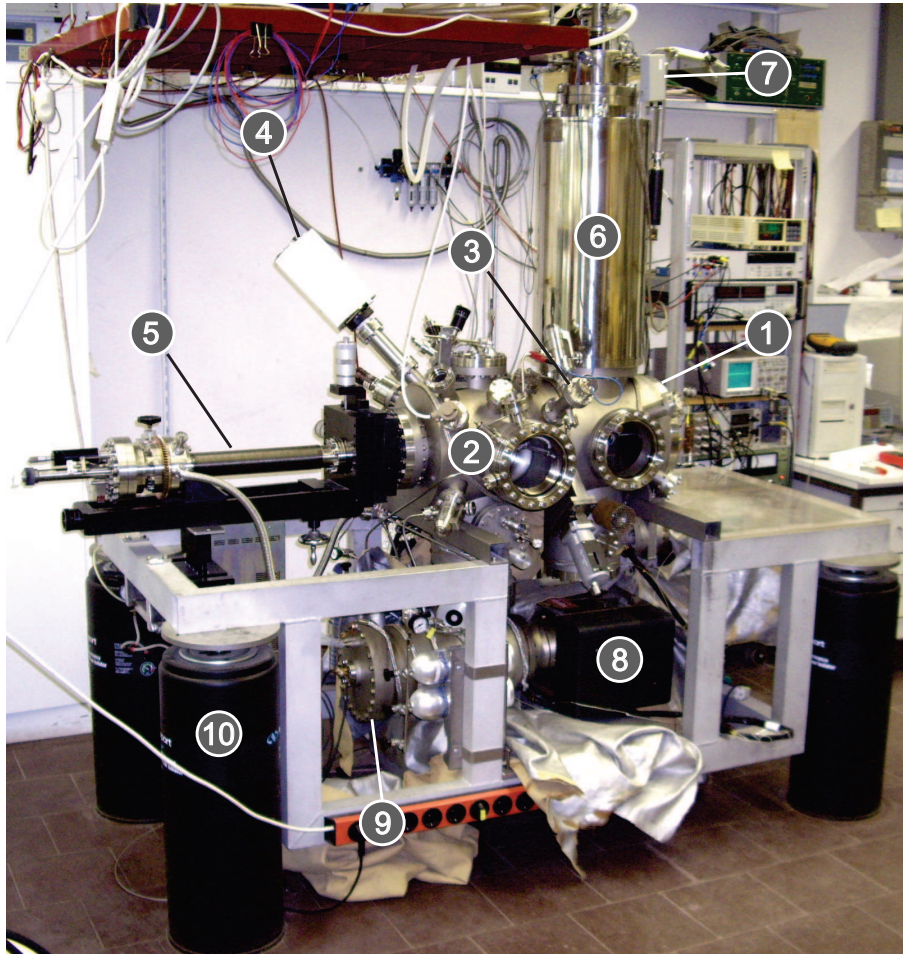


**Figure 1.8:** Experimental setup employed in this work. The UHV chamber is divided by a valve into the STM chamber containing the scanner (1) and the preparation chamber (2). The latter is equipped with a sputter gun with gas inlet (3) and a mass spectrometer (4). Sample transfer and cooling is performed with the manipulator (5). During measurements sample and scanner are cooled by a bath cryostat (6). (7) Preamplifier for the tunneling current. The chamber is pumped by an ion getter pump (6), a titanium sublimation pump (7) and a turbomolecular pump (not shown). The whole chamber rests on pneumatically damped feet (10). Photograph copyright by S. Selvanathan.

The manipulator is used to position the sample holder during sample treatment and for the subsequent transfer into the STM. It can perform motion in all three directions and 360° rotation around its axis. The manipulator contains its own helium cryostat to cool the sample down to below 70 K. This allows to modify the conditions during sample preparation, e.g. to limit

adsorbate diffusion, and to precool the sample prior to transfer into the STM.

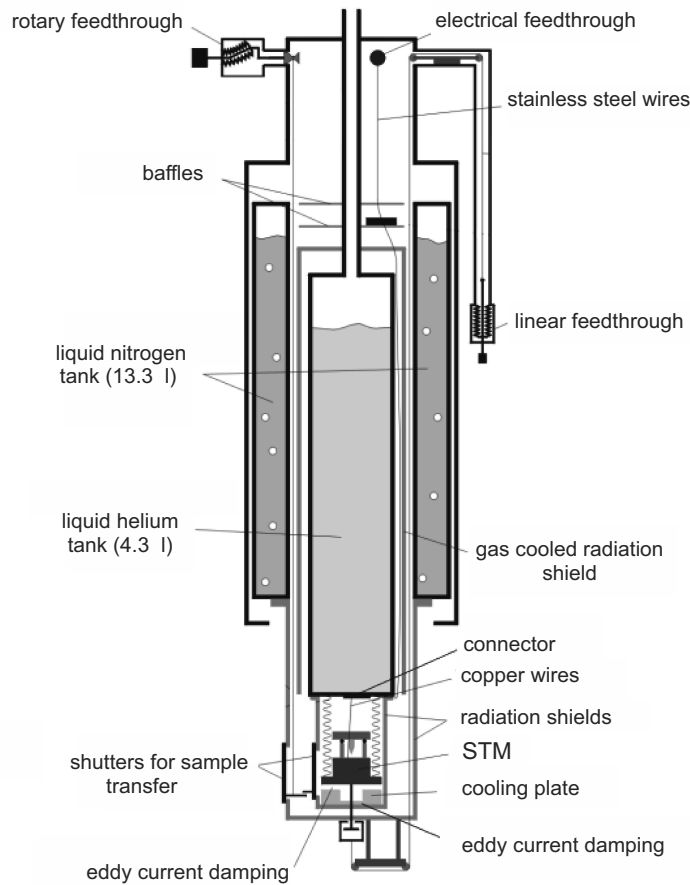


**Figure 1.9:** Sketch of the bath cryostat ((6) in Fig. 1.8). The scanner is suspended from the liquid-helium tank, which is surrounded by a liquid-nitrogen tank. Each tank carries a radiation shield which encloses the scanner. The mechanical feedthroughs at the top are used to operate the shutters and the pulley mechanism to pull the scanner onto the helium shield for cooling. From [48], reprinted with permission from S. Zöphel.

The scanner is attached to the bottom of a bath cryostat, consisting of a liquid helium tank (4.3 l) surrounded by a liquid nitrogen one (13.3 l), as shown in Fig. 1.9. In this way the sample and scanner can be maintained at a constant temperature of approx. 10 K and a temperature gradient is avoided. Performing measurements at low temperature has several advantages, among them an improved energy resolution by narrowing of the Fermi distribution. Furthermore, thermally induced processes such as adsorbate diffusion are suppressed, which is especially important for the study of weakly bound molecules that are too mobile to be imaged at room temperature. The stability is greatly enhanced at low temperature, with a drift of less than 1 Å/h, which allows to investigate a particular area for days at a time. With a cooled sample the helium lasts for about two days, which corresponds to a consumption of less than 0.1 l/h. The scanner is contained in two radiation shields made of aluminum that are attached to the helium and nitrogen tanks,

respectively. For enhanced cooling after sample transfer into the STM, the scanner head can be brought into contact with the helium shield by a pulley mechanism, which allows stable scanning at low temperature after a period of three to four hours. The shields furthermore act as cryopumps which likely leads to an improvement of the pressure inside the small volume with regard to the one measured on the outside. All electrical wiring is passed along the outside of the helium tank for cooling and the electrical feedthroughs are located at the top of the cryostat, which is also where the tunneling current preamplifier is connected (cf. (7) in Fig. 1.8).

### 1.4.3 Electronics and user interface

The scanner is operated with the "PSTMAFM" software developed by G. Meyer (commercially available from Createc). It allows to control all setting relevant for scanning, spectroscopy and manipulation (such as the feedback loop parameters) and to observe the recording of images and spectra in real time. The motion of the tip and the feedback loop is controlled by a digital signal processor (DSP), that communicates with the analog electronics via four 16-bit digital-analog and analog-digital converters (DACs and ADCs), as shown in Fig. 1.10.

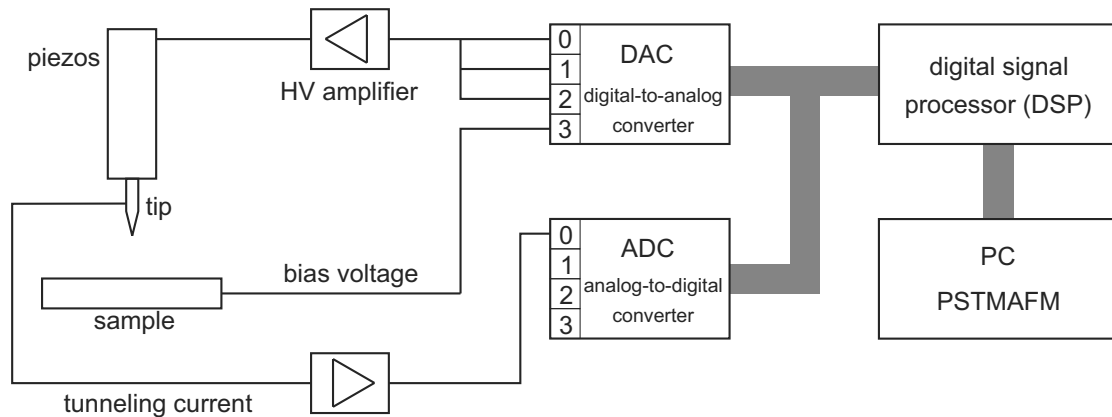


**Figure 1.10:** Schematic of the electronic components used for STM operation. The digital signal processor controls the feedback loop according to parameters set in the "PSTMAFM" software. The ADC and DAC converters connect the DSP to the analog electronics. Adapted from [48].

One DAC channel is used to supply the bias voltage, while the other three are used for the control of the piezo elements during scanning, coarse motion and automatic approach. The piezos require higher voltages than the maximal output of the DSP of  $\pm 10$  V, therefore the signal is passed through a high voltage amplifier (max output  $\pm 175$  V; variable gain of 1, 3, 10 and 30). The tunneling current is measured on the tip side of the junction and amplified by a Balzers I/V converter (variable gain of  $10^6$ ,  $10^8$ ,  $10^{10}$  and  $10^{12}$ , with a typical bandwidth during scanning of 10 kHz) located directly at the electrical feedthrough for noise reduction and returned to the DSP via one of the AD converters. In constant current mode, i.e. with an active feedback control, the current signal is compared with the set point current and the difference (error signal) is used to correct the height setting of the scan piezo.

## 1.5 Substrates: Au(111) and Au(100)

All experiments in this work were performed on gold single crystals. Gold is a transition metal with a fcc structure and a lattice constant of  $4.08 \text{ \AA}$  [49]. The employed surfaces were either the (111) or the (100) face. Both surfaces display a reconstruction, i.e. a divergence from the regular atomic lattice in the bulk. Gold is one of the few fcc metals whose (111) face is characterized by a reconstruction. Its investigation in STM was instrumental for unveiling the structural details. Direct determination of the atomic positions allowed to remove ambiguity and resolve the contradictions between models proposed on the basis of other experimental techniques. Thus, Barth et al. could confirm the stacking-fault-domain model, which consists of a periodic transition from fcc to hcp stacking resulting from a uniaxial and nearly uniform contraction of the topmost hexagonal layer [50]. Contraction takes place along the  $[1\bar{1}0]$  direction by an average of  $4.5\% \approx 0.13 \text{ \AA}$ . As a consequence, 23 surface atoms are placed on top of 22 bulk atoms in a  $\begin{pmatrix} 22 & 0 \\ -1 & 2 \end{pmatrix}$  or  $(22 \times \sqrt{3})$  unit cell as shown in Fig. 1.11. In the fcc and hcp regions (depicted black and dark gray) the atoms are situated in threefold hollow sites, whereas in the transition regions (light gray) they occupy quasi-bridge sites. Therefore, the latter regions appear as stripes of higher corrugation that form pairs running perpendicularly to the contraction, i.e. in the  $[11\bar{2}]$  direction. The vertical displacement in these stripes amounts to about  $0.2 \text{ \AA}$  as measured in STM. In addition to a vertical displacement the transition between fcc and hcp leads to a lateral displacement along  $[11\bar{2}]$  that was found to be approx.  $0.9 \text{ \AA}$ , in agreement with a hard sphere model.

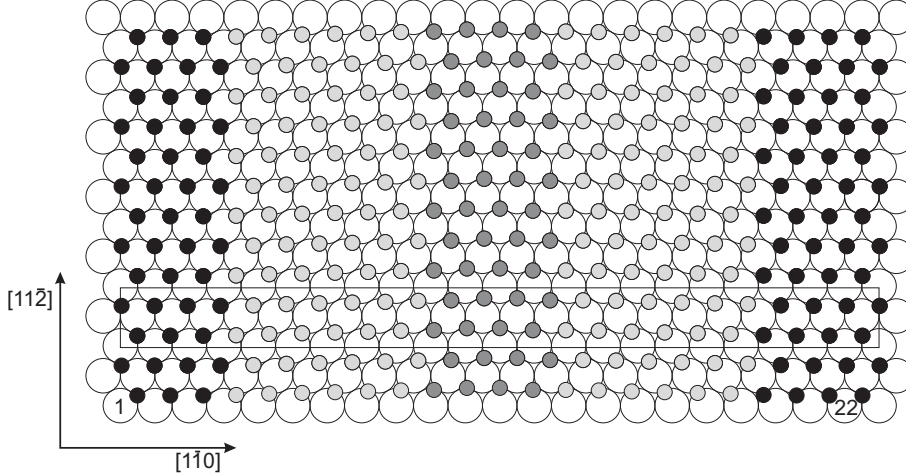


**Figure 1.11:** Sketch of positions of the first two atomic layers inside the domains of the herringbone reconstruction. Topmost layer atoms depicted with smaller diameter for better visibility. The atoms in the hcp regions (black, dark gray) occupy threefold hollow sites, the ones in the transition regions (light gray) quasi-bridge sites. The unit cell is enclosed by the box.

While the contraction takes place only along one direction, the surface is threefold symmetric. Thus, there appear three rotational domains of the above type. The transition between different domains is either facilitated by  $120^\circ$  bends of the corrugation lines that therefore continue in the next domain or their U-turn like termination by connecting two adjacent lines from within the same domain. A similar mechanism was observed at the step edges, which allowed to assign

the broader regions to fcc and the thinner to hcp stacking (based on the assumption that the atoms in the second layer occupy the regular bulk fcc positions which is therefore also true for the ones that sit on the lower terrace directly adjacent to the step edge). The reconstruction owes its name to the periodical bending of the corrugation lines on a larger scale, that leads to the appearance of regular patterns. These findings highlight the capabilities of the STM that allowed the observation of these superstructures.

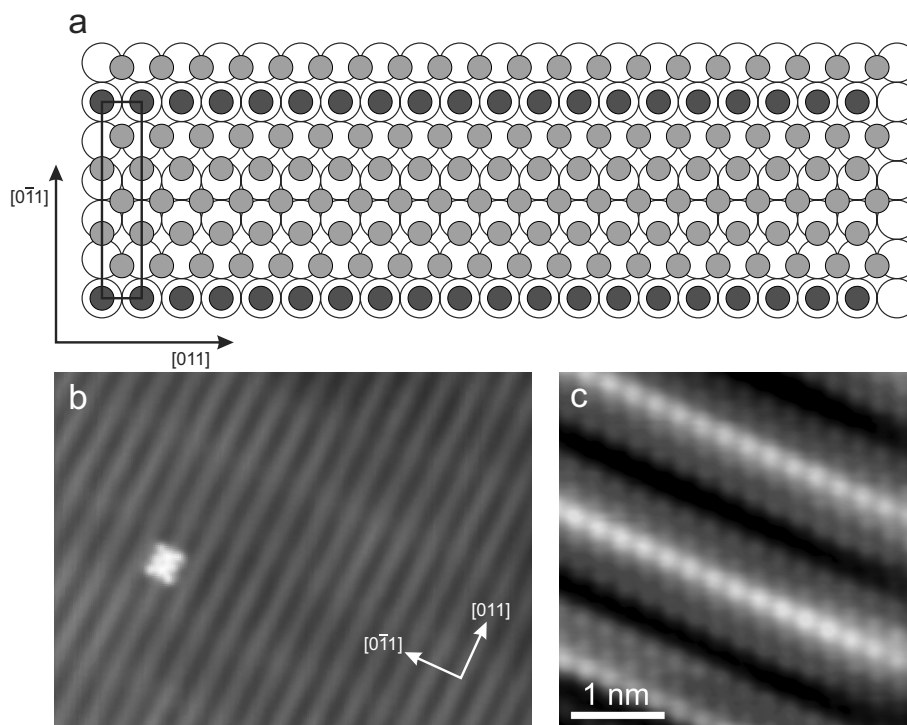


**Figure 1.12:** (a) Sketch of the first two atomic layers of the Au(100) surface. The topmost atoms are again shown with a reduced diameter for better visibility. The topmost layer forms a quasi-hexagonal lattice, the approximate unit cell is indicated by the box. The on-top situated atoms (colored dark gray) give rise to corrugation lines along the [011] direction. (b) STM image of Au(100) with a single TPP molecule,  $18 \times 24 \text{ nm}^2$ , 0.1 nA, 500 mV. (c) Au(100) imaged with atomic resolution, 100 mV, 40 nA (image (c) copyright by S. Selvanathan).

In the study of molecular adsorbates, the influence of the supporting surface has to be taken into account. Thus, the corrugation lines separating the fcc from the hcp regions constitute a small diffusion barrier [27]. Furthermore, the different stacking gives rise to a periodic potential modulation as was found in the study of the local properties of the surface state electrons [51]. This is furthermore reflected in a preferential adsorption of molecules on the fcc regions of the reconstruction [52], which could be considered as a form of templating. Moreover, the transition regions between the rotational domains (called "elbows") are oftentimes decorated with gold adatoms, which are therefore also preferred adsorption sites (especially at low coverage, most of the molecules are found at these sites). Despite the latter, the directing influence of the Au(111) surface is rather weak.

For an enhanced templating effect the Au(100) surface was chosen, because it features a stronger corrugation [53]. Despite the quadratic geometry of the underlying substrate atoms the topmost

layer of atoms forms a quasi-hexagonal structure as depicted in Fig. 1.12. The sketch in (a) shows an approximate structure, as in the real sample the topmost layer is incommensurate with the underlying lattice [54]. (Therefore, the  $5 \times 1$  unit cell indicated by the box is an approximated construct). As in the herringbone reconstruction, the atoms occupy different adsorption sites. The atoms that sit in on-top sites protrude the most from the surface (colored dark grey) and therefore give rise to corrugation lines in the  $[011]$  direction. These lines form extended domains (cf. Fig.1.12 (b)) that appear in two orientations perpendicular to each other due to the twofold symmetry of the bulk lattice. The distance between parallel lines is  $14.4 \text{ \AA}$  which lies in the range of the size of the employed molecules, which seems promising with regard to guiding the intermolecular interactions. Importantly, while the properties of Au(111) and Au(100) should be similar due to the identical chemical composition and similar lattice structure, the corrugation of the (100) face is larger at  $0.4 \text{ \AA}$ .

## 1.6 Molecules

The molecules that are employed in this work were synthesized in the group of S. Hecht at the Humboldt-Universität zu Berlin. A number of different varieties are used that however all derive from three molecular cores, porphyrin, fluorene and dithienylethene. The first two shall be introduced in this section as they have been investigated previously [55,56]. The dithienylethene has not been studied before and will therefore be discussed in detail in ch. 4.

### Porphyrin

Porphyrin is a heterocyclic compound, containing four pyrrole groups in a square and planar arrangement with their nitrogen atoms pointing inwards. The pyrroles are connected via methine bridges into a macrocycle that constitutes a highly conjugated system. Flat molecules with an extended  $\pi$  system such as porphyrin are favorable for the utilization at surfaces, because they tend to adsorb parallel to the surface [57]. Consequently, the functional groups positioned at their periphery will be pointing in-plane, which is optimal for intermolecular interaction. Porphyrins play a key role in many biological systems, most prominently in photosynthesis and the oxygen transport in red blood cells [58]. These functions are facilitated by forming a coordination complex with a metal ion that is located in the center of the macrocycle and that binds to the lone pair electrons of the four nitrogen atoms. Alternatively, instead of a metal atom, the center can also be occupied by two hydrogen atoms, in which case the porphyrin is termed "free-base". The latter type is employed exclusively in this work. The molecules are furthermore substituted with phenyl rings in their *meso*-position, i.e. at the bridging carbon atoms. These side groups are supposed to act as legs, to reduce the interaction of the molecular core with the surface and ensure sufficient mobility, which is crucial for the coupling in the on-surface-synthesis approach that is described in ch. 3. Thus, the basic building block is 5,10,15,20-tetraphenyl-porphyrin (TPP) as shown in Fig. 1.13. If the phenyl side groups are furthermore intended as binding sites, then they are to that end equipped with halogen atoms in the para position.

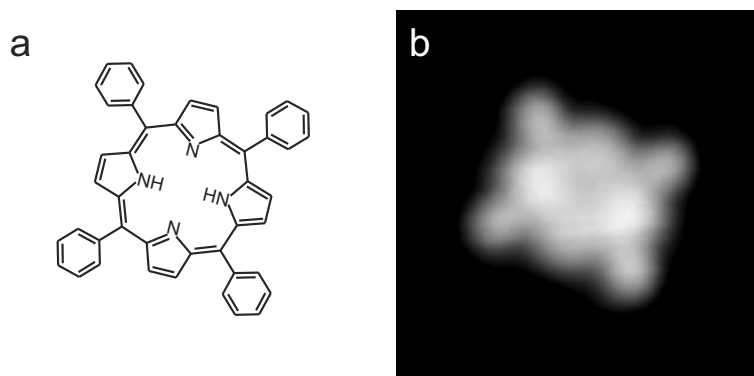


**Figure 1.13:** (a) Sketch of the chemical structure of tetraphenyl-porphyrin (TPP). (b) STM image of TPP on Au(100), image size  $3 \times 3 \text{ nm}^2$ , recorded at 500 mV, 0.1 nA. The four central lobes correspond to the pyrrole groups, the four outer ones to the phenyls. The molecule displays the saddle conformation (cf. main text).

The typical appearance of TPP is shown in Fig. 1.13 (b). The monomer therein displays a rhombic shape at the center with four protrusions at the corners that originate from the pyrrole groups. The appearance of the porphyrins is in accordance with previous studies and reflects the ring structure of the macrocycle [59]. Additionally, there appear four lobes protruding from the edges of the central frame, that are identified with the phenyl rings. The sketch in Fig. 1.13 (a) is rotated to appear in the same orientation (though not drawn to scale) as the monomer in the STM image. However, from the comparison of the two it is apparent that the conformation of the adsorbed TPP monomer does not conform with the square shape displayed in (a). It is known from previous studies that porphyrins adapt two different conformations termed "planar" and "saddle", in solution [60], but also adsorbed to a surface [61,62]. While in the former the macrocycle is nearly flat and its shape appears quadratic, in the latter the central frame buckles, with two opposite pyrrole groups pointing upwards and the other two downwards. It furthermore leads to a stretched appearance which also affects the angle at which the side groups extend from the central board. The shape of the monomer in (b) is clearly rhombic and the pyrroles to the left and right appear brighter than the top and bottom ones. Thus, its appearance agrees with the saddle conformation. In either conformation, the phenyl rings are inclined to form a dihedral angle with the macrocycle for sterical reasons.

## Fluorene

The realization of a molecular wire asks for a linear structure which efficiently facilitates charge transport. Extended  $\pi$ -conjugation and a small HOMO-LUMO gap are advantageous. Fluorene is a polycyclic aromatic compound that exhibits fluorescence (hence the name) and has been employed in light emitting diodes [63]. It is structurally similar to biphenyl. While in the latter, the phenyl rings are free to rotate with respect to each other, in fluorene planarity is enforced by a methylene bridge, which inhibits the rotation around the sigma bond connecting the two phenyl rings. Therefore, because the degree of pi-conjugation decreases with increasing dihedral angle, the bridging carbon ensures maximal  $\pi$  overlap between the phenyl groups, which enhances molecular conductance [64].

The molecules employed in this work, 7,7''-dibromo-9,9,9',9',9'',9''-hexamethyl [2,2':7',2'']terfluorene (DBTF), contain three of these fluorene units, as shown in Fig. 1.14 (a). The terminal phenyl rings are substituted with bromine atoms in the para position. These atoms are included to induce the connection to form chains by our method of on-surface-synthesis (cf. ch. 3). Each of the connecting carbon atoms are furthermore substituted with two methyl groups with the intention to reduce the adsorption strength to the surface and enhance diffusion, analogously to the side groups in the porphyrins. The monomers are usually evaporated from a quartz glass crucible at 270 °C onto the gold surface held at around room temperature. In STM images the monomers appear as three aligned larger protrusions with one additional smaller protrusion at each end, cf. Fig. 1.14 (b). The appearance agrees well with the calculated image in (c), which reveals that the three central lobes are caused by the dimethyl groups, whereas the smaller lobes can be identified with the bromine atoms. While in the gas phase the fluorene groups are free to rotate around the  $\sigma$ -bonds connecting them to trimers, the adsorption with their molecular

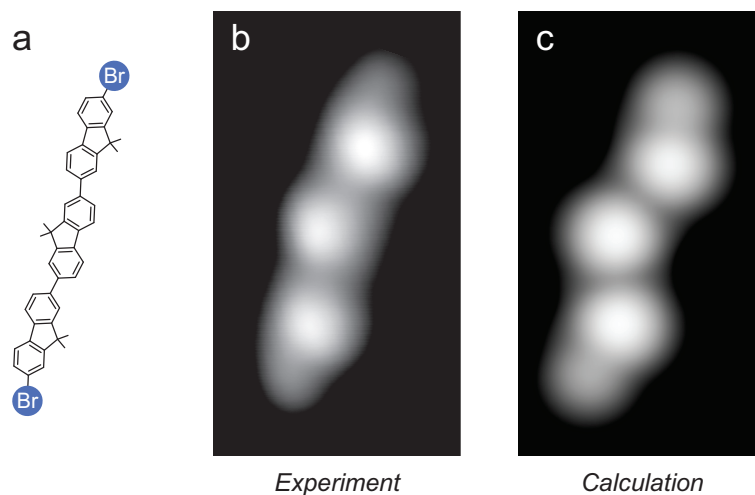


**Figure 1.14:** (a) Chemical structure of dibromoterfluorene (DBTF), (b) STM image of a DBTF monomer on Au(111) recorded at 500 mV, 0.1 nA. (c) calculated image using ESQC [65]. The image size for both (b) and (c) is  $2.5 \times 4.5 \text{ nm}^2$ . Adapted from [56].

board flat on the surface has them pointing either left or right with respect to the molecule's long axis. We observed a preferred 'zigzag' geometry ( $> 99\%$  of monomers) with the two outer groups pointing in one direction and the middle one in the other, as sketched in Fig. 1.14 (a). In addition to DBTF monomers, a variation of this molecule is employed that carries iodine instead of bromine and that is consequently called DITF.

## 2 Molecular wires connecting metallic and insulating surface areas

The introduction serves to give an overview of the development of nanoscale junctions based on studies from literature employing a variety of experimental techniques. It highlights the STM-based pulling technique that is employed in this work and concludes with the description of the outline of a novel configuration that features a single molecule in a horizontal rather than a vertical geometry. The realization and characterization of this setup is the subject of the experimental sections of this chapter. The oligo-terfluorene molecules that are employed to that end are made from DBTF monomers. The aim of the last section is to shed light on the polymerization process in which they are coupled into chains.

### 2.1 Introduction

Conductance measurements of microscopic junctions have been performed for several decades as a spectroscopic method [66] and for the study of transport phenomena, e.g. the tunneling through thin metal-oxide layers [7]. Junctions of exceedingly small size (nanometers) are of comparable length scale as the typical Fermi wavelength of metal electrons, therefore their behavior generally differs from the macroscopic one and requires a quantum mechanical description. Thus, such experiments offer the exciting opportunity to study quantum-mechanical effects. One peculiar example is the conductance quantization that is observed in atomic wires [67]. The progressive elongation and associated reduction in diameter, that is sketched in Fig. 2.1 (a), leads to a decreasing number of transverse modes in the wire (quantum point contact). Each such mode constitutes a conduction channel that contributes a conductance quantum  $G_0 = (2 \times e^2/h)$  to the electrical transport. Thus, the closing of a channel is reflected in a steplike decrease in the overall conductance of the junction. The conductance furthermore depends on the transmission  $T(E)$  which is the probability that an electron will propagate through a particular channel. If parallel channels add analogously to Ohmic conductors the total conductance of a wire is given by the sum of the transmissions of each channel. This is expressed by the Landauer formula [68]:  $G(E) = \sum_{ij} T_{ij}(E)$ . Utilizing molecules offers a promising way to introduce more specific behavior and functionality such as rectification or switching, because molecules have the advantage that their properties can be adjusted by synthetic design. One exciting prospect lies in the realization of molecular circuits. This requires the proper connection of molecules in networks, an issue which is treated in detail in ch. 3. Furthermore, a sensible assembly of the building blocks requires the detailed knowledge of their features. For molecular wires and functional units based on electrical transport (the prototypical example being the rectifier envisioned by Aviram and Ratner [69]), the most important property is their electrical conductance. This is why its study has been intensely pursued, both experimentally and theoretically. The measurement of electrical transport can furthermore be used for sensing application. Nanojunctions and -wires are of a similar length scale as chemical species that one wishes to detect. This potentially renders them extremely sensitive to the interaction with guest particles, down to the detection

of a small number of entities. The properties of the system can be monitored by recording its conductance. Molecular wires potentially offer the identification of chemical species through molecular recognition, i.e. the provision of groups that facilitate molecule-specific binding. For instance, by measuring  $I(V)$  curves on single-molecule junctions Tao et al. [70] could distinguish the complexation of different metal atoms by peptides. But also nanowires can be equipped with receptor groups that guest molecules can dock onto [71]. Changes in the conductance can be caused by the introduction of additional electronic states, changes in the charge distribution and conformational changes in the molecular wire.

Early studies performed conductance measurements of ensembles of molecules that included thin films produced through Langmuir-Blodgett or self-assembly methods sandwiched between electrodes. Using alkane chains in such a setup, Mann and Kuhn were able to confirm the exponential dependence of tunneling current on layer thickness [72]. Later studies have been performed by contacting upright-standing molecules in self-assembled monolayers (SAM) with the tip of a conducting atomic force microscope [73]. Samori et al. used this approach to measure the conductance of thiolated azobenzenes [74]. More spectacularly, the same group reported the photoisomerization of ensembles of the same molecule contacted by a Hg-droplet, wherein the molecular layer has to lift the droplet to return to the initial trans conformation [75]. In some studies the contact to the molecules has been enhanced using metal nanoparticles on top of the SAM [76]. Other experimental techniques include spectroscopy of donor-bridge-acceptor molecules [77] in solution and contact formation employing crossed wires or metallic beads [78]. A prominent class of molecules in transport measurements is that of DNA. For instance, Fink et al. used a metal tip to break and subsequently contact a single molecular chain spanning a hole microfabricated into a thin foil [79].

However, methods employing a large number of molecules can render the interpretation of the experimental findings difficult. Issues might include uncertainties of the transport pathway and experimental difficulties such as the formation of metallic bridges between the electrodes and inhomogeneous layer thickness. Furthermore, the characterization of single molecule functionality requires the investigation of single molecule junctions as the properties of interest can be veiled in setups containing many molecules in parallel, that might also give rise to collective effects.

Experimental techniques have been developed that constitute an intermediate between approaches investigating entire layers and ones that probe single molecules, most notably the mechanical break-junction (MBJ) technique [64, 80, 81]. This method allows the automated recording of large amounts of conductance data by repeatedly forming and breaking a metallic point contact sketched in Fig. 2.1 (a), usually in solution. Upon breaking of the metal contact, suitably substituted molecules can bridge the gap, allowing a conductance measurement of the newly formed junction, as sketched in Fig. 2.1 (b). However, the number of molecules and their arrangement are usually unknown and have to be inferred by statistical evaluation. In another notable example, Nuckolls et al. fabricated a device for the measurement of charge transport through molecules from carbon nanotubes [82]. To that end, a small gap was etched into the tube. Functionalized molecules were applied onto the sample from solution with the intention that they form covalent connections on both sides, thus bridging the gap. The whole structure was adsorbed on an insulating silica ( $\text{SiO}_2$ ) layer and its ends contacted with gold electrodes. Due to the horizontal

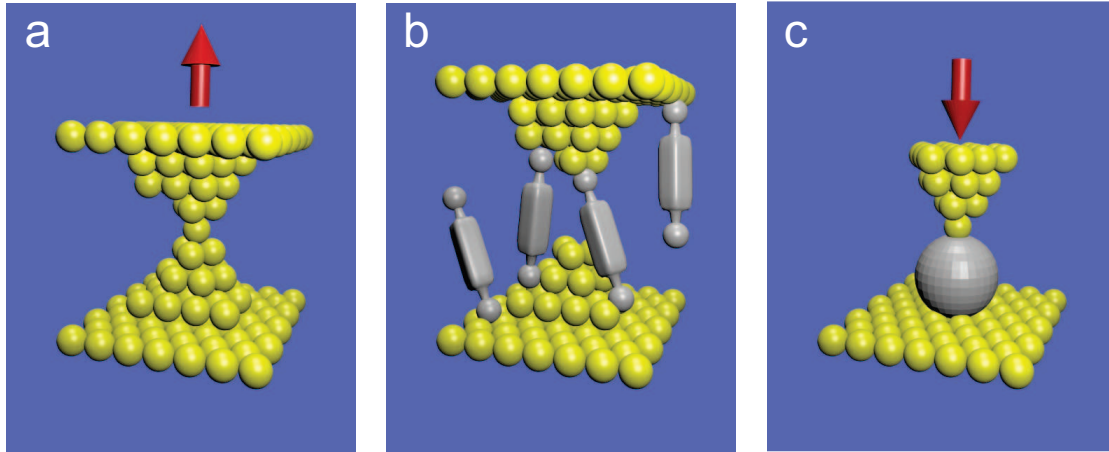


**Figure 2.1:** (a) Model of an atomic wire formed by bringing two electrodes into contact and subsequent retraction. (b) in the mechanical break junction setup, the eventual rupture of the metallic bridge can lead to a small number of molecules (gray) temporarily spanning the gap. (c) in the STM setup the tip can be brought into contact with a selected molecule without making tip-surface contact.

geometry the setup could be investigated with AFM, however the resolution was not sufficient to image the molecules inside the junction (or even determine a precise gap distance). Therefore, similar to the case of MBJ, information about the number and arrangement of the molecules had to be deduced indirectly. Using this setup the same group successfully investigated the switching properties of diarylethene molecules [83].

With the invention of STM it has been possible to measure the conductance of molecules in a defined configuration, allowing to address individual molecules in a controlled way. Joachim et al. reported the first successful formation of a metal-single molecule-metal contact using STM [84]. In this experiment the tip was extended towards individual  $C_{60}$  molecules adsorbed on a Au(110) surface until it formed mechanical contact (sketched in Fig. 2.1 (c)). For this configuration the corresponding electrical conductance was found to be of the order of  $10^{-4}G_0$ .

Dealing with single or a small number of molecules it becomes clear that the reproducible measurement of the electrical transport properties of individual molecules poses a challenge. In many cases the conductance recorded for one type of molecule differed by orders of magnitude. A central issue is the contacts between the molecule and the electrodes which in most cases are not known at the atomic scale and that can give rise to considerable changes in contact conductance. This can even lead to a conductance for one and the same junction that is variable over time. For instance, such behavior has been observed for thiolated molecules arranged in SAMs that can display stochastic switching due to a variable contact configuration [85]. However, a variation in conductance can also appear due to the intrinsic properties of the molecules. These include changes in conformation and electronic structure. While these kind of junctions can reveal interesting information about e.g. contact geometry, excitation thresholds or switching rates [86], random and uncontrollable changes in the conductive properties of functional units is unfavorable for inclusion into a single-molecule device. On the other hand, externally manageable variability opens the exciting possibility of tuning the charge transport by applying stimuli. Examples include the electromechanical modulation of the tunneling current. Tao et al. found that the force

exerted on a benzenedithiol between two gold electrodes can influence the electronic coupling and the relative position of molecular orbitals with respect to the Fermi energy of the leads [87], a parameter to which the conductance is sensitive. A similar observation was made previously by Joachim et al. [84] for conductance measurements while applying a small force to individual  $C_{60}$  molecules. Loertscher et al. observed the reversible switching of the conductance of phenylene-ethynylene derivative using a MBJ setup [81]. While an application as a molecular memory has been suggested for the latter, the thermal stability is probably not sufficient. A better chance is offered by switches, e.g. photochromic molecules in which an isomerization reaction leads to a change in the HOMO-LUMO gap. The change in electronic structure leads to a variation in charge transport through the junction. This will be discussed in ch. 4.

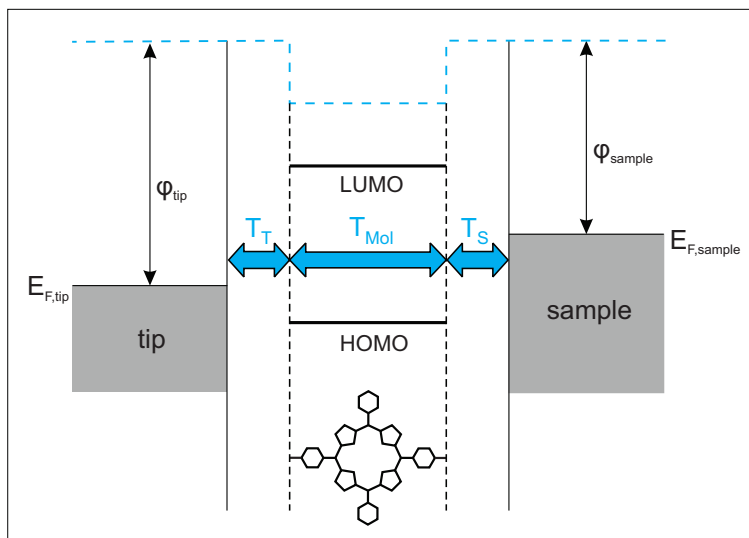


**Figure 2.2:** The tunneling current is determined by the transmission coefficients associated with the molecule  $T_{MOL}$  and the contacts to the tip and sample  $T_T$  and  $T_S$ .

Describing and predicting the behavior of molecular junctions is a complicated matter (also due to the size that can quickly become too large for computational modelling) and it is the object of intense theoretical study. A molecule placed between two electrodes constitutes an electronic tunneling pathway with a barrier that is generally lower than that of vacuum. The junction consists of three components: the metal leads, the molecule and the two contacts in between, as shown in Fig. 2.2. The metal surface is characterized by its work function  $\phi$  which is the energetic barrier for the electrons to escape from the bulk. In general, barriers can be overcome by supplying enough energy (over the barrier) or by tunneling, giving rise to two different transport mechanisms. The contacts can be characterized by their own transmission factors,  $T_T$  and  $T_S$ , which determine the contact conductance. The larger the distance the bigger is the corresponding barrier. Therefore, chemisorbed molecules usually exhibit higher contact conductance than physisorbed ones. The molecule in the junction modifies the tunneling barrier by the change of electrostatic potential. In the case of off-resonant tunneling the applied bias voltage is smaller than the distance of HOMO or LUMO from the Fermi energy. In this case tunneling is facilitated by the Lorentzian tail of the molecular states that are broadened due to the adsorption to the electrodes. This is called a tunnel channel [88]. (Since the molecular

orbitals possess a defined shape on the nanometer scale (and below) the tunneling pathways are spatially localized as well, which is the foundation of the resolution of the STM. [38]) Another important factor is the conjugation length which can change with the conformation of molecular subunits. Notably, this has been observed by Venkataraman et al. in a MBJ setup comparing different biphenyl derivatives linked to gold electrodes via amine groups [64]. The biphenyls were substituted to fix the dihedral angle  $\theta$  of the phenyl rings from planar (fluorene) to almost perpendicular (using methyl groups in the ortho positions). The conductance is found to decrease with decreasing  $\pi$ -conjugation as  $\theta$  increases in accordance with theoretical predictions.

A fundamental characteristic of an electrical conductor is the behavior of the conductance  $G$  as a function of its length  $L$ . While in Ohmic conductors the resistance  $R = G^{-1}$  grows proportional with  $L$ , it is constant for ballistic transport. The characteristic behavior of tunneling transport is an exponentially decreasing  $G$  with increasing  $L$ :

$$G(L) = G_c \times e^{-\beta \times L} \quad (14)$$

Therein,  $G_c$  is the contact conductance which is determined by extrapolation to  $L = 0$  and  $\beta$  is the inverse decay length.  $G_c$  depends on the electrode-molecule contacts. To measure this dependence with fixed contacts, e.g. employing dithiols in a MBJ setup, the usual approach is to synthesize a batch of molecules with an increasing number of units and then record the respective properties individually one after the other. For instance, such studies have been performed (type and number of units in parentheses) for porphyrins [89] (Zn-porphyrin derivative: 1-3), alkanes [90] (C-atoms: 6, 8, 10), peptides [91] (glycine sandwiched between cystein/cysteamine: 0-2), oligophenyleneimine [73] (phenyleneimine: 1 to 10) and carotenoid polyenes [92] (propenyl: 5, 7, 9, 11). Each species adds a data point from which one can deduce the function  $G(L)$ . This curve however is a compilation of the conductance values of different molecules with potentially different contacts, not a measurement along one and the same wire. Furthermore, most studies investigated only rather short molecules, because long and flexible chains would allow multiple connections and thus introduce a large amount of ambiguity into the current traces. Further complication stems from the need to substitute the chains to make them sufficiently soluble. Long side groups however lead to interactions and possibly additional and unwanted transport channels. Additional ambiguity is caused by the appearance of multiple peaks in conductance histograms gained from statistical evaluations of MBJ data. Thus, a new method that overcomes these limitations was devised for the continuous measurement of conductance along a molecular wire. It is employed for the investigation of the diarylethene switches in ch. 4 and furthermore serves for the formation of the structures discussed in this chapter. Therefore, it will be described in the following.

### 2.1.1 Pulling of molecular wires

Using the manipulation capabilities of the STM the end of a single molecular chain was contacted with the tip and gradually pulled off the Au(111) support with the intention that its other end

remains attached to the surface [56]. This would therefore result in a metal-molecule-metal junction. A similar scheme has been employed by Temirov et al. using PTCDA molecules [93]. However, this particular experiment did not allow an investigation of the length dependence. For the aspired kind of experiment the STM setup is uniquely suited. For one, the tip can be targeted at individual molecules with submolecular resolution, both laterally and vertically, which eliminates the requirement of the MBJ technique of repeatedly forming and breaking a gold bridge to trap molecules in between. Rather, the tip can be brought into close proximity with the site of the molecule intended for attachment without crashing it into the surface. Thus, both tip and surface routinely stay intact during the procedure which allows the imaging of the area both before and after the manipulation attempt. The images convey important information about the experiment, confirming the intactness of the molecule in question and the absence of defects in its vicinity. Furthermore, conformational changes resulting from the manipulation can be observed. The configuration with the molecule spanning the gap between the two electrodes constitutes a two-terminal conductance measurement setup.

Oligo-fluorene chains that are also in the focus of the present chapter have favorable properties for such an experiment: their molecular board consists of a conjugated carbon backbone to facilitate electrical conductance; the molecules are furthermore weakly adsorbed to the Au(111) surface and flexible. It is conceivable that situated at the ends of the chains there are radicals that can perform bonding to the tip. The chains are made from dibromoterfluorene monomers, cf. ch. 1.6, with the method of on-surface synthesis [55] that is discussed in ch. 3.1. Chain lengths of 100 nm are observed and the defect frequency is low. However the heating step also introduces anomalous connections that appear as kinks and junctions. This will be addressed in ch. 2.4.

For the conductance measurement, vertical manipulation was performed on the molecules. The desired configuration is sketched in Fig. 2.3 (a). To that end, the STM tip is positioned above the targeted site and the feedback loop is turned off. During the time interval of the manipulation the bias voltage and vertical displacement follow a chosen route. The resulting tunneling current reflects the developing state of the junction. To form a contact the tip is approached towards the surface and subsequently retracted to elongate the junction distance.

An excerpt of the current signal vs. the tip-surface distance for such a successful manipulation attempts is shown in Fig. 2.3 (b), which displays two branches labeled "approach" and "retraction". The experiment starts with the approach section and follows the typical exponential increase reflecting the tunneling barrier of vacuum. Zero height denotes tip-surface contact. Around 2 Å above the surface the current reaches saturation of the preamplifier at 100 nA (flat part). However, upon retraction the current signal follows a path with a slope that is different, i.e. less steep, than the one of the approach. This indicates that the molecule is located inside the junction lowering the tunneling barrier. Thus, a metal-single molecule-metal junction is successfully formed. The bond to the tip is sufficiently stable to lift the chain from the surface. Similar to the case of PTCDA [93] a pronounced dependence of the probability for bond formation on the site inside the chain that the tip is aimed at was observed. In agreement with the proposed presence of a radical produced by the dissociation of bromine [94], the highest likelihood for a successful attempt is at the apex of the chain.

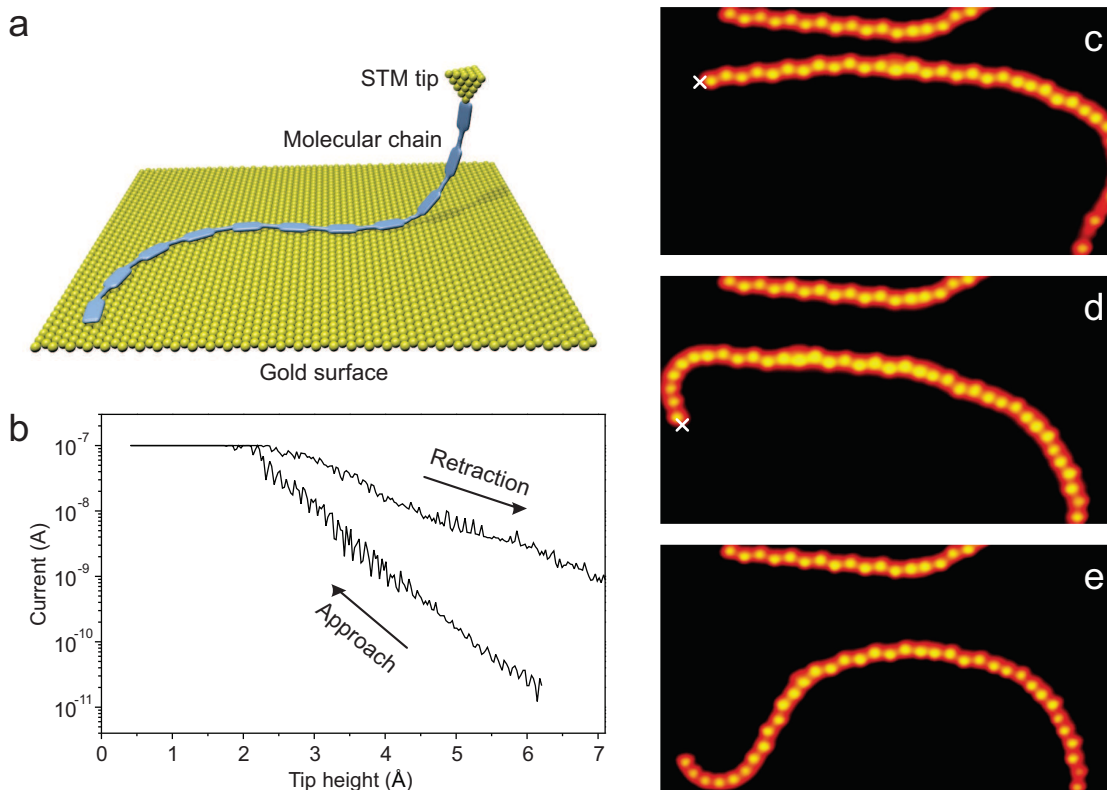


**Figure 2.3:** Contacting and pulling a single polyfluorene chain with the STM tip [56]. (a) Sketch of the proposed junction configuration. (b) tunneling current recorded during a pulling experiment, the initial approach branch can be clearly distinguished from the subsequent retraction branch. In between the current is constant due to the limited range of the preamp (in this case 100 nA). (c) - (e) series of STM images of the same area taken before and after vertical manipulation attempts at the positions indicated by the crosses. Image size  $13.7 \times 25.4 \text{ nm}^2$ .

In most cases the connection is broken before the chain leaves the surface. This is shown in Fig. 2.3 (c)-(e) which displays three consecutive images taken before and after lifting attempts. The tip is aimed at the position indicated with the cross. It can be seen that the chain changes its conformation upon manipulation, being pulled into the direction of the manipulation site and adopting a new curvature. These are remarkable changes considering the STM tip is only vertically approached to the surface and subsequently retracted. With the above interpretation however it is easily explained by the partial detachment of the molecule from the gold substrate. The lifting of chain segments several nanometers in length and their subsequent reattachment in a modified location offers a new manipulation modality with the prospect to surmount vertical obstacles such as step edges. This technique is employed in ch. 2.2. Note that the surrounding molecules (like the one to the top of the manipulated chain) stay fixed in space during the experiment and therefore serve as control objects, ruling out different modes of interaction.

In this way the junction conductance can be continuously measured up to separations of several nanometers. Small bias voltages on the order of 100 mV are applied to measure the transport properties of the molecule in the HOMO-LUMO gap. The curve follows roughly an exponential decay which is characteristic of tunneling, cf. eq. 14. As mentioned above, the contact conduc-

tance is found to scatter considerably. Values were obtained in the range of 10 to 500 nS (roughly  $1.3 \times 10^{-4}$  to  $6.5 \times 10^{-3} G_0$ ). The value of  $\beta$  on the other hand is characteristic of the molecular chain and is found to vary only little in different experiments employing different chains. A value of  $\beta = (0.38 \pm 0.09) \text{ \AA}^{-1}$  was obtained and corroborated by theoretical calculations of the same molecule yielding  $0.36 \text{ \AA}^{-1}$ . The calculations were performed by F. Ample and C. Joachim of Toulouse using the elastic scattering quantum chemistry (ESQC) approach [65]. For comparison, the inverse decay length that is initially observed during the approach tunneling through vacuum is  $\beta_{\text{vac}} = 2.4 \text{ \AA}^{-1}$ , i.e. considerably higher. A value of ( $\beta \approx 0.5 \text{ \AA}^{-1}$ ) appears to be characteristic of molecular chains for bias voltages in the gap, and has been observed for alkanes ( $\beta \approx 1.1 \text{ \AA}^{-1}$  [90]), peptides ( $\beta \approx 0.9 \text{ \AA}^{-1}$  [91]), carotenoids ( $\beta \approx 0.22 \text{ \AA}^{-1}$  [95]) and phenyleneimine ( $\beta \approx 0.3 \text{ \AA}^{-1}$  [73]). Notably, in the last study Frisbie et al. observed the transition from a tunneling to a hopping mechanism (although the exact number of molecules in the junction was unknown and estimated to be around 100). Furthermore, the continuous pulling method has been employed by Koch et al. for graphene nanoribbons which exhibited a  $\beta$  of around  $0.45 \text{ \AA}^{-1}$  [96].

For values of  $\beta$  of this magnitude, the conductance is decreasing rapidly, spanning several orders of magnitude over distances of a few nanometers. Therefore, such an experiment quickly exceeds the dynamic range of the preamplifier. Attempting to record the current at higher tip-sample separations could be facilitated by an increased contact conductance. This however would require a change in the chemical composition of the wire (e.g. using special anchoring groups [97]). Alternatively, it is expected that a smaller  $\beta$  is obtained by accessing the molecular resonances. The observed behavior is indeed a reduction in the attenuation factor with increased bias voltage and therefore a weakened dependence of the conductance on length. In this way the conductance through a single molecule could be continuously measured up to a length of 20 nm [56].

### 2.1.2 Decoupling molecules from the surface

In the previous section it has been outlined how the electrical transport through a molecular chain could be measured as a function of its length. Furthermore, geometrical information could be deduced from the conductance curves. However, this included using indirect evidence and the comparison with calculation. A more elegant setup might be imagined in a horizontal geometry which would allow the conductance measurement along a molecular chain in a stable configuration. Furthermore, potential integration into a device would include contact of the molecular wire with a suitable support that would need to be electrically insulating to separate different components from each other to avoid crosstalk. This however constitutes a challenge for the application of STM or conductive AFM, because the technique necessitates a conductive sample surface.

One approach to overcome this problem is to contact a single molecule adsorbed on an insulator with two (or more) tips [98]. Another way is to partially decouple the molecule using side groups or insulating layers. One notable example for the former is the 'Lander' molecule series [99] that was designed with the intention of lifting a central aromatic molecular board off the surface

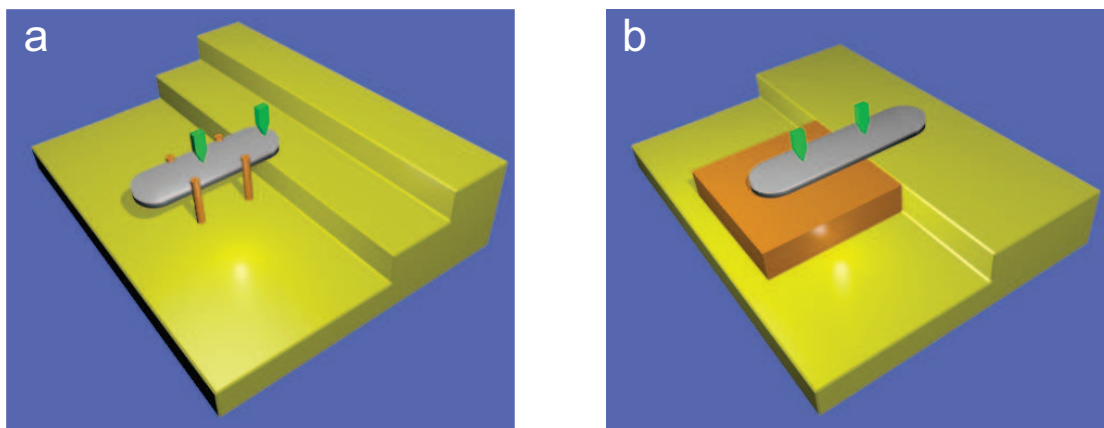


**Figure 2.4:** Horizontal conductance measurement setups, (a) the molecular board (gray) is decoupled from the metal substrate by spacer groups (orange), (b) the molecule is partially adsorbed to an insulating layer (orange). Green arrows denote the measurement points, the right of which is in both cases given by the attachment to a step edge. The tip constitutes the left one and is therefore spatially variable.

that it is deposited onto by spacer legs, as sketched in Fig. 2.4 (a). The central part potentially constitutes a molecular wire and is located at a height that is compatible with the contacting to a metallic pad or a step edge. The manipulation of the molecules and their interaction with the surface has been investigated by Moresco et al. [100] and Grill et al. [101]. These studies demonstrate a remarkable example for molecular wire lifted off a metallic support. While partial electronic decoupling from the surface was observed for the central board conductance measurement could not be performed on this system which was due to the legs attached to it that appear rather prominently in STM.

The other approach, introducing an insulating layer for the partial decoupling of the molecule offers a conceptionally more elegant approach, because it avoids the attachment of side groups to a particular molecule connected with changes in the electronic properties. Thus, it would allow the measurement of the unaltered properties of the wire. However, to perform conductance measurements the end of the molecule needs to remain in contact with the metallic surface which acts as the second electrode. Such a setup that is depicted in Fig. 2.4 (b) which includes part of the molecule adsorbed to a metal and the rest to an insulating island shown in orange had not been previously realized due to experimental challenges. These include the formation of long molecular wires and the preparation of insulating islands, followed by the partial transfer of the former on top of the latter. Especially the last step constitutes a serious difficulty because of the low diffusion barriers observed on insulating materials [102].

In the next section results on the successful formation of such a structure with parts of a molecule adsorbed to an insulating layer and the rest to the metal surface will be discussed.

## 2.2 Preparation of wires both adsorbed to NaCl and gold

Extended molecular wires of 100 nm and longer were successfully produced on Au(111) through the on-surface-synthesis process described in ch. 3.1. The polyfluorene chains constitute a suitable test case for measurement in the outlined arrangement - single molecules adsorbed partly to the insulator and partly to the metallic surface. It has been shown that thin films of insulators made of metal oxides and alkali halides can be produced on top of metal surfaces featuring only a single or a few atomic layers [103]. Due to their small thickness these layers can sustain tunneling and have been used in metal - metal-oxide - metal junctions for decades [66]. Controlling the number of layers of these islands promises the precise tuning of the interaction strength between molecules adsorbed on top with the metallic surface underneath as well as the barrier width and associated conductance that is introduced between the molecule and the surface. Sodium chloride has been chosen as insulating material, because it can be sublimed from an evaporator and continued growth of ordered layers can be facilitated by deposition of additional material. The preparation of thin NaCl films has been explored on metal surfaces, such as copper (including Cu(100), Cu(111), Cu(211) and Cu(311) [104–107]), on Al(100) and Al(111) [108], on Ag(100) [109] and Au(111) [110,111]. For the present study, also performed on a Au(111) surface, NaCl was bought commercially (Sigma-Aldrich, 99.999 %), ground to a powder and evaporated from a quartz crucible at around 800 K. NaCl is characterized by a large band gap of 8.5 eV, which it already exhibits for the bilayer [112]. For the preparation of NaCl on Au(111) a gap of approximately 9 eV was found for the bilayer with the valence and conductance band edge located at around 3.5 eV above and 5.5 eV below the Fermi energy. Deposition of NaCl onto Au(111) leads to the formation of (100)-oriented islands of increasing layers [111]. The surface of NaCl is non-polar and does not reconstruct. Multilayer growth starts before the gold surface is completely covered, thus leaving metallic regions that are better suited for tip treatment (cf. ch. 1.3.2) than the insulator islands. NaCl adsorbed on the gold does not lift the herringbone reconstruction and is even observed to cross step edges in what is called carpet-like mode [111,113]. The NaCl layers appear as protrusions in STM. The apparent height depends on the number of layers and measures approximately (for small bias voltages not exceeding 1500 mV; the geometrical height in parentheses) 2 Å (2.82 Å), 3 Å (5.64 Å) and 4 Å (8.46 Å), cf. the barrier model in Fig. 2.10 (a). In STM images of the (100) face with atomic resolution only one type of ion (the chlorine [108]) is imaged, forming a quadratic pattern characterized by the nearest neighbor distance of like ions which for bulk NaCl is 3.99 Å. The NaCl on Au(111) is slightly contracted with respect to the bulk distances and incommensurate with the substrate [111].

Attempting a deposition of the DBTF monomers on the pre-formed NaCl islands does not lead to polymers on top of these islands, because chain formation requires a heating step which is incompatible with a persistent adsorption on top of the insulator. Instead, molecular chains are found exclusively on the metallic parts of the sample, as shown in Fig. 2.5. This is due to the diffusion barrier that is greatly reduced on the islands compared with the areas of clean gold [102]. Because efficient diffusion is necessary for the coupling step, a decreased activation threshold would not circumvent this problem, e.g. by using the iodinated terfluorene (cf. 2.4). Therefore, it was attempted to perform the coupling on the metal parts of the surface and transfer

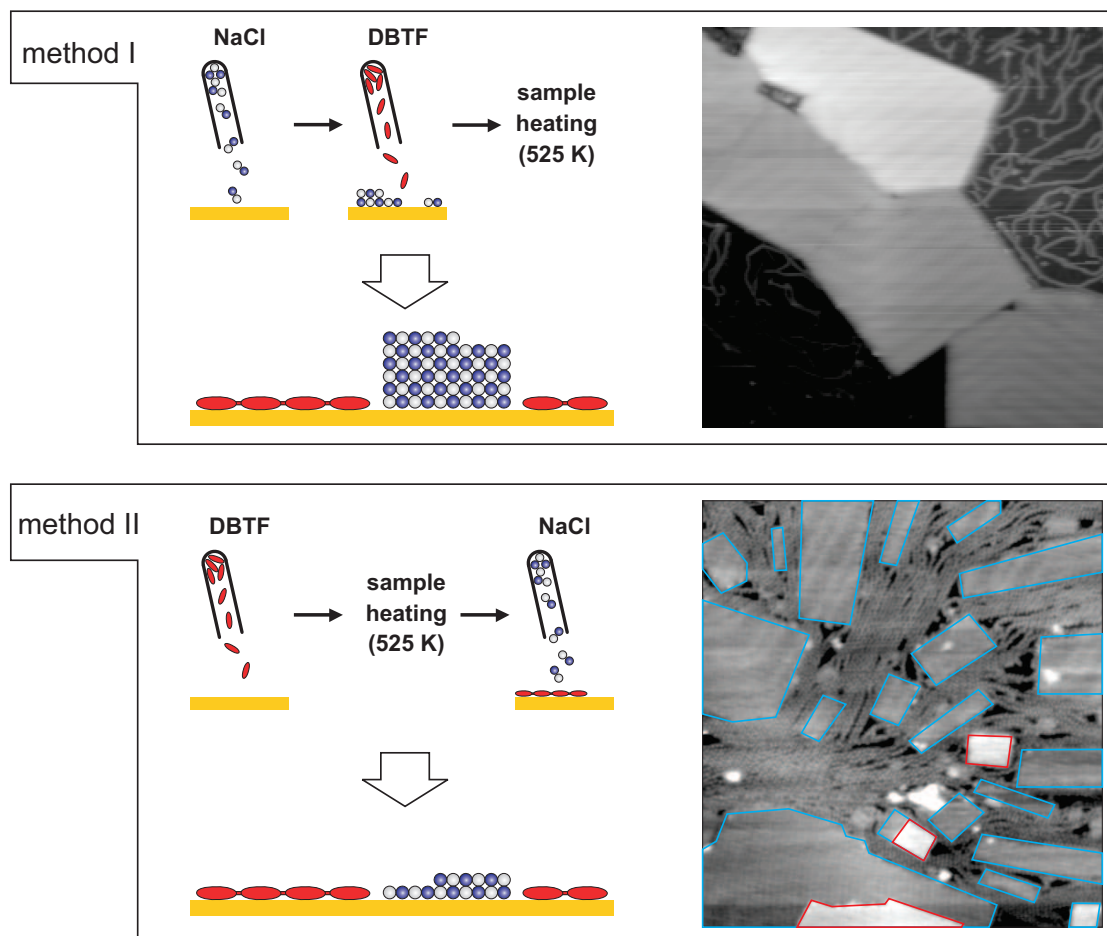


**Figure 2.5:** Polyfluorene wires and crystalline NaCl are prepared subsequently on a Au(111) surface [114]. Method I and II differ in the order of the preparative steps as shown in the sketches. Characteristic STM images are shown to the right (top:  $-1$  V,  $79$  pA,  $160 \times 160$  nm<sup>2</sup>; bottom  $-1$  V,  $10$  pA,  $75 \times 80$  nm<sup>2</sup>). The annealing of the NaCl (method I) leads to islands of increased height, whereas the film thickness can be restricted by deposition onto a slightly cooled sample (method II). In the bottom STM image NaCl monolayers (double layers) are highlighted by a blue (red) border. Most of the remaining space is covered by poly-TF chains.

the chains subsequently to the insulated regions.

Thus, one is confronted with the preparative choice to first grow the molecular chains or the NaCl islands. Fig. 2.5 displays a sketch of the preparative order and the resulting structures observed with STM. In method I the NaCl is deposited first, followed by chain precursors. Polymerization is induced subsequently by heating the sample surface with DBTF in the presence of NaCl. At the employed sample temperature of  $250$  °C, the NaCl is supposed to be mobile. Despite this, efficient chain formation is observed and the NaCl is found in crystalline islands, which is shown in the accompanying STM image. In method II the opposite order is followed, i.e. the chains are prepared first by sublimation of the DBTF and heating of the gold surface. Only after this polymerization step NaCl is deposited and is found to form crystalline islands in the presence of the molecular chains, as shown in the corresponding STM image.

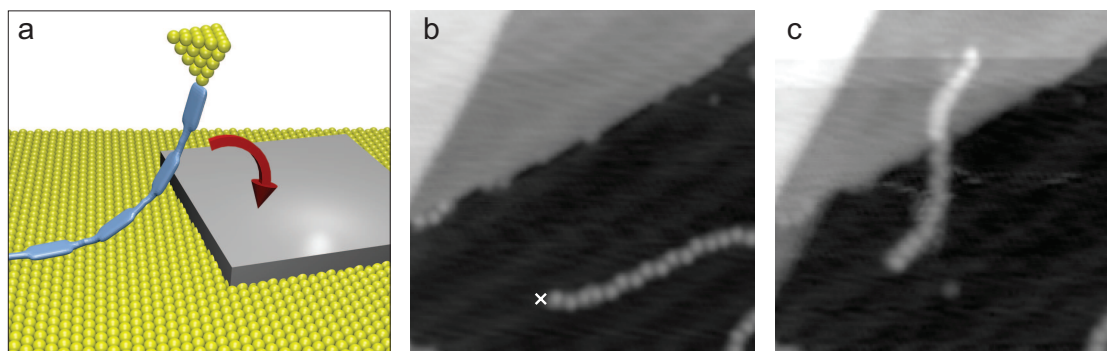


**Figure 2.6:** (a) Sketch of the intended manipulation, the polymer chain (blue) is pulled off the surface by the STM tip and dropped onto the NaCl (gray) when it detaches. STM images of a poly-TF chain before (b) and after (c) a manipulation attempt in which the end of the chain marked with the cross is attached to the tip. In (c) the upper part of the chain is adsorbed on a NaCl monolayer. Feedback parameters 5 pA,  $-1000$  mV, image size  $20 \times 20$  nm<sup>2</sup>.

It is one surprising result that the growth of the NaCl is apparently not negatively affected by the molecules. However, the presence of the chains is reflected by an increased ratio of long to short edge of the islands, something that is not typically observed for NaCl growth on clean gold. Thus, it was found that both methods successfully produce oligo-fluorene wires next to islands of NaCl of defined shape and crystalline order. The latter however differ in height depending on the preparative method. Salt island ripening is observed upon heating of the surface, which leads to an increased number of layers for method I, usually starting with three to five layers. Deposition of the NaCl onto the sample cooled to around  $0$  °C on the other hand limits the vertical growth and leads to islands of mostly one or two layers as shown in the bottom STM image in Fig. 2.5. Note that the wires were exclusively observed on the free metal regions of the surface while they did not appear on top of the salt.

While it is crucial that the chain growth is not inhibited by the NaCl islands and vice versa, the initial challenge remained, i.e. to achieve partial adsorption of a molecule on top of the insulator. The vertical pulling experiments (cf. ch. 2.1.1) suggest a way to that end: lifting the chains from the surface is in more than 90 % of attempts concluded by the detachment of the chain from the STM tip. It was shown above (Fig. 2.3) that the molecule usually covers a different area upon readsorption. This includes changes in lateral position of the whole molecule which is due to the fact that it is pulled laterally over the surface in the direction of the tip. Therefore, if the manipulation attempt is performed in the vicinity of the edge of an insulator island, the chain will be dropped on top with a certain probability, as sketched in Fig. 2.6 (a). Depending on the diffusion barrier of fluorene on NaCl it is therefore conceivable that this might lead to a stable realization of the intended configuration, similar to the one sketched in Fig. 2.4 (b), however without the need for a step edge. It was found that this is actually the case, as is shown in the STM images in Fig. 2.6 (b) and (c). In these images the bottom right corner shows the bare Au(111) surface with the poly-TF chains adsorbed to it, while the top left corner is covered with a NaCl monolayer. Image (b) was recorded before manipulation of the chain end indicated with the cross. As shown before, the interaction of the tip leaves the chain in a completely new

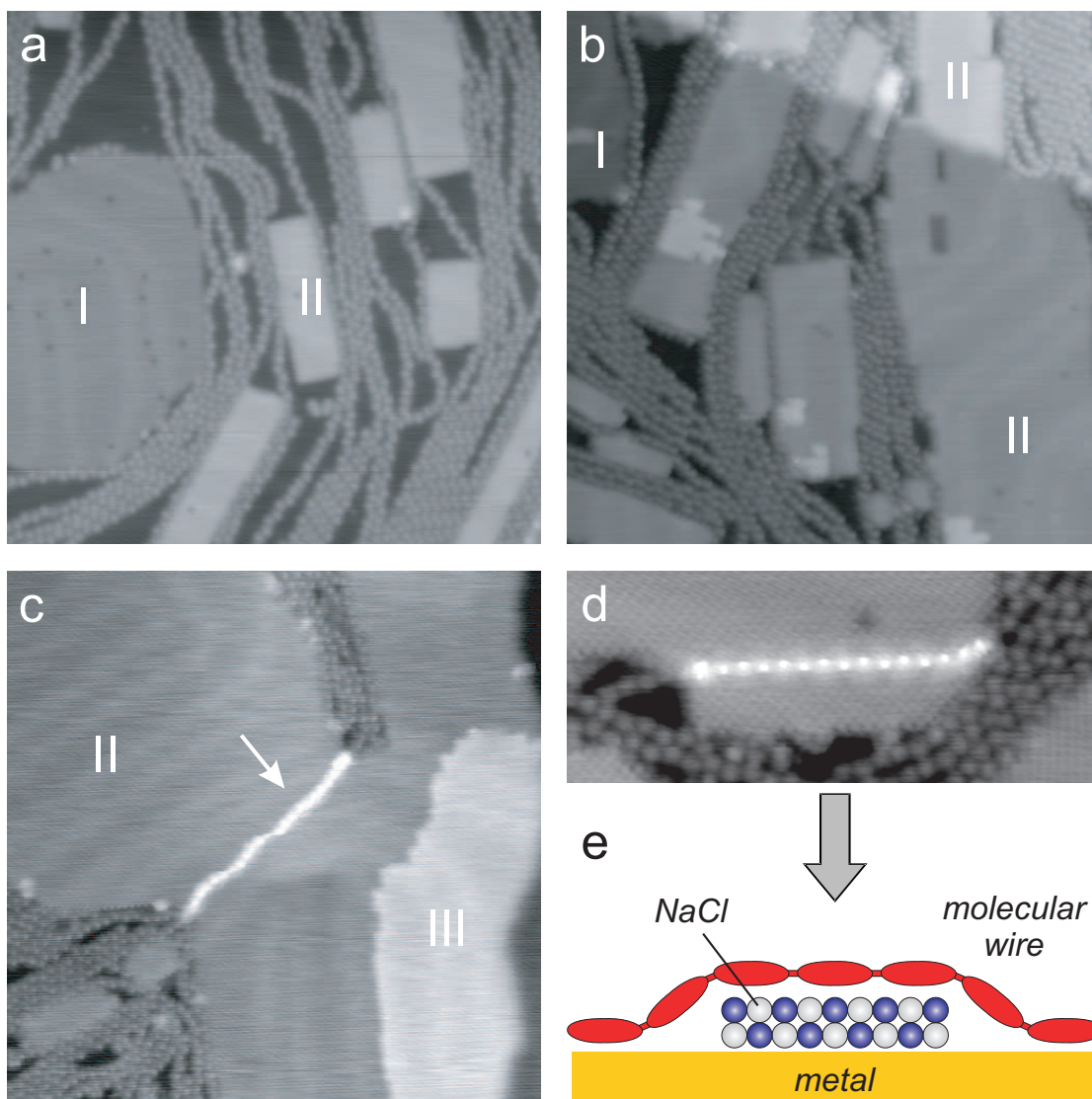


**Figure 2.7:** STM images recording the continued growth of NaCl islands on Au(111) in the presence of poly-TF chains [114]. NaCl coverage is (a) 0.4 ML, (b) 0.8 ML and (c) 1.2 ML (1 ML denotes the surface covered with a single layer of NaCl). Different layer thickness is indicated by roman numerals. Image size (a-c):  $45 \times 45 \text{ nm}^2$ . In (c) a chain is floating atop a insulating double layer, marked by the arrow. (d) STM image of a equivalent configuration in which the NaCl is atomically resolved. Image size  $9 \times 22.3 \text{ nm}^2$ . The structure is sketched in (e). Feedback parameters for all STM images  $-1000 \text{ mV}$ ,  $10 \text{ pA}$ .

position depicted in image (c) which shows the same region recorded after the manipulation. As is clearly visible a substantial part, i.e. more than one third, of the chain is adsorbed on top of the island, while the rest (the lower part) stays attached to the metal surface. Please note that the slightly fuzzy resolution in (c) is due to changes in the state of the tip, not because of damage caused to the sample. (Changes of this kind happen frequently upon manipulation and the resolution is usually restored by gentle tip treatment before resumption of the measurements, cf. ch. 1.3.2)

Before the discussion of the physical properties of the molecular chain it is worthwhile to take a look at an alternative method to produce the above configuration. It was observed that the lateral size of the NaCl islands can be increased by continued deposition. This is shown in Fig. 2.7. The insulator regions grow mainly laterally at the expense of the regions covered by the poly-TF chains. Due to their flexibility and weak adsorption to the surface these are laterally displaced up to a point when there remains not enough uncovered gold. At this stage the chains are forced to move vertically, i.e. on top of other chains or on top of salt islands. This leads to a particular geometry in which the chain is adsorbed on the gold on both ends, as shown in the STM image (d) and sketch (e). Thus, it is pinned on both ends in contrast to the configuration that was achieved by manipulation shown in Fig. 2.6. It was found that the arrangement with the chain adsorbed to the metal at both ends is more stable during imaging than the one that is only attached to the bare surface at one end. In agreement with studies investigating the adsorption of porphyrins on NaCl [102], the molecule - surface interaction strength decreases with an increasing number of layers. Thus, while imaging of a chain adsorbed on top of a single and a double layer of NaCl was feasible, no stable imaging of molecules on a trilayer could be performed, i.e. it was usually removed by scanning the tip over it. Another advantage over the pulling technique is that it avoids the random nature of the process, since there is only a little amount of control of the result of the detachment of the chain from the tip, which can require many attempts before a successful event. The extension of the NaCl islands on the other hand was observed to reproducibly produce the bridging configuration on one and two layers of NaCl, depicted in Fig. 2.7.

### 2.3 Electronic decoupling and conductance measurement

The novel configuration allows to study the electronic structure of different segments of one and the same molecular chain in different local environments. Through the application of a bias voltage the range of molecular states that facilitate the tunneling can be selected, as sketched in Fig. 1.4. Therefore, the recording of images of a molecule at different bias voltages can reveal

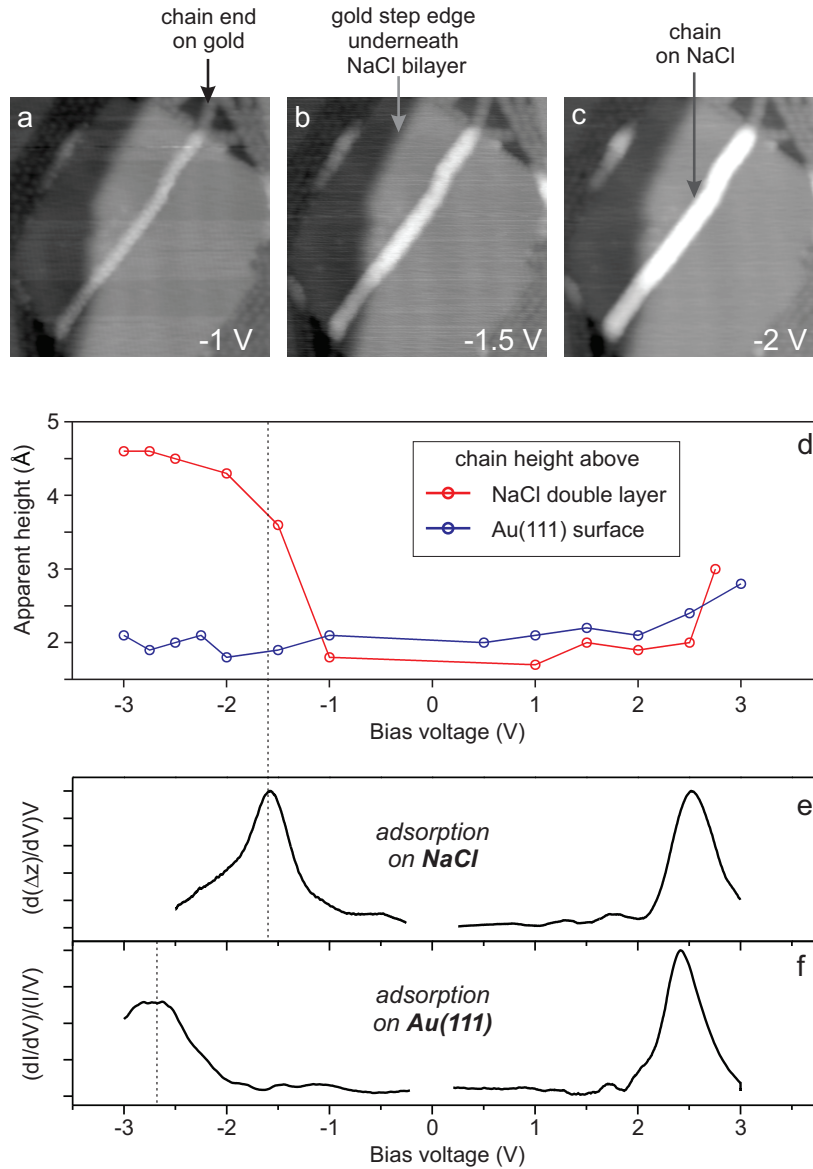


**Figure 2.8:** (a - c) STM images of the same region featuring a chain crossing a NaCl bilayer. Images were recorded at 10 pA and increasing bias as indicated in the images. Images sized  $21 \times 21$  nm<sup>2</sup>. From these image series apparent heights were measured, the results of which are compiled in (d). Apparent heights depending on the bias are shown for chains adsorbed on top of a bilayer as well as for the ends directly adsorbed to the Au(111) surface. (e) typical  $dz/dV$ -spectroscopy curve recorded at constant  $I_T = 0.1$  nA over a chain adsorbed on a bilayer NaCl and (f) differential conductance  $(dI/dV)$  curve recorded on top of a chain adsorbed to the gold. Adapted from [114].

the presence of its orbitals in dependence of energy. The results are shown in Fig. 2.8 for the case of a poly-TF chain adsorbed to gold with its ends and to a bilayer of NaCl with the center. While in the gap the tunneling current is almost constant, in the vicinity of a resonance the transmission is greatly enhanced leading to an increased tip height in constant current imaging. Fig. 2.8 (d) records this apparent height on top of the respective substrate, i.e. gold for the chain ends adsorbed on the metal and the monolayer and bilayer of NaCl for the section adsorbed on top of the insulator. A considerable change is visible between  $-1$  V and  $-2$  V, shown in the STM images (a) to (c). In the latter the chain appears much brighter both with respect to the part adsorbed to the gold and the same chain at lower bias. This change is reflected as the steep increase in apparent height starting at  $\approx -1$  V. A similar onset is visible on the positive sample bias side (probing unoccupied states) at around  $\approx 2.5$  V. On the bare metal surface on the other hand, the apparent height is almost flat with a shallow increase towards higher bias voltages. These results are corroborated by spectroscopy. Fig. 2.8 (e) and (f) show spectroscopy recorded on top of the chains on gold (f) and on top of a bilayer of NaCl (e).

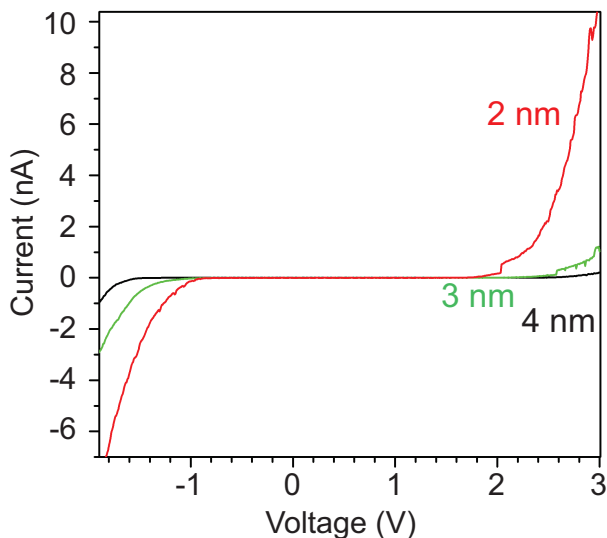


**Figure 2.9:**  $I(V)$  curves recorded for a tip-molecular chain-surface junction [56], cf. also ch. 2.1.1. The pulling is stopped at three different heights as labeled.

While on gold the range of  $|V| < 3$  V is accessible with  $I(V)$ -spectroscopy (constant height) the investigation of the chains on the insulator islands require  $z(V)$ -spectroscopy (constant current) to limit the current that flows in the junction. While the LUMO is located at about the same energy  $E_{\text{LUMO}} = (2.4 \pm 0.1)$  eV as on the bare gold surface, there is a considerable shift on the side of occupied states from  $E \approx (-2.7 \pm 0.1)$  eV on Au(111) to  $(-1.6 \pm 0.1)$  eV on top of the insulating bilayer. Thus, the location of the molecular orbitals coincides with the onset of the increase in the apparent height in imaging. These results show the existence of a state (presumably the HOMO) on the side of the occupied states that is suppressed because of the adsorption of the molecule to the metal surface. However, it reappears if the chain is adsorbed to a bilayer of NaCl. Due to the particular adsorption configuration the electronic states of one and the same chain are subject to different environments depending on whether they belong to the middle bridging part or the terminal sections. Unlike for the ends adsorbed to the bare metal

surface the energetic shifting, broadening and quenching is reduced for the segment adsorbed on top of NaCl. Thus, the spectroscopic results indicate that it is possible to achieve partial electronic decoupling for a molecular chain and to investigate its orbitals in dependence of their local atomic-scale environment.

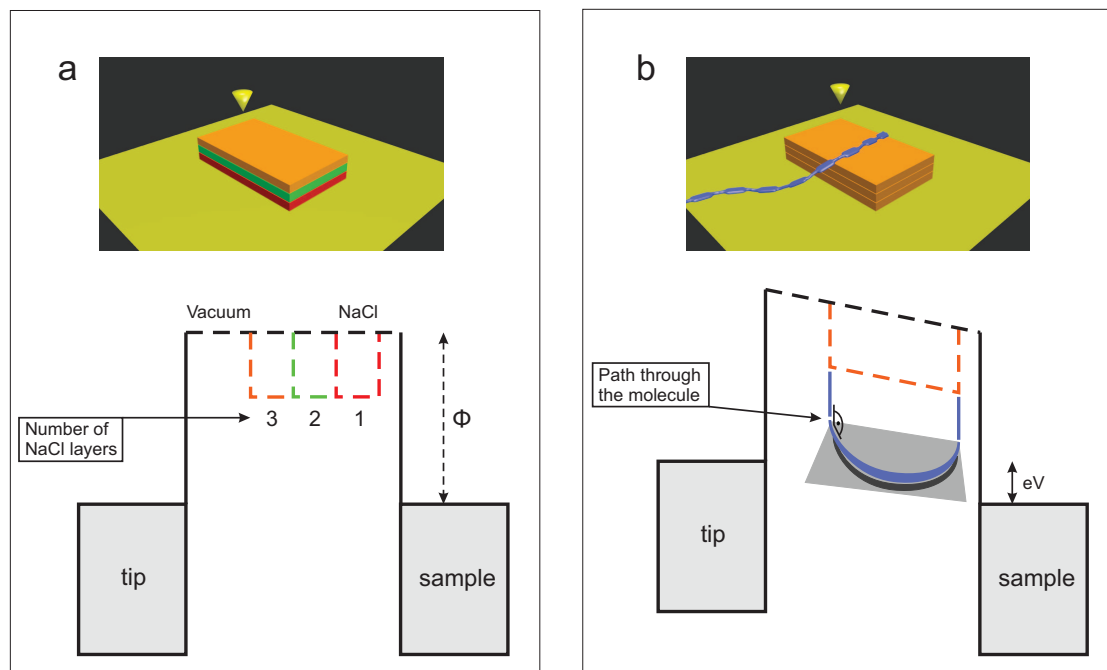


**Figure 2.10:** (a) model of layers (red, green, orange) of NaCl on a metal surface and their effect on the tunneling barrier, shown below. (b) model of a triple NaCl layer (orange) on a metal surface. The salt island is crossed by a molecular chain (blue) which introduces an additional horizontal tunneling pathway. The associated tunneling barriers differ in width and height as indicated in the sketch below. The path through the molecular chain (blue) proceeds horizontally which is expressed in the pseudo-2D depiction.

While recording differential conductance curves jumps are frequently observed, which reflects the fact that the chains are only weakly adsorbed on top of the salt layers. Since the chains are attached on both sides by the adsorption to the gold substrate they have only a small amount of leeway for such motion. This behavior is reminiscent of the wagging motion performed by the porphyrin chains on Au(111) at elevated temperatures (cf. Fig. 3.22). This motion that has not been observed for poly-terfluorene chains on Au(111) might be thermally induced, but it is also possible that it is caused by the interaction with the STM tip, despite the small tunneling current of 10 pA. Sudden movement of chains on NaCl were observed during scanning. The chains usually display a homogeneous contrast without intramolecular features when imaged at higher bias voltages as shown in Fig. 2.8 (c). This could also be due to the excitation of the motion caused by resonant tunneling [115]. The horizontal geometry of the wires adsorbed on the salt allows the measurement of the decoupled molecular states. It is interesting to compare this to the configuration in which the chain is spanning the gap between the surface and the tip, cf. Fig. 2.3 (a). To that end pulling experiments were performed as described in ch. 2.1.1. At certain heights the pulling was then stopped and  $I(V)$  sweeps were recorded. Exemplary curves are shown in Fig. 2.9 for three different tip-sample distances at 2 nm, 3 nm and 4 nm.

Because the bias is increased to several volts the conduction is not generally off-resonant anymore. The curves show an onset to increased conductance at about  $-1$  V and  $2$  V, which is in good agreement with the onset of the conductance peaks for chains on bilayer NaCl, cf. Fig. 2.8 (e). The application of larger tunneling bias and the corresponding increase in the current is likely to lead to the detachment of the wire from the tip. It would be tempting to calculate the decay length  $\beta$  from the  $I(V)$  curves at different heights depending on bias voltage. However, different current curves like the ones shown in Fig. 2.9 are associated with contact conductances that, as described above, vary considerably and therefore prohibit to determine  $\beta$ .

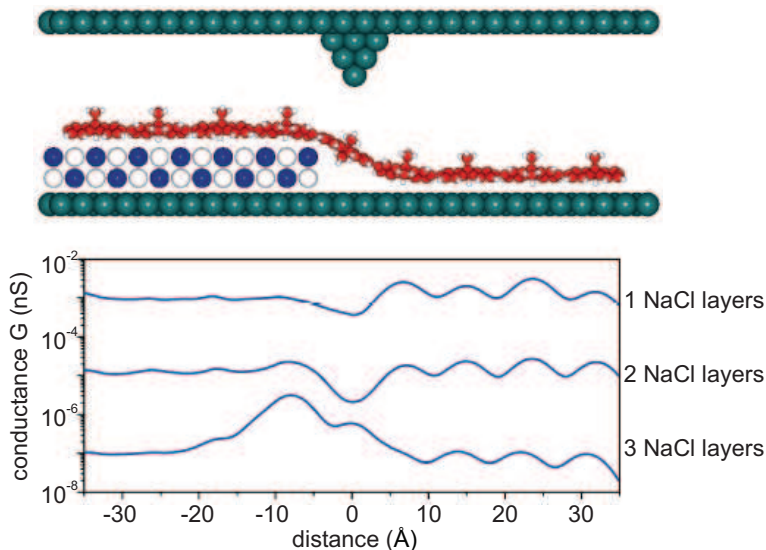


**Figure 2.11:** Top: tunneling junction model consisting of the tip and sample and a molecular chain adsorbed on NaCl on the left side and gold on the right. This structure constitutes the defect in the ESCQ [65] transport calculations. Bottom: conductance curves calculated for the system comprising one, two and three layers of NaCl. The x-axis is scaled to the model shown above, the curve is acquired by 'scanning' the tip at a constant height ( $10$  Å above the first NaCl layer). Calculation and copyright by F. Ample and C. Joachim.

A chain on top of the insulator opens a new transport pathway in addition to the direct tunneling. It is conceivable that electrons travel horizontally along the molecule instead of tunneling vertically through the insulator. Due to the different geometry and chemical composition the two competing pathways are characterized by a different length and a different barrier height, as sketched in Fig. 2.10 (b). While naturally the width of the NaCl is smaller than the length of the chain segment leading to the gold surface the tunneling barrier (sketched in orange) and the associated decay length of  $\beta = 1.2$  Å $^{-1}$  is larger. The path through the poly-TF wire (blue) on the other hand is longer, but characterized by a lower  $\beta = 0.36$  Å $^{-1}$  [56].

The product of distance and  $\beta$  appears in the exponential attenuation factor that determines the transmission, cf. eq. 14. The above values allow a simple estimation of the two pathways. The exponential factor for a triple layer of NaCl is  $3 \times 2.82$  Å  $\times 1.2$  Å $^{-1} \approx 10.15$ . The factor for the corresponding molecular wire segment is  $4 \times 9$  Å  $\times 0.36$  Å $^{-1} \approx 13$ . This is the result assuming that at least four bridging fluorene units at a length of  $9$  Å each are required to accommodate a horizontal adsorption geometry on both the metal and the insulator. Thus, a minimum of

three to four NaCl layers are needed to measure a substantial current through the wire, whereas otherwise the tunneling through the NaCl dominates. This estimate is corroborated by STM images that show a homogeneous contrast along the wire on top of the NaCl bilayers up till the edge of the thin film, reflecting the predominant transport through the latter. On the other hand, examples of molecular chains adsorbed on a triple layer of NaCl have not been observed as it is probably not stable enough. The above estimate is furthermore confirmed by calculations, shown in Fig. 2.11, which reports the first appearance of a current modulation along the wire at a thickness of three NaCl layers. For that height (lowest curve) the constant height calculation finds an increase towards the NaCl edge between around  $-20 \text{ \AA}$  and  $-10 \text{ \AA}$ , which is caused by significant conduction along the wire into the substrate.

## 2.4 Theoretical polymer length distribution

It is an interesting question how the reaction of organic molecules is influenced by the presence of a metal surface. The catalytically enhanced reactivity is one (also technologically) very important aspect and its study is in the focus of the surface science approach. For instance, it was found by Saywell et al. for the coupling of DBTF molecules on a stepped Au(10,7,7)-surface that the catalytically active locations are the kink sites along the step edges [116]. Another important aspect in this regard is the dimensionality of the reaction. While the polymerization in solution is a three dimensional process, diffusion and coupling is confined to two dimensions in our method (cf. Fig. 2.12, particle on the terrace). An attachment to a step edge or similar corrugation originating from a surface reconstruction can lead to a further restriction to one dimension [117, 118] (Fig. 2.12, particle at the steps). While the task to resolve such processes is not a trivial one, important information can be obtained by the study of the products [30].

One feature of the product of our coupling process is its length/weight distribution. In chemistry the molecular weight is an important property of a polymer. Unlike compounds made by other processes, polymers are polydisperse, meaning that its individual molecules differ in the number of units. This is an inherent feature caused by the statistical nature of the coupling and appears without the presence of defects or contamination. Therefore, its weight has to be characterized by a distribution. Knowledge of this distribution can potentially give important insight about the formation process. So far, such an investigation has not been performed for a 2D-confined polymerization.

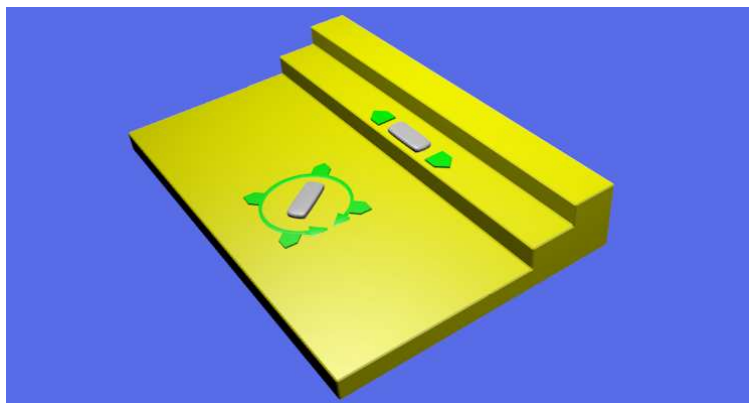


**Figure 2.12:** Sketch of the dimensionality of diffusion on the surface (molecules shown in gray): while the molecule on the terrace (left) is allowed to rotate around  $z$  and to diffuse in  $x$  and  $y$  (2D), the diffusion for the molecule on the step edge (right) is restricted to that direction (1D).

The common approach to the description of products formed in solution is by assuming an equal reactivity of all reactive groups, i.e. at every point in time the probability to react is the same for all functional groups [119]. In particular this is independent of the number of monomer units attached to a specific group. To determine the length distribution on the basis of this assumption one can imagine a random experiment, in which black and white stones are drawn from a hat, simulating the formation of a chain. White appears with a probability  $p$  and signifies that the last group has reacted, i.e. the chain keeps growing (more stones are drawn). The value of  $p$  is equal

to the fraction of the reacted groups. Black appears with probability  $(1 - p)$  and signifies that the last group has not reacted, which terminates growth of the chain. Therefore, the probability of the appearance of a particular chain with  $n$  units is equal to the product of the probabilities of one black and  $(n - 1)$  white stones:

$$W(n) = p^{n-1} \times (1 - p) \quad (15)$$

The absolute number of chains of length  $n$  at a given time  $t$  can be calculated by multiplying with the number of such random experiments (which is equal to the total number of chains  $N_{\text{total}}(t)$ ). The parameter  $t$  is given by the time at which the polymerization is interrupted (by cooling the sample to cryogenic temperature), but it also depends on the temperature during the coupling.

$$N_n(t) = N_{\text{total}}(t) \times (1 - p) \times p^{n-1} \quad (16)$$

Because the number of molecules (linear molecule with one functional group at each end) is always half that of the reactive groups it can be expressed by the number of monomers  $N_0$  present at the start of the reaction:  $N_{\text{total}}(t) = N_0 \times (1 - p)$ . In combination one finds:

$$N_n(t) = N_0 \times (1 - p)^2 \times p^{n-1} \quad (17)$$

This function is called the *most probable distribution*, because of its good description of the products formed under a variety of circumstances [119]. The fact that the number of monomers will always remain the maximum of all chain lengths can be explained with the observation that although the number of monomers is decreased forming dimers and attaching to other chains, longer chains keep reacting in the same amount. Therefore their relative numbers will decrease as well. Fig. 2.13 shows the distribution for three different values of  $p$ . The corresponding average molecule lengths are 100 (red), 20 (blue) and 10 (green).

In the following the length distribution of polyfluorenes formed on a Au(111) surface will be discussed. In chemistry, the experimental determination can be performed with different techniques, which will in general yield slightly different results, as each method is usually biased towards larger or smaller molecules. In our case, the individual chains' number of segments can be counted without ambiguity. The only limitation are molecules adsorbed to step edges, which are not sufficiently resolved and chains that leave the image, which as a result cannot be counted. As a consequence, the distribution is somewhat biased towards smaller chains.

#### 2.4.1 Length distribution of polyfluorene chains on Au(111)

The investigation of the length distribution of the chains allows to address the question whether and how the adsorption on the metal surface influences the polymerization process. For instance,

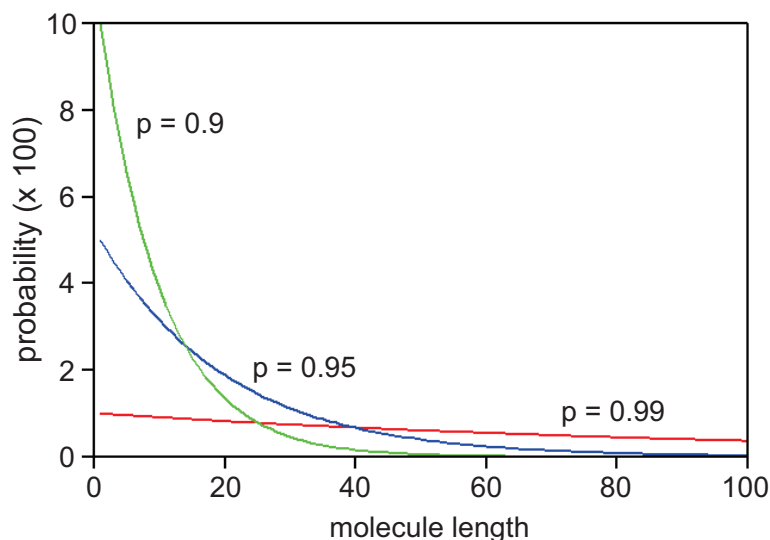


**Figure 2.13:** 'most probable distribution' for three different values of  $p$ .

does it follow the most probable distribution outlined above, which relies on the assumption of equal reactivity of all functional groups present at a certain time, no matter how many chain segments are attached to them? To this end DBTF monomers were deposited onto a Au(111) surface. Subsequently the polymerization was induced by heating the sample (cf. ch. 3.1) and studied with STM. The number of terfluorene (TF) segments of the observed chains ( $N_{\text{chains}} = 1003$ ) were recorded and the results are shown in Fig. 2.14.

The distribution 17 (red line) shows a general agreement with the histogram (red bars), indicating that it can at least be used as a starting point in the description of the latter. The MPD only uses the number of monomers ( $N_0 = 5108$ ) and the probability  $p$  that a group has already reacted (initially there are  $2 \times 5108 = 10216$  such groups; at the time of counting they are reduced to twice the number of chains = 2006. This gives  $p = (10216 - 2006)/10216 \approx 0.8$ .) This would imply that the reactivity of groups attached to longer chains is not substantially reduced. From this one could in turn conclude that the mobility of those chains is not considerably reduced, either.

However, upon closer inspection one notices deviations between the curves. Disregarding the number of monomer counts the distribution rather seems to follow a Gaussian shape, leveling off as the chain length approaches one. The only apparently good agreement at  $N=1$  is revealed to be spurious if one considers the tendency of the brominated precursor to form defects in the form of kinks and junctions (one such instance indicated by the solid arrow in Fig. 2.14). This is due to the necessity of the heating step to 200 °C for the initiation of the coupling reaction (cf. ch. 3.1). Since such connections do not constitute 'legal' links, they were disregarded and two separate chains were entered into the histogram. Disqualification of these chains leads to a considerable reduction of counts at  $N=1$ . The blue bar shows the number of monomers ignoring the ones that potentially form such a bond. (Because the chains don't necessarily lie isolated on the surface this determination cannot be unambiguously done and has been omitted for longer chains that are more likely to lie adjoining to other chains, cf. Fig. 2.14 dashed arrow). Updating

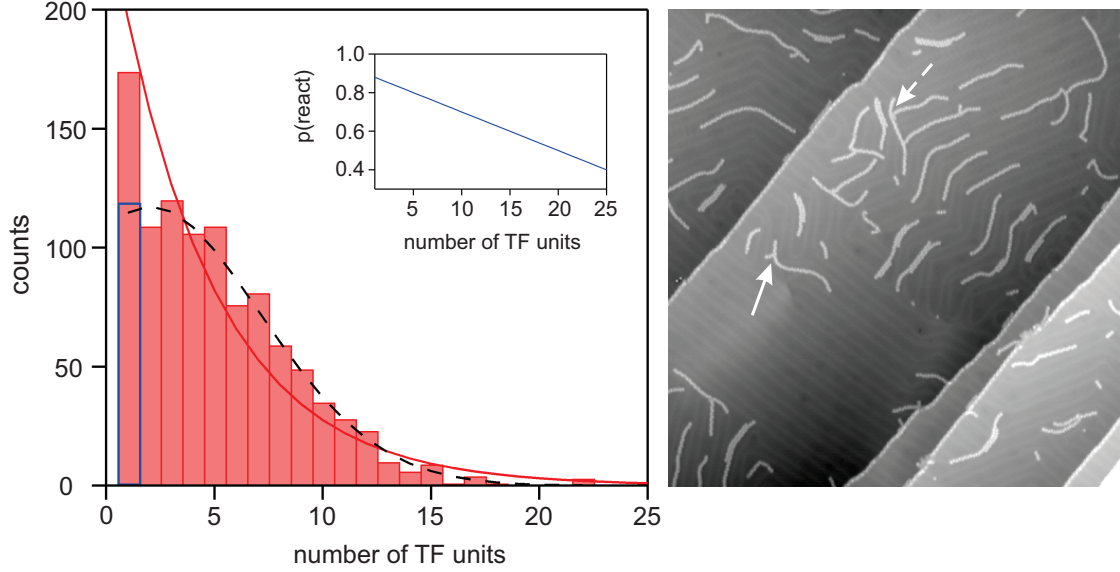


**Figure 2.14:** (Left) Length histogram of 1003 polyfluorene chains from a preparation of DBTF on Au(111). The length is counted in multiples of three, since the monomer comprises three units. Red line: 'most probable distribution' (parameters in the text). Dashed line: fit of function 18, using a probability  $p$  that depends on the number of segments in the chain (as shown in the inset). (Right) Exemplary STM image used for the histogram. Feedback parameters: 0.1 nA, 500 mV, image size  $128 \times 135 \text{ nm}^2$ . (At increased magnification, the lobes associated with the fluorene are easily discernable, cf. Fig. 2.3).

the first count makes the deviation of the curve obvious. Apparently the initial assumption is not fulfilled anymore. However, since the deviation is not so large, one could try to salvage the theoretical model with a correction. The probability  $p$  appears to have a dependence on the number  $N$  of chain segments.

$$N_n(t) = N_{\text{total}}(t) \times \prod_{k=1}^{n-1} p(k) \times (1 - p(n)) \quad (18)$$

$p$  is assumed to decrease linearly with  $N$  (as shown in the inset of Fig. 2.14), i.e. the likelihood to attach monomers to a chain drops with each additional unit. The dashed curve in Fig. 2.14 is a fit using function 18 to the corrected histogram, in which the probability is the free parameter (shown in the inset). The total number of chains  $N(t)$  is not given by the simple dependence on the probability anymore. However, the number is known from the counting procedure (giving a total of 948 chains in the corrected histogram). The dashed curve displays a good agreement with the experimental counts, whereas the probability for short chains is close to the value found for the MPD. Thus, it can be concluded that the deviation can be accounted for by this dependence of the probability  $p$  on  $N$ . The leveling of the curve as  $N$  approaches one can be explained by the reduced mobility of the longer chains which leads to a reduced reaction probability. Furthermore the higher likelihood of adsorption to step edges could play a role. As a consequence, the number of small oligomers decreases more quickly than that of the longer ones.

The influence of kinks and junctions on the distribution can be eliminated by the use of dif-

ferent monomer building blocks. Iodinated precursors constitute an elegant alternative to the brominated ones in this regard. In agreement with different studies [120] we found that the iodophenyl-bond is dissociated catalytically on Au(111), starting around 200 K. For instance, following a preparation of iodinated porphyrins on a Au(111) surface held at RT we observed dimers and other small oligomers, as described in ch. 3. A deposition of these molecules onto the sample at 60 °C leads to efficient coupling producing long chains. The same behavior is observed for the terfluorene substituted with iodine (DITF). This fact renders the heating step to 200 °C, which is needed for the activation of DBTF molecules and which leads to defects, superfluous. As a consequence, kinks and junctions are virtually non-existent.

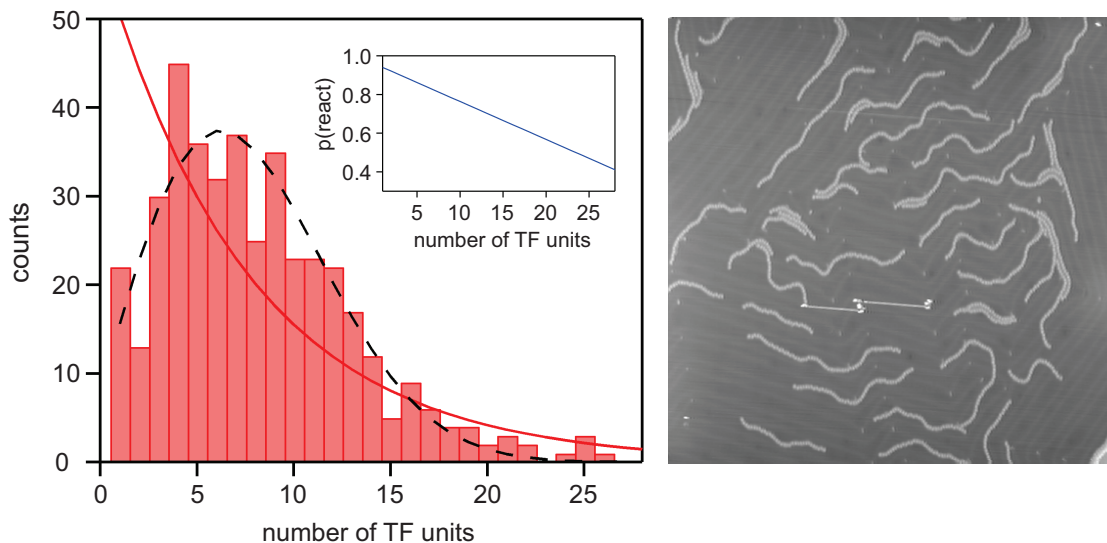


**Figure 2.15:** (Left) Length histogram of 412 polyfluorene chains from a preparation of DITF on Au(111). Red line: length distribution according to eq. 17. Dashed line: fit of function 18, using a variable probability  $p$  (as shown in the inset). (Right) Exemplary STM image used for the histogram. Feedback parameters: 0.1 nA, 500 mV, image size  $134 \times 136 \text{ nm}^2$ . The number of kinks and junctions is greatly reduced. The chains appear a little fuzzy caused by surrounding iodine adatoms.

Fig. 2.15 shows the histogram of chains made of DITF. The average reaction probability  $p \approx 0.88$ , i.e. the reaction has proceeded further than the product shown in Fig. 2.14. In this case the deviation from function 17 (red curve in Fig. 2.15) is immediately obvious: the histogram (total number of chains  $N_{\text{total}} = 412$ ) reaches a maximum at around six TF units and then decreases as  $N$  goes towards one. Therefore, the 'most probable distribution' is not a good description any more. However, a fit of function 18 as performed for the case of DBTF yields the dashed curve in satisfactory agreement with the histogram. While the initial probability is slightly higher, the slope of  $p$  is almost identical to the one shown in Fig. 2.14 ( $-0.0199$  for the former and  $-0.0196$  in the present case), which corroborates the description. Since the product of the surface coupling is the same in both cases, one can (disregarding differences in coverage and effects caused by kinks and junctions) also consider the two histograms as snapshots of the reaction taken at a different times. While in the first example the monomers are still the most frequent species, the process is more advanced in the second case, i.e. a depletion of the monomers has already set in, whereas numbers of the longer chains do not decrease in a similar quantity. This is a qualitative difference to the curves shown in Fig. 2.13. If the reaction were kept progressing one would

expect the peak of the histogram to further shift towards a greater number of chain segments.

Another interesting property is the interplay between activation and diffusion. While both are thermally induced, one could imagine that the rates at which the molecules are activated and diffuse play a role in the produced structures. The above process can be thought of as the limiting case in which the monomers are rapidly diffusing at the employed sample temperatures, at which the activation starts to set in. That could however change if the intact monomers were deposited onto a cold sample which would then subsequently be heated to the minimal activation temperature (at which point the diffusion might still be slow).

## 2.5 Conclusion

In conclusion, the simultaneous adsorption of one and the same molecular chain on metallic and insulating areas has been demonstrated for the first time. The poly-fluorene wires could be partly transferred to NaCl islands grown on top of Au(111) by means of vertical manipulation with the STM tip. This method could be complemented by a preparative approach which relies on the controlled increase of the insulating material. It was shown that the continued supply of NaCl leads to the crystalline and lateral growth of the islands at the expense of the areas covered by the polymeric chains. Ultimately, this forces the molecules on top of the insulator which routinely produces the intended configuration with a chain pinned at both ends to the gold surface while its center bridges the salt layer. Tunneling spectroscopy revealed the partial electronic decoupling, i.e. that of the chain segment on top of the thin film, which was furthermore corroborated by the recording of  $I(V)$  curves in a pulling geometry, i.e. with a wire suspended between the tip and the sample, with the onset of resonances at the same energies. The novel configuration should be applicable to carry out single-molecule conductance measurements, provided that the conductive properties of the wire are able to compete with the tunneling through the salt.

Furthermore, the on-surface-synthesis of oligo-terfluorene has been investigated to advance the understanding of the coupling process by examination of the reaction products. The polymer length distribution has been determined from STM images and modeled with a distribution function. Comparison revealed a departure from the 'most probable distribution', which is based on the assumption of equal reactivity of all reactants and which provides a good description for many solution-formed polymers. The deviation could be corrected by making the reaction probability dependent on the polymer chain length leading to a satisfactory agreement between the experimental observation and theoretical description. It is therefore concluded that the reaction probability of the activated species decreases with increasing polymer length, which is most likely a consequence of longer chains' reduced mobility. Furthermore, it could be demonstrated that the formation of defects which are caused by the heating step can be suppressed by employing iodinated precursors that perform the polymerization at considerably lower temperature.



### 3 Covalent linking using a hierarchical approach

This chapter is concerned with the formation of molecular structures at surfaces. The introduction provides a brief overview focussing on studies dealing with sub-monolayer coverages studied under vacuum conditions. While these aggregates are mostly based on non-covalent bonds, recently the fabrication of stable networks formed by on-surface polymerization has been demonstrated, which has since attracted a lot of attention. The aim of the experimental sections is to advance the control of the polymerization process and study the novel structures that result from it.

#### 3.1 Introduction

Two different approaches exist for the formation of microscopic structures at surfaces, which can be described by 'top-down' and 'bottom-up'. In the first one which has been predominantly employed so far, lithographic methods are used to etch miniaturized components from semiconductor material, which is the basis of today's microelectronics technology. This method contains inherent problems associated with further size reduction, for instance the optical diffraction limit and the devices' unclear properties as their dimensions are reduced further. The opposite 'bottom-up' approach tries to overcome these issues by minutely building up the functional units from their atomic or molecular components and then contact those building blocks to integrate them into a device architecture. Two different strategies can potentially be employed to that end: (1) the formation of individual structures by nano-fabrication, e.g. using the STM tip [121] or even a large array of tips [122]. (2) Alternatively, the components can be instructed to carry out the construction spontaneously, performing self-organization. Self-organization processes are responsible for the formation of complex matter on many different length scales including living organisms and therefore are of fundamental interest in their own right [123]. These processes proceed 'under the pressure of information' as Lehn puts it [124], meaning that the employed building blocks aggregate according to the properties encoded into their structures. Initially in the chemists' domain, the relevance for physical and biological systems renders the field multidisciplinary. The motivation to investigate self-organization and resulting structures is obvious, to gain an understanding of how such development takes place and also to employ such processes in the laboratory, for instance for the fabrication of the above-mentioned molecular nanostructures.

One very elegant way to implement this concept for the formation of regular patterns of defined shape is to utilize molecular recognition, in which the units diffuse and selectively and spontaneously arrange themselves based on the interaction of complementary functional groups [125]. This allows for a fast and parallel formation process and the advantage over the assembly of structures in a molecule-by-molecule fashion in terms of efficiency and precision is immediately obvious. A prerequisite is the sufficient mobility of the building blocks, which is fulfilled in the fluid phases but also on smooth surfaces. The latter leads to a reduction of the dimensionality of both the diffusion and the resulting structures.

The structures made of molecules that were developed and studied with STM and other surface-sensitive techniques were until recently made mostly by molecular self-assembly (disregarding self assembled monolayers [126,127] in which the molecules are grafted onto the surface by linker groups and that differ in properties). It has been shown that molecular self-assembly, derived from supramolecular chemistry and based on weak non-covalent interactions, can be used to produce intricate networks of predetermined shape by the use of specially designed molecules [57, 125, 128]. The assembly is determined both by the interaction between molecules and surface and the molecules with each other. Flat aromatic compounds are frequently employed, because they tend to adsorb with the molecular board parallel to the metal surface. Examples include porphyrins [129] and coronenes [130]. This geometry has the advantage that substituents at the periphery are arranged in-plane and can be used to facilitate the interaction among the molecules. (It is furthermore advantageous for the investigation with STM). The types of interaction at one's disposal through the inclusion of suitable substituents include hydrogen and metal coordination bonding as well as van-der-Waals and dipolar interactions.

### Van der Waals interaction

Interaction can be caused by the presence of permanent or induced electrical dipoles in the molecular species. Permanent dipoles can be generated by polar groups. Notably, this was realized by Yokoyama et al. through the substitution of porphyrins with cyanophenyl groups [131]. By specific placement of the substituents they were able to produce trimers, tetramers and chain structures in a predictable way (cf. Fig. 3.1 (A)). In another study, Bartels et al. [132] investigated the influence of thiol and halogen substituents on the assembly of phenyl groups and attributed the formation of honeycomb structures to quadrupolar interactions. The interaction can have an attractive but also repulsive effect [133]. For instance, charging of Sn phthalocyanine on Ag(111) gave rise to dipoles perpendicular to the surface plane resulting in a repulsive interaction, which in turn led to the isolated arrangement of the molecules [134].

London dispersion forces constitute a weak, non-specific and non-directional interaction between atoms and molecules. They play an important role in the interaction of noble gas atoms and the dimers of halogens [135]. They are caused by fluctuations in the spatial electron distribution that give rise to temporary electric dipoles, which in turn induce dipoles in neighboring molecules that result in an attractive interaction. This interaction quickly decreases with distance ( $\propto r^{-6}$ ). Since the polarizability increases with the size of the molecule the dispersion forces increase as well. Van der Waals radii can be determined from the equilibrium distances in molecular crystals that typically lie between 1 and 2 Å. (A smaller distance can be an indication for covalent bonding.) The interaction increases with surface contact of two molecules, which leads to a tendency for the formation of close-packed islands. The dispersion interaction is present between all atoms and molecules and contributes also to the binding energy of crystals and covalent bonds, although usually its relative impact is small. Lastly, the van der Waals interaction can also play a substantial role in the bonding and conductance of metal-molecule-metal junctions as recently observed by Venkataraman et al. in break-junction experiments [136].

## Hydrogen bonding

Hydrogen bonding takes place between an electron-deficient hydrogen and the lone pair of an electronegative atom (N, O, or F). It has been successfully employed for the formation of molecular structures and studied with STM [137–145]. In contrast to dispersion interactions, hydrogen bonding is directional. Water molecules constitute the model system, however H bonding is also found in many biological systems, because biomolecules contain many nitrogen and oxygen atoms that can take part in such bonds, most significantly realized in the pairing of DNA bases. DNA bases highlight the principle of molecular recognition, with selective binding of adenine to thymine and guanine bonding to cytosine. They are rather compact and planar and therefore favorable for a study using STM [137, 139, 143, 144].

Other notable examples of hydrogen-bonded structures investigated at surfaces include a porous honeycomb network by Beton et al. realized from a mixture of PTCDI and melamine [140], which was used for the trapping of clusters of  $C_{60}$ . Stoehr et al. were able to build regular patterns from perylene derivatives on a Cu(111) surface [141]. Interestingly, the bonding capability of these molecules has to be turned on through the partial dehydrogenation of the molecules by means of a heating step. Thereupon, different aggregates are formed depending on the employed coverage. One of them, a honeycomb structure, was employed subsequently for the trapping of the free electron gas of the Cu(111) surface state [145], resulting in the formation of a new band structure. Regular honeycomb structures were also produced from anthraquinone on a Cu(111) surface by Bartels et al. [142], with pore sizes several times the size of the building blocks forming the network (cf. Fig. 3.1 (C)). These structures can only be explained by the interplay between the attractive hydrogen bonds together with a repulsive interaction between the molecular units and highlight the notion that a proper understanding of a system's features could lead to the ability to control its shape and properties.

## Metal coordination bonding

Metal complexes are of substantial importance in many biological systems. The textbook example is the compound formed by porphyrins and metal cations, a system instrumental for the oxygen transport in animals and also photosynthesis in plants [58]. In porphyrins the four pyrrole groups' nitrogen atoms can donate electrons to an atom in the center of the macrocycle. This makes porphyrins, like the structurally related phthalocyanines, tetradentate ligands. These molecules were investigated adsorbed at metal [146] and semiconductor [147] surfaces. In the cited studies, the metal ion could be reversibly exchanged between the 'up' (pointing towards the vacuum) and 'down' (pointing towards the surface) conformation, constituting a molecular switch. Interestingly, it was shown that the metalation can also take place for the molecules already adsorbed on the surface [148]. It was found that the reaction proceeds with high yield even at room temperature. More importantly for the formation of supramolecular structures more than one molecule can coordinate to a metal atom, which renders it an intermolecular junction. Vertical arrangements could be realized for sandwich type double deckers [149] which

are studied as potential molecular rotors, however mostly in solution. For the formation of two-dimensional arrays, molecules can be equipped with donor atoms at their periphery. Regular and extended networks could be produced, in some studies facilitated through a codeposition with metal atoms [150–154]. Notably, Kern et al. reported on the complexation of different organic ligands to iron atoms on a Cu(100) surface to form rectangular multicomponent networks that displayed error-correction [150] (cf. Fig. 3.1 (B)). It was shown in the same group that such structures can be made to cross step edges [151]. Villagomez et al. could show the connection of wheeled monomers via Cu adatoms to form linear 'trains' [152]. Since many organic molecules potentially constitute ligands and because of the ubiquitous supply of adatoms at metal surfaces, there is often the possibility for the formation of such complexes.

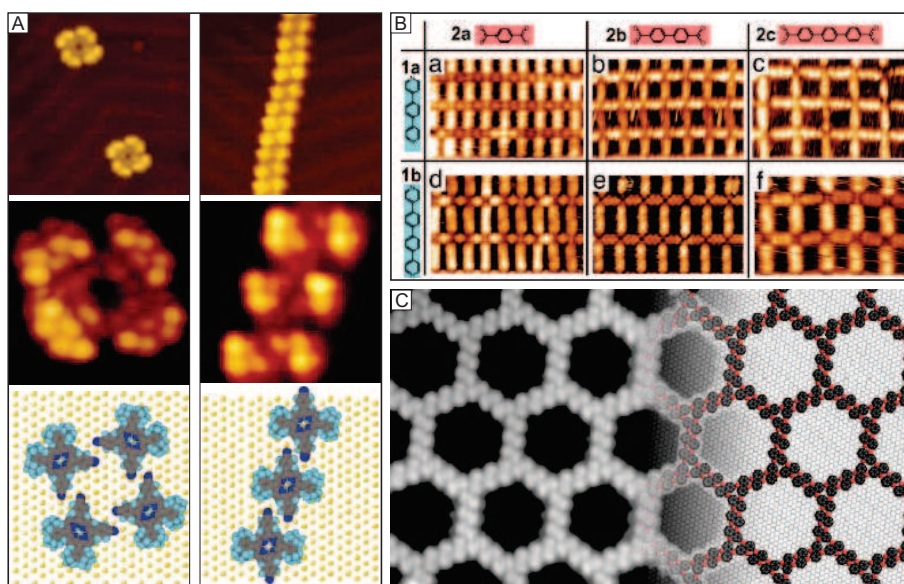


**Figure 3.1:** Structures formed by molecular self-assembly. (A) porphyrins arranged in tetramers (left) and chains (right) by dipolar interaction, reprinted by permission from Macmillan Publishers Ltd: Nature [131], copyright (2001); (B) rectangular networks formed by metal coordination from different combinations of two ligand molecules (red/blue) together with Fe adatoms, from ref. [150], Copyright (2007) National Academy of Sciences, USA.; (C) honeycomb network made of anthraquinone molecules interacting via H bonds, from ref. [142]. Reprinted with permission from AAAS.

It has been shown in the studies cited above that intricate patterns can be produced by molecular self-assembly on metal surfaces and that the architecture can be encoded into the molecular building blocks which follow these instructions spontaneously on a large scale (cf. Fig. 3.1). The formation process is thermodynamically controlled, i.e. the formed structures depend only on the stability of the final products, enabled by the reversible nature of the bonding. While this allows error correction, it comes at the expense that the resulting assemblies, relying on non-covalent interactions, will probably not be stable enough to be incorporated into an application working at or above room temperature.

## Covalent bonding

Only covalent bonds deliver the stability to the structures required for above-room temperature working conditions. Networks interconnected by covalent bonds possess another advantage which lies in the fact that they in principle allow efficient charge transport. This is crucial with regard to functional units whose features are based on electrical conductance, such as diodes or switches (cf. ch. 4.4) and of course also for the molecular wires interconnecting these components. Furthermore, at the length scale of atoms and molecules the electronic properties form a close relationship with the size and architecture of the molecular structures which opens the possibility of tuning them by the design of the networks. This is something that has been successfully attempted e.g. for graphene nanoribbons that exhibit different HOMO-LUMO gaps depending on their width and edge shape [155].

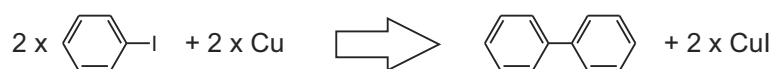


**Figure 3.2:** Ullmann reaction scheme, as realized for single molecules using the STM tip [41].

Studies of individual networks and also potential application of such structures in devices require the introduction of a surface. One hypothetical route towards this goal might be the synthesis of covalent arrays in solution and their subsequent deposition onto a sample. However, the large molecular weight of such a structure precludes its intact sublimation due to the high temperatures that would be required. A preparation from solution on the other hand bears the disadvantage of contamination with solvent (and ambient) molecules. Furthermore, solution-based synthesis demands the introduction of large solubilizing side groups, detrimental to an efficient design of such a network. This renders an on-surface synthesis approach the most promising. Furthermore, the breaking and subsequent formation of covalent bonds to yield new species at surfaces is of paramount importance in the field of heterogeneous catalysis. An early example is the Ullmann coupling [156] reaction, in which halogen-aryl bonds are cleaved in solution in the presence of copper, resulting in the coupling of the aryl groups (cf. Fig. 3.2). However, the controlled formation and observation of a covalently connected species at surfaces had not been shown at the single molecule level until Hla and coworkers could demonstrate the coupling analogously to the Ullmann reaction of individual phenyl rings at a copper surface by employing bias pulses from an STM tip [41]. This study is a showcase for the capabilities of the STM: iodophenyl molecules were identified at the step edges and the C-I bond dissociated using tunneling electrons (Fig. 3.3 a). The process was found to be a one-electron process and damage to the aromatic ring could be excluded by the use of bias voltages below those capable of dissociating either C-C or C-H bonds. Then the tip was employed in lateral manipulation mode to remove the iodine and move two such activated phenyl rings together (Fig. 3.3 c and d). In a third step the two rings were connected, again using excitation by tunneling electrons (Fig. 3.3 e).

The process depends on the relative orientation of the two phenyl groups that is stabilized by bonding to the step edge. The authors assume that the voltage pulse induces a rotation leading to an alignment of the reactive groups. However, the simultaneous formation of many covalent bonds to produce predefined molecular patterns on a surface in a self-organized fashion remained

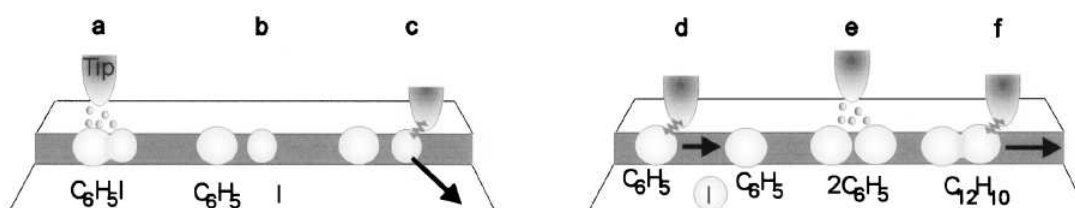


**Figure 3.3:** Schematic steps of the Ullmann type reaction of individual iodophenyl molecules as described in the text (image from Ref [41], Copyright (2000) by The American Physical Society).

an open challenge.

The first realization of the fast and parallel formation of molecular networks stabilized by chemical bonds on a metal surface was performed in 2007 [55]. For this study, porphyrin was chosen as the central molecular building block. Derivatives of these molecules featuring bromophenyl legs were synthesized by S. Hecht and M. Peters at the Humboldt Universität Berlin. It could be shown that using such precursor molecules, chains and also extended networks could be produced (cf. Fig. 3.5 (a) - (f)). Like in the single-molecule chemistry described above, the working principle is based on the fact that the carbon-bromine bond is the weakest inside the molecule and can be split off selectively. Importantly, this can be induced without damaging any other parts inside the molecule as all the other bonds are sufficiently high in energy. Furthermore, a strong bond is formed subsequently between the halogen and surface metal atoms [157], which makes the C-Br bond scission thermodynamically favorable. The network formation takes place in two steps, (1) activation of the precursors and (2) connection of the reactive units, cf. Fig. 3.4. The first step, i.e. the dissociation of the bromine from the molecular core, was induced thermally. Since the molecules are applied to the surface by thermal evaporation, the activation can already take place during deposition. It was found that for the porphyrins the critical evaporator temperature lies within practical bounds for the sublimation of the monomers. This range is given by the temperatures at which a fraction of a monolayer can be produced between tens of minutes (at the onset of a measurable signal from the quartz crystal microbalance) and a few seconds (which is the minimal time needed to operate the shutter of the evaporator). As a consequence, the molecules can already be activated during the deposition. They then reach the surface in reactive form. Another possibility is to keep the evaporator temperature below that critical temperature. In this case intact monomers can be observed with STM. This could be demonstrated by the controlled dissociation of the bromine atoms, which happens at around 2.2 V. Subsequently, the Br atom is usually observed at a close distance but separated from the molecular core and can be further removed by lateral manipulation as in the dissociation of iodophenyl described above. Both procedures will render the molecule reactive, likely with a radical in position previously connected to the bromine (denoted by dots in Fig. 3.4). Subsequently, while the monomers diffuse over the sample surface they can form a new covalent bond via these reactive sites in an addition reaction. This is why a sufficient mobility is crucial for step (2). The only residue of the polymerization is in form of the halogen atoms that can be viewed as protecting groups. No other by-products are formed in the reaction. Furthermore, the bromine is usually not observed on Au(111) and is expected to have desorbed at the elevated temperature [158].

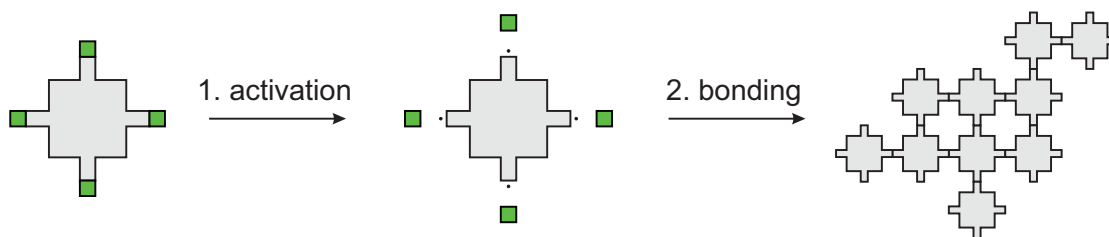


**Figure 3.4:** Schematic representation of the two-dimensionally confined polymerization. (1) The monomers (gray) can be activated by dissociation of the halogen atoms (green) both during evaporation and on the sample. (2) the coupling reaction is facilitated by surface diffusion.

The covalent linking of organic molecules using this approach to form two-dimensional structures at (mostly metal) surfaces has attracted considerable attention [159–161]. The method described above has been successfully employed for a number of molecules [94, 116, 118, 120, 162–167], highlighting the generality of the approach. One-dimensional structures could be successfully produced. For instance, the group of Rosei reported the successful formation of polyphenylene [164] (cf. Fig. 3.5 (g)) and -thiophene [165] from bromine and iodine functionalized precursors. In the former study different placement of the halogens resulted in straight and zig-zag structures in a predictable way. For both systems they identified an intermediate stage of monomer bi-radicals stabilized by the surface. These molecules are bonded to surface atoms (the resultant structures are sometimes called ‘protopolymers’ [168]) and require an additional heating step to induce coupling. As was shown for the tetra-brominated porphyrins, monomers equipped with more than two coupling moieties can be used to realize two-dimensional structures. For instance, the Fasel group reported the formation honeycomb networks made of cyclohexaphenylene (yielding ‘porous graphene’ [163] - cf. Fig. 3.5 (h)) and another made of triphenylamine derivatives [120]. Notably, the same group observed the coupling of brominated anthracene and tetraphenyl-triphenylene derivatives, the product of which could be converted into graphene nanoribbons of different shapes by a cyclodehydrogenation reaction [169]. Furthermore, honeycomb networks made of phenyl rings were reported by Gutzler et al. [162] (cf. Fig. 3.5 (i)) and also Blunt et al. [170].

In all studies the surface was found to play an active role, apart from supplying a support for the polymerization process. It confines the reaction to two dimensions, influencing molecular conformation, mobility and arrangement of the precursors, a notion that is further investigated in ch. 3.2. In some cases it is found to stabilize radical intermediates, while in most cases it plays a catalytic role, assisting the monomer activation and also cyclization reactions. It was shown that different metals and crystal faces can be utilized and that the properties of the surface can have a profound influence on the polymerization. For instance, different morphologies were found for the formation of one and the same type of honeycomb network on the (111) face of Au, Ag and Cu and ascribed to the difference in diffusion barrier height [94]. Successful studies using different molecules employed surfaces such as Cu(110) [164], Cu(111) [94, 162, 166], Ag(111) [120, 169] and Au(111) [94, 169].

It is noteworthy that a similar process could even be induced on a bulk insulator [171]. Kuehnle and coworkers could confirm that the process works analogously to that on a metal surface.

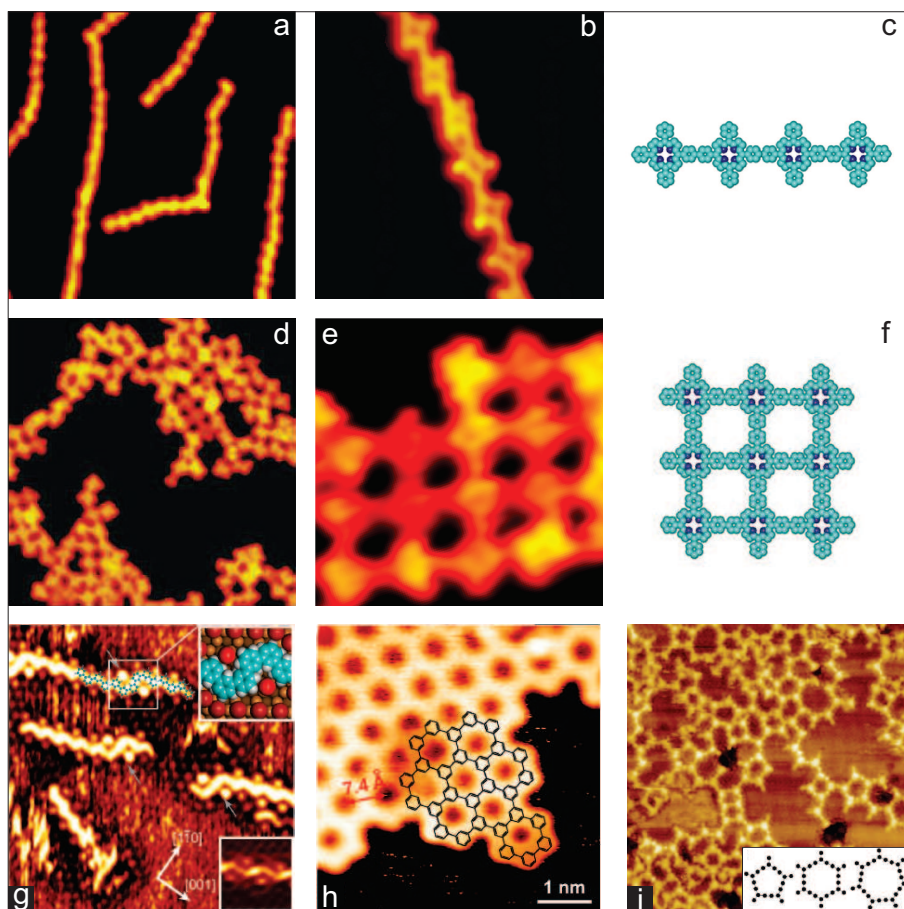


**Figure 3.5:** Covalent molecular aggregates formed by an 'Ullmann-like' on-surface-synthesis process, i.e. based on halogenated precursors. (a) - (f) oligomers made of tetra-phenyl-porphyrins. While the precursor featuring two bromine atoms in a *trans* configuration results in linear chains (a) - (c), substitution of the phenyls in all four directions with bromine leads to two-dimensional network growth (d) - (f) (from ref. [55]). The process is not limited with regard to the building blocks, other examples include (g) chains made from phenyl, from ref. [164], Copyright 2009 Wiley-VCH Verlag GmbH & Co. KGaA, Weinheim; and also porous networks like the ones shown in (h) and (i), reproduced from ref. [163] and [162], respectively, with permission from The Royal Society of Chemistry.

However, due to the reduced adsorption energy special care had to be taken that the precursors do not desorb during the heating step. This was facilitated by the inclusion of carboxylate groups linking to the calcite insulator surface.

Besides the Ullmann-type process outlined above, covalent networks at surfaces can be produced employing different linking chemistries. For instance, Raval et al. observed the connection of tetra(mesityl) porphyrins on a Cu(110) surface (cf. Fig. 3.6 (a)) [172]. The missing row reconstruction of this surface is found to have an influence on the orientation of the small networks. The same crystal face of gold is used by Zhong et al. for the coupling of alkanes [117], which are found to arrange along the surface corrugation (shown in Fig. 3.6 (d)). Successful covalent coupling was furthermore observed by Stoehr et al. [173], investigating the coupling of carbenes made from pyrimidine derivatives to produce linear chains (cf. Fig. 3.6 (b)) and by Weigelt et al. [174]

who realized a crosslinked copolymer by formation of imine bonds. Porte et al. [175] investigated the formation of Fe phthalocyanine networks on the (111) face of Au and Ag (cf. Fig. 3.6 (c)). The same growth is furthermore claimed to proceed on NaCl islands on top of Ag(100). Similar to the study of the adsorption of polyfluorene wires on NaCl islands [114] the adsorption of the networks commences only after saturation of the metallic areas of the sample (cf. ch. 2.2). The same group reported on the formation of extended networks using precursors substituted with boronic acid groups that form boroxine rings with the elimination of water on Ag(111) [176]. Exposing networks linked by boroxine rings to a humid atmosphere at increased temperature, Lackinger et al. observed the ripening of the structures, facilitated by the reversibility of the previously formed bonds [177]. This allows a limited error-correction, however at the expense of reduced network stability. This kind of dynamic covalent coupling [178] is in principle very attractive, however it offers no routes towards the coupling of monomers to yield carbon-carbon bonded conjugated structures. In most cases the polymerization is induced thermally and the monomers are arranged in non-covalent structures as the ones described above before the heating step.

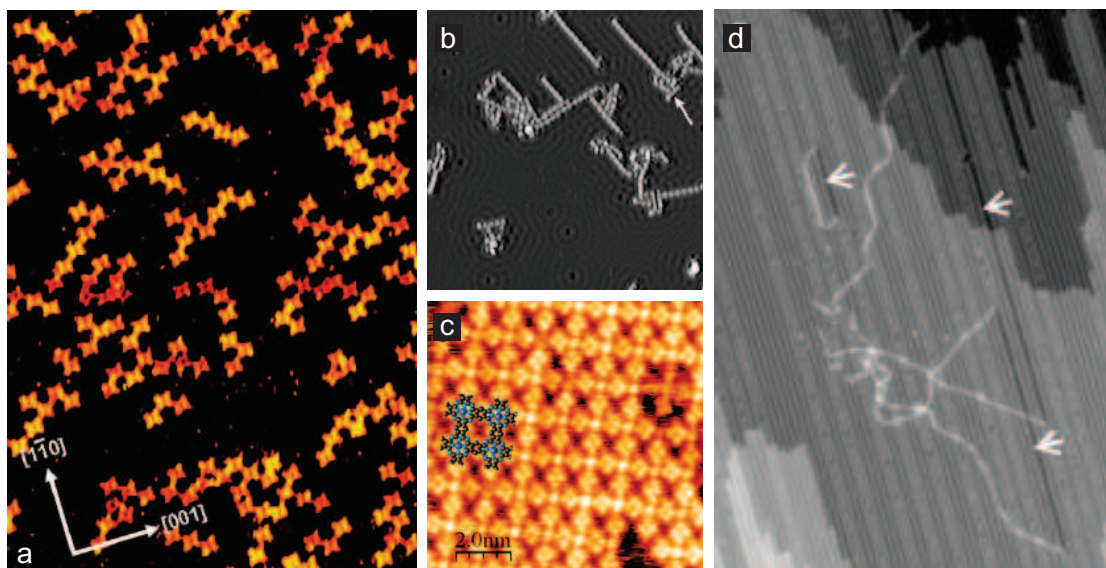


**Figure 3.6:** Examples of structures formed by surface-confined synthesis based on different (“non-Ullmann”) coupling. (a) tetramesityl-porphyrin networks on Cu(110), reproduced from ref. [172] with permission from The Royal Society of Chemistry; (b) chains made of TAPP (a compound based on pyrimidine) on Cu(111), from ref. [173], Copyright 2008 Wiley-VCH Verlag GmbH & Co. KGaA, Weinheim; (c) Fe-phthalocyanine networks on Ag(111), reprinted (adapted) with permission from ref. [175]. Copyright (2011) American Chemical Society; (d) alkane chains coupled on Au(110), from ref. [117]. Reprinted with permission from AAAS.

Despite the considerable success in the formation of otherwise inaccessible structures, the covalent linking confined to two dimensions leaves room for further study and optimization. The drawback of the reactions described above is their limitation to one-step processes with all the monomers being activated (more or less) at once. Thus, experimental outcomes were characterized by non-selective linking and a rather low level of control. This precluded the formation of more sophisticated structures and led to rather simple architectures. As a consequence, if

one were to employ different molecular building blocks, this would lead to a random coupling (sketched for the one-dimensional case in Fig. 3.7 (a)) or in the case of complementing reactants to strict alternations, i.e. the repeat unit consists of two different structural units, (b). This is the case for the sketched bifunctional units (forming two connections, e.g. DBTF) or polyfunctional (facilitating more than two bonds, such as Br<sub>4</sub>TPP). On the other hand, separating the activation, e.g. to different temperature ranges, would result with high likelihood in the formation of block copolymers as sketched in (c). However, the controlled coupling of different types of molecular components acting as wires, diodes and switches is critical for the realization of functional structures at the molecular level, e.g. the envisioned molecular circuitry. In this regard, the need for an interconnection following a specific design in a minutely guided process is obvious.

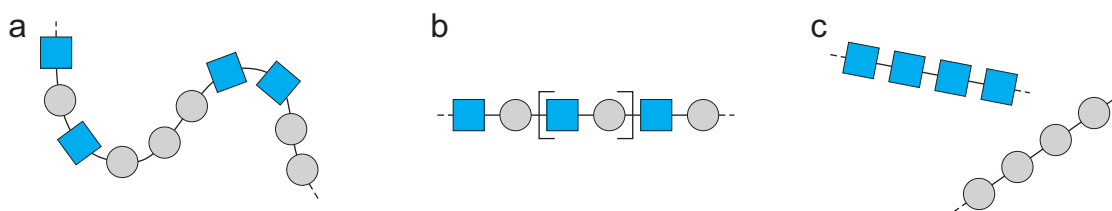


**Figure 3.7:** Sketch of the outcome of simultaneous activation of two different di-valent building blocks (blue, gray) (a) with random and (b) complementing coupling (repeating unit in brackets). (c) Sequential activation on different building blocks leads to the formation of block copolymers.

Furthermore, an important motivation for an improved coupling scheme stems from the pursuit of regular structures. Due to the non-reversible nature of the covalent bonds the possibility of error-correction as illustrated for the structures formed by molecular self-assembly is prohibited and defects cannot be repaired once the network formation has taken place. (An example is sketched in the inset of Fig. 3.5 (i) which depicts the intended hexagonal shape (center) next to non-optimal pentagonal and heptagonal ones that are also observed experimentally.) Therefore, it is crucial to address this issue already during the coupling and focus on the reduction of linking errors. One approach relies on the size of the reactants. To start with a greater number of correctly assembled monomers leads to a reduction in the number of defects per surface area in the resulting networks. It has been shown that linear chains can be grown virtually defect-free, which therefore makes them an attractive starting point for two-dimensional growth. The prearrangement of the precursors can play an important role as well. While steric hindrance can result in the formation of defects, it is conceivable that a preorganization of the molecules can also facilitate an improved network formation. It is the subject of the following experimental sections to address these issues by the realization of a stepwise on-surface coupling process. The goals are the reduction of the defect density by exerting a guiding influence on the intermediate products and the selective coupling by the controlled provision of reactive sites.

## 3.2 Hierarchical growth - experimental results

Our approach to address these issues relies on specially instructed monomers. Building on the study described above [55], we chose porphyrin derivatives with an improved design: the substituents were chosen in such a way as to program the monomers for a hierarchical growth [179]. The approach aims at dividing the reaction into different steps allowing their separate and subsequent activation.

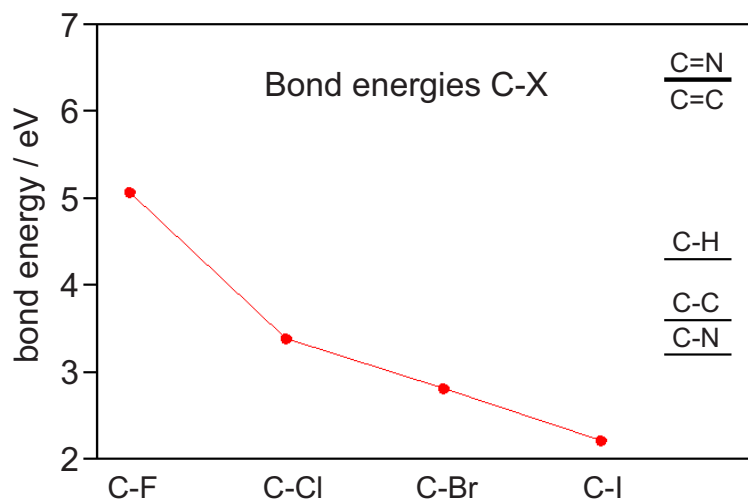


**Figure 3.8:** Mean binding energies of the halogens fluor to iodine with carbon. [135]

To that end, bromophenyl and iodophenyl groups are attached to the porphyrin's *meso* position in *trans*-Br<sub>2</sub>I<sub>2</sub>-tetraphenylporphyrin (Br<sub>2</sub>I<sub>2</sub>TPP) in a *trans* configuration as shown in Fig. 3.10 (a). These latently reactive halides are employed to facilitate the activation and subsequent coupling. The working principle relies on the decreasing binding energy with carbon as one goes along the halogen group (cf. Fig. 3.8). In general, it depends on the order (single, double, etc.), on the length of the bond (generally increasing binding energy with decreasing length) and its polarity. As the electronegativity is reduced going from fluor towards iodine, the polarity of the bond and therefore the ionic contribution is reduced. Thus, the expectation is that the iodophenyl bond will be dissociated before the bromophenyl one. In this way the molecules are instructed to participate in two polymerization directions, i.e. first performing linear chain growth and then two-dimensional network growth in a second step.

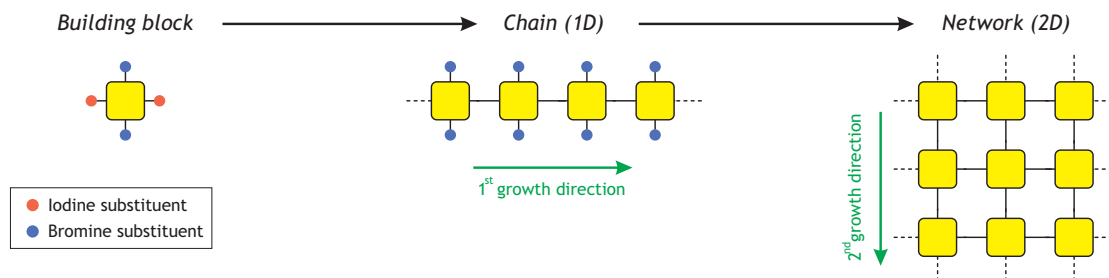


**Figure 3.9:** Sketch of the reaction sequence guided by the information encoded into the molecular precursors leading to a hierarchical coupling pathway.

The porphyrin monomers are deposited from a Knudsen cell at 320 °C onto a Au(111) surface. If the surface is held at room temperature, the molecules already perform coupling to form short oligomers, mostly dimers and a small fraction of larger structures. A representative overview image is shown in Fig. 3.11 (a). A survey of this preparation revealed 18 % monomers, 59 % dimers, 17 % trimers and 5 % tetramers for the 1360 oligomers counted. These are exclusively linear chains and no two-dimensional growth has been observed. The porphyrin macrocycles appear among rows of small bright lobes. Upon closer inspection it is found that these lobes decorate the apices of each chain as is visible in the magnified image in Fig. 3.11 (b), which shows an island consisting of dimers. The regular assembly of the molecules leads to the rows of bright lobes (two of them are indicated by dashed lines in the magnification). While individual chains such as the dimer shown in Fig. 3.10 (c) can easily be separated from such assemblies by lateral manipulation, cf. ch. 1.3.1, they cannot be divided further in this way. This indicates that partial activation is already taking place at these temperatures either at the surface or during the evaporation process. A dissociation at the surface is in agreement with studies that observed the catalytically induced cleavage of carbon-iodine bonds on Au(111) starting at around 200 K [180].

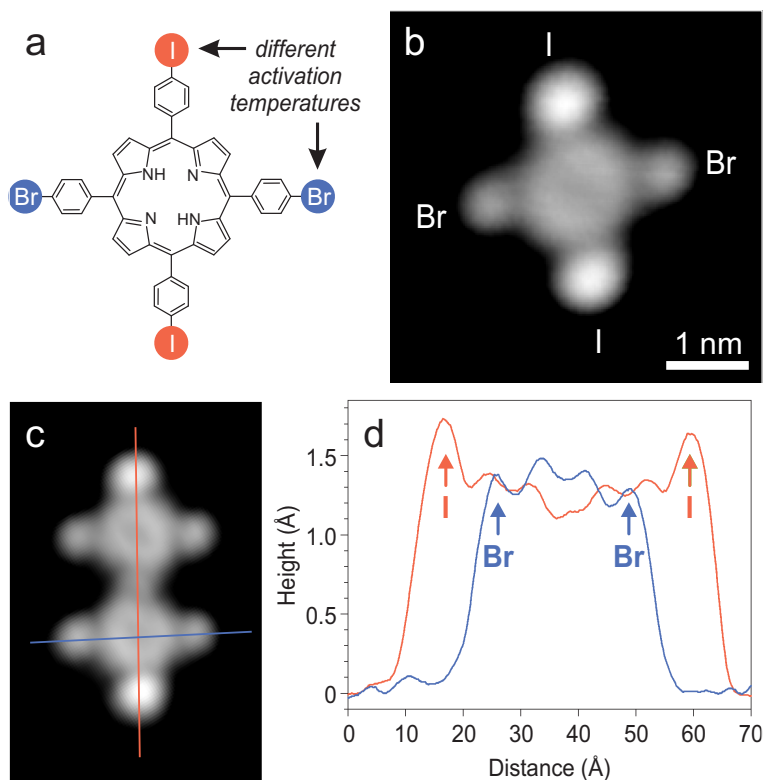


**Figure 3.10:** The employed monomer [179]. (a) Sketch of the chemical structure of  $\text{Br}_2\text{I}_2\text{TPP}$ ; (b) STM image of a  $\text{Br}_2\text{I}_2\text{TPP}$  monomer on Au(111), feedback parameters 0.5 V, 0.1 nA; (c) STM image of a dimer of  $\text{Br}_2\text{I}_2\text{TPP}$  on Au(111) image size  $4.3 \times 6.5 \text{ nm}^2$ ; (d) height profiles along the line scans indicated in (c).

To investigate the polymerization process, the first objective is to identify the components of the molecules visible in STM images recorded with submolecular resolution. The molecules display the appearance typical for porphyrins that reflects the ring structure of the macrocycle, with four protrusions in a rhombic shape associated with the pyrrole groups. Additionally, some of

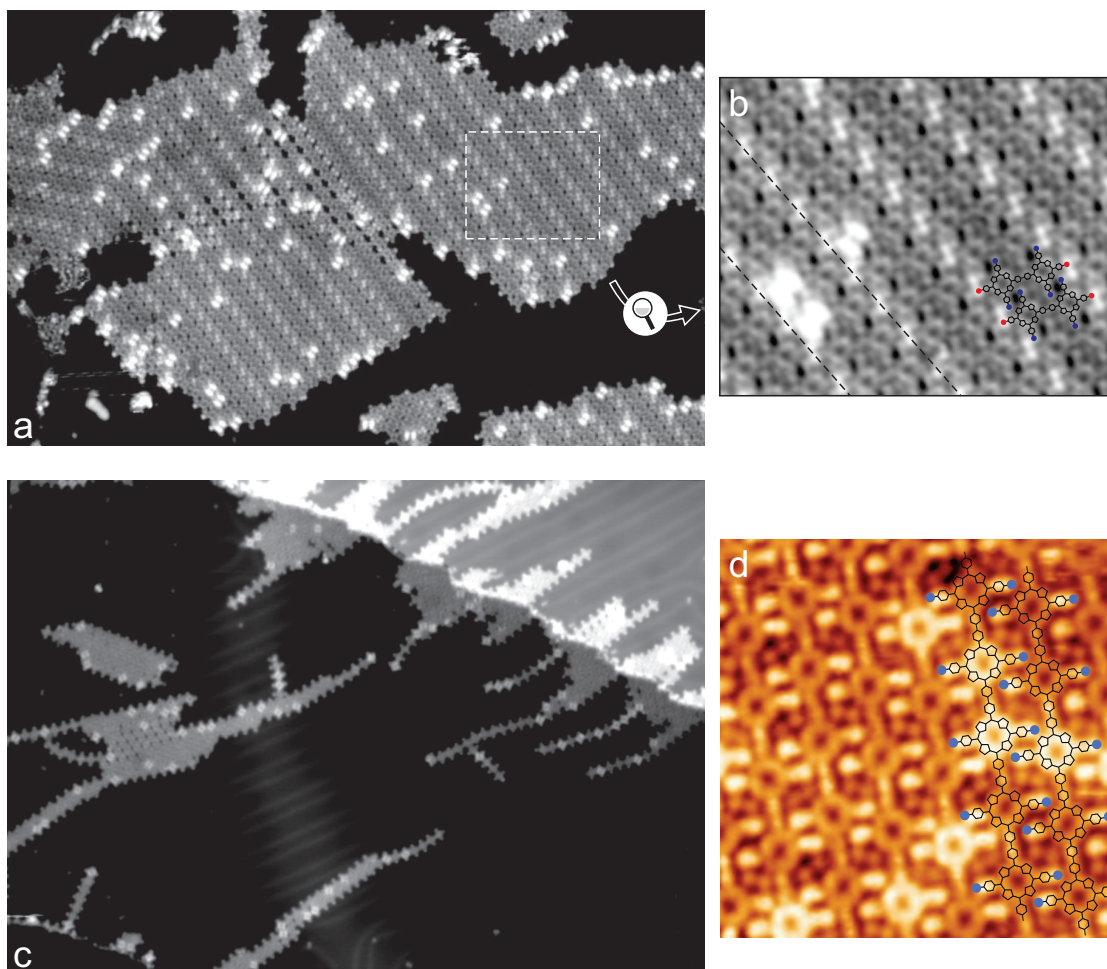


**Figure 3.11:** STM images of  $\text{Br}_2\text{I}_2\text{TPP}$  on Au(111). (a) recorded after deposition of the molecules on a sample held at room temperature, image size (a)  $50 \times 80 \text{ nm}^2$ ; (b) magnification of the boxed area in (a), sized  $12 \times 15 \text{ nm}^2$ , showing rows of dimers. (c) and (d) recorded after the first heating step at  $120 \text{ }^\circ\text{C}$  for 5 min, (c) sized  $85 \times 120 \text{ nm}^2$ ; (d) close-packed chains are assembled in islands, image size  $10 \times 10 \text{ nm}^2$ . Bias voltage (a) - (c) 1 V; (d) 0.3 V; tunneling current for all 0.1 nA. Sample temperature during scanning (a) - (c) 10 K, (d)  $70 \text{ }^\circ\text{C}$ .

the molecules appear brighter than the surrounding ones (three of them are visible directly next to the dashed lines in the magnified image of Fig. 3.11 (a)), which is attributed to the interaction with gold adatoms [181]. On the other hand, the identification of the two different types of halogenated side groups poses a challenge since the assignment, unlike in the case of  $\text{Br}_4\text{TPP}$ , is ambiguous. However, they are characterized by different apparent heights in STM images, which were utilized to compare them to the bromophenyl and iodophenyl substituents on molecules that were synthesized with only one type of halogen atom.

Fig. 3.12 shows the height profiles across single molecules with different substituent arrangements. The two molecules used for comparison (at the center/right of the figure) consist of a porphyrin core with bromophenyl (center) or iodophenyl (right) groups at the *meso* position (i.e. attached to the methine bridges) in a *trans* configuration. However, unlike the  $\text{Br}_2\text{I}_2\text{TPP}$  molecule, they do not possess halogen substituents in the orthogonal direction, where phenyl

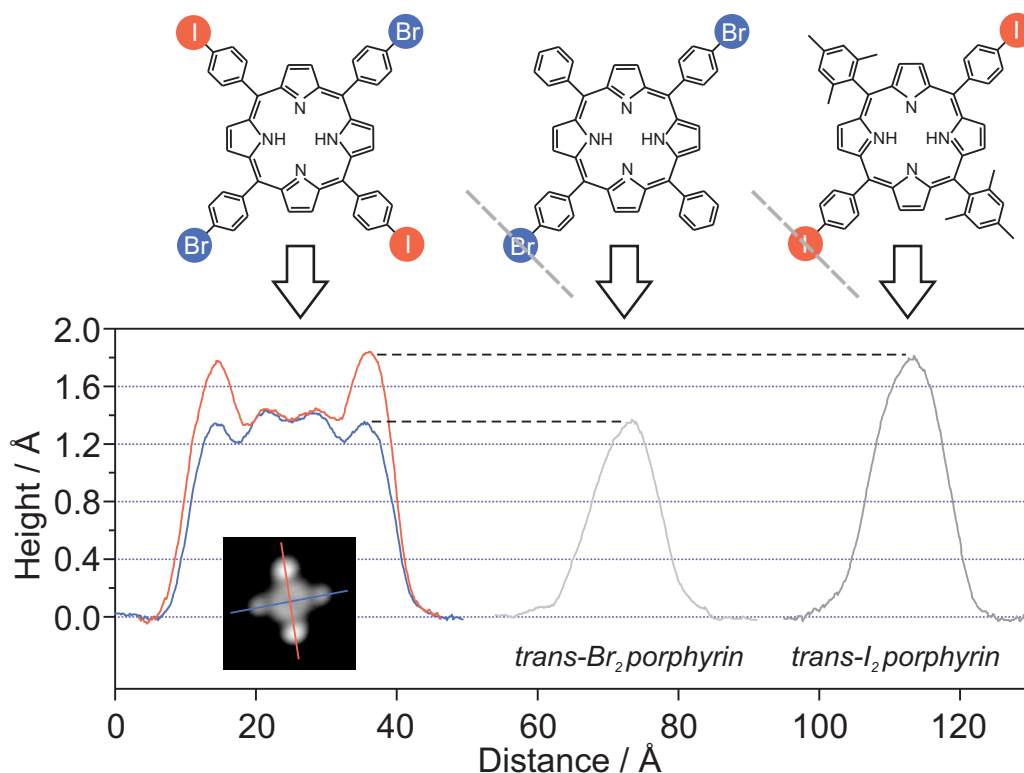


**Figure 3.12:** Height profiles and chemical structures of the molecules used for the assignment of the two halogen types to the side groups of  $\text{Br}_2\text{I}_2\text{TPP}$ . Left:  $\text{Br}_2\text{I}_2\text{TPP}$ , center and right: singly-substituted porphyrin derivatives for comparison. The position of the height profiles over the halogen atoms are indicated by the dashed grey lines.

(center) and mesityl (right) groups are attached (those side groups are not expected to have an influence on the appearance of the halogenated legs). Line scans performed across those groups (cf. Fig. 3.12) show good agreement between the bromine atoms and the lower protrusions on the  $\text{Br}_2\text{I}_2\text{TPP}$  side groups and likewise of the iodine atoms with the higher protrusions. This allows the identification of the substituents for the monomers and the products of the subsequent polymerization steps. The brighter protrusions (apparent height of  $(1.7 \pm 0.1) \text{ \AA}$ ) thus represent the iodine substituents, while the bromine legs appear lower at  $(1.3 \pm 0.1) \text{ \AA}$ .

On the other hand, a different appearance without a distinct protrusion is observed after halogen dissociation, cf. ch. 1.3, as shown in Fig. 3.13. To that end, the tip is positioned above the position marked with the  $\times$  in (a) and the bias is increased gradually to 2.5 V, inducing the cleavage of the carbon-bromine bond. Accordingly, in the image (b) recorded subsequently, the atom is sitting at a small distance, as marked by the arrow. (While the bromine atoms could be removed from the molecular frame in this way, attempts targeting the iodine atoms were unsuccessful. This could be due to lateral motion induced by the tunneling electrons, as shown in Fig. 3.13, which terminates the current through the targeted position).

As for the short oligomer chains shown in Fig. 3.11 (a), the brighter protrusions are exclusively observed at the apex of the long axis, which indicates partial iodine dissociation and connection of the corresponding sites. In contrast, the side groups at the short axis (appearing lower) stayed entirely intact and there were no perpendicular connections observed. It can therefore be

concluded that the bromine is still bonding to and protecting its phenyl groups. Thus the appearance of the dimers and short oligomers corroborates that the process is initiated as intended. A dissociation at the surface is in agreement with studies that observed the catalytically induced cleavage of carbon-iodine bonds in iodobenzene on Au(111) starting at around 200 K [180].

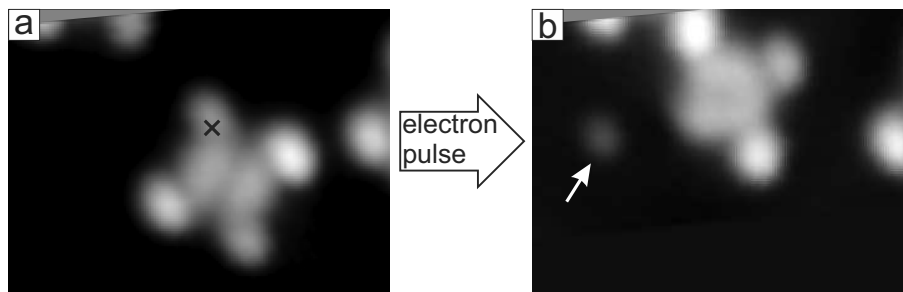


**Figure 3.13:** STM images before (a) and after (b) the application of a pulse of tunneling electrons in the position marked by the  $\times$ . The manipulation induces the dissociation of the bromine atom (marked by the arrow) and a rotation of the whole molecule by  $90^\circ$ . Image size  $4.5 \times 6 \text{ nm}^2$ , feedback parameters 500 mV, 0.1 nA.

The dimers and short oligomers constitute a snapshot of the process which has already proceeded one step into the reaction, i.e. to the center of Fig. 3.9. To monitor the whole connection sequence from the monomer building block via an intermediate reaction product to the final network structure a premature activation was inhibited by deposition of the monomers onto a sample cooled to 80 K. In agreement with the above interpretation the molecules appear as monomers, cf. Fig. 3.10 (b), whereas dimers etc. were not observed. While they are found to aggregate in small islands (cf. Fig. 3.14 (a)) indicating their mobility at even these low temperatures they only weakly interact as all of their substituents remain in the protected state (confirmed by lateral manipulation). The absence of the yet-to-be-formed chemical connections is obvious from the distance and arrangement of the molecules that features the substituents in a close-packed and interleaved arrangement. It is thus shown that it is possible to initiate the process from the very starting point.

As outlined above the first step is initiated by supplying thermal energy. To induce an efficient chain formation the sample temperature is raised above room temperature. For the selectivity of the process it is crucial that the temperature ranges corresponding to the activation of the different substituents, i.e. iodine and bromine, do not overlap, as this would lead to a random connection. In a recent study [182] conducted by a different group it was observed that the choice of substrate can play a decisive role for the value of the temperature thresholds. In one case this led to simultaneous activation and consequently loss of selectivity. The Au(111) surface (and also its (100) face as shown below) turns out to be suitable in this regard. Upon annealing the substrate to  $120^\circ\text{C}$  efficient chain formation is observed, cf. Fig. 3.14 (b). Furthermore, from STM images it can clearly be seen that the substituents perpendicular to the long axis remain intact and the smaller lobes associated with the bromine withstand the heating step. The chains are found to assemble into ordered islands interlocking their side groups as shown in Fig. 3.11 (d). Note that the gaps that form between the bromophenyl groups of neighboring chains are filled with two lobes each that could be caused by the iodine atoms that are expected to remain on the surface at the employed temperatures. The different nature of the intramolecular bonds

stabilizing the chains and the intermolecular interaction leading to island formation can be seen from spectroscopy and manipulation (cf. below).

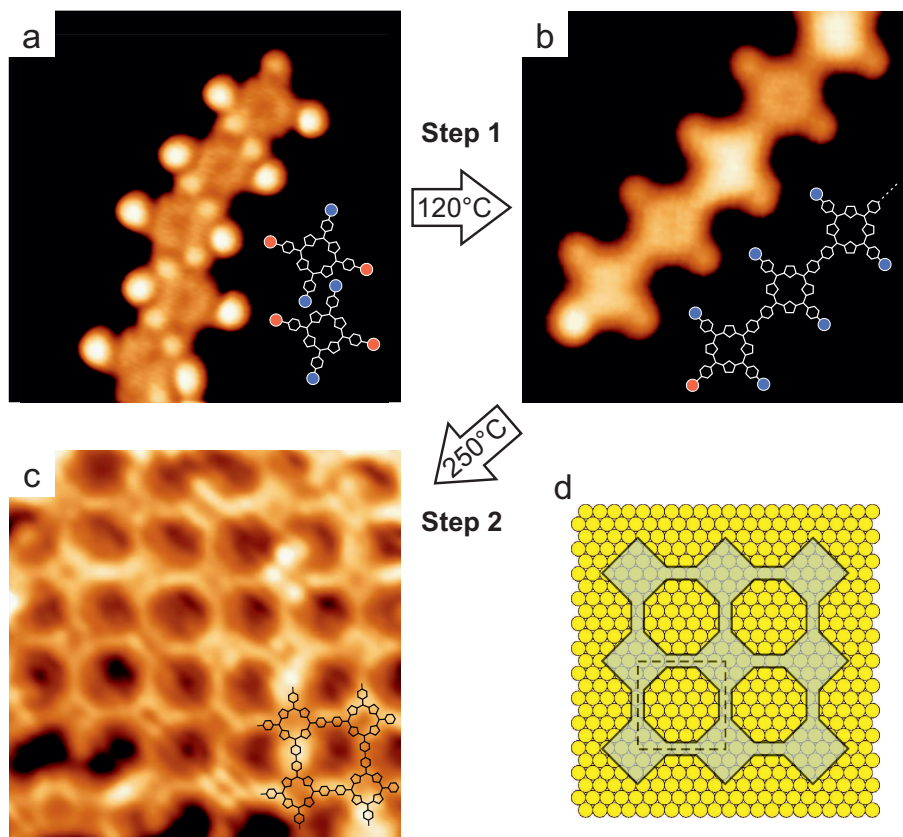


**Figure 3.14:** STM images of  $\text{Br}_2\text{I}_2\text{TPP}$  on  $\text{Au}(111)$ , (a) after deposition onto the sample cooled to 80 K, (b) after heating to 120 °C and (c) after heating to 250 °C. The corresponding chemical structures are indicated. Images (a) and (b) sized  $8 \times 8 \text{ nm}^2$ ; (c) imaged at 180 °C and sized  $10 \times 10 \text{ nm}^2$ ; (d) sketch of a porphyrin network with the underlying surface atoms (same scale).

In the previous study [55] a characteristic resonance was observed at 3 eV above the Fermi energy located directly and exclusively at the position of the connection point between two porphyrins. Theoretical calculation revealed that this peak is associated with a covalent bond which gives rise to an interaction between the  $\pi$  orbitals of the coupled phenyl rings and does not agree with any other type of intermolecular interaction. Thus, it represents a convenient fingerprint for the covalent nature of the formed bonds as it can be probed locally for individual molecules by STM spectroscopy. The same fingerprint was observed on the interconnected  $\text{Br}_2\text{I}_2\text{TPP}$  molecules, where it is visualized by bias-dependent imaging (Fig. 3.15). The similarity with the previously studied  $\text{Br}_n\text{TPP}$  molecules (the 'n' denotes the different number of substituted bromine atoms) confirms the existence of identical intramolecular bonds in the present case. While connected molecules appear in homogeneous contrast at low bias voltages, bright protrusions become visible at the connecting bridge if the bias voltage is raised to 3 V (marked by an arrow in Fig. 3.15).

Further indication of covalent linking is obtained by lateral manipulation. Fig. 3.16 shows an excerpt of a series of STM images that document the tip-induced modifications that were induced in between their recording. To that end after completion of each image the tip is brought into

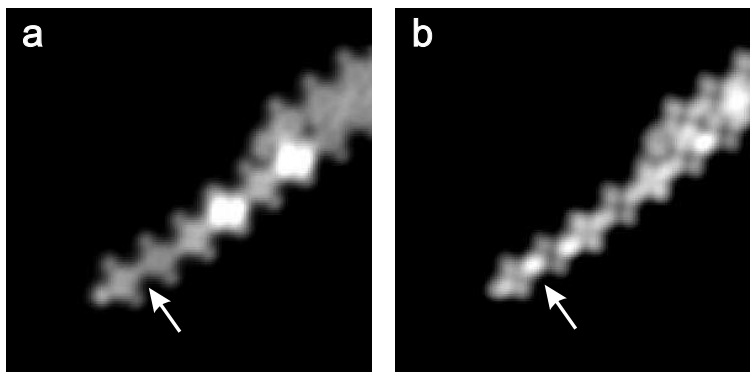


**Figure 3.15:** STM images of molecular chains formed by heating the Au(111) sample prepared with  $\text{Br}_2\text{I}_2\text{TPP}$  precursors to  $120^\circ\text{C}$  for 5 min. (a) and (b) show the same area at a bias voltage of 1 V and 3 V, respectively and a tunneling current of 0.1 nA. Image size  $15 \times 15 \text{ nm}^2$ . The arrow indicates a bond position that appears as a protrusion in (b).

closer contact and instructed to follow the path indicated by the arrow. It is seen that the targeted chain can be progressively peeled off the island that it is attached to on the left side. Like in this example, islands can generally be divided easily into separate chains, whereas the separation of a chain into segments was never observed. Thus, Fig. 3.16 highlights the difference between strong intramolecular coupling and the weak intermolecular interaction inside the islands. By performing vertical manipulation it was moreover possible to extract a single chain from the inside of a close-packed assembly, leaving behind a jigsaw puzzle piece like gap in the island (cf. Fig. 3.17 (a)). To that end the tip was brought rather forcefully into contact with the island that was intact prior to the manipulation. Upon retraction the tip left behind the small crash site indicated by the arrow. Furthermore, it also removed a chain from the previously close-packed island. As shown for the wires made of poly-terfluorene (cf. ch. 2.1.1) only a strong, i.e. covalent interaction can reasonably be responsible for the vertical removal of such a structure. Analogously to those conductance measurements, this renders the poly-TPP chains applicable for pulling experiments [56]. Both lateral and vertical manipulation is facilitated by the flexibility of the chains, which is reflected in the readily inducible curvature visible in the images of Fig. 3.16.

The molecular flexibility furthermore gives rise to a wagging motion which is sometimes observed even if the temporal resolution of image recording is not sufficient to resolve such a dynamic process (e.g. the rotation of molecules at surfaces [183]). However, a whole molecular chain performing a pendulum-like oscillation has not been observed in STM so far. This is what is sometimes found for TPP-chains with one end connected (e.g. to a larger network) while the other end is free to move over the surface. In that case, we observed a wagging motion that cannot be resolved down to 10 s per frame. Consequently, we observe the envelope of the motion, as shown in Fig. 3.22 (a). Their appearance becomes more frequent in images taken at higher temperature, as the surface diffusion is thermally activated.

For the verification of the growth process, the second coupling step remains to be demonstrated starting from the islands shown in Fig. 3.14 (b). As mentioned above the formation of chains is facilitated virtually defect-free. Thus, it is an ideal starting point for the initiation of two-

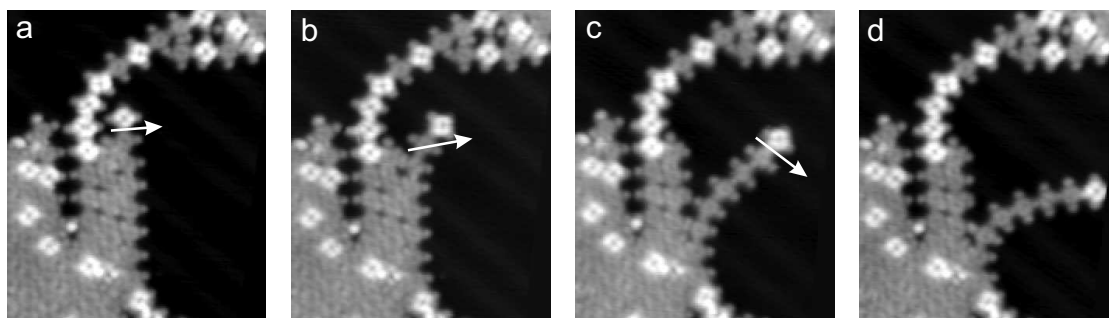


**Figure 3.16:** Series of STM images taken between lateral manipulation with the STM tip. Image size  $20 \times 24 \text{ nm}^2$ , scanning parameters 1 V, 0.1 nA, manipulation parameters 20 mV, 20 nA, during manipulation the tip follows the path indicated by the arrow (after completion of the image).

dimensional network growth. From temperature dependent STM measurements we could determine the temperature threshold for the activation of the brominated substituents which lies at  $200 \text{ }^\circ\text{C}$ , i.e. comfortably above the temperature range relevant for the deprotection of the iodinated side groups. Upon raising the sample temperature above this value, extended porphyrin networks were observed, as shown in Fig. 3.14(c) (cf. Fig. 3.19 (a) for an overview image). The sample temperature was usually increased to and for five minutes held at  $250 \text{ }^\circ\text{C}$  to induce efficient activation and coupling. The observations therefore cover the entire polymerization process, starting from the monomer building blocks, via the intermediate one-dimensional chains, towards the completely interconnected architecture marking the reaction's final product. It therefore constitutes the first realization of a hierarchical covalent coupling process at a surface and the observation of all of its reaction stages. The networks are porous structures as shown in the sketch of Fig. 3.14 (d). The unit cell of  $17.6 \times 17.6 \text{ \AA}^2$  contains approx. 43 gold atoms, of which roughly 30 atoms are covered by the network, leaving 13 atoms exposed (estimate based on STM images which depends on the tip condition). These structures could therefore potentially be employed as templates for other species, e.g.  $\text{C}_{60}$  as used in the work of Blunt et al. [170].

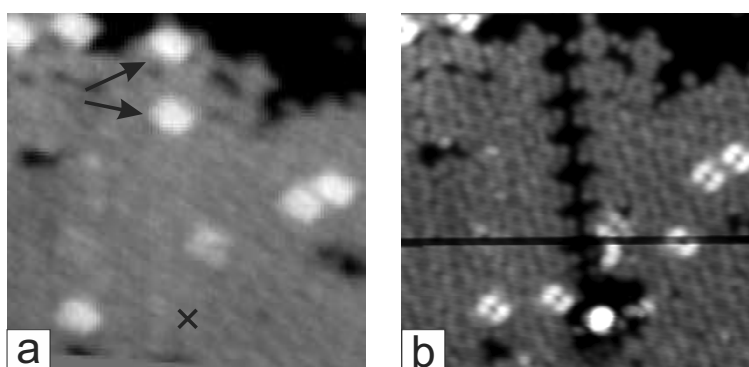


**Figure 3.17:** STM images of an island of porphyrin chains taken (a) before and (b) after the tip was brought into contact at the position indicated by the x. Images sized  $17 \times 17 \text{ nm}^2$ , feedback parameters 1 V, 0.1 nA. Despite the low resolution in (a) the pattern of bright molecules is visible; two of them belong to the chain that is removed by the tip (marked by the arrows).

It is immediately obvious that the network structure is less dense than the close-packed islands of chains. Therefore, sub-monolayer coverages are employed to allow an unhindered two-

dimensional coupling. With these results we have access to the same architectures, i.e. two-dimensional porphyrin networks, via two different paths, one produced through the non-specific, one-step reaction [55] employing the monomers solely equipped with brominated substituents and the other stemming from the hierarchical approach described above. This allows a quantitative comparison.

### 3.2.1 Thermal desorption spectroscopy

To further elucidate the polymerization process, thermal desorption spectroscopy (TDS) measurements were performed to complement the investigation using VT-STM. To observe the halogen dissociation steps, the masses corresponding to bromine and iodine (plus some control masses) were monitored (test mass: 76 - 78; Br: 79; HBr: 80; I: 127; HI: 128). To that end, a Au(111) sample was prepared with Br<sub>2</sub>I<sub>2</sub>TPP at sub-monolayer coverage, placed directly in front of the QMS at a distance of approx. 3 cm and heated while recording the spectra. The increase of temperature was controlled manually and the temperature increased at approx. 20 K/min. Representative results are shown in Fig. 3.18.

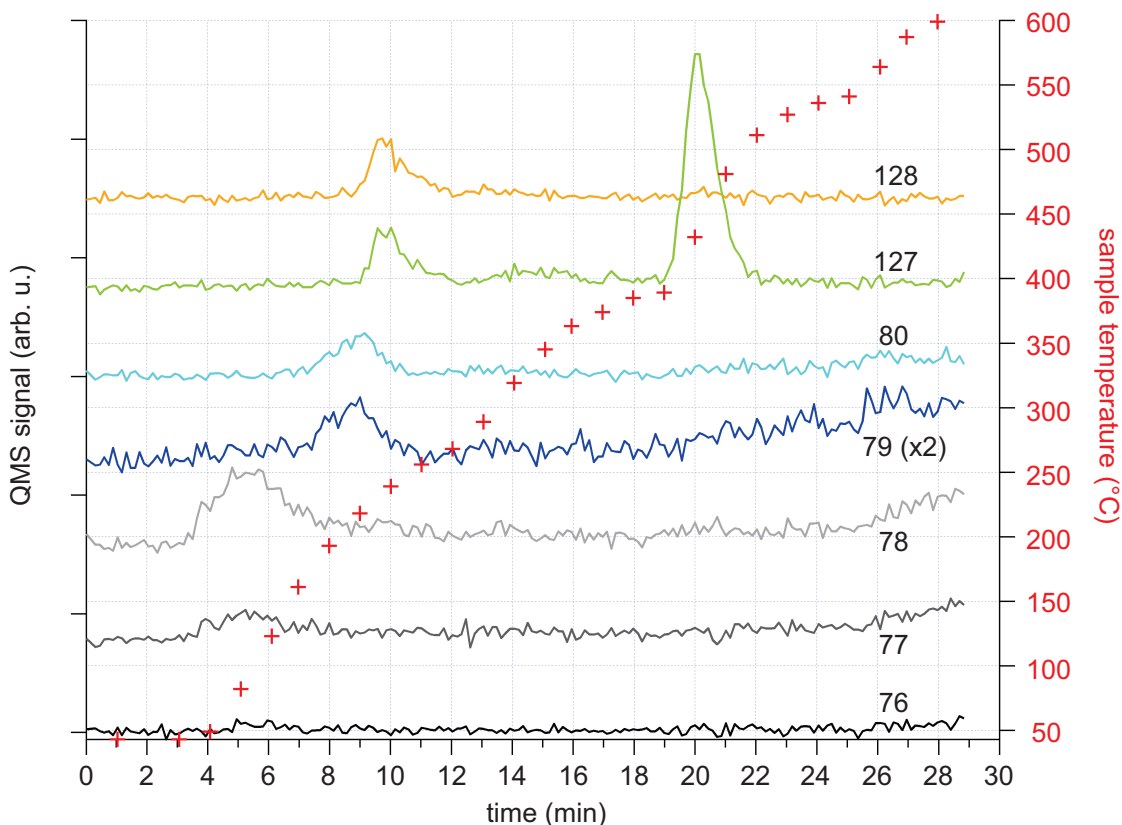


**Figure 3.18:** TDS signals of Br<sub>2</sub>I<sub>2</sub>TPP on a Au(111) sample. The recorded masses are indicated next to the traces; traces are offset vertically for better visibility. The temperature is indicated by the red markers and axis to the right. The temperature curve was controlled manually and therefore appears slightly wavy. The data is not corrected for spectrometer sensitivity and molecular ionization cross-section.

In the interpretation of the data, different processes have to be distinguished that can cause peaks in the curves. (1) Halogens are dissociated and immediately leave the sample, (2) previously dissociated halogens that stayed attached to the surface desorb at higher temperature, (3) cracking patterns: fragments of the molecules desorb and are dissociated in the QMS and (4) regurgitation and wall displacement effects [184]: gases pumped by the ion getter pump can lead to the detection of other species that are released from the pump by reaction and displacement processes.

The bromine trace (79) shows one clear peak at around 200 °C, whereas the iodine one (127) shows two, at around 230 °C and another at 430 °C. The detection of bromine coincides with the second activation step of Br<sub>2</sub>I<sub>2</sub>TPP (process 1) and thus corroborates the interpretation from STM. The iodine on the other hand is known to adsorb to the gold after dissociation and leave the Au(111) surface at around 680 K (type 2) [180], which agrees well with the second I desorption peak. The origin of the first peak however is unclear. If the signal was caused by the direct desorption after dissociation, one would expect an earlier occurrence, as substantial dissociation is already observed at 120 °C in STM. To exclude the possibility that the peak is caused by fragments other than the iodine, the experiment was repeated by the porphyrin with four bromine atoms (Br<sub>4</sub>TPP), which displayed no signal at all at m=127/128. In this way, a displacement effect by the bromine (that desorbs slightly before the first iodine peak) could be excluded as well. Therefore, both peaks can be identified with the iodine. Performing TDS on a clean Au(111) sample showed a flat trace at all observed masses. Upon sublimation of the molecules from the evaporator, molecules will likely also cover the sample holder next to the gold sample that is also heated during the desorption experiments. To exclude the possibility that the signal originates from molecular fragments that desorb from the sample holder, a tantalum plate (without sample) was dosed with Br<sub>2</sub>I<sub>2</sub>TPP. No peaks were observed in the subsequently recorded TDS spectra at m=127/128. Another cause for the first iodine peak might be desorption of the activated porphyrin after bromine dissociation. However, other fragments such as phenyl are not observed at the same temperature. Thus, while the TDS signal of the Br<sub>2</sub>I<sub>2</sub>TPP corroborates the proposed activation process, the first iodine peak requires further investigation.

### 3.2.2 Network size

To judge the influence of sequential activation and substrate-directed diffusion on the quality of the networks, it is necessary to quantify the network size of a given preparation. This task requires a statistical analysis of the networks, i.e. to determine the number of building blocks in each network. We have presented such an evaluation for the case of chains made of poly-terfluorene. In the investigation at hand the matter is complicated by the growth in two directions and the fact that building blocks can remain in place even without the realization of all intended reaction partners. Thus, a definition is needed of what is considered a network. Simply counting all connected monomers is not sufficient, because the objective of the Br<sub>2</sub>I<sub>2</sub>TPP molecules is to form *two-dimensional* architectures realizing all possible interconnections, i.e. up to four at each building block. However, while the molecules are found to assemble in networks that are spanning the entirety of terraces, the size of regular sections is generally limited by two types of defects:

Missing and incorrectly formed bonds. The former is caused by bonds that are not realized (see Fig. 3.20 (b)) or missing monomer building blocks (e), whereas the latter originates from the different conformations of the porphyrin monomers (c) and/or bending/mismatch of the net (f). This kind of defect is intrinsic to the growth mechanism and caused by the flexibility of the monomers. Similarly, Porte et al. [182] observed the appearance of polygons ranging from squares to nonagons with only about 30% of the pores exhibiting the hexagonal structure lowest in energy for networks made of phenyl and boroxine rings. The fact that the distribution of polygons did not respond to attempts to optimize the reaction conditions led them to the assumption that the system is close to equilibrium and that these kinds of defects cannot be avoided. DFT calculations performed for the structurally similar benzenediboronic acid by the same group [185] revealed that introducing stress into the pores (going from hexagons to pentagons or heptagons) is associated with only a small energy penalty. Note that an STM image containing triangular and pentagonal defects, sketched in (c) and (f), respectively, is presented in Fig. 3.19 (b).

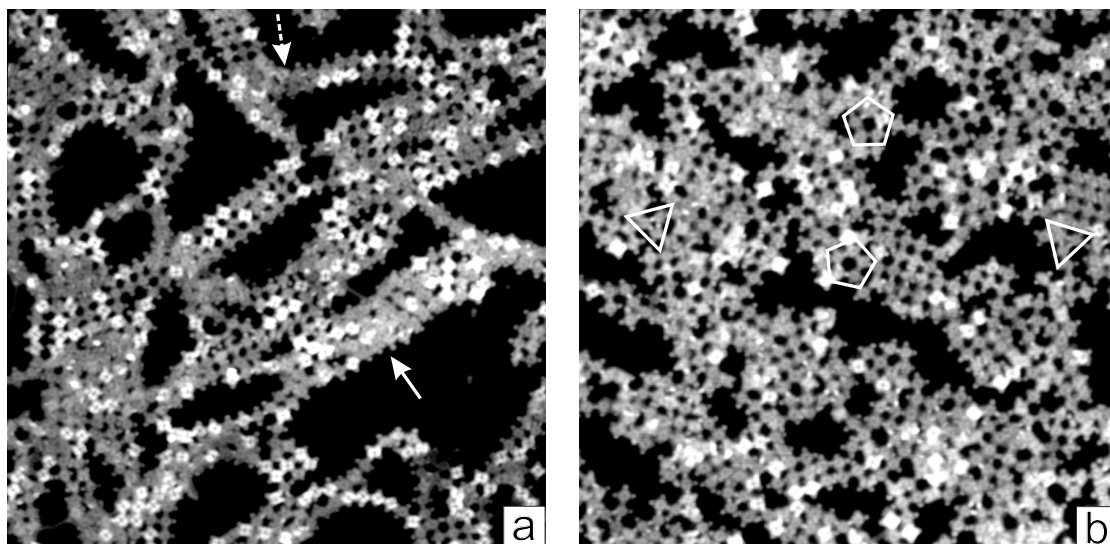


**Figure 3.19:** LT-STM images of (a)  $\text{Br}_2\text{I}_2\text{TPP}$  molecules and (b)  $\text{Br}_4\text{TPP}$  molecules on a Au(111) sample that was heated to 250 °C for 5 min. Parameters for both images: size  $62.5 \times 62.5 \text{ nm}^2$ , feedback parameters: 1 V, 0.1 nA. Defects as indicated by arrows and shapes discussed in the text.

In this study, we define two counting conditions:

- 1) Each molecule in a network must be part of a  $2 \times 2$  square sub-unit to be considered. For instance, Fig. 3.20 (a) shows a case where all connected building blocks are counted. On the contrary, only 6 molecules of the network are considered in (e), because (1) is not fulfilled by the two molecules attached at the left.
- 2) A molecule is only counted, if all possible bonds to the super-network are realized. This is why in Fig. 3.20 (d) two monomers are disqualified.

It is important to note that the determination of network sizes can be complicated by a low resolution of the STM images. An example is highlighted in Fig. 3.19 (a) by the solid arrow. The locally reduced contrast is likely caused by iodine adatoms filling the networks' pores. Fur-

thermore, networks that leave the boundaries of an image have to be disregarded. Consequently, we considered only such networks for the statistical analysis that are imaged with intact bonds and porphyrin cores at low bias voltage.

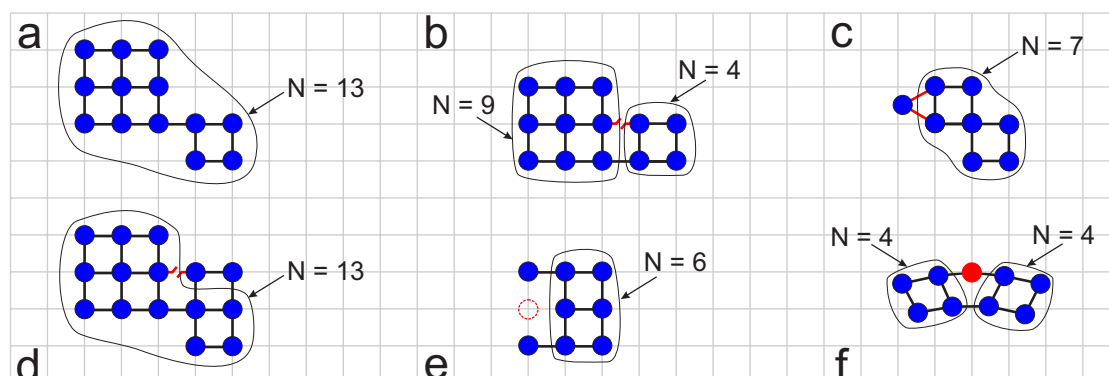


**Figure 3.20:** Models of networks formed by  $\text{Br}_2\text{I}_2\text{TPP}$  molecules.  $N$  indicates the number of monomers counted for a given network (contained by the line). (b-f) exemplify the types of defects that limit a network's size. If there are different possibilities to count, the biggest network is selected, for instance  $N=13$  in (d).

One could be tempted to try to visualize the interconnection of the building blocks using the above-mentioned technique of imaging at a 3 V bias to detect the empty orbital associated with the covalent bond. While this is certainly a possibility for individual (small) chains and networks, fast scanning at a high bias is likely to induce changes to both the sample and the tip, leading to loss of resolution. Another option might be to employ automatic image analysis methods. However, because in our case the differences in appearance are quite minute and a judgment of a bond requires several factors such as geometry, the assessment of a program would introduce too large an error in the counting procedure.

The results of the counting are presented in Fig. 3.21. Although the networks in all cases are highly interconnected (meaning that isolated segments are rarely encountered), most of the monomers are found in regular structures of  $2 \times 2$ . However, it can be seen that the network size distribution of the  $\text{Br}_2\text{I}_2\text{TPP}$  preparation (b) decreases more slowly than the  $\text{Br}_4\text{TPP}$  one (a). That means that for the former a bigger number of building blocks is found in larger networks. Therefore, it can be concluded that the hierarchical process has an ordering influence on the network formation, resulting in a higher degree of regularity. For instance, the number of triangular defects is reduced approximately by a factor 3 with regard to networks formed by the one-step process.

Thus, this conceptual approach can be utilized to enhance the regularity of the produced networks. In networks formed from the one-step-connecting  $\text{Br}_4\text{TPP}$  non-orthogonal links are frequently observed, forming local structures such as triangles or pentagons (cf. Fig. 3.19 (b)). These are intrinsic defects and originate from the flexibility and different possible conformations of the precursor molecules and the low barrier of the connection reaction. For instance, if a building block that is already attached to some network structure connects to another unit (with one of its remaining reactive sites) while the unit twists away from its minimal potential energy

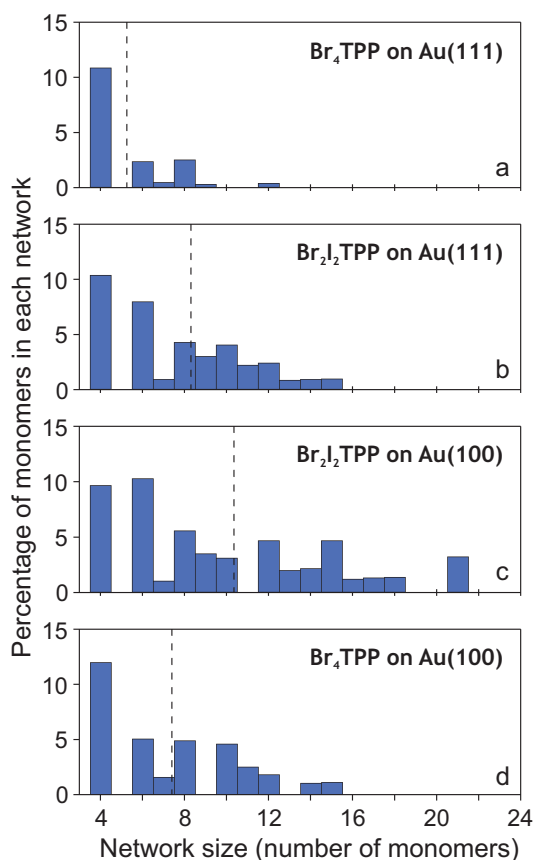


**Figure 3.21:** Size distribution for hierarchical and non-hierarchical growth [179]. Histograms of the network size are shown for Br<sub>2</sub>I<sub>2</sub>TPP and Br<sub>4</sub>TPP on Au(111) and Au(100) respectively. The column height reflects the fraction of monomers that are part of a network size indicated on the bottom axis. Vertical dashed lines denote average network sizes. Total number of monomers, defining 100% (including non-regular structures and monomers) is  $\approx 1200$  in each case.

position, then the resulting structure can deviate from the ideal square geometry (cf. Fig. 3.20 (c) and (f)). Such defects can perpetuate themselves, because they lead to further mismatch, leaving activated building blocks in the vicinity of the defect without a reaction partner. Thus, the regularity decreases and the network size is lowered. Due to the nonreversible nature of the coupling the possibility for self-repair, which is a key feature for structures formed by molecular self-assembly, is prohibited.

By following our strategy of hierarchical growth an improved regularity is obtained as the network formation is separated into two consecutive steps. One advantage lies in the fact that the formation of linear chains takes place virtually defect-free. Therefore, when the dissociation of iodine substituents leads to the formation of linear porphyrin chains with intact bromine-protected groups pointing sideways, these chains can be regarded as the second growth step's starting monomers. These 'monomers' of course are so large that they could not be deposited onto the sample surface intact by thermal evaporation [186]. However, from STM images one can observe another important factor which also contributes to improved network regularity: The covalently bound chains favor the agglomeration to islands in which they are arranged in

a parallel fashion, cf. Fig. 3.11 (d). The equidistant side groups interlock, resembling gears. In this arrangement the distance between neighboring chains is minimized. This is the starting point for the second step, the dissociation of the bromine atoms and a connection of the chains to networks. The parallel and one-on-one pre-arrangement of the potentially reactive sites leads to a further reduction of defects.

One can imagine this effect to work similar to a zipping-mechanism (as sketched in Fig.3.22 (b)): when the reaction starts at a given point along the chain, all the other connection points are already perfectly aligned, while the incorporation in a linear structure reduces the individual unit's inclination for twisting.

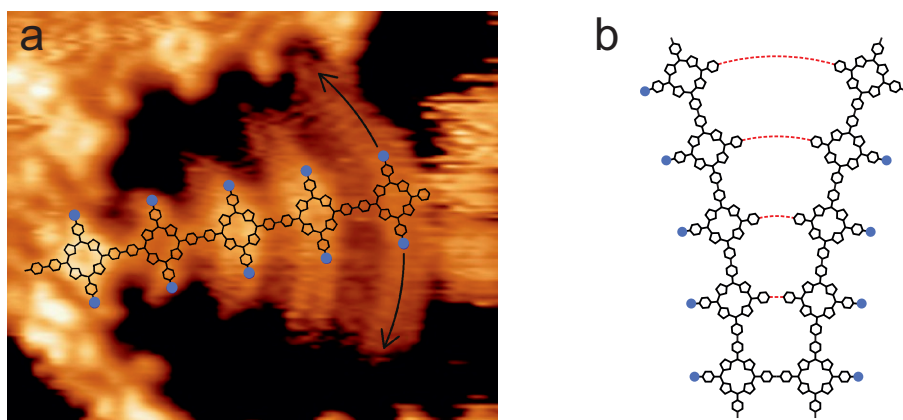


**Figure 3.22:** (a) STM image of a chain fixed at the left side performing a wagging motion, image size  $10 \times 12 \text{ nm}^2$ , sample temperature  $90 \text{ }^\circ\text{C}$ . (b) tentative model of the zipping mechanism - the to-be-formed connections are indicated by the red lines.

However, there is one caveat: if these parallel running chains bend, which is frequently observed when they become longer, then this can again cause mismatch. If the bending becomes too strong, the matching between convex and concave faces can be disturbed. An example is indicated by the dashed arrow in Fig. 3.19 (a). This can then lead to the formation of pentagons as shown in Fig.3.20 (f). This effect can be reduced by keeping the chains straight. One could imagine to employ more rigid building blocks. This would however constitute a restriction for properties of the monomers. A more elegant solution would be the directing influence of the surface, which is discussed in the next section.

### 3.2.3 Substrate-directed growth

As outlined above, employing a hierarchical process allows to program the system to move along a given reaction path that proceeds via intermediate products. The possibility of influencing these intermediates offers another attractive control mechanism. One could e.g. think about letting the system evolve into different directions by applying external stimuli. The influence of the arrangement of the intermediates has already been mentioned above. Thus, an auto-templating effect has been observed, i.e. the spontaneous alignment of the first stage products - the chains - before the start of the second growth step. However, on a Au(111) surface this prealignment lacks a clear directional preference and it is probably of diminished effect at higher temperatures.

A deliberate and controlled prearrangement of the intermediate is therefore a desirable goal. To that end, the interaction of the surface with the molecules was employed.

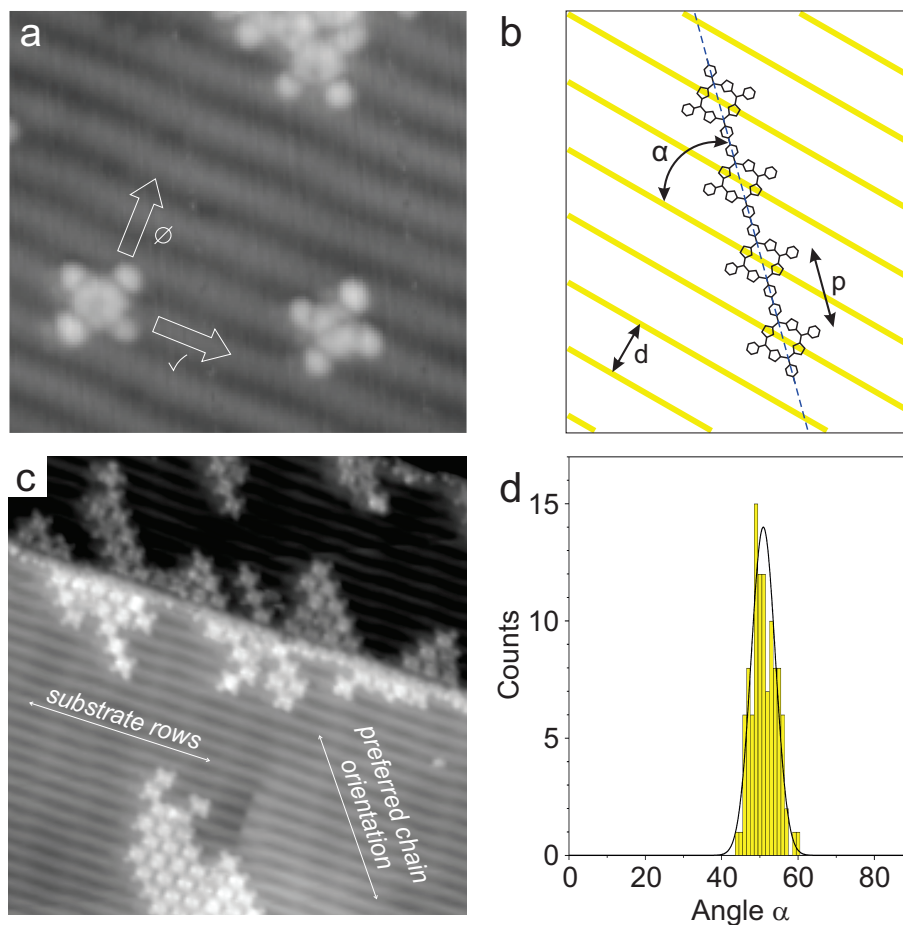


**Figure 3.23:** Steering the polymerization using a corrugated surface [179]. (a) STM image of non-activated  $\text{Br}_2\text{I}_2\text{TPP}$ ,  $12 \times 13 \text{ nm}^2$ , the arrows denote the directions of high and low diffusion barrier. (b) Model of the adsorption of a chain with the monomers atop the rows. (c) STM image showing the characteristic alignment of the porphyrin chains after the first step,  $42 \times 42 \text{ nm}^2$ , (d) angular distribution for 100 chains as shown in (c).

Until now, the gold substrate has been used as a support, confining the motion and orientation of the porphyrins to 2D, and acting as a catalyst for the halogen dissociation. However, the surface can also exert a directing influence. Specifically, structured surfaces constitute an attractive alternative to the relatively flat Au(111) that can be employed for templated growth of molecular structures. If one wanted to remain on one specific low-index plane, one has the possibility to introduce corrugation by utilizing surfaces vicinal to it, which is effectively the same crystal face separated by step edges. However in this case the corrugation is always identical to the height of the step edge. The diffusion barrier across step edges is rather high and the applicability for two-dimensional growth is questionable. Furthermore, the reduced size of the terraces leads to a reduced number of monomers available for polymerization, which in one case has resulted in rather short chains [116]. In one notable example network growth was observed to extend over step edges [151]. However, in this case non-covalent networks were investigated. While

the crossing of step edges is observed for chemically coupled arrays, e.g. for porphyrin chains, this is in contradiction with the notion of templating. In comparison with the vicinal surfaces of Au(111), the Au(100) face has favorable properties: the top layer atoms are arranged in a quasi-hexagonal pattern like the Au(111) and possesses a higher corrugation (ca. 0.4 Å). This is caused by a surface reconstruction forming linear stripes of elevated atoms in the  $[0\bar{1}1]$ -direction, cf. ch. 1.5. If the polymerization includes a heating step, this reconstruction has to remain stable up to the employed temperature, otherwise the templating effect is lost. In the Au(100) case the  $5\times 1$  reconstruction has been observed up until temperatures of 350 °C using LEED [187]. This is much higher than the 200 °C temperature threshold needed for the activation of the brominated precursors.

After deposition onto Au(100), the  $\text{Br}_2\text{I}_2\text{TPP}$  monomers display the desired behavior as they preferentially adsorb atop of the rows, cf. Fig. 3.23 (a). Furthermore, from lateral manipulation it is found that the motion along the rails has a lower barrier than the one perpendicularly to it. This is reflected in the lower resistance (smaller tip-sample separation) needed to push a particular molecule across the corrugation. For a more quantitative evaluation a time- and temperature-dependent investigation would be necessary (cf. e.g. [31]). Thus the (100) face constitutes a new influence for the system while the polymerization is found to function as on the previous (111) surface. Indeed, by heating the sample to 120 °C the first reaction step is readily induced on this surface, yielding chains (cf. Fig. 3.23) and a further annealing to 200 °C efficiently produces two-dimensional networks (cf. Fig. 3.24).

Because of additional interactions that are present inside polymeric structures it is not *a priori* clear whether the adsorption behavior is still the same for the chains and networks. The monomer distance inside the chains is fixed, therefore they would have to rotate with respect to the rails to accommodate the preferred adsorption configuration. From a simple geometrical model, the chains would be expected to form a specific angle with the rails that would effect the atop-position for every monomer inside a (straight) chain. The  $d = 14.4$  Å separation of the rails and the  $p = 17.6$  Å distance of the porphyrin monomers calls for a  $\alpha = 55^\circ$  angle, as shown in Fig. 3.23 (b). This alignment is actually observed: Fig. 3.23 (c) shows the characteristic alignment of the porphyrin chains, that lie very straight and along a clear preferential direction, even when agglomerating in islands. Fig. 3.23 (d) displays the corresponding histogram compiling the orientation of 100 straight chains with respect to the surface rails, that shows a narrow distribution around an angle of  $51^\circ$ , which is close to the anticipated one (Fig. 3.23 (b)).

The requirement for the networks is more stringent with each monomer connected in two directions, considerably increasing the degree of interconnection. This would necessitate not only a particular orientation of the networks with respect to the underlying corrugation but also a deformation to obtain the favorable angle observed above for both edges of the array if each building block in the network were to adsorb in identical sites on the Au(100) rows, cf. Fig. 3.24 (a). Experimentally, this deformation is only observed for the smallest of networks ( $2\times 2$ ), whereas for larger assemblies the intramolecular interaction prevails and imposes a rectangular geometry on the architecture. This is shown in Fig. 3.24 (b) which displays a STM image of a larger network. The angle  $\beta$  is close to  $90^\circ$  which means that the registry of the monomers with the underlying rails is abandoned, most likely because the networks achieve an energetically favorable confor-

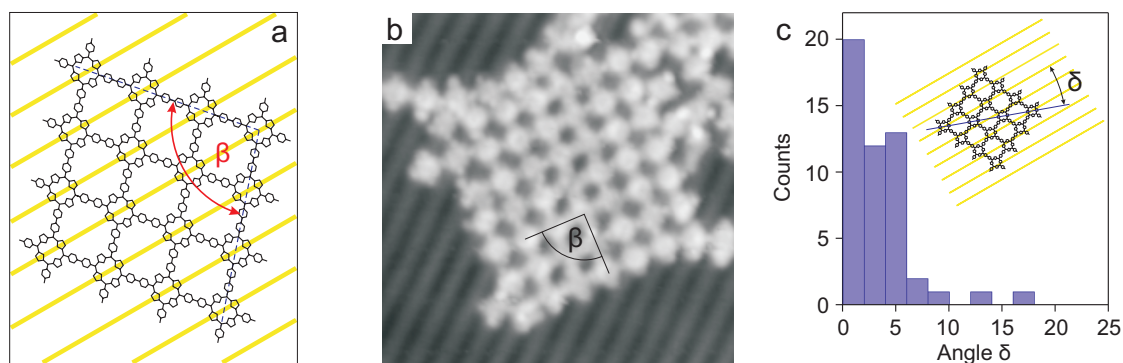


**Figure 3.24:** Porphyrin network on Au(100), (a) model of the network distorted to realize the on-top adsorption of every monomer; (b) STM image of a porphyrin network after the second activation step, feedback parameters 0.5 V, 0.1 nA, image size  $20 \times 20 \text{ nm}^2$ ; (c) histogram of the distribution of the angle between the gold rails and the network diagonal of 50 networks.

mation in the undistorted array. The preferential orientation of the networks remains, however, which is displayed in Fig. 3.24 (c): the networks are found to form an angle of approx.  $45^\circ$  with the surface rails.

Thus, we see a clear directing influence of the surface corrugation on the orientation and diffusion of the monomers and chains and the orientation of the networks. It is plausible that this could play an important role in processes that are facilitated by diffusion, especially the inter-connection of the chains. Since the bending and the more random orientation of the chains was found to promote disorder and defects in the structures grown on Au(111), employing the structured (100) face could be expected to improve network regularity. To put this to the test a network size distribution was compiled as for the networks grown on Au(111). The result shown in Fig. 3.21 (c) displays a clear tendency towards larger networks compared with histogram (b), corroborating this assumption. This improvement is a consequence of the positioning of the intermediates and therefore especially effective in the hierarchical linking process. To highlight this fact we performed the same experiment on Au(100) however employing the mono-functionalized  $\text{Br}_4\text{TPP}$ . While in the corresponding distribution a regularity-enhancing effect of the surface corrugation is also visible, cf. Fig. 3.21 (d), the distribution is clearly surpassed by the  $\text{Br}_2\text{I}_2\text{TPP}$  one. (Actually the mean network size of  $\text{Br}_2\text{I}_2\text{TPP}$  is larger on either surface).

### 3.2.4 Formation of co-polymers

So far the hierarchical approach has been used to increase the regularity of the products. The directing influence through the separation of the reaction into different steps was discussed in the last section. A greater potential of the process however lies in the controlled formation of more sophisticated structures that are not accessible by a non-hierarchical approach. To demonstrate this effect, the formation of a copolymer consisting of two components was attempted.  $\text{Br}_2\text{I}_2\text{TPP}$  was deposited onto Au(111) together with DBTF (cf. Fig. 3.25 (c)) to produce a 2D network structure. If the sample is cooled during evaporation, both species are initially non-activated. Ideally, heating the sample would lead first to a formation of linear chains of porphyrins anal-

ogously to the process described above. Since the porphyrins' side groups and the ends of the terfluorene molecules are protected by bromine atoms, they would both stay intact at this first stage and not participate in the reaction. Only in a second step, i.e. upon heating up to at least 200 °C would those groups then be deprotected and perform coupling. Such a combination of molecules has not been investigated before, therefore it is not *a priori* clear whether it would actually link or rather lead to separate block polymers (or rather networks and wires). A considerable reduction in the linking probability between different compounds is conceivable and might even be prohibited for steric reasons. This would be detrimental for the generality of the approach.

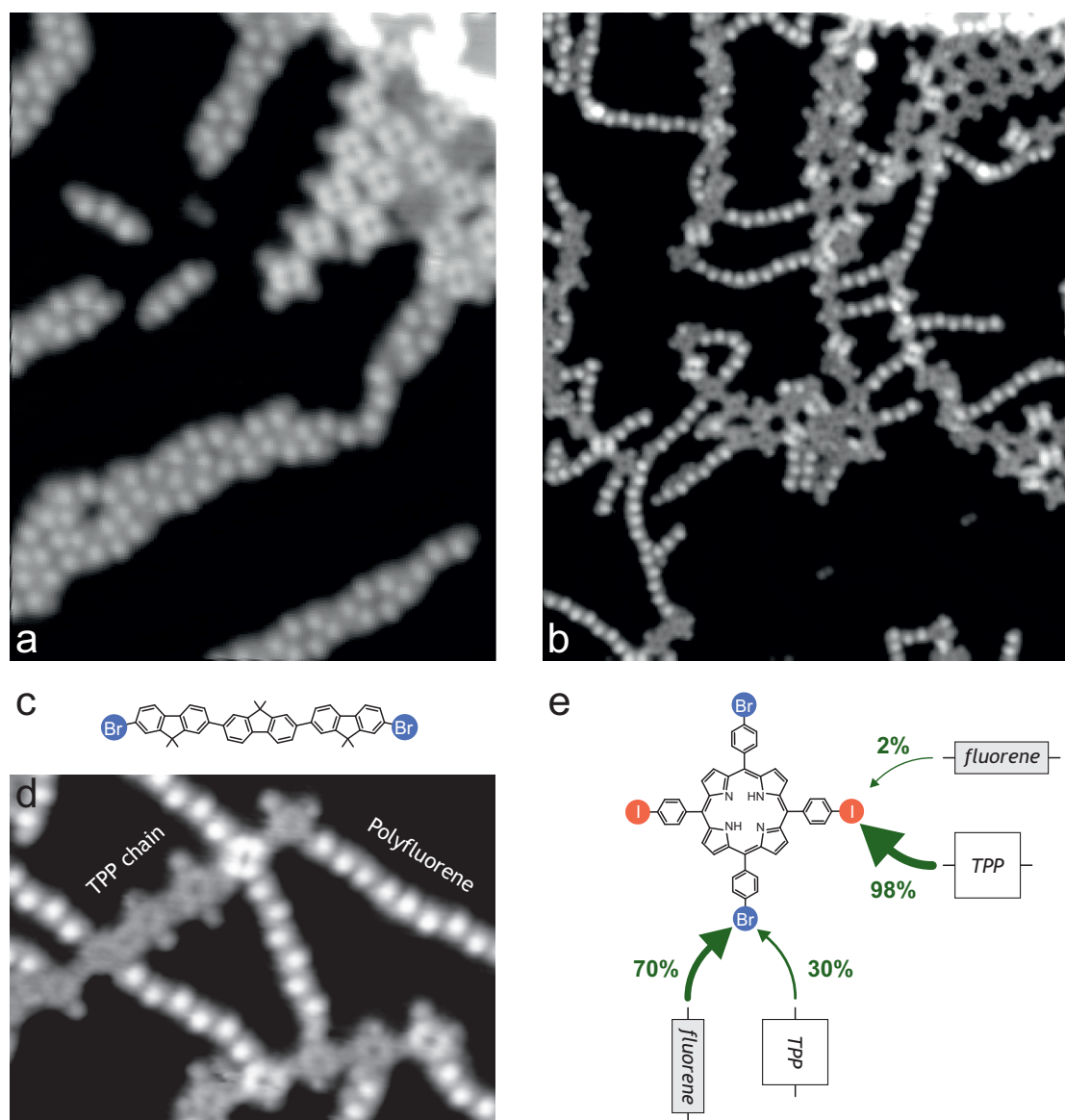


**Figure 3.25:** Copolymers by hierarchical growth [179]. (a) STM image of  $Br_2I_2TPP$  together with DBTF deposited onto Au(111) at 50 °C,  $18 \times 24 \text{ nm}^2$ , (b) STM image of the same sample after a heating step to 250 °C,  $33 \times 40 \text{ nm}^2$ , (c) chemical structure of DBTF, (d) high-res STM image of the copolymers,  $13 \times 18 \text{ nm}^2$ , (e) analysis of the porphyrin and fluorene attachment to the porphyrin binding sites (number of porphyrin sites  $n_I = 489$ ,  $n_{Br} = 269$ )

Fig. 3.25 (a) shows the two types of molecules after deposition onto Au(111) at 50 °C. While the porphyrins are observed to form short covalent chains (upper right corner) in accordance with the results presented above, the DBTF molecules are found non-activated and arranged in weakly bound islands (as confirmed by lateral manipulation - the two monomers in the top left of the image have been detached from the island with the tip). It was found that an efficient coupling is induced upon heating of the sample to 250 °C. The two different molecules intermix, leading to chains of porphyrins perpendicularly interconnected by wires of oligo-terfluorenes, as shown in Fig. 3.25 (b) and (d). Thus, they effectively form a ladder structure. An analysis of the connection highlights the high selectivity of the process, cf. Fig. 3.25 (e). Only a very small number of fluorenes is found to connect to the long axis of the porphyrin chains (and exclusively at the ends), whereas most of them attach to the previously bromine-functionalized legs. On the other hand, the larger part of the porphyrin building blocks are found in chain structures, while coupling of adjacent chains to 2D-networks leads to a 30% connection during the second stage (an example is shown in the upper right corner in (b)). This however does not affect the selectivity of the cross-coupling.

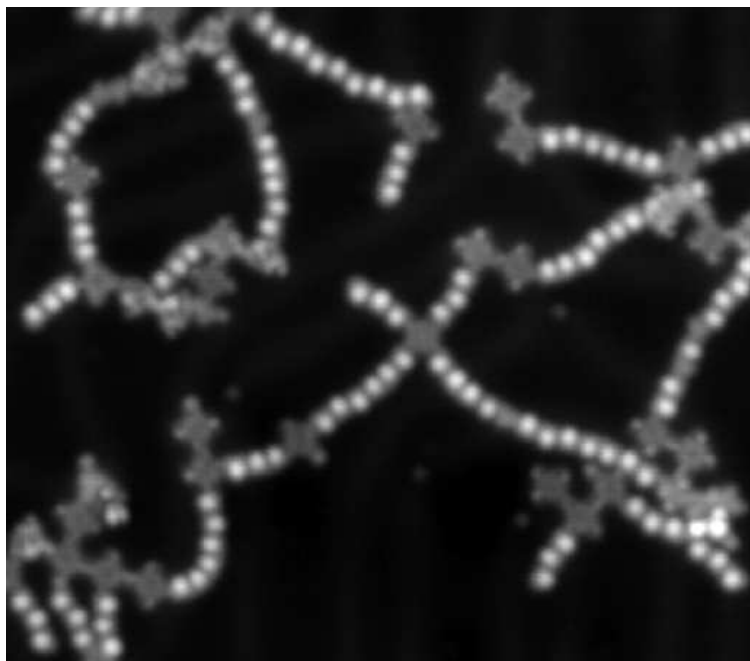


**Figure 3.26:** STM image of a copolymer formed from Br<sub>4</sub>TPP and DBTF by heating the Au(111) sample to 250 °C for 5 min. Image size 27 × 31 nm<sup>2</sup>.

To contrast these results we performed the same experiment via a non-hierarchical pathway using the Br<sub>4</sub>TPP molecule together with DBTF. Due to the simultaneous activation of all protected groups, random structures are observed in the STM images, cf. Fig. 3.26. These results underline the potential of the hierarchical process and are very encouraging for the controlled incorporation of functional units. They pave the way for the fabrication of more complex architectures.

To complete the above investigation copolymer formation was attempted on the corrugated Au(100) surface. In this case the corrugation is also found to influence the polymerization. While no extended islands are observed for the weakly bound monomers (Fig. 3.27 (a)), after heating the

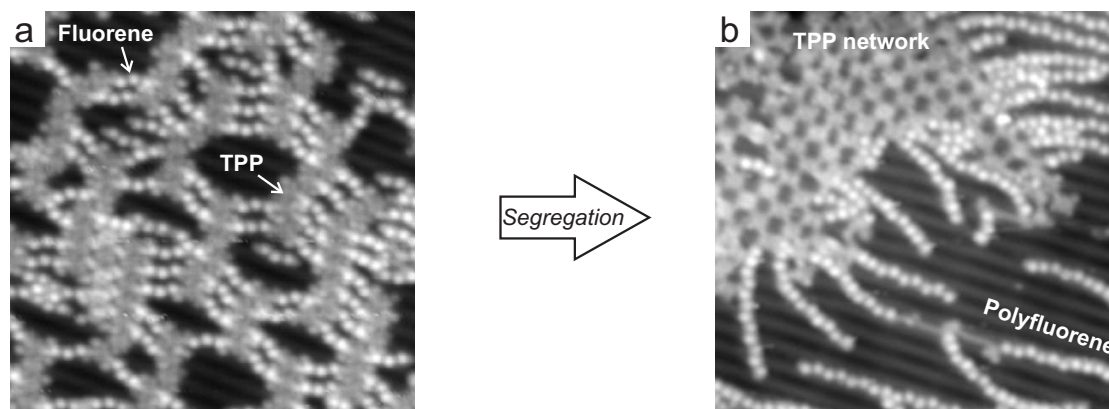


**Figure 3.27:** STM images of Au(100) prepared with a mixture of Br<sub>2</sub>I<sub>2</sub>TPP and DBTF [179]. (a) before and (b) after heating the sample to 250 °C. Both images sized 32 × 32 nm<sup>2</sup>.

two different molecules are found connected but with a rather low degree of mixing (Fig. 3.27 (b)). Starting from the mixed phase, this result is rather surprising. It hints at an efficient formation of islands made of porphyrin chains into which only a small number of terfluorenes are diffusing prior to the second heating step. A further elucidation of the dependence of the resulting architectures on the preparation parameters would be highly interesting and might lead to the possibility to steer the products into different directions.

### 3.3 Conclusion

In conclusion, a hierarchical approach has for the first time been realized and investigated for the covalent coupling of organic molecules on a surface under UHV conditions. Employing different halogen atoms in the monomers, stepwise activation of reactive sites could be demonstrated through their selective dissociation, which provides a new element of control of the polymerization. Using scanning tunneling microscopy both at cryogenic and at elevated temperature, the entire process could be monitored from the intact monomers via the one-dimensional chains to the two-dimensional network structures.

Building on these results the approach was employed to tackle two important challenges that exist for surface-confined polymerization: (1) Covalent networks formed at surfaces have been characterized by low regularity and a high number of defects. This is due to the fact that because of the non-reversibility of the coupling, the structures cannot perform error-correction as is possible in molecular self-assembly. (2) The architectures produced so far display a low level of complexity, mostly consisting of a single molecular component or in the case of complementary linking groups of a strict alternation. However, aiming for the fabrication of functional structures, e.g. by utilization of molecular switches, a controlled and selective integration is required. These issues, that are both a consequence of the one-step linking approach that has been exclusively employed in previous studies, could be successfully addressed by employing hierarchical synthesis.

Experiments showed that the polymer networks formed from the stepwise process were enhanced considerably with regard to the size and regularity, which was revealed by the direct comparison

of equivalent porphyrin networks formed by the hierarchical and non-hierarchical process. The origin of the improved interconnection could be identified as the low-defect coupling of the chain intermediates and their subsequent arrangement in islands of regular order which is conserved during the second coupling step and reflected in the two-dimensional structures. In addition to the adsorbate-adsorbate interaction it was demonstrated that the influence of the surface could be used to steer the coupling process by utilizing the reconstructed (100) face of gold, whose corrugation lines act as rails for the diffusion of porphyrin building blocks which leads to another improvement of the network quality. With regard to the directing influence, the hierarchical approach was put to the test by the covalent connection of two different species, terfluorene and porphyrin. After applying stepwise activation, STM images showed extended and intermixed copolymers. Importantly, an examination of the newly formed bonds revealed that binding did not take place randomly, but rather with a high degree of selectivity. The resulting structures are not accessible through the previous one-step processes, highlighting the potential of the new means of controlling the on-surface polymerization that has been demonstrated by the hierarchical approach.



## 4 Polymerization and isomerization of dithienylethene

This chapter is concerned with switches at surfaces and more specifically with molecular isomerization. In the introduction, examples from literature are discussed to highlight the relevant concepts and give an overview of the state of the art, before the molecule that is the subject of this study - dithienylethene - is introduced. The subject of the three following experimental sections is the characterization of the DTE monomers, their polymerization employing on-surface coupling and finally their manipulation, which includes attempts to induce their isomerization.

### 4.1 Introduction to molecular switches

Switches are components connected to an input and an output that can reversibly toggle a signal on and off depending on their state that can be set externally. The term is used in a more general way to denote systems that feature (at least) two meta-stable states (bistability) which can be changed reversibly by an external stimulus. A number of properties need to be considered to judge the usability of a particular switch whether it be a micro- or macroscopic system. Among those properties is the stability of the participating states. These have to be sufficiently stable and not revert back spontaneously to the other form. Another criterion is fatigue resistance, i.e. how many switching cycles a system can sustain. To employ a switch, the two states should possess features that substantially differ from one another to facilitate unambiguous read-out (ON/OFF-ratio). Moreover, it is mandatory that the state can be determined without its alteration, i.e. the reading process should be non-destructive and not induce switching. With application in mind, other issues are the reliability and directionality of the switching process and furthermore the addressability in case one is dealing with a collection of switching units. Examples of switches are numerous and a few examples will be compiled in the following (of course focussing on microscopic systems).

Switches are intensely studied in surface science. The prototypical switch is the field effect transistor found in great number in any electronic circuit. In transistors the physical quantity that is changed is the density of charge carriers. The state of the switch is read out by measuring the conductance across the junction (signal quantity). A similar effect has been observed for semiconducting nanowires, in which the adsorption of charged species to the surface can affect the conductance through the wire [71]. Interestingly, this doping can be rendered chemically sensitive by the selective binding of molecular species to the wire (thus constituting a sensor). Another technologically important example at surfaces encompassed in the broader definition of a switch are memory elements, realized e.g. by small areas of thin magnetic films. In these the system is toggled between different states that are represented by different stable direction of the magnetization. Thus, regions with up and down directions could constitute magnetic bits, 0 and 1, respectively. The orientation influences the electrical resistance which offers a method for read-out. Hard disk drives are commercially available today that feature a memory density of one terabit per square inch, which corresponds to an edge length per bit on the order of 25 nm. It is a current challenge to further reduce such structures' sizes to the length scale of atoms

and molecules for the realization of an even higher storage density. The capability of the STM to assemble and investigate structures made of individual atoms has facilitated the fabrication of a number of such structures at the nanometer scale. Notable examples include the vertical manipulation of a single atom [35], the change in bonding angle of Si surface atoms [188] and the lifting on In atoms in small indium chains on a InAs surface [189].

Rather than with atomic structures, this chapter will be concerned with small organic molecules. Molecular switches constitute an important class of compounds holding great potential as functional units, whose utilization could conceivably allow the realization of novel applications in areas such as molecular electronics, functional surfaces, data storage and sensing. Such expectations are based on their diverse and synthetically tunable properties [190]. An important such property is their ability for isomerization, which is the process of transforming one molecular species into another without altering the chemical composition. This can entail only geometric modifications through the rotation around chemical bonds, but also their rearrangement. Model systems and associated processes are provided by nature. One of the most relevant is probably retinal [191], which facilitates human vision through a *cis-trans* photoisomerization from 11-*cis*-retinal to the all-*trans*-retinal that induces a conformational change in a connected protein upon absorption of a photon. This in turn leads to a cascade of electrochemical signals that are transmitted via the optic nerve to the brain where the information is processed.

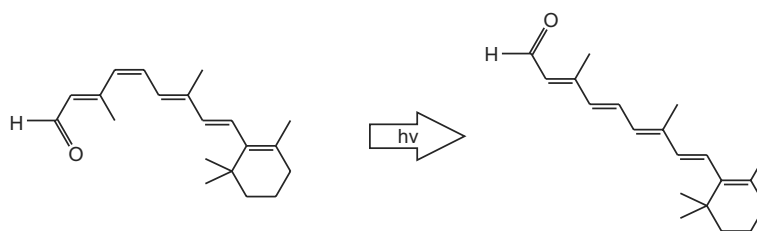


**Figure 4.1:** *Cis-trans* isomerization of retinal

Important for the characterization of a switch is the nature of the excitation and molecular states responsible for the isomerization, as well as that of the property employable for the read-out. Light, electric and magnetic fields, electrical current, heat and mechanical forces are among the stimuli available to induce the change from one state to the other [190]. Fig. 4.2 (a - c) shows a sketch of a bistable system featuring two potential minima separated by a barrier. In (a) the crossing is facilitated by climbing the vibrational states of the electronic ground state, e.g. by supplying thermal energy. In (b) the molecule is raised to an excited electronic level, e.g. by absorption of a photon of appropriate energy. It then evolves on the respective potential surface and if the life time of the excited state is long enough (solid line), it can transition to the other ground state minimum upon relaxation. In (c) the transition is facilitated by a deformation of the potential which can for instance be associated with an ionic state or caused by a strong electric field. The state can then be identified by observing the change in e.g. mechanical, electronic, optical or magnetic properties. The description of a switch mentions first the excitation, such as photo- or electro-, followed by either the nature of the induced change, e.g. -chemical or -mechanical or that of the feature used for read-out, e.g. -chromic or -conductive. For instance, if a molecule's absorption spectrum is switched by light, it is termed photochromic; if its optical

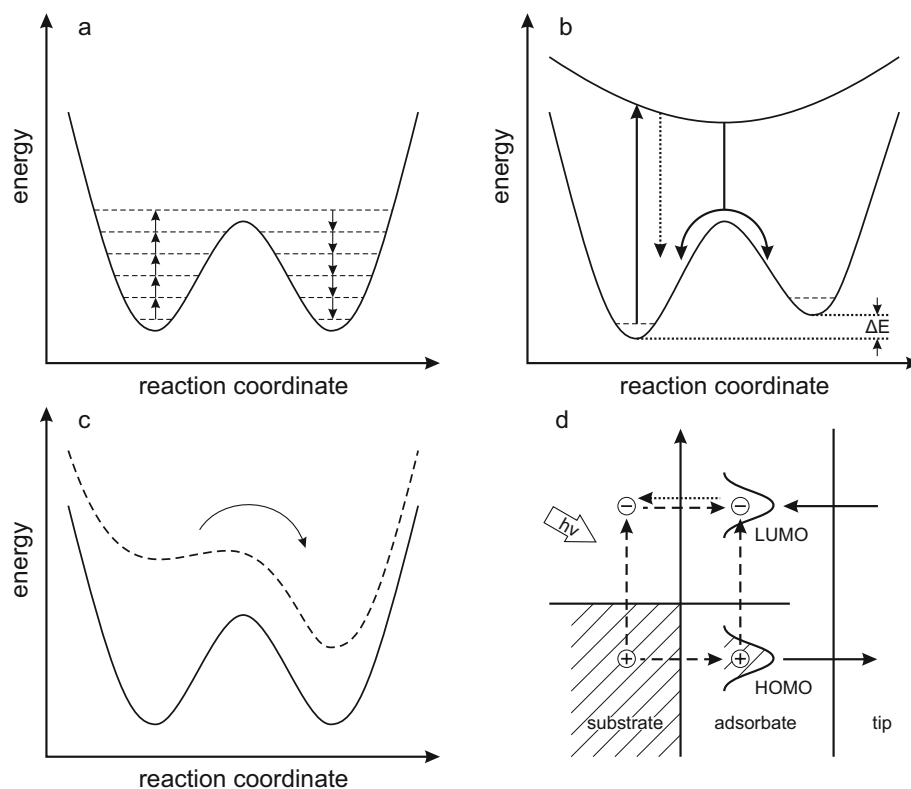


**Figure 4.2:** (a-c) Bistable energy potential landscape featuring two minima separated by a barrier. The reaction coordinate could be for instance the bond angle in azobenzene or the distance between the carbon atoms that perform bonding in the DAE molecules (cf. below). In (a) the barrier is crossed by thermal energy, climbing up and down vibrational states. In (b) electronic excitation is sketched, in which the molecule is raised onto the upper curve, where it can evolve before relaxation back to the ground state. (c) Transition from one minimum to the other induced by a deformation of the potential energy surface (dashed line). This can happen through an ionic state, e.g. by electron attachment/detachment in electrochemistry or by the application of an electric field. (d) sketch of the different excitation paths, dashed lines represent photoexcitation (intramolecular excitation or excitation of surface electrons and charge transfer to the molecule); solid lines denote ionic resonances by tunneling to/from the LUMO/HOMO. Deexcitation is shown by the dotted line.

properties are changed by electrons however, it is called electrochromic, etc.

Incorporating a switch into a device such as a circuit will necessitate the contacting of the molecule to either other molecules or a surface or most likely both. Such contact, for instance the physisorption to a metal surface, will generally constitute a non-negligible influence on the properties of the molecule. With regard to the switching ability it was found that while some molecules retain the behavior observed in solution, in many cases the isomerization is inhibited [192–195]. Among the reasons for the suspended functionality are fast relaxation of excited states responsible for the switching due to coupling with surface electronic states, i.e. the system would not evolve far enough to the right in Fig. 4.2 (b) before relaxation into the ground state takes place (dotted arrow). Another reason can be steric hindrance, which effectively restricts the reaction coordinate to a range that cannot facilitate the transition to the other state. And lastly an unfavorable influence of the adsorption on the potential energy surface governing the isomer-

ization process could prevent the isomerization, e.g. if the barrier separating the two minima is retained despite ionization in (c) [196]. On the other hand, in some cases switching is observed for molecules that do not switch if not in contact with the surface [86]. For instance, this can be caused by changes in the coupling with the electrodes. However, these kind of processes have to be differentiated from intrinsic switching which is caused by the isomerization of a molecule. Predicting the behavior of molecules on surfaces or contacted between leads still poses a serious challenge.

Some of the earliest efforts aimed at switching individual molecules at surfaces were made in the Rieder group at the Freie Universität in Berlin [101,197], employing the STM tip to mechanically induce conformational changes. This requires the availability of different stable geometries that can arise from the adsorption to the surface at low temperatures. Performing manipulation on porphyrin molecules substituted with (3,5-di-tert-butyl)-phenyl legs, Moresco et al. achieved their reversible rotation around the  $\sigma$ -bond connecting them to the macrocycle between two different states, one almost coplanar to the surface and one perpendicular to it [197]. The corresponding difference in electrical conductance could be utilized to read the state of the molecule. A similar behavior was observed by Grill et al. for Lander molecules that possess a molecular board lifted from the surface by side groups (sketched in Fig. 4.3 (a)) [101]. The legs are found to adopt a tilted geometry, which defines two states, one for each direction along the molecular board. It was demonstrated that these are readily convertible with the STM tip without effecting a change in lateral position. In these examples the conformational change is facilitated by the combined potential of tip and surface.

However, isomerization at a surface can also be induced by different kinds of excitations as was demonstrated soon thereafter for *cis-trans* isomerization. This is a different type of conformational switching in which the two different states are stabilized by a double bond in compounds such as azobenzenes, stilbenes and di-benzene-imines. The azobenzene molecule (cf. Fig. 4.3 (b)) constitutes a model system and is well suited to serve as an illustration for the different kinds of effects that can arise from the adsorption to a metal surface, because it is one of the most intensely studied systems that actually still display reversible switching after adsorption, for certain surfaces that is [15,192,193,198–203]. Like the diarylethenes, azobenzenes are photochromic switches [204]. The isomerization can be induced by light irradiation (either  $n-\pi^*$  or  $\pi-\pi^*$  transition with different excitation wavelengths and following different mechanisms – inversion or rotation). Azobenzenes have been called "first-generation" photochromic switches [204], because the *cis-trans* back-switching can be induced thermally.

The switching of molecules adsorbed to a surface depends on many factors. For the unsubstituted azobenzenes as well as the one with one tert-butyl-leg on each phenyl ring in the para position adsorbed to a Au(111) surface the photoisomerization was found to be suppressed and all molecules stayed in the energetically more favorable *trans* form [192]. The light-induced reaction was observed only for the molecule with two tert-butyl groups attached to both sides (3,3',5,5'-tetra-tert-butyl-azobenzene, "TBA", cf. Fig. 4.4), indicating that the reaction can be recovered by reducing the strength of the molecule-surface interaction. While adsorption to a surface can negatively influence a molecule's functionality it can also open up new reaction path-

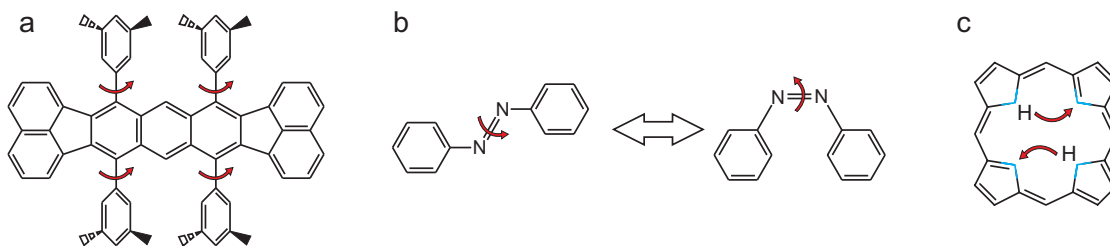


**Figure 4.3:** Chemical structure of three of the switches discussed in the text. (a) Lander molecule [101], the tert-butyl groups (sketched as wedges) lead to an out-of-plane rotation of the phenyl legs. Adsorption leads to two stable tilt angles, one for each direction along the long axis of the molecule. Due to steric reasons switching always includes simultaneous rotation of both legs on a given side, (b) azobenzene [203], left: the planar *trans*, right the 3-dim *cis* conformation, (c) free-base porphyrin in which the four central nitrogen atoms (blue) provide bonding sites. The red arrows indicate the switching mode, in (a) / (b) rotation around a single/double bond, in (c) the tautomerization of the central H atoms [205].

ways, for instance supplying electrons and holes upon irradiation. Hagen et al. investigated the photoexcitation mechanism of TBA on Au(111) and found a process mediated by the substrate [206]. They proposed that holes are created in the gold d-bands that are transferred to the HOMO of the molecule, resulting in a positive ion resonance that facilitates the *trans-cis* switching. The STM opens new switching modalities as has been shown employing the same molecule and surface and inducing the reaction by applying bias pulses. Henzl et al. investigated an azobenzene derivative ("Disperse Orange 3") with two additional substituents ( $\text{NO}_2$ ,  $\text{NH}_2$ ) that showed reversible switching on Au(111) upon application of bias pulses from the STM tip [200]. Both directions of the isomerization are characterized by a threshold in the reaction yield (at around 650 meV) which led to the conclusion of a process induced by vibrational excitation mediated by inelastically tunneling electrons. Similarly, Choi et al. reported that the unsubstituted azobenzene molecule can be switched reversibly between the *trans* and the *cis* forms by the application of tunneling electrons [201]. The process is polarity-dependent and the required bias agrees with the energetic positions of the molecular states, indicating that in this case the process is facilitated by resonant tunneling. Yet another mechanism was demonstrated by Alemani et al. for the reversible and repeated switching of TBA [15] (cf. Fig. 4.4 (a) and (b)). Interestingly, it was found that the bias necessary to induce the switching process depends approximately linearly on the tip-sample separation for distances greater than 10 Å. This behavior is in contrast to the constant energetic thresholds observed before. Furthermore, switching could also be achieved at a large distance at virtually zero tunneling current which rules out the excitation by tunneling electrons in this case, leading to the conclusion that the strong electric field is responsible for the process. This theoretically predicted [207] mechanism is probably based on the deformation of the potential energy surface, cf. the sketch shown in Fig. 4.2 (c). Surprisingly, the molecules lost their switching ability on either Cu(111) or Au(100) [193], highlighting the sensitivity on the molecule-surface interaction. Furthermore, the importance of the balance between the adsorbate-adsorbate and the adsorbate-substrate interaction was revealed in a notable study by Dri et al. investigating the TBA molecule substituted with an additional methoxy group (M-TBA) [202], leading to two remarkable findings. Firstly, of the four different however similar types of island assemblies that were observed only two displayed switching while

the other two did not. And secondly, of the two that could be switched the molecules showed a peculiar dependence of the isomerization probability on the individual molecule's lateral position with respect to the substrate lattice. Interestingly, this led in one case to the appearance of a rectangular lattice of *cis* molecules (cf. Fig. 4.4 (c)) while the switching in the other case followed the ridges of the Au(111) herringbone reconstruction. These selected studies are meant to highlight the fact that the surface can considerably change the behavior of switches adsorbed to it and also introduce new pathways for the isomerization that might hold interesting properties and allow novel modes of interactions with the molecules.

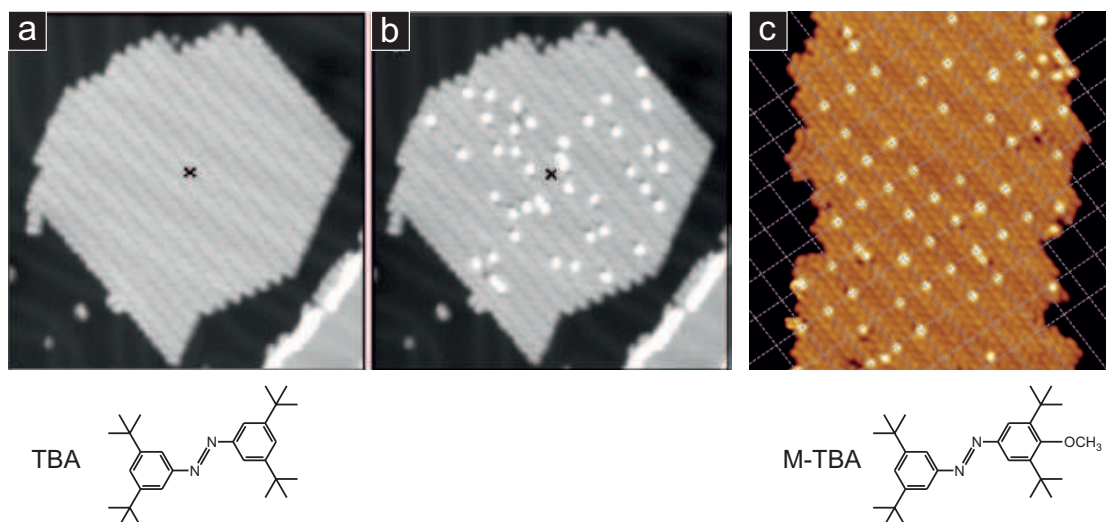


**Figure 4.4:** Islands of TBA before (a) and after (b) bias pulses from the STM tip applied in the position of the  $\times$ . While the island is all in the *trans* conformation in (a), the bright spots in (b) correspond to molecules in the *cis* form. Images  $37 \times 37 \text{ nm}^2$ , reprinted (adapted) with permission from ref. [15]. Copyright (2006) American Chemical Society. (c) Islands of M-TBA after the application of bias pulses. In this case the bright *cis* species is found preferentially in a rectangular lattice which depends on the registry with the substrate lattice.  $29.2 \times 28.5 \text{ nm}^2$ , reprinted by permission from Macmillan Publishers Ltd: Nature Nanotechnology [202], copyright (2008). Chemical sketches of the molecules in the *trans* form are shown below the STM images.

The substantial geometric changes by conformational switches, such as the *cis-trans* isomerization, have been put to use spectacularly in "motor" molecules that were shown to perform directed motion upon excitation with tunneling electrons [208]. However, strong conformational changes render these units incompatible with a rigid incorporation into a network, which is one of the main requirements of molecular electronics. Fortunately, there are other types of isomerizations and molecules that display virtually no conformational changes during switching. The tautomerization of the central hydrogens in macrocyclic molecules such as free-base porphyrins and related compounds constitutes an example [205, 209, 210]. The two hydrogens are bonded to opposing nitrogen atoms resulting in two different configurations that are equivalent under a  $90^\circ$  rotation of the entire molecule (cf. Fig. 4.3 (c)). Liljeroth et al. demonstrated the associated rotation of the electronic states of individual phthalocyanine molecules [209]. The switching was induced by tunneling electrons and reflected in the orientation of the orbitals, their features clearly visible and unperturbed by the metallic substrate by the introduction of thin insulating

NaCl layers. Since the switching entails only the change in position of two protons to the adjacent pyrrole groups, the isomerization proceeds without changes in conformation or adsorption, but causes a measurable change in the conductance of the molecule measured over its side arms. A similar behavior was reported for tetraphenylporphyrin (TPP) directly adsorbed onto a Ag(111) surface in a study by Auwaerter et al. [205] Interestingly, the bistable system could be turned into a four-level switch by the application of a bias pulse leading to the removal of one of the central hydrogen atoms. This results in four available positions for the remaining hydrogen, which can be detected as they give rise to a difference in tunneling current for the tip held at a fixed position. Another type of molecule that can perform isomerization without pronounced conformational changes are the diarylethenes that will be discussed in the following.

#### 4.1.1 Diarylethene molecular switches

After this brief overview, the focus will now be set on the switch that was studied in this work, namely diarylethene ("DAE"). Diarylethenes belong to a class of molecules in which the isomerization is performed by the formation/dissociation of a covalent bond associated with an intramolecular ring-opening/closure. Other members of this class are the furylfulgides and spiropyrans [211]. Like azobenzene, the diarylethenes are photochromic molecules. As noted above the name implies that these are compounds that change their color (absorption spectrum) under light irradiation. Although the application of such molecules as memory has been proposed as early as 1956 [212] and despite considerable interest in the development of e.g. optoelectronic components [213], the implementation has been relatively slow. The main reasons lie in most photochromic compounds' thermochromism, i.e. the change of color at elevated temperatures (without light) and insufficient fatigue resistance. In 1988, Irie reported a new type of photochromic molecule that overcomes these drawbacks [214]. In diarylethenes a type of molecule was found that combines thermal stability with high fatigue resistance. For instance, the isomeric states of some DAE derivatives were found to be stable at elevated temperatures (80 °C) for months at a time, whereas the ring-opening and -closing reactions could be repeated for tens of thousands of cycles in air while still displaying ample properties [215].

The parent material of DAE is stilbene. Like azobenzene stilbene undergoes a *cis-trans*-isomerization [196, 198, 216], cf. the reaction between (1) and (2) in Fig. 4.5. On the *cis* side, stilbene undergoes a cyclization reaction yielding dihydrophenanthrene (3), which is basically a ring-closed DAE. This in turn can be irreversibly oxidized to phenanthrene (4). To harness the cyclization process between the *cis* and the dihydro species two challenges have to be met: first, the competing reactions into *trans*-stilbene and phenanthrene have to be suppressed and secondly the open- and closed-ring forms (2 and 3) have to be rendered stable against thermally induced switching. For the former issue, the structure is modified as indicated in Fig. 4.5. The *cis* form is locked by introduction of a bridging unit (sketched in blue). To protect the *ortho* position of the aryl groups, the hydrogens are exchanged for methyl groups that are more stable with respect to oxidation (sketched in orange). For the stability of the ring-open and -closed forms it was found in calculations [217] that an important factor is the type of aryl groups connected to the ethene. The energy barrier between the respective ground state energies of the two isomers

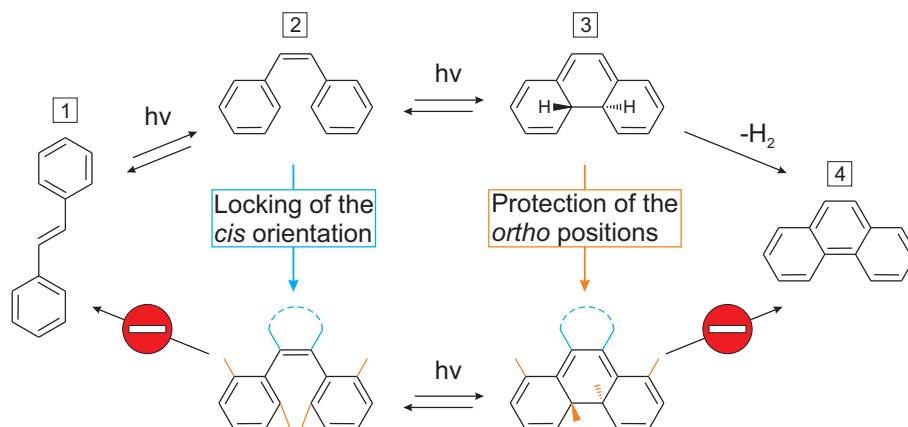


**Figure 4.5:** Photochemical reactions of stilbene (1, 2), the 'parent material'. Reactions competing with the cyclization/cycloreversion between *cis*-stilbene (2) and dihydrophenanthrene (3) yield *trans*-stilbene (1) and phenanthrene (4). These reactions are inhibited by the substitution with groups shown in blue and orange (described in the text).

is found to depend on the difference between them (cf.  $\Delta E$  in Fig. 4.2 (b)): While for a large difference in energy  $\Delta E$  the barrier is small it increases with a decreasing  $\Delta E$ . Irie found that the replacement of the phenyl rings with heterocyclic groups leads to a reduction of this gap. The reason for this is that the shift in energy caused by a change in aromaticity upon cyclization or cycloreversion is large for phenyl and smaller for the heterocyclic groups. Therefore, it is favorable to utilize aryl groups with low aromatic stabilization energy. Thiazoles and thiophenes constitute the best systems in this regard. The latter type, as sketched in Fig. 4.6, is employed in this study. The use of these particular aryl groups is reflected in the name of the compound, namely dithienylethene ("DTE").

The isomerization of DAE molecules has several advantages. For one, the switching process involves only a small geometrical change, which renders it compatible with the rigid incorporation into a covalent network, unlike e.g. the ring-opening/closing of spiropyrans. It has been shown that the isomerization can take place inside a single crystal without altering the crystal structure [215,218]. In a notable study [219] the small geometrical changes of the individual molecules could be utilized to induce reversible changes in the macroscopic shape of a thin crystal that could even be employed to perform mechanical work. Moreover, the switching is accompanied by a large change in some of its physical properties (ample ON/OFF-ratio). Because the  $\pi$  electrons in the open-ring form are localized on the thienyl groups, the 'R' groups attached to it shown in Fig. 4.6 (left) will not communicate with each other. Upon cyclization the carbon atoms participating in the formation of the bond perform a change in hybridization from  $sp^2$  to  $sp^3$  and the molecule establishes a linearly conjugated  $\pi$ -electron system between the 'R' groups (indicated in blue in Fig. 4.6, right). This change in the electronic properties leads to a change in the absorption spectrum and also a substantial shift of the molecular conductance  $G$ , which can be read out in two-terminal current measurements. It is interesting to note that the dependence of the conjugation on the switching state can be reversed by attachment of the thienyl group in the 2- rather than the 3-position (as is the case in Fig. 4.6), which would render the ring-open form the high-conductance state. In addition to the photochemical isomerization, it was shown

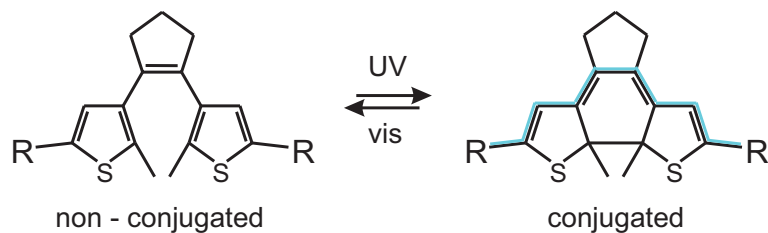


**Figure 4.6:** Chemical structure of dithienylethene (DTE) in the ring-open (left) and ring-closed (right) form. The cyclization/cycloreversion leads to a marked difference in the interaction between the substituents "R", (left) R groups not interacting, (right) R groups interacting via the path highlighted in blue.

that DTE can be switched by reduction/oxidation in an electrochemical cell [220].

The isomerization of individual and also ensembles of DAE molecules adsorbed to (in most cases metallic) surfaces have been investigated with different techniques [83,95,221–231], mostly attempting photoexcitation. Fig. 4.7 shows the chemical structure of some of the employed molecules. Most studies have utilized compounds substituted with thiol groups to facilitate chemical bonding to metal surfaces or nanoparticles, resulting in a vertical arrangement in self-assembled monolayers (SAMs). Conductance measurements are performed in this arrangement in a MBJ or STM setup. Using an STM based setup, He et al. found that irradiation of (1) sketched in Fig. 4.7 attached to a gold sample led to the change in the ratio of the abundance of subsequently recorded conductance peaks associated with the open- and closed-ring forms (using an STM-based setup) and concluded reversible switching [95]. Dulic et al. employed a MBJ setup to record the conductance of (2a) while illuminating the junction [221]. In a small number (10) of attempts a sudden decrease in the conductance was observed and ascribed to the ring-opening. On the other hand, an increase in the conductance associated with ring-closure could not be observed, indicating that this reaction, unlike in solution, is not active in contact with the gold. It was proposed that this is due to quenching of the excited open state by the surface electronic states. The same process (ring-opening) is observed for the similar molecule (2b) connected to a gold surface, isolated in a mixed SAM and measured with STM [223]. Illumination of the SAM leads to the disappearance of the bright protrusions identified with the closed-ring species which is also attributed to the cycloreversion reaction. Using the same method and alternating visible and UV irradiation reversible switching is reported for molecule (3) arranged in SAMs [224], which is an indication that the type of the linking to the substrate is crucial for retaining the functionality of the molecules [222].

In a different approach, Arai et al. combined the isomerization in solution with a surface by performing STM at a solution-graphite (HOPG) interface [226]. Two different DTE derivatives are investigated, one of which contains two coupled switches. Only the smaller part of the molecules are located at the surface, while the larger part exists in solution, which is where the photochromic reactions take place upon irradiation. While the surface doesn't play a role in the isomerization in this case, reversible switching is observed and the change in the species in solution is reflected in differently ordered molecular islands. Another interesting investigation of DAE is described by Whalley et al. [83]. Small gaps etched into electrically contacted carbon nanotubes

were utilized to realize a molecular junction employing molecules (4a) and (4b). It was found that both displayed unidirectional switching (ring-closure) when irradiated with UV light, reflected by a sudden current increase. However, the attachment to the CNT apparently inhibits the back-reaction under visible light. Nonetheless, this technique constitutes an interesting alternative to the thiol-based approach for the measurement of the molecular conductance, although also in this case the exact number and arrangement of the molecules in the junction is not known.

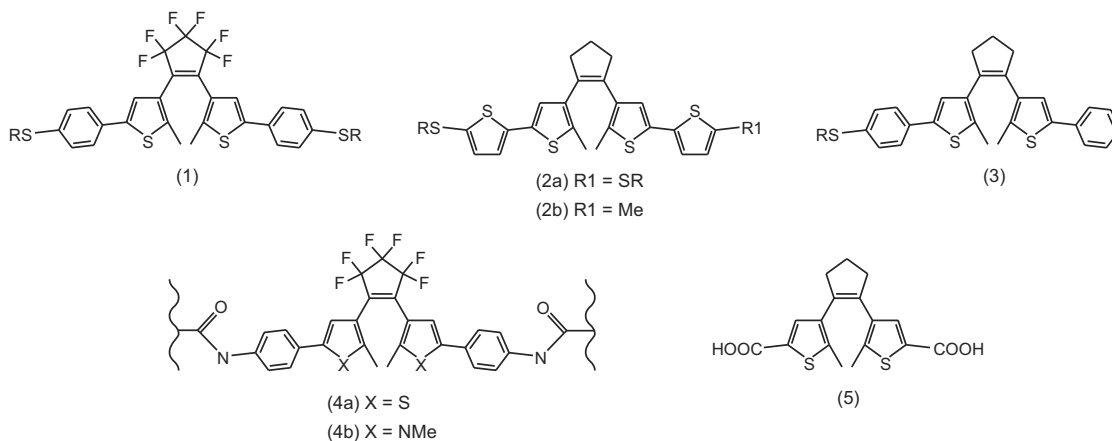


**Figure 4.7:** Chemical structures of the molecules discussed in the text (only shown in the ring-open form). "R" denotes protective groups that are dissociated to facilitate the metal-sulfur bond. The wavy lines next to (4) signify attachment to carbon nanotube edges. (1) - [95], (2) - [221, 223], (3) - [224], (4) - [83], (5) - [228]

In approaches depending on a statistical evaluation, the simultaneous presence of two isomers can obfuscate results. Furthermore, intramolecular resolution in STM that could be used to unambiguously identify molecular species and infer details about their conformation is seldom achieved in self-assembled monolayers and judging the switches' state from their apparent height in SAMs is complicated by stochastic blinking [85], an effect in which molecules change their appearance depending on the binding of the sulfur to the substrate.

All mentioned studies have investigated switching of the DAE connected via linker groups (or in solution), while there are few that examine their properties directly adsorbed to a surface with STM under UHV conditions. One of them is the study by Coudret et al. in which the DTE (5), shown in Fig. 4.7 was deposited onto a Cu(111) surface [228]. However, it was concluded that the molecules do not perform isomerization which was attributed to the strong interaction with the surface.

To summarize, in most studies it is found that DAE molecules displaying efficient and reversible switching in solution only show a limited performance or even no switching at all once contacted to a metal surface. As mentioned above, they have this in common with most other switches. The reasons for this change in properties include steric hindrance, the efficient deexcitation (quenching) of the excited state responsible for the isomerization or an unfavorable modification to the potential energy surface. Furthermore, until now, in studies investigating single DAE switches these molecules were almost exclusively grafted onto a surface by linkers and arranged in SAMs, i.e. a vertical geometry, whereas no assembly and connection neither into weakly nor

strongly coupled molecular structures has been investigated. A great and so far unused potential of the switches however lies in the possibility to realize the switch states 'ON' and 'OFF' in an electronic circuit, given that they could be properly contacted. In such a setup one could envision the switches to control the flow of electrical signals through the network. To this end one has to make sure - by adequate design of the molecules, the right choice of surface [193] and a suitable covalent connection - that the switching properties of the molecules are not inhibited. Attempts to that end will be described in the following.

## 4.2 Characterization of diarylethene monomers on Au(111)

I have investigated different halogenated and non-halogenated dithienylethene (DTE) switches as shown in Fig. 4.8 on a Au(111) surface. Since the retention of the switching ability turned out to be a major complication for molecules going from solution to adsorption onto a surface, utilizing a surface with little reactivity appears to be the most promising approach. Gold is the least reactive among the coinage metals and the (111) face is characterized by small corrugation, which is why it is favorable for the present study.

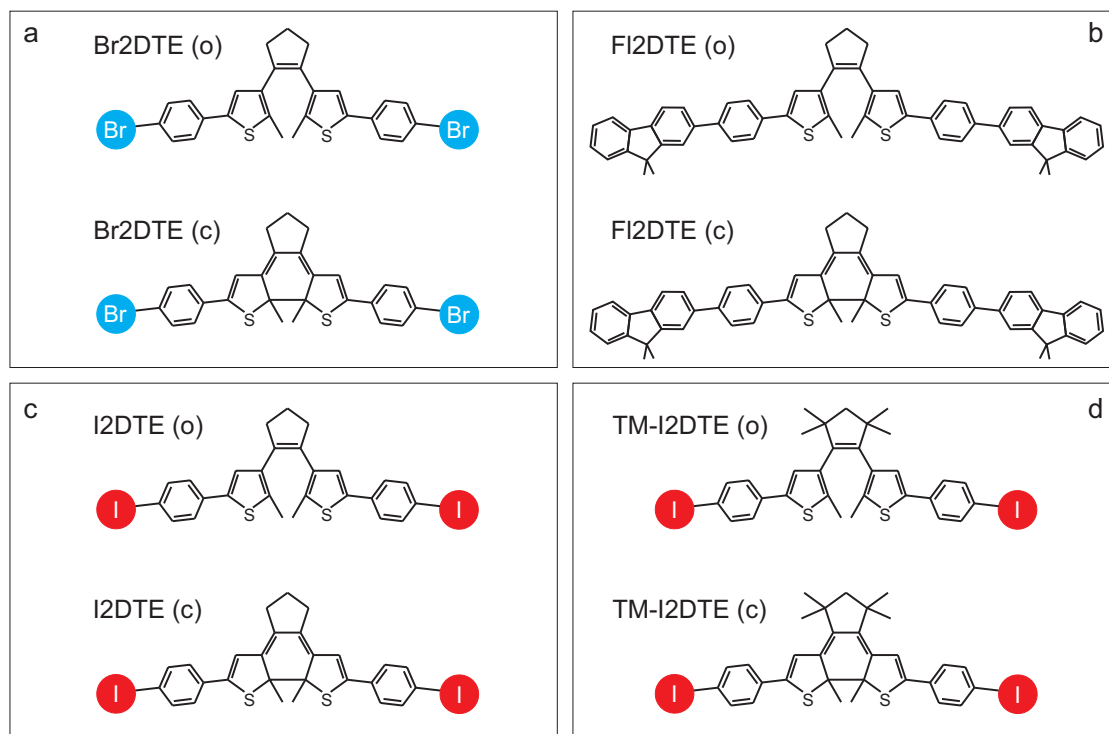


**Figure 4.8:** Chemical structure of the investigated switch molecules in the open (o) and the closed (c) form. All molecules possess a dithienylethene switch moiety with an additional phenyl attached to each thienyl group. The compounds intended for polymerization (a, c, d) are substituted with halogen atoms (bromine or iodine) on the para-position of the phenyl rings, whereas the molecule shown in (b) features fluorene groups instead. In chemical terminology the compounds (in the open-ring form) are called 1,2-Bis-(2-methyl-5-(4-brom-phenyl)-thien-3-yl)cyclopent-1-en (a), 1,2-Bis-(2-methyl-5-(4-(9,9-dimethylfluoren-2-yl)phenyl)-thien-3-yl)-cyclopent-1-en (b), 1,2-Bis-(2-methyl-5-(4-iod-phenyl)-thien-3-yl)cyclopent-1-en (c) and 1,2-Bis-(2-methyl-5-(4-iod-phenyl)-thien-3-yl)-3,3,5,5-tetramethyl-cyclopent-1-en (d).

Despite the fact that switches such as azobenzene molecules are intensely studied, experiments on DAE molecules directly adsorbed on metal surfaces, i.e. in a planar geometry and not grafted via linker groups, are rare [228]. Since no previous work exists for this particular molecule on Au(111) the first imperative is to characterize and identify the structures found on the surface. The switching is potentially influenced by the local environment and the conformation of the molecules. For instance, the appearance of the switching lattice (cf. ch. 4.1.1) caused by the registry of the adsorption position with the surface found for azobenzene derivatives [202] would

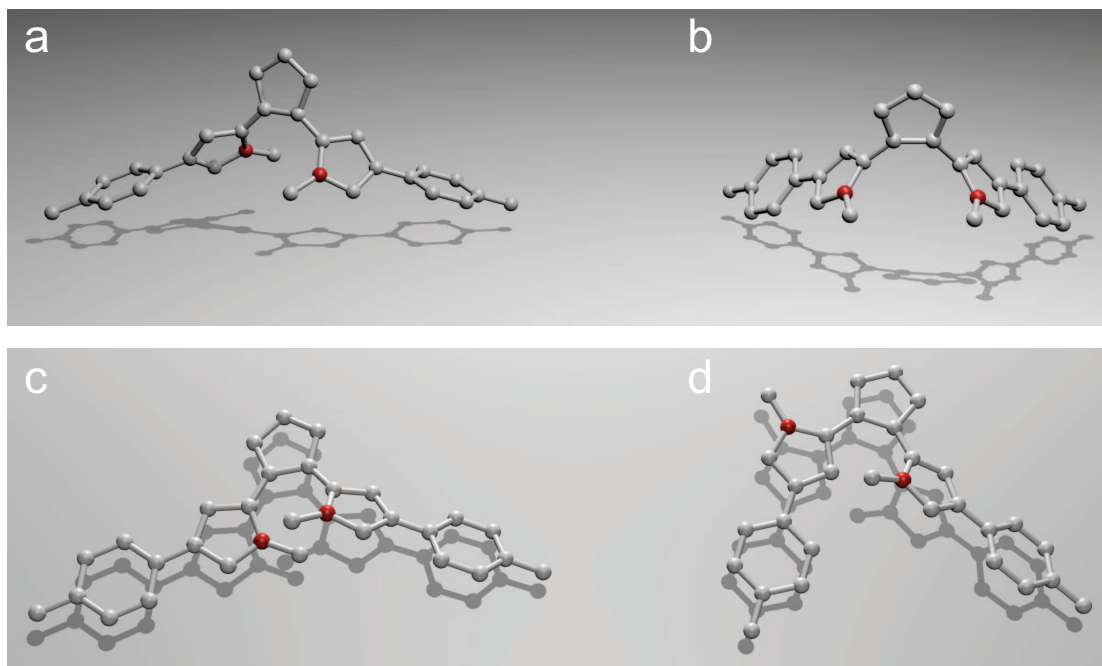


**Figure 4.9:** Sketches of the different conformations of DTE. The carbon atoms that participate in the cyclization reaction are shown in red. (a) extreme conformation of DTE displaying C<sub>2</sub>-symmetry and (b) mirror-symmetry. These two conformations could both perform a ring-closing reaction. The influence of the surface is considered in (c) and (d). While the proximity of the carbons in (c) would allow the cyclization in (c) the rotation of the left leg in (d) prevents it.

hardly have been accessible with integrating techniques, such as UV-vis spectroscopy. Furthermore, it was observed that the light irradiation could induce not only *cis-trans* isomerization but also the transformation of ordered into disordered structures. Therefore the local examination of the surface using STM is instrumental for a detailed and quantitative description of the molecular structures and their behavior. Important aspects include their adsorption, conformation and agglomeration into islands. Based on these observations a prediction can be attempted which structures can potentially be switched and which cannot. It is convenient to start with the examination of the monomer building blocks, as they are almost identical to the repeating unit in subsequently to be formed polymeric structures. The use of the brominated precursors is advantageous in this regard, because the monomers are stable when deposited onto a sample held at room temperature (cf. ch. 4.3). In solution the open molecules can be expected to form two extreme conformers, cf. Fig. 4.9, that are interchangeable by a rotation around the  $\sigma$  bond connecting the ethene with the thiophene ring, yielding a mirror-symmetric one with both legs pointing in the same direction (b) and a conformation with C<sub>2</sub> symmetry (a). However, due to adsorption on a surface a more flat-lying conformation is likely as shown in (c) and (d). The carbon atoms that form the new bond in the ring-closing reaction are highlighted in red. While in (a) to (c) these carbons are close enough to take part in a bond, the conformation shown in (d) does not allow it. An interesting question in this regard is the effect of the thienyl groups on adsorption. Groups containing sulfur, especially thiols, are popular for their tendency to bind to gold surfaces and their use in e.g. SAMs is a standard technique [223, 224]. In this experiment

however, the binding of the thienyl groups to the surface would very likely be detrimental to both the interconnection process and the switching ability of the molecules.

#### 4.2.1 Open-ring brominated DTE

These molecules ( $\text{Br}_2\text{DTE(o)}$  in Fig. 4.8) were evaporated at  $135\text{ }^\circ\text{C}$  from the Knudsen cell at a rate of approximately  $0.05\text{ ML/min}$ . The molecules are found in two different conformations, a linear and an angled one. At low coverages the molecules are forming small islands on the *fcc* regions of the herringbone reconstruction (cf. Fig. 4.10). Furthermore, single molecules decorate the elbow sites. The reconstruction is not adversely affected by the molecules (also at higher coverages) which is a first indication for a weak interaction with the molecules.

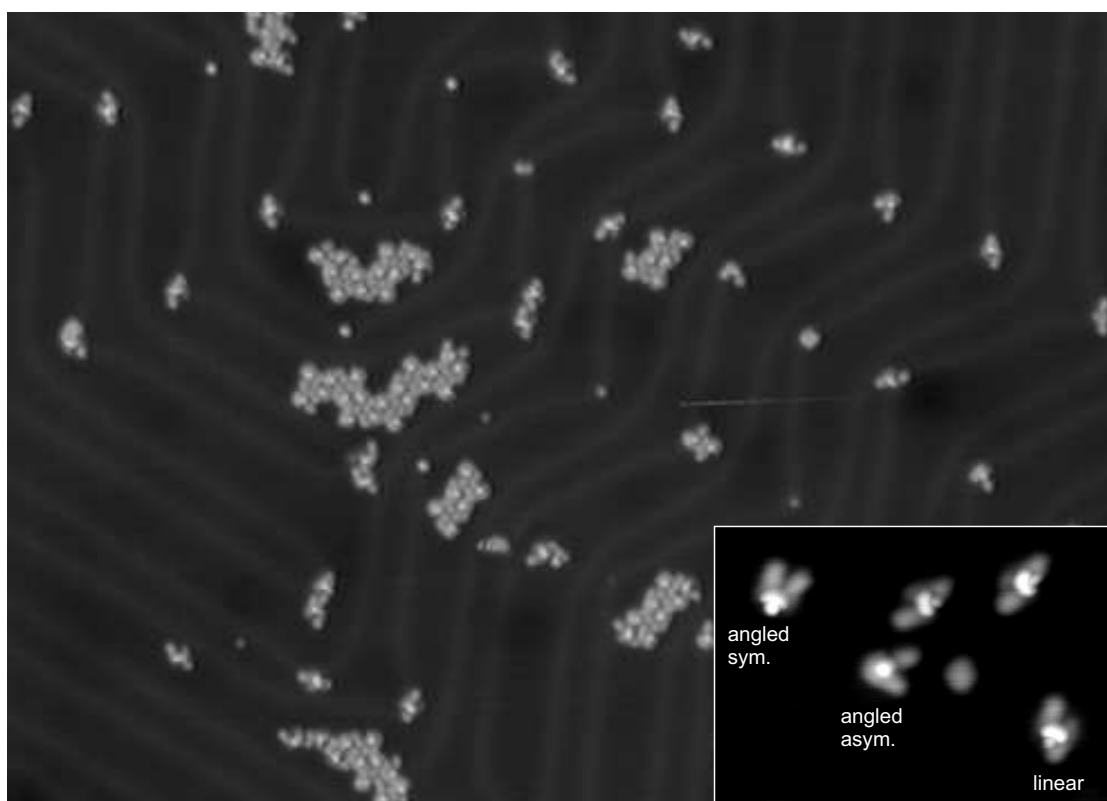


**Figure 4.10:**  $\text{Br}_2\text{DTE(o)}$  on Au(111) imaging set point  $0.1\text{ nA}$ ,  $500\text{ mV}$ . Image size  $50 \times 70\text{ nm}^2$ . The inset shows an enlarged image ( $9 \times 13\text{ nm}^2$ ) of five single molecules, two angled and three linear conformers. The single lobe is probably a small cluster of gold typically situated at the elbow sites.

The weak adsorption is also observed during lateral manipulation with the STM tip. This is corroborated by calculation, which finds no chemisorption of the thienyl groups with the surface with the molecule lying approximately flat on the surface (calculations performed by M. Grisolia and C. Joachim [232]). The majority of molecules is found in the angled conformation ( $> 93\%$ ). For this conformation the appearance in STM images is slightly asymmetric with two legs of different length and a brighter protrusion in the center, cf. the one labeled "angled asym." in Fig. 4.10. An enlarged STM image of an assembly of molecules in this conformation is shown

in Fig. 4.11. One of the monomers is encircled by the dashed line. The legs together with the central lobe form an angle of about  $90^\circ$ . The identification of the legs with the bromophenyl groups and the central part with the switching DTE unit is straight forward and agrees well with the calculated image that is shown in the inset in the lower right corner. It corresponds to the geometry that is shown in Fig. 4.9 (d): One leg (the one appearing longer) is tilted so that its thienyl's sulfur and the methyl group are pointing slightly upwards giving rise to the central bright lobe. The other leg (appearing shorter) is lying virtually flat and in plane with the cyclopentane ring and with the sulfur atom pointing outwards. Around the central protrusion there appears a ribbon at approximately the same contrast as the legs. This can be ascribed to the cyclopentane ring together with the methyl and thienyl groups from the shorter leg. The small gap in the ribbon is likely caused by the thienyl group that is tilted towards the surface on the leg appearing longer. This is in agreement with the calculated image which displays an area of reduced conductance at that location (indicated by the arrow). The distance measured from STM images between the ends is  $(1.1 \pm 0.1)$  nm which is in agreement with the calculated monomer (including the surface), in which the Br - Br distance is 1.05 nm. These angled conformers are not expected to be switchable for the geometric reasons discussed above. The islands formed from these conformers build units of three (more seldom four) molecules (as shown in Fig. 4.11). This close-packed arrangement is typical for structures formed by the weak van-der-Waals interaction. In this geometry the bromine atoms on the longer legs are pointing towards the neighboring molecules' sulfur atom. It is conceivable that this results in the formation of a halogen bond [233].

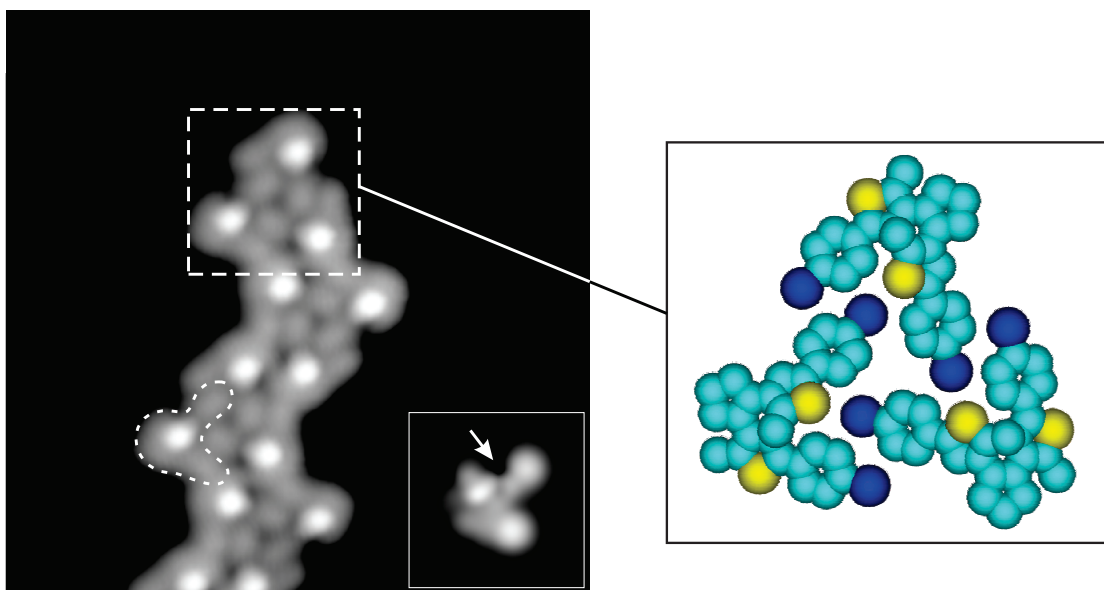


**Figure 4.11:** STM image of an island of  $\text{Br}_2\text{DTE(o)}$  molecules, feedback parameters 0.1 nA, 500 mV,  $10 \times 10 \text{ nm}^2$ . The dotted outline contains one angled monomer. The dashed box contains three switch molecules in the typical unit as shown in the model on the right hand side. Color code: sulfur yellow, bromine blue, carbon cyan. The inset (bottom right of the STM image, copyright by M. Grisolia) shows a calculated image of a single monomer in the same orientation and conformation as the lower left one in the model (same scale as the STM image) [232].

The linear and less frequently ( $< 7\%$ ) observed conformer is found mostly isolated at the her-

ringbone elbow sites. In STM images it typically shows a characteristic appearance of three lobes in the central part connected to two legs, as shown in Fig. 4.12. What is striking about its appearance is that it also does not appear symmetrical. The explanation is that this open-ring monomer is not found standing upright as depicted in Fig. 4.9 (a) but rather lying on the side as sketched in (c). Accordingly, the features labeled (1) and (2) in Fig. 4.12 can be identified with the thienyl groups. One of the methyl groups is located on top of the other and forms a combined protrusion together with the ethene group (1). On the other side of the molecule there is a less bright protrusion (3) that fits well as the cyclopentane ring in this interpretation. Depending on which methyl group lies on top of the other, two mirror-symmetric conformers are observed as is visible from Fig. 4.12. Models of the two enantiomers in the STM image are shown to the right. Observing both forms next to each other also proves that the appearance is not an artefact caused by the tip. Again, the identification is corroborated by the calculated image (shown in the inset), that reproduces the appearance of the monomer in the top right corner. From the above deliberations a molecular unit in this conformation would be a promising specimen for switching attempts, because of the proximity of the key carbon atoms.

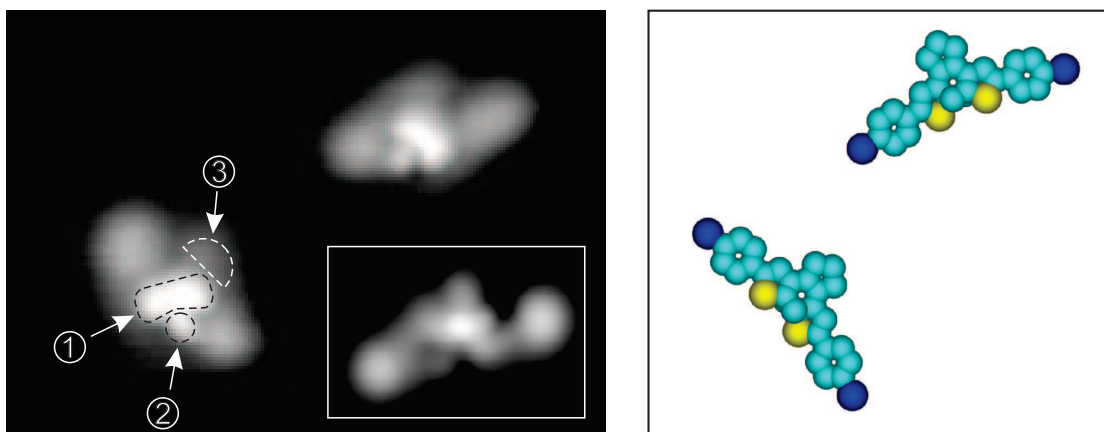


**Figure 4.12:** (left) STM image of a two linear conformers of  $\text{Br}_2\text{DTE(o)}$ . feedback parameters 0.1 nA, 250 mV, image size  $5 \times 7 \text{ nm}^2$ ; (right) model of the two monomers (color code as in Fig. 4.11). The inset shows a calculated image of a monomer (drawn at the same scale, copyright by M. Grisolia) in the same conformation and orientation as the top right one in the model [232].

While the angled conformers arrange in the regular islands described above, the linear species is found mostly isolated and the orientation of the individual molecules is only given by the interaction with the surface. The orientation of the long axis of the molecules is anisotropic, as is shown in the histogram in Fig. 4.13. About half of the molecules are oriented along the direction of the herringbone corrugation. In this case the interaction with one of the adjoining ridges is dominating, leading to narrow peaks. Approximately the other half lies directly and tangentially at the elbow site and the long axis is roughly given by one of the crystal axes. In this case the counts are distributed around these angles (indicated by the grey arrows) as the elbow sites are not perfect.

For the measurement of the electronic states, these molecules are not well suited as the application of a bias of around 2 V will induce the dissociation of the bromine atoms from the frame of the

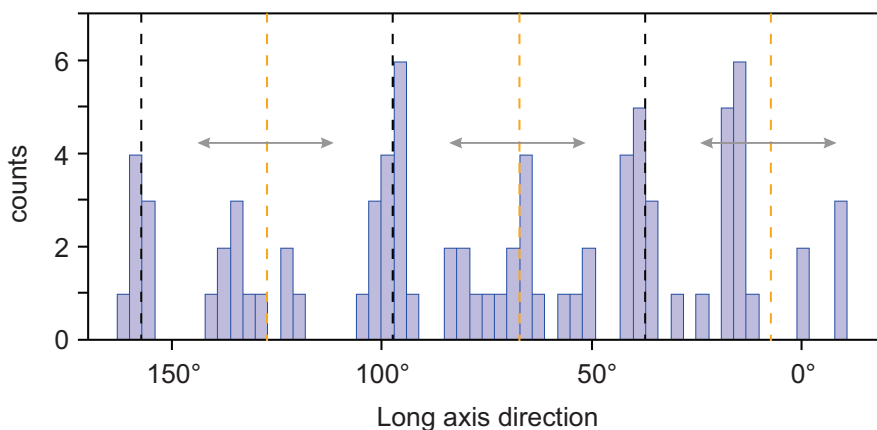


**Figure 4.13:** Histogram of the direction of the long axis of 83 linear conformers of Br<sub>2</sub>DTE(o). The direction of the herringbone ridges are indicated by the black dashed lines, the gold crystal axes in orange.

molecules [55]. However, in this bias range the features in differential conductance ( $dI/dV$ ) correspond to those of the Fl<sub>2</sub>DTE(o) molecules (cf. below).

#### 4.2.2 Closed-ring brominated DTE

These molecules ((Br<sub>2</sub>DTE(c)) in Fig. 4.8) were evaporated at 140 °C from the Knudsen cell at a rate of approximately 0.1 ML/min. Fig. 4.14 (a) shows an STM image of their typical appearance. The greater part are found in a linear conformation (around three quarters) and the rest in an angled one, cf. Fig. 4.14. The angled species appears identical to the asymmetric ring-open angled conformation described in section 4.2.1. One of these units is framed with a dashed line. They are not compatible with the closed form corresponding to Fig. 4.9 (b) because they are not symmetric.

The appearance of the monomers shown in Fig. 4.14 is puzzling. In STM images recorded at 500 mV bias the linear molecules appear at a lower height than the ring-open isomers. This is surprising, because the closed isomer is expected to display a reduced HOMO-LUMO gap which would likely give rise to an enhanced transmission and therefore an increased apparent height at the same feedback parameters. Furthermore, they display a nearly homogeneous contrast in STM images, whereas the calculation (cf. the inset in (a)) shows a bright protrusion in the center. These are strong indications that the observed molecules do not correspond to the closed-ring monomers shown in Fig. 4.8 (a). A possible explanation for the deviating appearance might be that the ring-closed species is not stable during the evaporation process, which could lead to both cycloreversion and oxidation to yield the ring-open form and a structure similar to phenanthrene, respectively. For the latter case, the molecules would be planar, having lost the methyl groups that protrude from the surface and thus would be more similar to the almost featureless graphene nanoribbons [96]. Attempting a comparison with the latter, profiles were taken across the center of the switches (feedback parameters 500 mV, 0.1 nA), revealing the height at  $(1.8 \pm 0.1)$  Å.

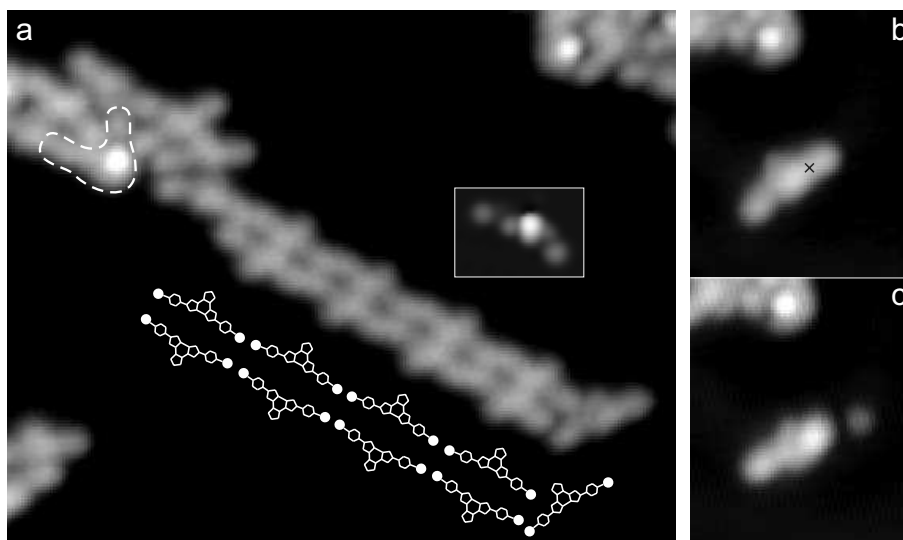


**Figure 4.14:** STM images of a preparation of Br<sub>2</sub>DTE (c) on Au(111), (a) showing a double row of molecules that is sketched below. A single linear molecule is visible at the end of the chain. There also appear a smaller number of the asymmetric angled conformer (enclosed by dashed line), image size  $12 \times 15 \text{ nm}^2$ . The inset shows the calculated image of a linear closed monomer drawn at the same scale, copyright M. Grisolia [232]. (b) and (c) display the same area before (b) and after (c) the controlled dissociation of one bromine atom by means of a bias pulse, cf. ch. 1.3.2 (location of the tip during the manipulation indicated by the  $\times$ , images sized  $5 \times 6 \text{ nm}^2$ ), all images recorded at 500 mV, 0.1 nA.

Line scans across the graphene ribbons on Au(111) at the same feedback parameters show a comparable apparent height of  $(1.9 \pm 0.1) \text{ \AA}$ . (Since the LUMO of these chains is located at 1.6 eV, the difference in electronic structure should not distort the comparison too much.) On the other hand, the presence of the bromine atoms can be confirmed by a controlled dissociation with an electron pulse from the STM tip at 2 V as for the open-ring monomer. An example of such a manipulation is shown in Fig. 4.14. In (c) the bromine is separated from the rest of the molecule by a small distance.

### 4.2.3 DTE with fluorene

For the DTE-conductance switch, the goal is ultimately to connect it from both sides with molecular wires. This is already programmed into the monomer unit discussed above, with the bromine intended to supply appropriate connection sites, according to the on-surface synthesis approach described in ch. 3.1. The switches equipped with two units of fluorene (labeled "Fl<sub>2</sub>DTE" in Fig. 4.8) represent an intermediate step in which the switching unit is connected from both sides to the shortest possible wire of the above type. The study of these molecules yields important insight because it circumvents complications in the linking process (cf. ch. 4.3) and can therefore serve as a reference system. The monomers furthermore don't contain halogens that in the previous section precluded the recording of differential conductance beyond the bias voltage sufficient to dissociate the carbon-bromine bond.

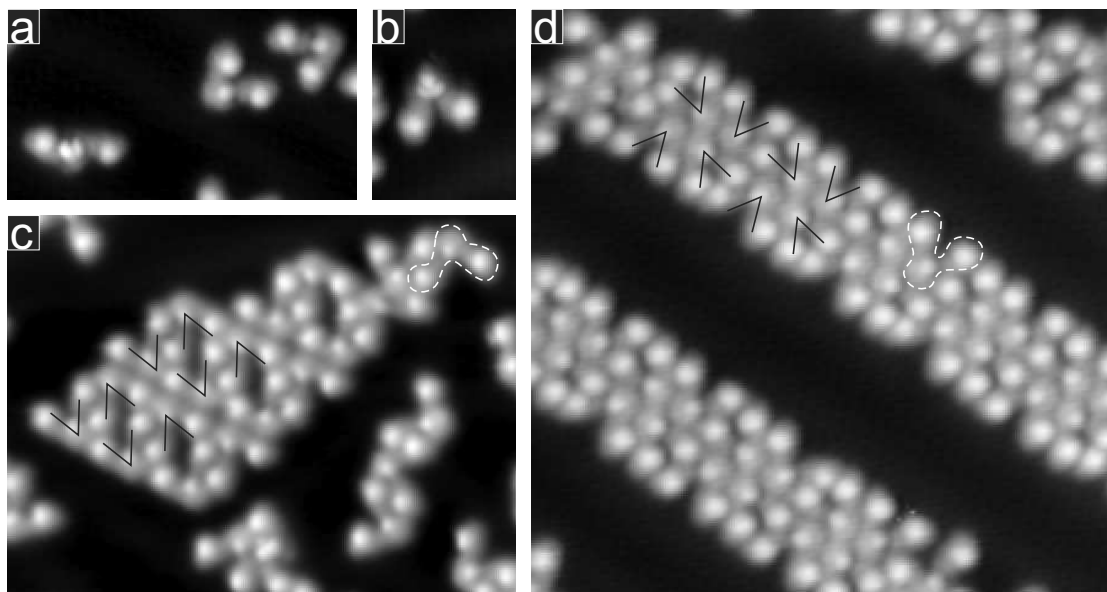


**Figure 4.15:** STM images of  $\text{Fl}_2\text{DTE(o)}$  on  $\text{Au}(111)$ . (a) one linear and two angled conformers, (b) one symmetric angled conformer, (c) and (d) differently ordered islands. Some of the molecules are highlighted by 'V's. The border of a single molecule is outlined by the dashed line in (c) and (d). Image size  $6 \times 11 \text{ nm}^2$  (a),  $6 \times 4.5 \text{ nm}^2$  (b),  $12 \times 16 \text{ nm}^2$  (c) and  $17 \times 17 \text{ nm}^2$  (d). Feedback parameters for all: 500 mV, 0.1 nA.

The molecules were evaporated at a temperature of  $205 \text{ }^\circ\text{C}$  at a rate of rate  $0.4 \text{ ML/min}$ . Imaging the molecules on the  $\text{Au}(111)$  surface, the central part appears like the one described for  $\text{Br}_2\text{DTE}$  (o), displaying either the angled conformation with the bright central lobe or the linear structure with intramolecular contrast, as shown in Fig. 4.15 (a). In addition, the molecules possess a bright protrusion on both ends which can be identified with the fluorene groups. The angled conformer can be transformed into a linear one and vice versa by means of manipulation with the STM tip. Furthermore, similar to the case of DBTF [56], the angle of the molecule is altered by rotation of the fluorene around the  $\sigma$ -bond connecting it to the phenyl group. This is most apparent by the difference in angles that is observed in the angled conformers. A symmetric angled conformation is observed, albeit with a very low frequency (less than 1 % in over 400 molecules). It can however be produced by lateral manipulation, as the example shown in Fig. 4.15 (b). The appearance of this conformer is consistent with the one sketched in Fig. 4.9 (b). While most molecules appear intact, some fragmentation has taken place and some of the monomers are found missing fluorene legs. The amount of fragments is around 10 % of the observed units. Considering that such a dissociation produces at least two fragments one can conclude that the amount of damaged molecules is closer to 5 %. These might give rise to a mobile species that is periodically visible between the static  $\text{Fl}_2\text{DTE}$  islands. Thus, mostly intact deposition of these minimally contacted switches is possible. The angled  $\text{Fl}_2\text{DTE}$  molecules form islands of limited order on the fcc regions of the herringbone reconstruction, such as the ones shown in Fig. 4.15 (c) and (d). While the island in (c) derives from the typical zigzag stacking (cf. the three units at the lower right corner) and displays open pores, the island in (d) appears close-packed with a windmill-like motif as highlighted by the arrow heads. Interestingly, there

doesn't appear to be any difference in the appearance and arrangement between preparations of the open- and closed-ring isomers. This behavior is in partial accordance with the results for the brominated switches, in that the preparation of Br<sub>2</sub>DTE (c) would yield monomers displaying the angled conformation that is only compatible with the ring-open isomer. On the other hand, a flat and featureless species such as the ones in the double row shown in Fig. 4.14 has not been observed for neither form of Fl<sub>2</sub>DTE.

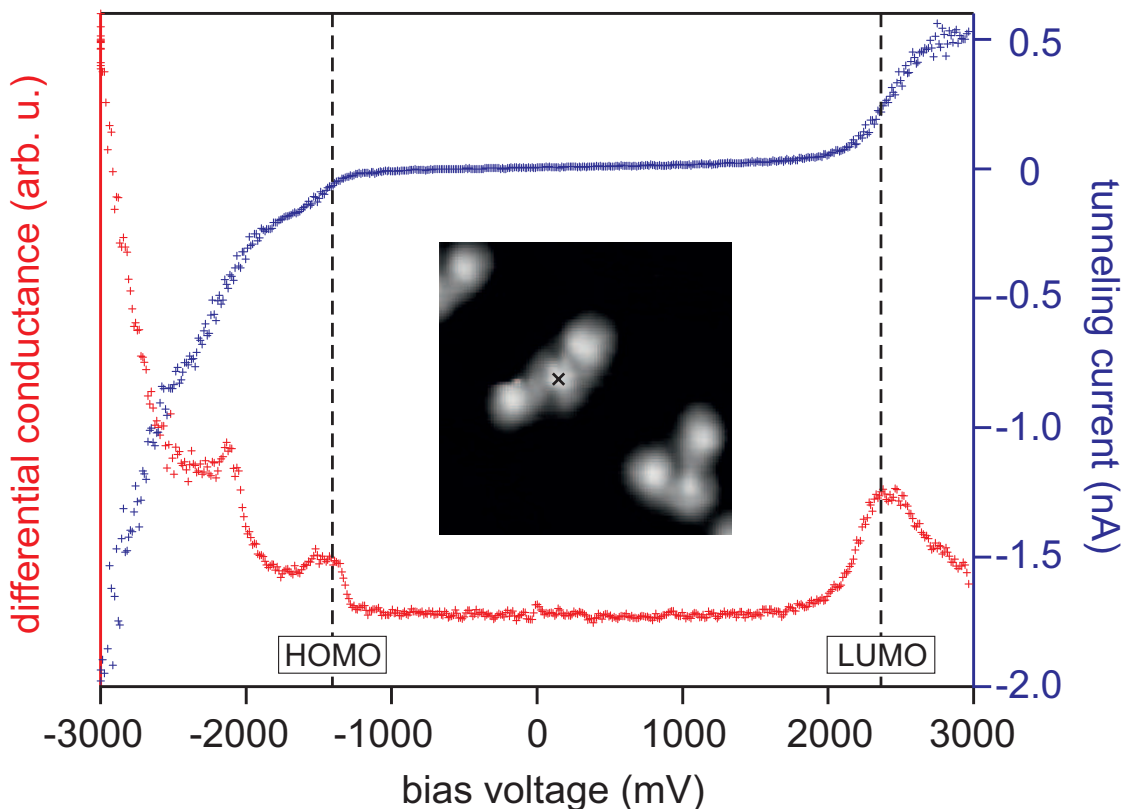


**Figure 4.16:** Tunneling current (blue) and differential conductance signal (red) recorded over a linear monomer of Fl<sub>2</sub>DTE (raw data, lock-in modulation amplitude = 10 mV, frequency = 723 Hz). The inset shows the STM image recorded beforehand (image size  $7 \times 7 \text{ nm}^2$ ). The position of the tip during the spectroscopy measurement is indicated by the cross. HOMO and LUMO are indicated by dashed lines.

The identification of the angled conformers with the open-ring switch is straight forward for geometric reasons and is corroborated by the interconvertibility into the linear form by lateral manipulation. The assessment of the linear species on the other hand is more complicated, because its shape is compatible with both the open- and closed-ring forms. As will be shown, the recording of differential conduction ( $dI/dV$ ) traces allows the unambiguous assignment of the respective state to a particular monomer. A characteristic curve recorded on the center of a linear Fl<sub>2</sub>DTE is shown in Fig. 4.16. The states of the linear conformers are found at  $E_{\text{HOMO,lin}} = (-1.25 \pm 0.05) \text{ eV}$  and  $E_{\text{LUMO,lin}} = (+2.5 \pm 0.1) \text{ eV}$ , whereas the angled conformers display theirs at  $E_{\text{HOMO,ang}} = (-1.12 \pm 0.08) \text{ eV}$  and  $E_{\text{LUMO,ang}} = (+2.5 \pm 0.2) \text{ eV}$ . Thus, the surprising and central result is that the features are the same for spectra taken on the linear as well as the angled conformers. Furthermore, they are identical for the preparations of open- and closed-ring Fl<sub>2</sub>DTE. Since the angled conformer is incompatible with the closed species and

since from experiments in solution the cyclization is expected to lead to a considerable change in the HOMO-LUMO gap, it can be concluded that the observed isomer of  $\text{Fl}_2\text{DTE}$  is always the ring-open form. Thus, it seems to be the case that the isomers do not stay in the closed-ring form, but are modified in the evaporation process, similar to what was observed for  $\text{Br}_2\text{DTE}$  (c).

The understanding of the appearance and more importantly the spectroscopic signature of the monomers constitute an important prerequisite for gaining control of the switching functionality of the DTE. While the features in the spectrum shown in Fig. 4.16 reflect read-out of the open ("Off") state, it remains to be seen if the closed ("On") state can be produced and if its properties differ sufficiently from its isomer. However, before addressing this issue I will turn to the coupling of the monomers to covalently bonded structures, since the ultimate goal for the switches is to include them into a network mimicking a circuit-like architecture. The incorporation of functional units into a network has not been demonstrated so far. Most importantly, the properties of the switching center must not be adversely affected by the connection to not suppress its functionality.

### 4.3 Polymerization of dithienylethene

The focus of the present section lies on the fabrication of covalently linked structures on a Au(111) surface, applying the knowledge that has been gained from the investigation of the fluorenes (cf. ch. 2.2) and the porphyrins (cf. ch. 3.2). However, unlike the chains and networks produced so far, the intended structures will be the first to carry functional units in the form of the DTE switches described in ch. 4.2.

#### 4.3.1 Structures made from Br<sub>2</sub>DTE

Performing variable-temperature STM on the porphyrin monomer, a threshold of 200 °C was determined for the activation of the bromophenyl side groups. To induce efficient polymerization, i.e. enhanced dissociation and diffusion, the sample was usually heated somewhat higher, to 250 °C. Since the Br<sub>2</sub>DTE monomers are equipped with identical side groups, the same method was employed with the intention to produce chains of DTE switches interconnected by covalent bonds. Fig. 4.17 (a) shows the typical appearance of the resulting structures observed with STM after the heating step and subsequent cooling to 10 K. Coupling has indeed taken place and dendritic structures are found mostly adsorbed on the fcc regions. There appears to be a repulsive interaction between the molecules as they are mostly found isolated. This could be Coulomb repulsion caused by charging of the molecules. While the coupling of the DBTF molecules gave rise to a small amount of branching defects (cf. ch. 2.4), the oligomers formed by Br<sub>2</sub>DTE are characterized by a large number of junction connections. Indeed, purely linear structures are rarely observed, as shown in Fig. 4.17 (a). Structures of recurring shape can be found, e.g. linear structures that bear a resemblance to the monomers (circled) and X-shapes that could correspond to dimers (squares). The geometry and the stability of the structures (as confirmed with lateral manipulation) indicate that the Br<sub>2</sub>DTE monomers can participate in another, unintended type of coupling reaction. This was corroborated by a separate experiment in which non-halogenated DTE molecules were heated on a Au(111) surface. The appearance and stability of the resulting structures were similar to that shown in Fig. 4.17 (a). The cause for this coupling might lie in the thienyl units, because they are not present in the other types of monomers investigated so far. Thus, the coupling of the Br<sub>2</sub>DTE turned out to be problematic and did not produce the intended results. In an attempt to ameliorate the outcome the preparative procedure was changed into a copolymerization, employing Br<sub>2</sub>DTE together with DBTF, cf. ch. 1.6. The intention was to connect the switches from both sides with molecular wires, and simultaneously reduce the number of erroneous connection by the dilution of the DTE by terfluorene. Fig. 4.17 (b) shows the two molecules co-deposited onto a Au(111) surface at room temperature. At the coverages employed (less than half a monolayer) both types of monomers are found to form small separate islands that are characterized by the order that was observed for the individual molecule, i.e. double rows for DBTF (solid arrow) and triangles for Br<sub>2</sub>DTE (dashed arrow). Fig. 4.17 (c) shows the same preparation after a heating step of 200 °C lasting for five minutes. As is visible from the image the two different species intermix efficiently to form covalently bound structures, as was observed for the mixture of terfluorene and porphyrin (cf. ch. 3.2). Furthermore, the

number of DTE bonds of the unintended type is reduced by the presence of the terfluorene. Chains of fluorene containing single, i.e. non-branching, switches are regularly observed. An instance of the smallest switch unit contacted on both sides is shown in Fig. 4.17 (d).

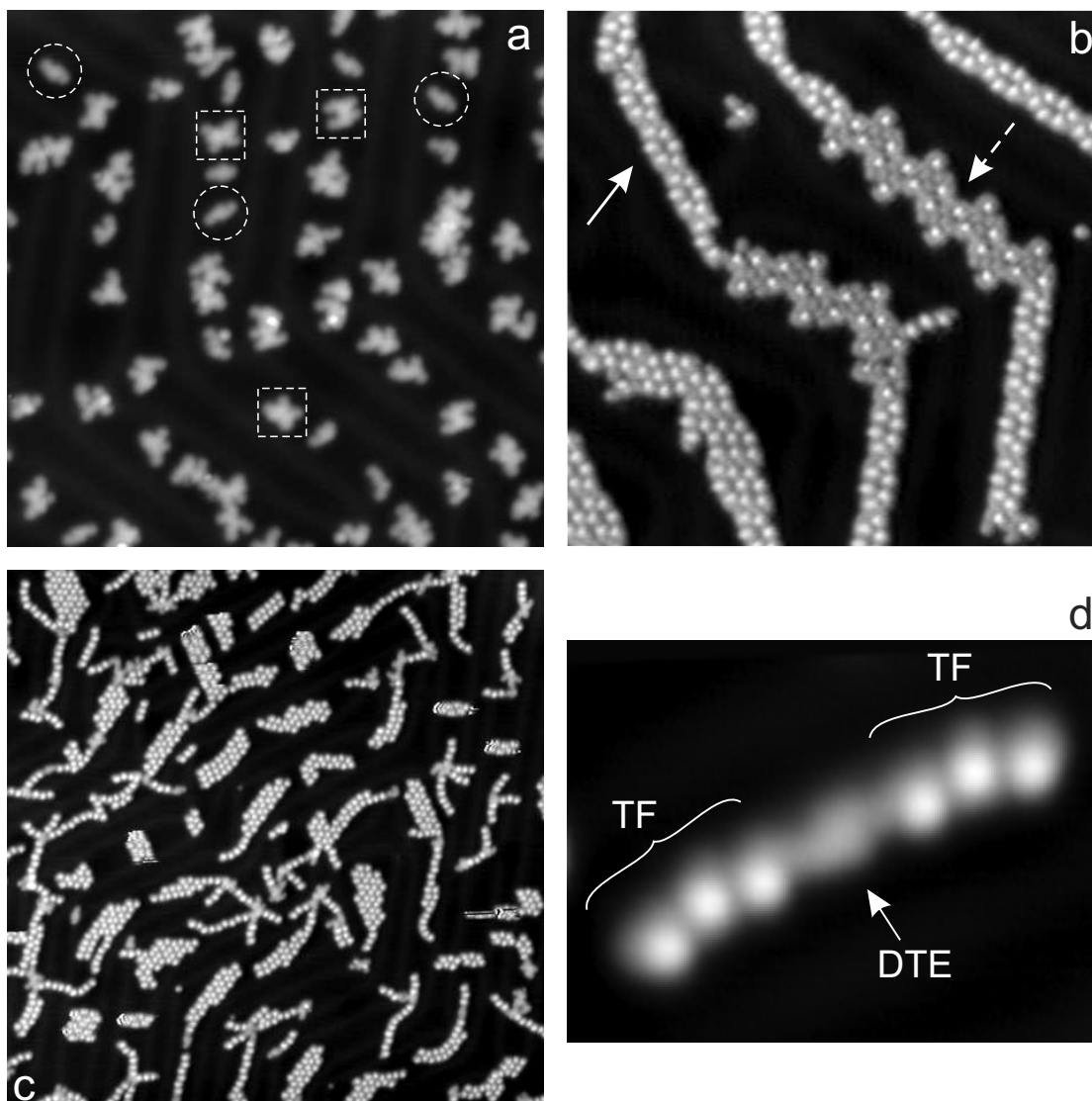


**Figure 4.17:** (a) STM image of the Br<sub>2</sub>DTE molecules on Au(111) after the application of a heating step (250 °C, 5 min), 33 × 33 nm<sup>2</sup>. (b) STM image of a codeposition of Br<sub>2</sub>DTE (dashed arrow) and DBTF (solid arrow) on Au(111) before the heating step (28 × 28 nm<sup>2</sup>). The same preparation after a heating step 5 min at 250 °C is shown in (c) (67 × 67 nm<sup>2</sup>). (d) high resolution image of a TF-DTE-TF molecular chain (6 × 8 nm<sup>2</sup>). Imaging parameters for all: 500 mV, 0.1 nA.

However, the reaction of the unknown type coupling DTE units cannot be suppressed altogether and therefore branched structures are still present. Like in the case without DBTF the switches are found in several appearances. DTE units forming a link in a chain appear in an angled as well as a linear form. While the incorporation into chains is successfully performed and switches such as the one in Fig. 4.17 (d) are frequently observed, the appearance of the DTE moiety is changed from the intact one described in section 4.2.1. After the heating step, i.e. going from Fig. 4.17 (b) to (c) the DTE assumes a lower apparent height and homogeneous contrast, similar to what was

observed for the preparation of closed-ring Br<sub>2</sub>DTE, cf. section 4.2.2. More specifically, the central protrusion with the intramolecular features identified with the methyl group appears to be absent. Thus, while the DTE segment can still be identified (this is not possible any more for the structures display in Fig. 4.17 (a)), the intactness of the switching moiety cannot be confirmed from the images. Therefore, while the configuration shown in Fig. 4.17 (d) is favorable for e.g. pulling experiments, the presumed damage inflicted to the switching unit by the heating step made it necessary to adapt the coupling process.

### 4.3.2 Oligomeric chains made from I<sub>2</sub>DTE

As shown in ch. 2.4, the iodinated terfluorene (DITF) requires a lower activation energy which leads to the growth of extended chains already at room temperature. The omittance of the heating step allows the connection of these precursors yielding virtually defect-free structures. It was therefore attempted to apply this successful approach to the switch molecules by employing iodinated DTE precursors (labeled I<sub>2</sub>DTE (o) in Fig. 4.8) with the intention of avoiding both the branching type of coupling as well as the modification to the functional unit. The structures that are observed after the deposition of I<sub>2</sub>DTE on Au(111) held at room temperature are shown in Fig. 4.18. Different from the appearance of the brominated monomers forming interlocked islands, the molecules appear as chains of switches. Unlike the case shown above (Fig. 4.17) chain formation connects the central units via the legs of the switches and no signs of branching are observed. Equally as important, the central unit appears to be unchanged with regard to the appearance of the intact monomers (cf. section 4.2.1). A repeating unit is circled in the inset of Fig. 4.18. The connection between the units is homogeneous and no boundary is visible any more. The molecules' central part displays the characteristic bright lobe with the surrounding brim as shown in Fig. 4.11. The bright feature originates from the thienyl group that is slightly tilted upwards located at the inside of the angle (the corresponding methyl groups are displayed as small wedges in the inset of Fig. 4.18). The DTE display an asymmetric shape and their orientation can be inferred by the brim, which displays a gap on the side where the methyl group is pointing inwards (cf. Fig. 4.9 (d)) on the leg that appears longer for the monomers. For this angled conformer there are three different types of connections possible: long-long, long-short, and short-short, as sketched at the bottom of Fig. 4.18. All three types of connections are represented in the high-res inset. The most frequently observed is the long-short combination with a distance of  $(13.8 \pm 0.5)$  Å as measured from STM images (distance 'd' in the sketch). This is compatible with a calculated chain that predicts a distance of 14.8 Å between neighboring units' protruding methyl groups. (The calculation is for a molecular chain in the gas phase [234]). Most importantly for the corroboration of the intactness, recording differential conductance curves (cf. Fig. 4.19) show the same features in dI/dV curves as the intact DTE monomers shown in Fig. 4.16, whereas the stability of the newly formed bonds was asserted in many instances of manipulation with the STM tip. Both of the latter points will be discussed in detail in ch. 4.4.

The chains are mostly located on the fcc regions of the herringbone reconstruction and the largest part is observed in a zigzag conformation with a smaller number of linear segments in between.

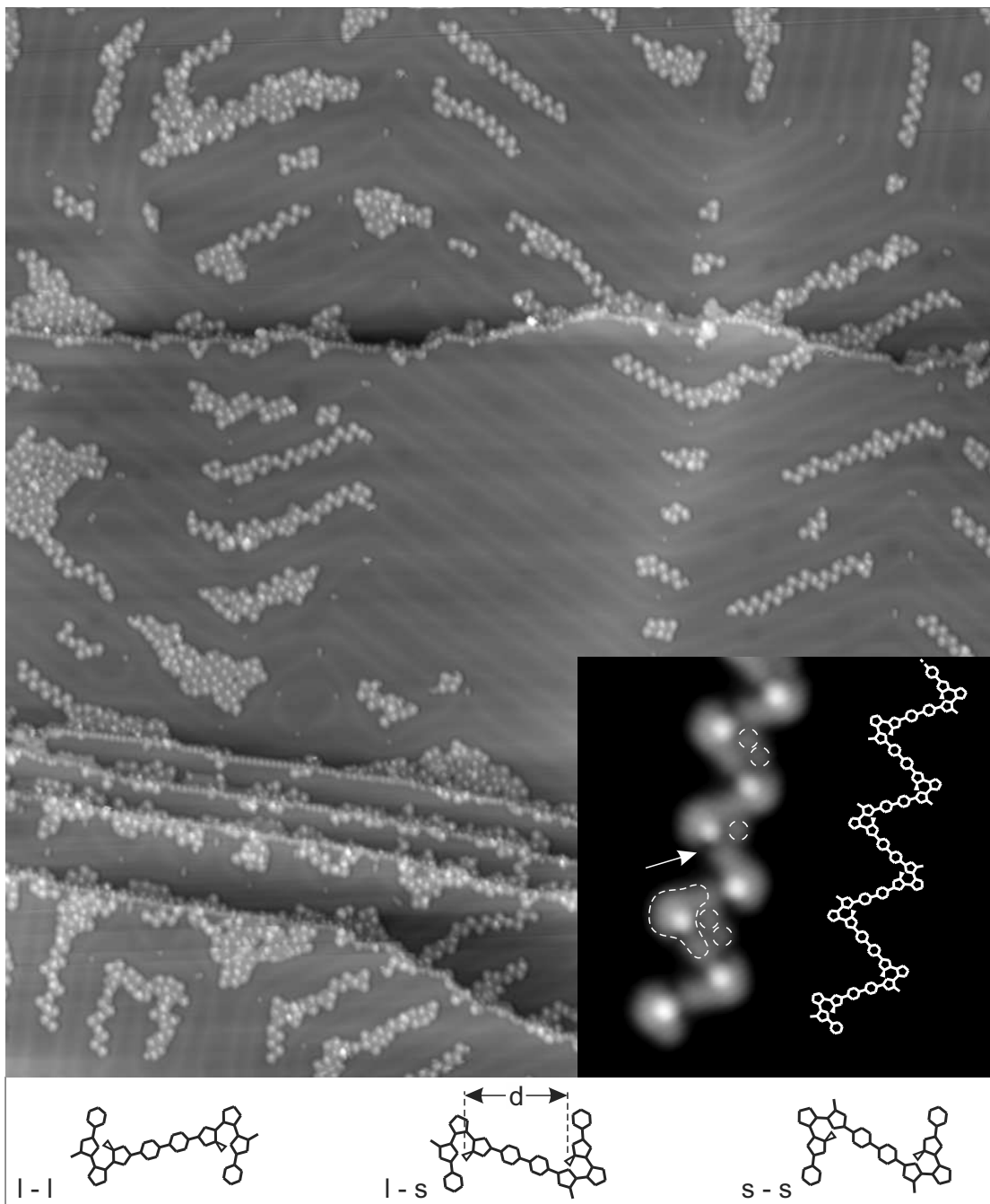


**Figure 4.18:** Overview image of  $I_2DTE$  deposited onto  $Au(111)$  at room temperature. Image size  $130 \times 140 \text{ nm}^2$ ,  $-500 \text{ mV}$ ,  $0.1 \text{ nA}$ . Several horizontal step edges separate the terraces occupied with molecular chain structures. The inset shows a high-resolution segment of an oligo-DTE chain with a sketch of the according chemical structure. Image size  $9 \times 9 \text{ nm}^2$ ,  $500 \text{ mV}$ ,  $0.1 \text{ nA}$ . The arrow denotes the position of a gap in the brim (cf. main text). The dashed circles highlight lobes that likely are iodine adatoms from the activation process. Since the units are not symmetrical, there appear three different types of connections, as sketched below the STM images. All three types can be distinguished in the inset.

In some cases the gaps in the side of the chains appear filled with adatoms (marked by dashed circles in the inset of Fig. 4.18), which can lead to a slight reduction in contrast. As these atoms were not observed for the molecules without iodine, the identification suggests itself. At this low coverage, chains are observed isolated as well as arranged in islands.

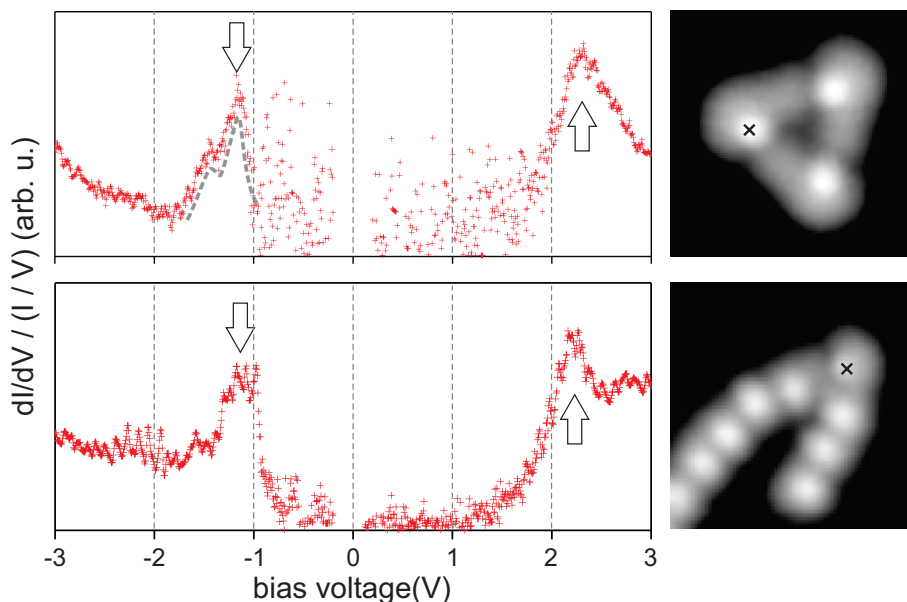


**Figure 4.19:** Normalized  $dI/dV$ -spectra recorded on a DTE unit in a homopolymer and a copolymer as indicated by the  $\times$  in the STM images to the right. (top) Cyclic DTE trimer,  $3.5 \times 3.5 \text{ nm}^2$ . (bottom) DTE contacted from both sides with TF units,  $5 \times 5 \text{ nm}^2$ . Both images recorded at 500 mV, 0.1 nA. The HOMO (LUMO) is indicated by the down (up) arrows. Intervals of small differential conductance signal, i.e. mostly in the gap, are sensitive to the enhancement of noise by the normalization procedure, which is especially visible in the top graph. Therefore, a curve is added to the HOMO in this spectrum as guide to the eye.

The present findings point to the conclusion that the produced structures displayed in Fig. 4.18 are indeed the intact and covalently coupled DTE. This is the first realization of such a structure on a surface. Such a chain coupling several switches into one entity is very interesting in itself. For instance, thinking in terms of information storage eight units in one asymmetric compound such as the segment shown in the inset of Fig. 4.18 could be used to store one byte of information. (The shown area provides space for at least four such chain segments, i.e. 4 byte/ $100 \text{ nm}^2$ , which is equivalent to more than 25 Tbyte per square inch). It has to be noted that the predominant conformation is the angled one (as the ones shown in the inset) that was identified as the non-switching one above. This might be considered as a drawback. However, as will be shown below, for cyclization of individual units this poses a surmountable challenge, while for the parallel switching of a large number of such molecules the inclusion of additional groups during synthesis could be attempted to ensure a favorable, i.e. the linear, conformation on the surface. (This will be addressed below with the TM-I<sub>2</sub>DTE molecules). By heating the surface it could be shown that these structures withstand a heating step to 100 °C. Continued coupling is observed upon these annealing steps producing longer chains, whereas the characteristic features of the repeating units remains unchanged. This is analogous to what was observed for DBTF, cf. ch. 2.4.

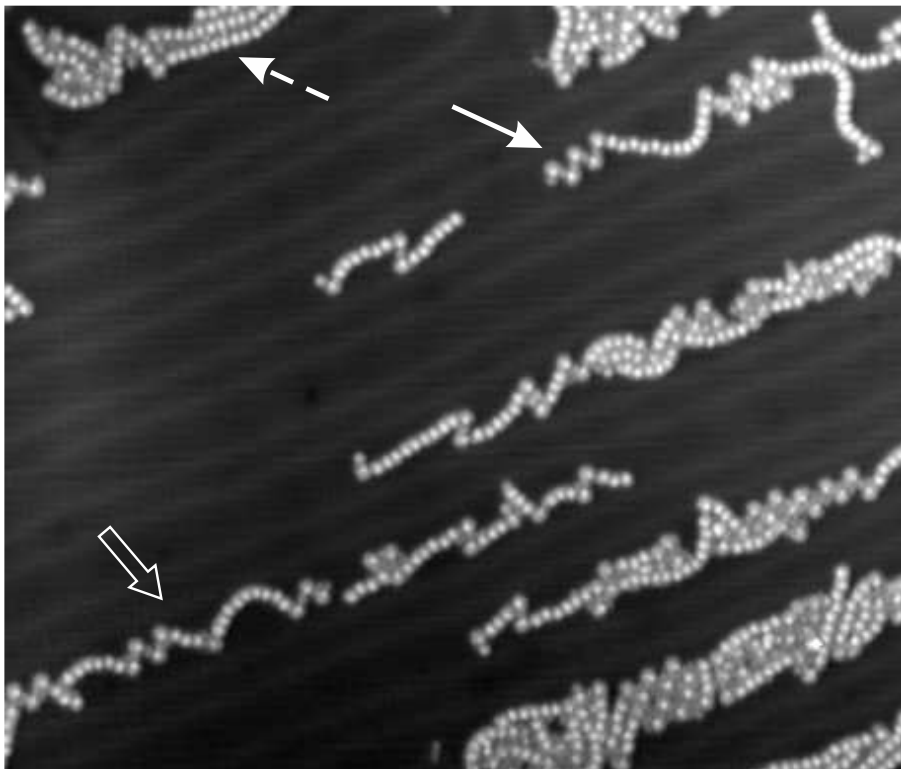


**Figure 4.20:** STM image of a copolymer of terfluorene and dithienylethene on Au(111), parameters 500 mV, 0.1 nA, image size  $55 \times 65 \text{ nm}^2$ . Solid and dashed arrows highlight homopolymer sections, the hollow arrow points at an intermixed segment.

The intact connection of the DTE by the above method paves the way for the contacting of individual switches with molecular wires that could not be realized using the brominated precursors, because the switches sustained damage during the heating step. To that end  $\text{I}_2\text{DTE}$  was deposited together with DITF onto Au(111). Since both types of molecules activate at the same time and because the formation of block copolymers was to be avoided, the deposition had to take place simultaneously, much like the case of DITF and  $\text{Br}_2\text{I}_2\text{DTE}$  (cf. ch. 3.2). The resulting structures are shown in Fig. 4.20. The coupling appears to have taken place efficiently and randomly as expected. While homopolymer segments as indicated in the figure by the solid (DTE) and dashed (TF) arrows are also present, there appears a sufficiently large number of intermixed chains that possess isolated units of one type contacted on both sides by the other (as pointed out by the hollow arrow).

While the poly-TF segments appear with a smoother curvature to accommodate the preferred fcc regions of the herringbone reconstruction, the switches predominantly display the characteristic angled shapes (cf. Fig. 4.21). The intramolecular appearance is in marked contrast to the one observed after the heating step that was required by the bromine-substituted monomers, cf. Fig. 4.17 and identical to the one observed for the individual monomers and inside the DTE homo-polymers, cf. Fig. 4.18. Examples for DTE contacted from both sides with terfluorene are shown in Fig. 4.21. As before, the linear DTE species is seldom found. The switch segments have been investigated with  $dI/dV$ -spectroscopy and their differential conductance signature (cf. Fig. 4.19) is in agreement with the one of the fluorenylated monomers and the DTE units in ho-

mopolymer chains. Therefore it can be concluded that the switches covalently couple with the terfluorene units without damage or significant alteration of their conformation, adsorption or electronic structure. In all cases a binding of the thieno groups to the gold that has been suspected of causing a detrimental influence on the switching behavior [231] has not been observed.

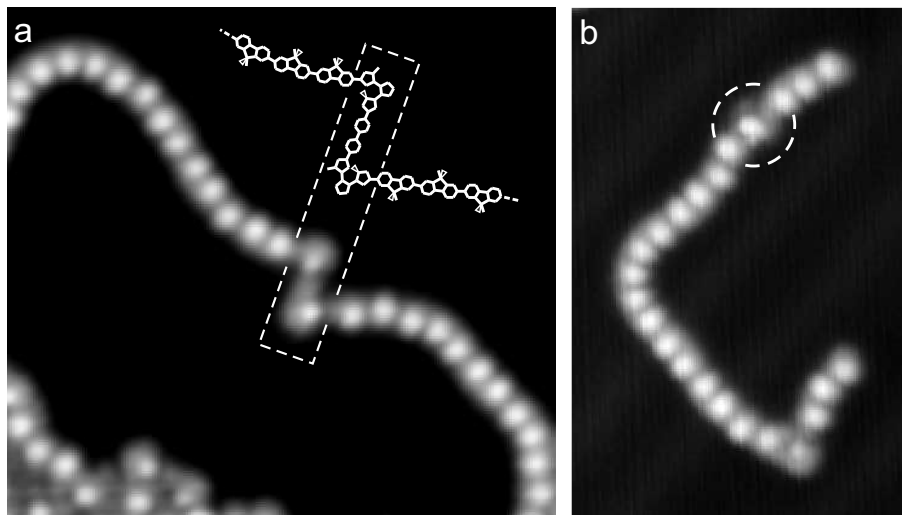


**Figure 4.21:** High-resolution STM images of copolymer chains. (a) DTE-dimer contacted from both sides by long TF chains. The chemical structure is shown as a sketch (enlarged for better visibility). The box encloses the two switches. (b) Example of two switches inside a chain, but this time separated by five units of TF. One of the DTE units has been transformed into the linear conformation (circled). Parameters 500 mV, 0.1 nA, image sized  $14 \times 15 \text{ nm}^2$  (a) and  $10 \times 15 \text{ nm}^2$  (b).

### 4.3.3 Oligomeric chains made from TM-I<sub>2</sub>DTE

Despite the fact that thienyl groups don't appear to form strong bonds to the gold surface, a decoupling of the switching unit might be advantageous for improved performance [192]. Furthermore, as pointed out above, the conformation that is expected to facilitate switching - the linear one - usually constitutes just a fraction of the observed molecules, which is unfavorable, e.g. if one were to try isomerization of the adsorbed molecules on a larger scale by light irradiation. As a remedy it was suggested above that the adsorption and conformation could potentially be influenced by adding appropriate side groups to the molecule. The DTE unit comprising only 15 carbon atoms is rather small and therefore the options are limited without causing a considerable alteration. The cyclopentane ring is a promising candidate in this regard. A substitution with fluorine (F6) has been employed in the past [83, 225]. In the present study a monomer equipped with two di-methyl side groups was employed instead, as sketched in Fig. 4.8 (d).

Fig. 4.22 (a) shows an image of a preparation of TM-I<sub>2</sub>DTE on Au(111) held at room temperature. Differently ordered islands are observed as highlighted by the arrows, displaying linear stripes (solid white) of different periodicity, stacked ordered arrays (hollow white) and disordered regions (black). At first glance, these differences in assembly are puzzling. However, judging from the molecular dimensions the activation has not been complete, i.e. not all iodine sub-

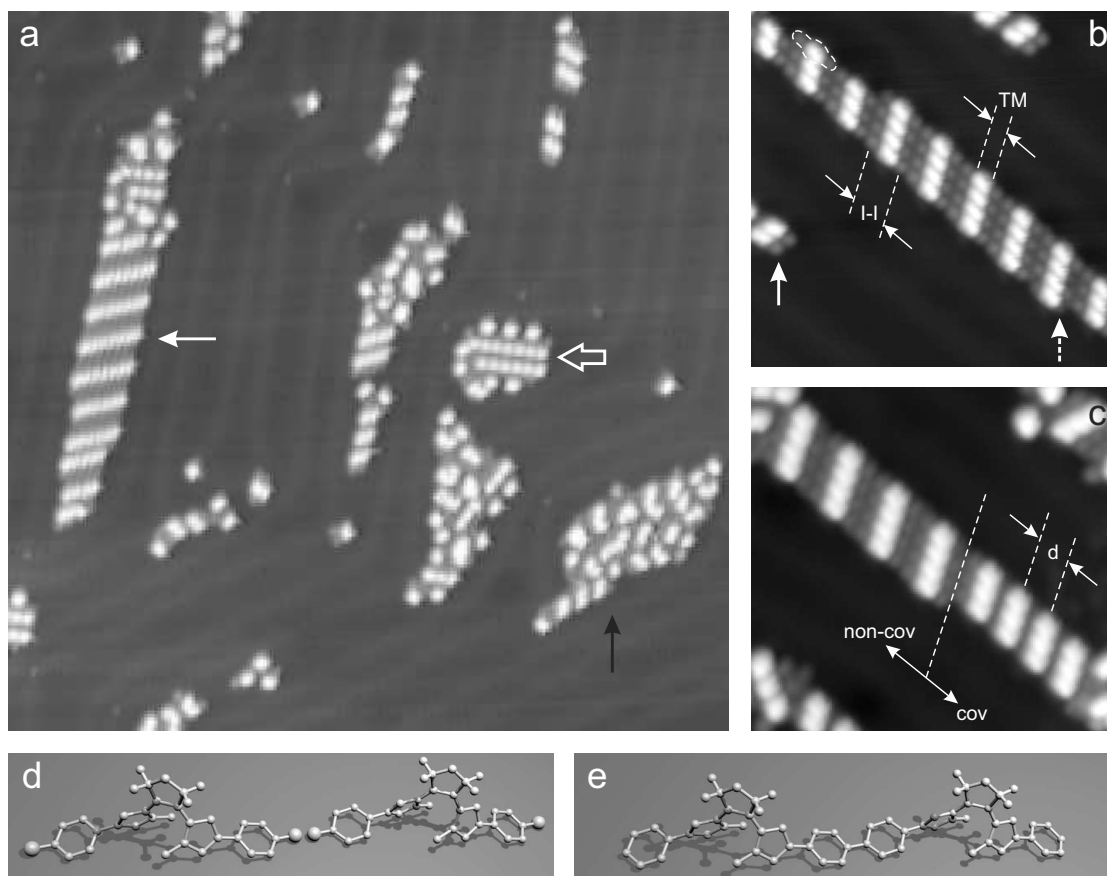


**Figure 4.22:** STM images of TM-I<sub>2</sub>DTE deposited onto Au(111) at room temperature. (a) overview image sized  $60 \times 60 \text{ nm}^2$ , the arrows denote different types of islands as discussed in the text, (b) high resolution image of an island as the one indicated by the white arrow in (a), image size  $17 \times 17.5 \text{ nm}^2$ , the arrows highlight differently terminated monomers, (c) image of a boundary between islands made of non-covalently and covalently linked molecules (as sketched in (d) and (e)), image size  $15 \times 16 \text{ nm}^2$ . Bias voltage for all:  $-500 \text{ mV}$ , tunneling current of (a) and (c)  $50 \text{ pA}$ , (b)  $100 \text{ pA}$ .

stituents have been dissociated from the molecules, similar to what was observed for Br<sub>2</sub>I<sub>2</sub>DTE (cf. ch. 3.2), causing different types of structures. This is corroborated by lateral manipulation, in which monomers are easily identifiable, cf. Fig. 4.23. Their appearance, as shown in Fig. 4.22 (b), is changed with regard to the DTE without tetramethyl. The molecules display a brighter protrusion in the center with a width of  $(9.9 \pm 0.4) \text{ \AA}$  (marked "TM" in (b)) and two smaller lobes at the ends at a distance of  $(18.6 \pm 0.6) \text{ \AA}$  (marked "I - I"). These are in good agreement with the calculated distances of the dimethyl groups and the space between the iodine atoms for the calculated TM-I<sub>2</sub>DTE in the linear, up-right standing conformation depicted in Fig. 4.9 (a). There, the distances measure  $9 \text{ \AA}$  and  $18.4 \text{ \AA}$ , respectively (calculated with Hyperchem for the gas phase [234]). Because of the absence of peaks on the central feature, the width of the central group is measured as full width at half maximum and therefore the van-der-Waals radii of hydrogen are included in the width). Thus, the identification with the iodinated precursors is straight forward. In the lower right corner in Fig. 4.22 (b), a monomer is visible that has been activated, i.e. the outer lobes associated with the iodine are absent (dashed arrow) in contrast to the appearance of the intact ones (solid arrow). On the other hand, other assemblies, such

as the islands indicated in (a) by the hollow white and black arrows are incompatible with the non-coupled monomers. This is highlighted in Fig. 4.22 (c) which display the transition between non-covalently (upper left) and covalently (lower right) connected switches (sketches are shown in (d) and (e)). While the former displays the same distances as the ones in (b) the bright tetramethyl lobes in the latter are more closely spaced at  $(17.0 \pm 0.4) \text{ \AA}$  (marked as distance "d"). The molecular mechanics calculation, again for for up-right standing form, predicts a distance of  $17.8 \text{ \AA}$ , which is slightly higher because the covalently connected chain bends in the gas phase, which is inhibited by the presence of a surface. Furthermore, the protrusions corresponding to the iodines are absent in these chains. It bears mentioning that the monomers as shown in Fig. 4.22 are found almost exclusively in this linear, upright standing conformation that has not been observed before. Thus, it can be ascribed to the presence of the two dimethyl groups that appear to take part in a stabilizing lateral interaction.

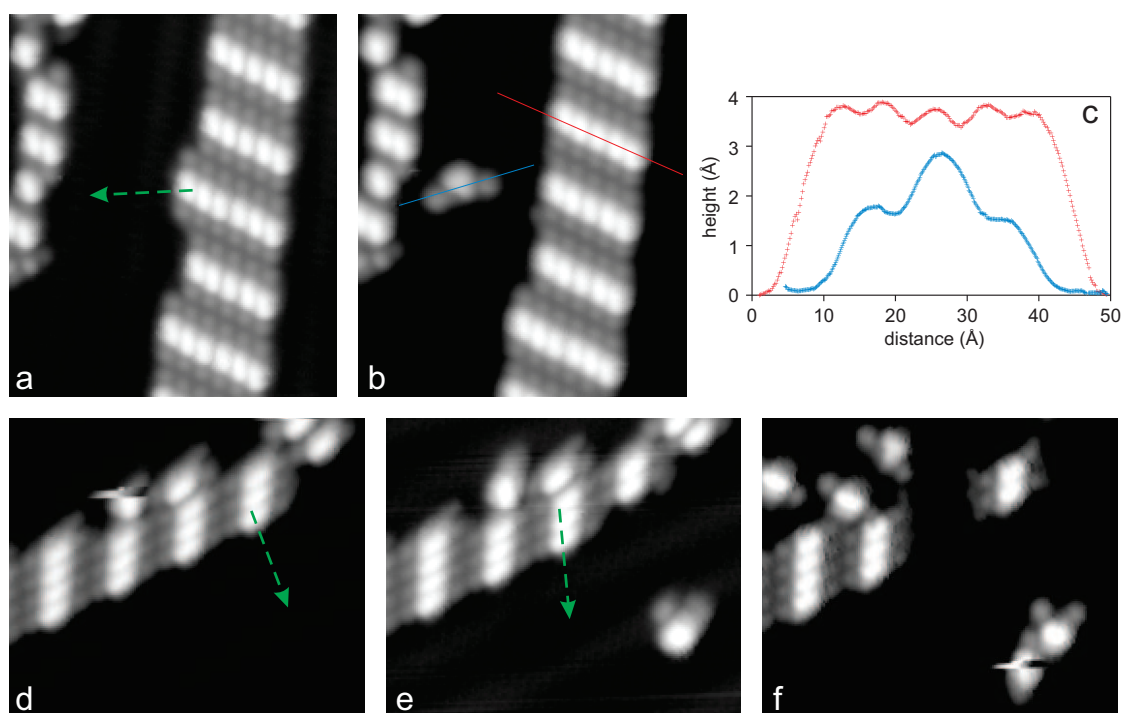


**Figure 4.23:** Examples of lateral manipulation with the STM tip as indicated by the green arrows. (a) before and (b) after such a manipulation, (c) shows line scans across the molecules as indicated in (b). (d) - (f) shows another example, wherein an entire column is removed from the island. Images (a) and (b) sized  $12 \times 14 \text{ nm}^2$ , bias voltage 500 mV; (d) - (f) sized  $11 \times 13 \text{ nm}^2$ ,  $-500 \text{ mV}$ ; all images' tunneling current 0.1 nA.

Fig. 4.23 shows lateral manipulation experiments of the weakly bound monomers undertaken to learn more about the conformation. The tip follows the path as indicated by the green arrows. (a) and (b) record the successful detachment of a single monomer from an island, which corroborates the interpretation of Fig. 4.22. Interestingly, the appearance of the molecule is changed afterwards. The central segment that appears as a bright and linear shape bridging the outer lobes in the island is turned into a triangular shape imaged at lower height. Line scans shown in (c) document this change: while the bright lobes in the island displays a height of approx.  $4 \text{ \AA}$ . the isolated monomer appears at most at  $3 \text{ \AA}$  (recorded at the same feedback

parameters). Considering only the geometry for a moment, for the linear monomer lying on the side as sketched in Fig. 4.9 (c) the additional dimethyl groups should appear at a comparable height as the central protruding methyl which would explain the triangular shape. It appears that the interaction with the adjacent units is necessary to accommodate the linear up-right standing conformation and that a detachment leads to a change in adsorption geometry. Another example is shown in Fig. 4.23 (d) - (f). In a first step, a single monomer is detached as before. However, afterwards, the observed conformation is not the linear but an angled one, analogous to the example discussed above. However, due to the homogenous contrast of the center, the distinction between the symmetric and asymmetric (angled) forms is not unambiguous any more. In a second step, a whole column of switches is removed from the island, which shows that the interaction between adjacent stacks is rather weak.

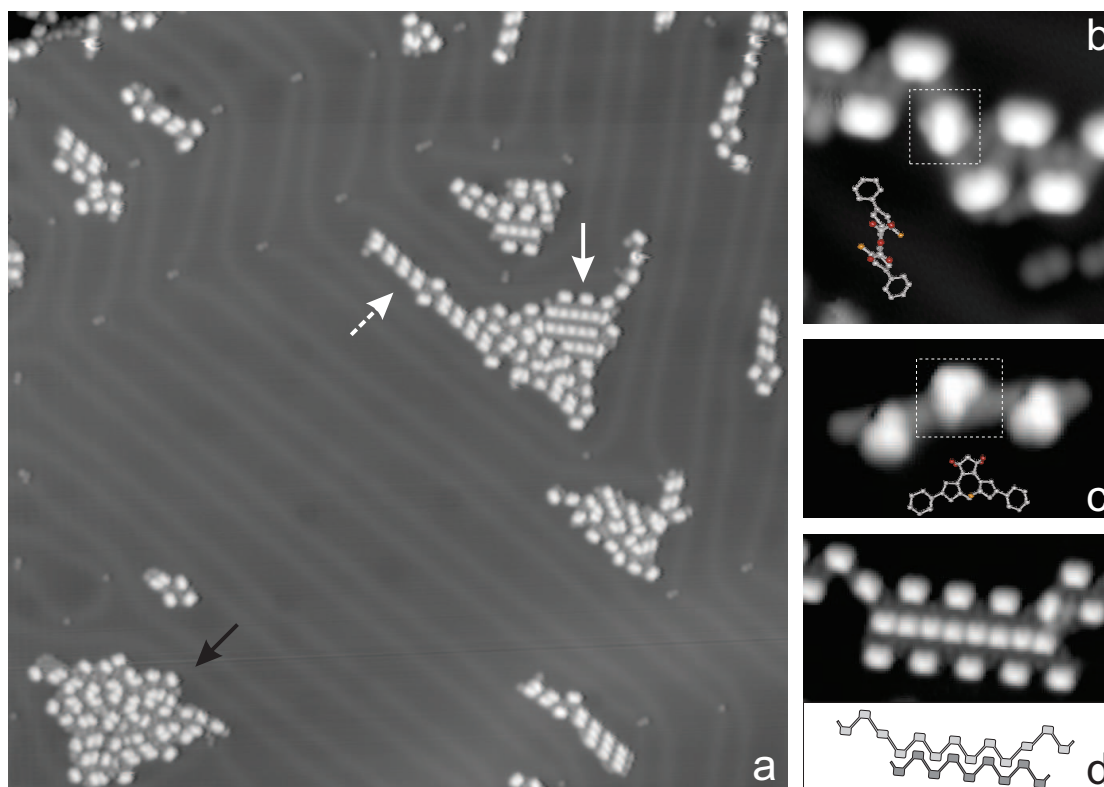


**Figure 4.24:** STM images of TM-I<sub>2</sub>DTE after a heating step (100 °C, 5 min), (a) overview image 70 × 70 nm<sup>2</sup>, (b) high-res segment of a chain 7 × 7 nm<sup>2</sup>, all shown units are in the angled conformation, except for the one contained in the box. For the latter a sketch is shown; (c) a trimer in the sideways-linear conformation, 4 × 7 nm<sup>2</sup>, the boxed unit is again represented by a sketch; (d) image of a regular island of the same ordering as the one indicated by the arrow in (a), 7 × 13 nm<sup>2</sup>, the stacking is sketched below. Bias voltage for all images −500 mV, tunneling current (a) 100 pA, (b) - (d) 50 pA.

The same conformations of the TMDTE repeat unit - linear up, linear sideways and angled - are observed in the covalently connected chains as well, giving rise to differently shaped islands. To induce an efficient polymerization, the surface prepared with the TMDTE chains was subjected to a 100 °C heating step that was found previously to leave the DTE molecules intact. In that way the non-activated islands in Fig. 4.22 are consumed by coupling. The resulting coupled structures are shown in Fig. 4.24 (a). In the linear chains (dashed arrow), the up-linear conformation is

predominantly found, with the occasional angled conformer unit to accommodate bends. Images recorded at high resolution show that the central protrusion associated with the tetra-methyl is slightly slanted with respect to the long axis of the chain, which gives the repeat units a shape resembling a % sign. This becomes especially visible for units that were separated from their neighbors. An example is shown in Fig. 4.24 (b), in which the boxed unit bridges two chain segments made of the angled conformers. The linear unit is shown as a model, which corresponds to the top view of the one shown in Fig. 4.9 (a). In the model, the protruding carbon atoms (the two dimethyl groups and the top one of the cyclopentane) are highlighted in red to account for the central bright bar shape. The two methyl groups pointing left and right (colored orange) give rise to the small lobes, one on each side. As shown in Fig. 4.23 the upright conformation doesn't appear to be the most stable for the switches without lateral neighbors. Fig. 4.24 (c) shows a trimer that was detached from an island by lateral manipulation. Rather than the straight bar center, the three units display a triangular shape as the one observed for the isolated monomer in Fig. 4.23 (b). As the legs are pointing at an angle of almost  $180^\circ$  the conformation is identified with the linear-sideways one with alternating direction, depicted as an inset. As the islands grow, the molecules prefer the angled conformation in which adjacent chains form indented structures with each other. These structures account for most of the angled conformers present on the surface. These can be disordered as the one in Fig. 4.24 (a - black arrow) or locally ordered (a - solid arrow) and (d). It is interesting to note that the protrusion associated with the tetramethyl appears contracted in the indented structure with respect to the outer ones (cf. the central horizontal row in Fig. 4.24 (d)). The indentation is the reason for these small and closely spaced lobes. However, the appearance is identical once the interlocking is lifted by manipulation.

As for the monomers, from images one cannot conclude whether these angled units are in a symmetric (i.e. likely isomerizable) or non-symmetric (non-isom.) form. However, since the linear chains account for about half the repeat units of the presented preparation, this results in a large increase of switches that are, at least judging from their conformation, potentially switchable. Note that the linear species was found very infrequently for the chains consisting of DTE. Therefore, the declared goal to increase their percentage is successfully accomplished by only a small change to the molecular structure, i.e. the attachment of two dimethyl groups to the cyclopentane ring. As chains appear to be the preferred shape for smaller coverage, this might constitute a route for an even higher ratio of favorable to unfavorable conformation.

## 4.4 Manipulation of oligo-DTE

In the last sections it was described how the DTE switches appear on the surface, as unreacted monomers and covalently connected in chains, the latter both as homopolymer and as copolymer together with terfluorene. The characterization and successful polymerization provide the necessary groundwork for the manipulation of the switches. In this chapter, I will address the modifications that can be induced in the described structures, most importantly the isomerization. The STM tip constitutes an ideal tool in this regard, as described in ch. 1.3. For connected or individual molecular switches, in order to harness the reduction in size of the individual unit, the addressability has to be provided. However, stimuli such as light or electric fields do not deliver single molecule addressability. It has been attempted to create compounds of connected DTEs with different optical signatures ("multicolor") for selective optical switching [235], but examples containing DAE units that deliver the full intended functionality are rare [236]. Addressing individual units spatially instead of spectrally, these difficulties can be avoided by inducing the switching with the STM tip. For switches on a metal surface, it has been shown that an isomerization can be induced by tunneling electrons [193, 201] and electric field [193] as well as light irradiation [192]. As the tunneling current can be applied with submolecular resolution, units can be affected individually, possibly even when they are connected to an oligomer. (While the targeting of single nanometer-sized molecules employing the electric field of the STM tip is probably not feasible, its operational radius can be as small as tens of nanometers [15] and can even have a local influence if combined with the tunneling current [28]).

As the DTE is intended as a conductance switch in a molecular wire, switching by passing a current along the latter would be advantageous. As sending a current through a single molecular wire is inhibited by the presence of the metal surface the pulling approach, that has been described in ch. 2.1.1, is again applied. Similar to the effect of applying voltage pulses from the STM tip separated by a vacuum gap, the resulting behavior might be different however due to the geometry of the participating molecular orbitals.

The crucial question is whether the molecules can switch, i.e. whether the functionality that has been shown in solution can be preserved upon first the adsorption on the metal and second the incorporation into the chains.

All described switches and chains of switches have been subjected to voltage pulses of different bias and current, both separated from the STM tip by a vacuum gap and in the junction geometry in which the molecule forms a bridge between the tip and the sample. As will be shown, differential conductance ( $dI/dV$ ) spectroscopy constitutes the appropriate tool for the determination of the isomer's state. Suitable parameters have to be identified for the read-out, since the required bias sweeps can again be considered as switching attempts, whereas accidental ring-closure or -opening has to be avoided. Considering the brominated monomers, the readily dissociable carbon-halogen bond prevented the recording of  $dI/dV$ -spectra at bias voltages beyond 2 V. In this bias window switching has not been observed. The isomerization of the dissociated DTE (i.e. the ones without the bromine substituents) has not been attempted due to the uncertainty about the condition of the molecule. The DTE switch with fluorene groups at each end constitute a more promising candidate. Voltages as high as 3 V could be applied

without inflicting damage. However, with these molecules the results remained inconclusive. The DTE units coupled to chains made from iodinated precursors (cf. Fig. 4.18) on the other hand did display an interesting behavior upon manipulation and the following results are to prove that isomerization can indeed be induced for selected units inside these oligomers. Since they turned out to be the best system in this regard, it will be described in greater detail.

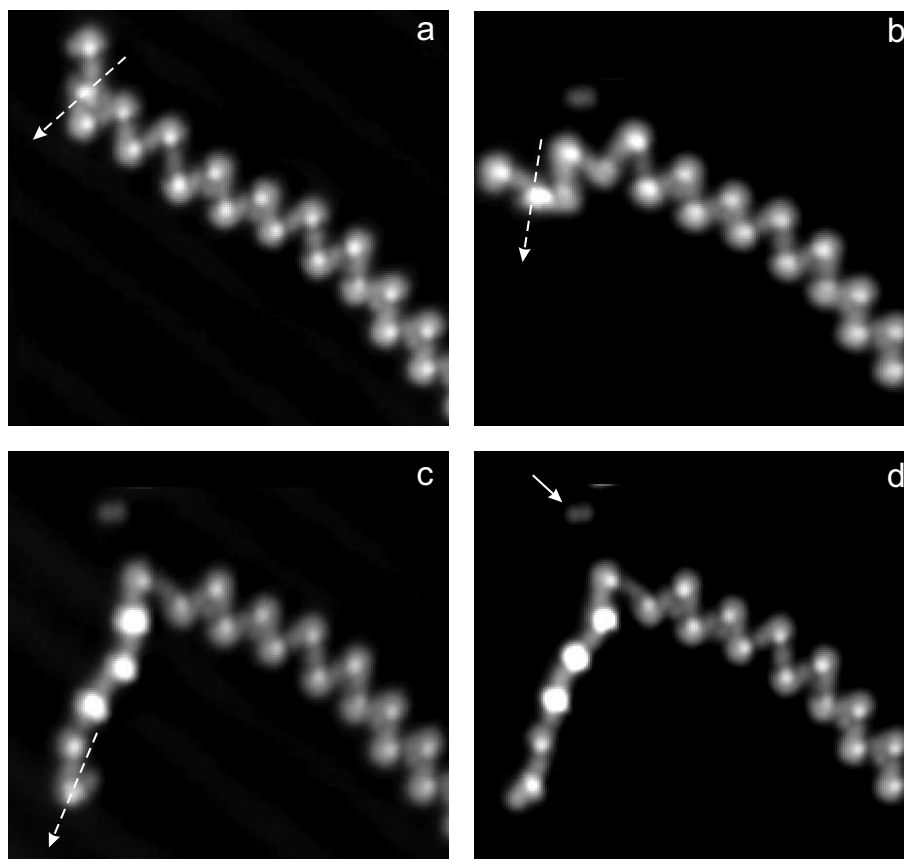


**Figure 4.25:** Sequence of STM images of the same surface area showing a chain made of DTE in between lateral manipulation attempts (the path of the tip during manipulation is indicated by the dashed arrows). Images sized  $15 \times 16 \text{ nm}^2$ , 500 mV, 0.1 nA. The second DTE unit in the chain (crossed by the path of the tip in (a)) is found in the linear form without any external modification. The solid arrow in (d) highlights adatoms that previously resided next to the molecule.

However, before turning to the isomerization, another issue has to be addressed. In the previous section it was noted that the angled conformation that was predominantly observed for these molecules is likely not suitable for performing the isomerization reaction, i.e. ring-closure, because the carbon atoms taking part in the formation of the new bond are not adjacent and cannot approach each other due to the adsorption to the surface. Speaking in terms of Fig. 4.2, the reaction coordinate is restricted to one of the minima, whereas the other is not accessible while the molecule stays in contact with the surface. Fortunately, favorable conformers can be produced by manipulation as shown in Fig. 4.25. The images document the outcome of a series of attempts of lateral manipulation employing the STM tip, leading to the progressive unfolding of the chain. Afterwards, the five terminal DTE units' conformation is rendered linear. Additionally, instances of the linear species are also regularly found, albeit with low frequency. An example is the second

segment in Fig. 4.25 (a) that was observed without any previous modification. While both types of linear units were investigated with  $dI/dV$  spectroscopy and subjected to switching attempts (as discussed below), the ones that were natively found offer a more convenient starting point. This is because of their intramolecular features that are the same as the one found for the monomers, cf. Fig. 4.12, which allows to unambiguously assign a conformation. This is oftentimes not as easily possible for the ones that were prepared afterwards, as is visible for the ones shown in Fig. 4.25. While the chain is rendered linear, there is the possibility of different adsorption geometries that are stable at low temperature. However, due to the gentle parameters employed (usually 20 mV and 20 nA in constant current mode) a manipulation-induced damage is unlikely and was not observed in the differential conductance signal. Thus, both types of switches are candidates for the cyclization reaction.

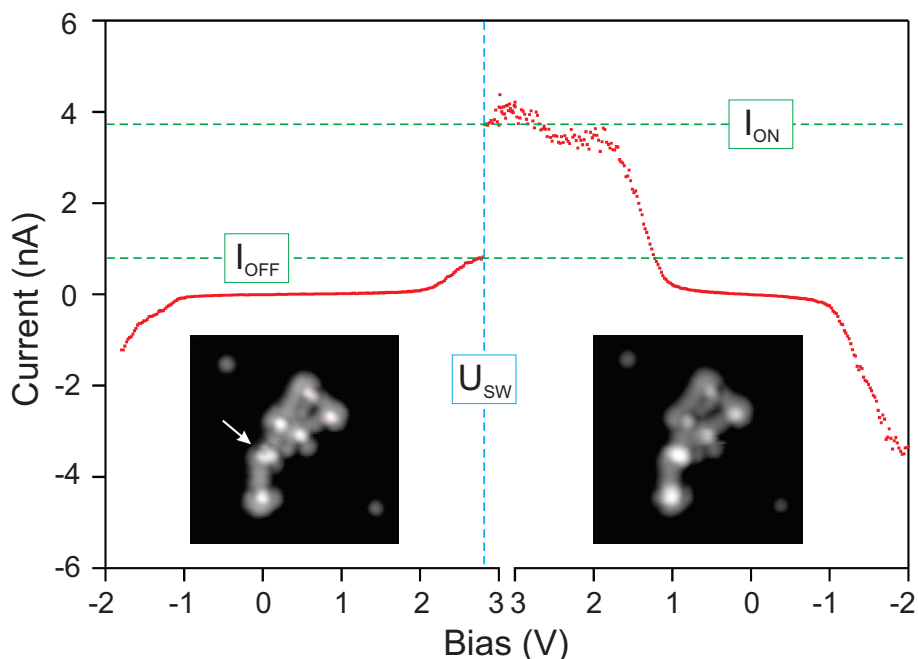


**Figure 4.26:** Current signal in dependence of the bias voltage recorded on top of a DTE molecule on Au(111). Close to three volt (labeled "U<sub>sw</sub>"), the current exhibits a jump, followed by a different backward trace. The inset shows STM images ( $-500$  mV,  $0.1$  nA,  $8 \times 8$  nm<sup>2</sup>) taken before and after the bias pulse. The targeted unit is indicated with an arrow.

Commencing the discussion of the isomerization, Fig. 4.26 shows the current signal recorded during one of the switching attempts in the non-contacted configuration, i.e. with the molecules separated from the tip by several angstroms. The tip is aimed at the center of the unit indicated by the arrow in the inset and the feedback loop is interrupted for the duration of the voltage pulse. The bias voltage is then ramped up from  $-2$  V up to  $+3$  V (bias applied to the sample). The bias is held for a short moment (the immediate reversal of the bias was in some cases found to cause artefacts in the  $dI/dV$  signal) before being ramped down again to the initial value. This procedure is followed to observe if any changes occurred during the bias sweep. The whole curve was recorded in 40 s. Approximately the first half of the signal appears smooth and gives rise to the typically observed signature in  $dI/dV$  (cf. Fig. 4.19). Close to 3 V however (labeled as U<sub>sw</sub>), the curve displays a discontinuity in which the current (labeled as I<sub>OFF</sub>) experiences a sudden

increase. Afterwards it proceeds smoothly again starting from a magnitude approximately 4 times higher (labeled as  $I_{\text{ON}}$ ) as the bias returns to its initial value. STM images are recorded before and after each such attempt. In many cases in which a trace of this type is recorded, small changes in the appearance of the unit are observed afterwards. Imaging at  $-500$  mV in the gap it usually displays a slightly changed (usually increased) height and less intramolecular features (as shown in the inset of Fig. 4.26). Attempts in which the subsequent images display dissociation or debris are disqualified.

Of a total of 917 such attempts performed on oligo-DTE, 58 traces (6.3 %) displayed a behavior that indicated a modification. All except one of these were observed on a linear conformer unit (57 in 842 attempts, or 6.8 %) and only one on an initially angled unit (1 in 75, or 1.3 %). However, in the latter the unit was located at the end of a chain. Therefore, with only one of its legs connected it is likely that in this case the DTE possessed the necessary freedom of movement to perform the ring-closure. Thus, the behavior during voltage pulses is in agreement with the interpretation that the linear conformation indeed constitutes the isomerizable form, whereas the angled one usually does not switch. 51 of the successful attempts displayed a clear jump in the current assignable to a certain bias voltage such as the one shown in Fig. 4.26. In all these cases the jump is observed between 2.5 V and 3 V with an average value of  $\bar{U}_{\text{sw}} = (2.9 \pm 0.2)$  V. Note that this current signature is only observed in one polarity with the sample on positive bias with respect to the tip. The average ratio between  $I_{\text{ON}}$  and  $I_{\text{OFF}}$  at the respective switching bias is  $4.3 \pm 2.6$ .

The different current trace after the jump is accompanied by a modified differential conductance ( $dI/dV$ ) signal which reflects changes in the density of states. The  $dI/dV$  signal is recorded together with the current by means of a lock-in amplifier using the following parameters:  $\nu = 723$  Hz,  $A = 20$  mV, time const = 100 ms. To ensure that the tip is in proper working condition (clean metal) spectra are recorded alternately on the molecule and the bare metal surface, which is characterized by the Au(111) surface state [51, 237]. The  $dI/dV$  signal is the most important indication for successful isomerization, because in the case of ring-closure the HOMO-LUMO gap is reduced due to the electrons' delocalization over the entire molecule and the resulting change in quantum confinement. Fig. 4.27 (a) shows exemplary  $dI/dV$ -signals taken on DTE units connected in chains that didn't previously display a current jump event like the one shown in Fig. 4.26. While the sweeps shown in Fig. 4.27 extend up to 3 V, a bias value high enough to cause the discontinuity in the current as described above, in these curves the forward and backward ramp show identical features and the sum of the traces is shown in the figure. The positions of the features in (a) marked with the solid arrow (HOMO) and dashed arrow (LUMO) are in agreement with the spectrum taken on  $\text{Fl}_2\text{DTE}$  (cf. Fig. 4.16) and thus indicative of the intact, ring-open isomer.

As stated above, the second half of the current trace shown in Fig. 4.26 is associated with a different  $dI/dV$ -signal. It is reassuring that this new curve is stable and usually allows continued recording. Fig. 4.27 (c) shows characteristic spectra (again the sum of forward and backward traces) taken on top of a unit for which a successful current jump event has been observed. While the highest occupied orbital (solid arrow) appears nearly at the same energy as before, the peak associated with the lowest unoccupied orbital is shifted downwards

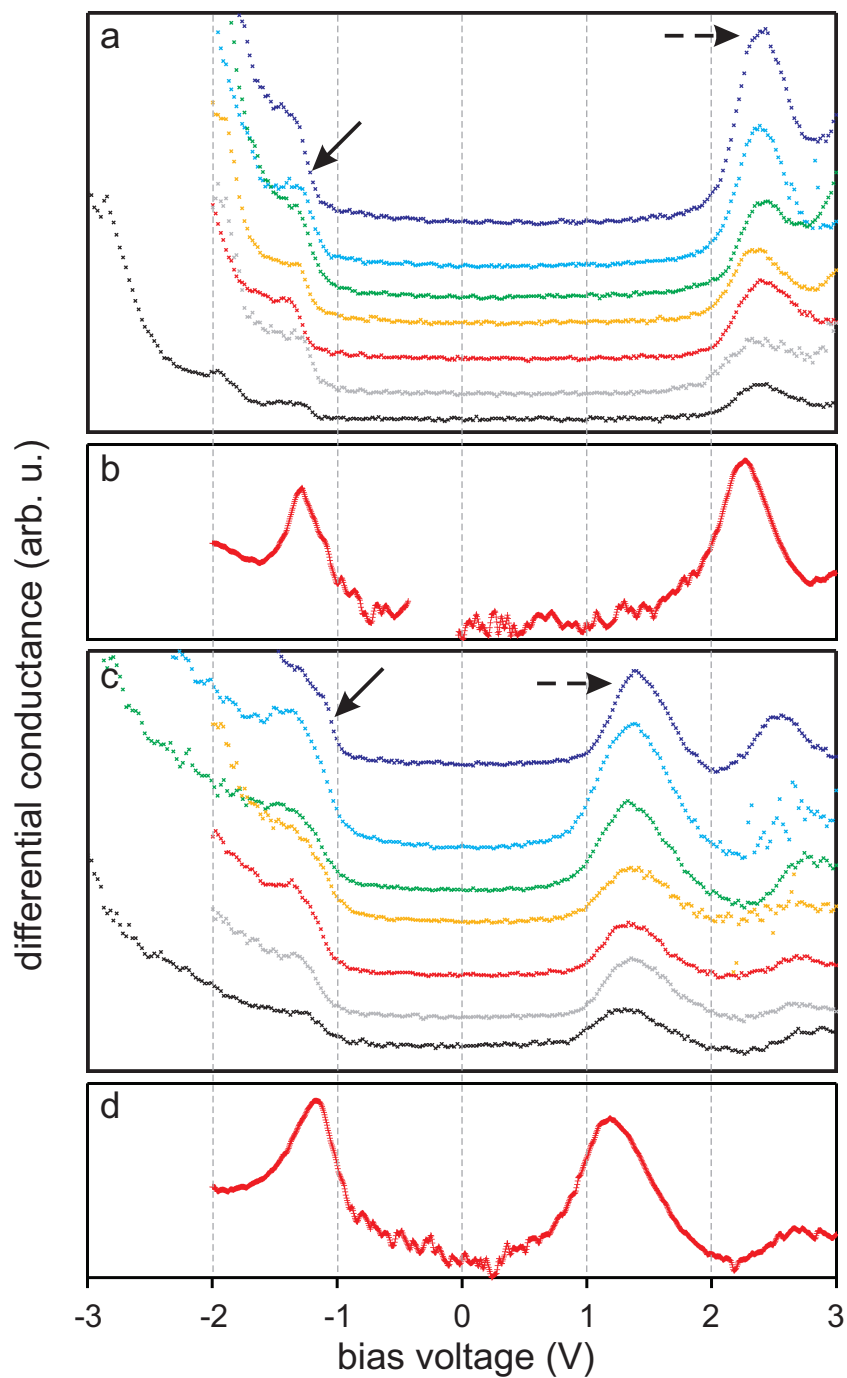


**Figure 4.27:** Characteristic differential conductance signals recorded on top of different DTE units connected in chains. The spectra in (a) agree with the ring-open isomers. In the unmodified spectra, the HOMO usually appears as a shoulder (solid arrow). (b) shows the sum of 16 normalized spectra (including those shown in (a)). Spectra like the examples shown in (c) are observed after current jumps like the one shown in Fig. 4.26. (d) Sum of 17 normalized spectra of the latter type, including those shown in (c). The spectra in (a) and (c) are shifted vertically for better visibility.

considerably by approx. 1 eV. The positions of the HOMO and the LUMO for the ring-open molecule are found to be (averaged over 155 dI/dV curves)  $E_{\text{HOMO}} = (-1.2 \pm 0.1)$  eV and  $E_{\text{LUMO}} = (2.3 \pm 0.1)$  eV. Evaluation of the individual HOMO-LUMO distances resulted in a gap of  $E_{\text{gap}} = (3.5 \pm 0.1)$  eV. These values are read from the normalized spectra ( $\frac{dI/dV}{I/V}$ ) as shown in Fig. 4.27) (b), since in the raw data the HOMO is oftentimes only visible as a shoulder on the occupied side. Evaluation of the modified curves like the ones shown in (c) was performed in the same way yielding  $E_{\text{HOMO}} = (-1.2 \pm 0.1)$  eV and  $E_{\text{LUMO}} = (1.2 \pm 0.2)$  eV with an average gap of  $E_{\text{gap}} = (2.3 \pm 0.1)$  eV. (As the current discontinuity is a relatively rare event, the number of averaged spectra is smaller in this case, counting 72.) The error in the above values reflects the deviation present in the energy of the dI/dV features. These might be caused by differences in the local environment of the unit and also small differences in the exact location of the tip, both laterally and vertically. The central result is that the change in the differential conductance signal entails a strong shift of the LUMO (whereas the position of the HOMO is almost unchanged) which results in the reduction of the HOMO-LUMO gap by more than 1.1 eV on average.

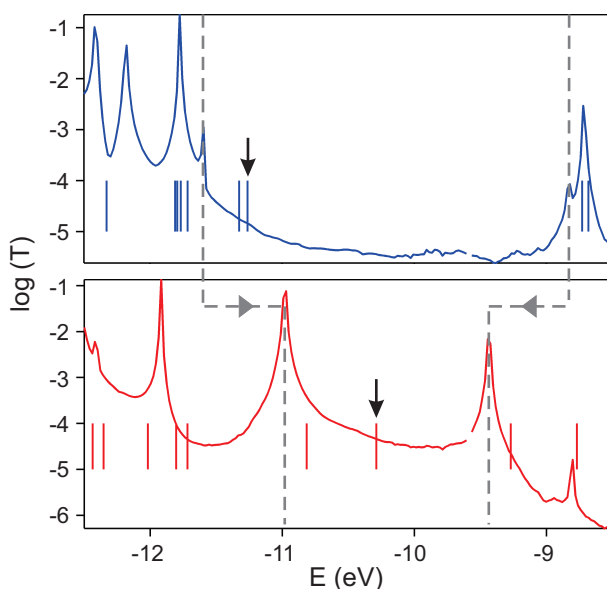


**Figure 4.28:** Transmission spectra ( $\log T$ ) calculated for the open (top) and closed (bottom) linear unit ( $\text{Br}_2\text{DTE}$ ). The vertical lines denote the levels of the free molecules (HOMO levels indicated by the arrows) that are broadened and shifted due to the adsorption to the gold surface (continuous lines). Calculation by M. Grisolia and C. Joachim, CEMES-CNRS, Toulouse.

The energetic shift found in dIdV-spectroscopy can be compared with the theoretical curve shown in Fig. 4.28. It displays the transmission of the calculated  $\text{Br}_2\text{DTE}$  monomer taking into account the influence of the surface. The discrete levels of the molecules in the gas phase are broadened and shifted to resonances. While an absolute placement of the levels is not possible due to ambiguity in the position of the Fermi level, energetic differences can be examined. While the size of the calculated gaps is smaller than the experimentally observed ones, the change going from the ring-open to the ring-closed isomer (indicated by the dashed lines) is approx. 1.2 eV, which is very close to the experimentally observed value of 1.1 eV. Furthermore, cyclic voltammetry measurements (performed by M. Pätzelt and S. Hecht) display a gap of 3.35 eV for the open isomer of  $\text{Fl}_2\text{DTE}$  and 2.0 eV for the closed one, i.e. a difference of 1.35 eV.

Thus, the collected information about the behavior of the molecules, i.e. the observation of the current jump, the emergence of a modified differential conductance signal with a smaller HOMO-LUMO gap – virtually only observed on the suitable conformers – and the agreement of the gap with both the prediction of calculation and complementary experimental techniques show that the ring-closing process could indeed be induced by the application of a bias pulse. This result is an important step to show the viability of the molecule as a functional unit on the surface. Since the process is only observed for positive sample bias polarity (tunneling into the empty molecular states) and at a magnitude at which the LUMO (or possibly also higher states) are accessible, it is likely that the process is facilitated by resonant tunneling. On the contrary, the behavior is not indicative for vibrational excitation by (off-resonant) inelastically tunneling electrons and no switching was observed for large tip-sample distances, i.e. without tunneling electrons. Thus, the first half of the switching cycle has been observed. On the other hand, the reversibility of the process cannot be automatically assumed. For instance, Feringa et al. reported that while the ring-opening of a (differently substituted) DTE molecule is still allowed by the attachment to gold electrodes, the reverse process is prohibited by the introduction of gold electronic states [221].

This is more so the case, since the magnitude of the bias required to induce the isomerization is in principle large enough to induce the breaking of bonds inside the molecules. While it is unlikely that random damage inflicted on the molecule leads to a recurring signature in differential conductance, this possibility could elegantly be excluded by restoring of the ring-open spectral fingerprint. The low probability of the tip-induced ring-closure poses a challenge in this regard, because it is the only way to produce the 'on'-state species, since this isomer did not withstand the evaporation procedure, as described above. Furthermore, if the probability of the back reaction was equally low, this would render the chance of a successful observation of an entire switching cycle very small. Nonetheless, the reappearance of the initial spectrum was observed several times, as shown in Fig. 4.29. It shows a selection of a series of bias ramps recorded on top of one and the same DTE unit inside a chain (linear unit indicated by the arrow). Spectra that are identified with the ring-open isomer are colored red, those of the ring-closed form blue. Initially, as shown in (c), the unit display the characteristic signal of the ring-open switch. However, in (d) a switching event is observed and the backward trace (blue) follows a different curve analogously to what was observed in Fig. 4.26 for the current signal. The same curve is recorded in the following spectrum (e). However, in one of the subsequent attempts the peak characteristic for the closed form at +1.2 eV vanishes and the open-ring peak at around 2.3 eV is recovered (f). This alteration is observed several times, always on the same unit. Unlike the current jump observed for the cyclization reaction, the reverse process is not associated with a clear signal that could be used to pinpoint the cycloreversion to a specific bias to help to elucidate the mechanism.

It is worth noting that the feature associated with the HOMO is more pronounced for the ring-closed form (blue curves) than the ring-open ones (red). This and the application of rather low set-point currents to avoid damaging the molecule might be the reason for the temporary loss of a clear feature on the side of the occupied states (negative bias) for curves (f), (g) and (j). However, a clear step is observed in (i) which together with the fingerprint at around 2.4 eV indicates the return to the initial open form. Furthermore, after 35 such attempts the appearance

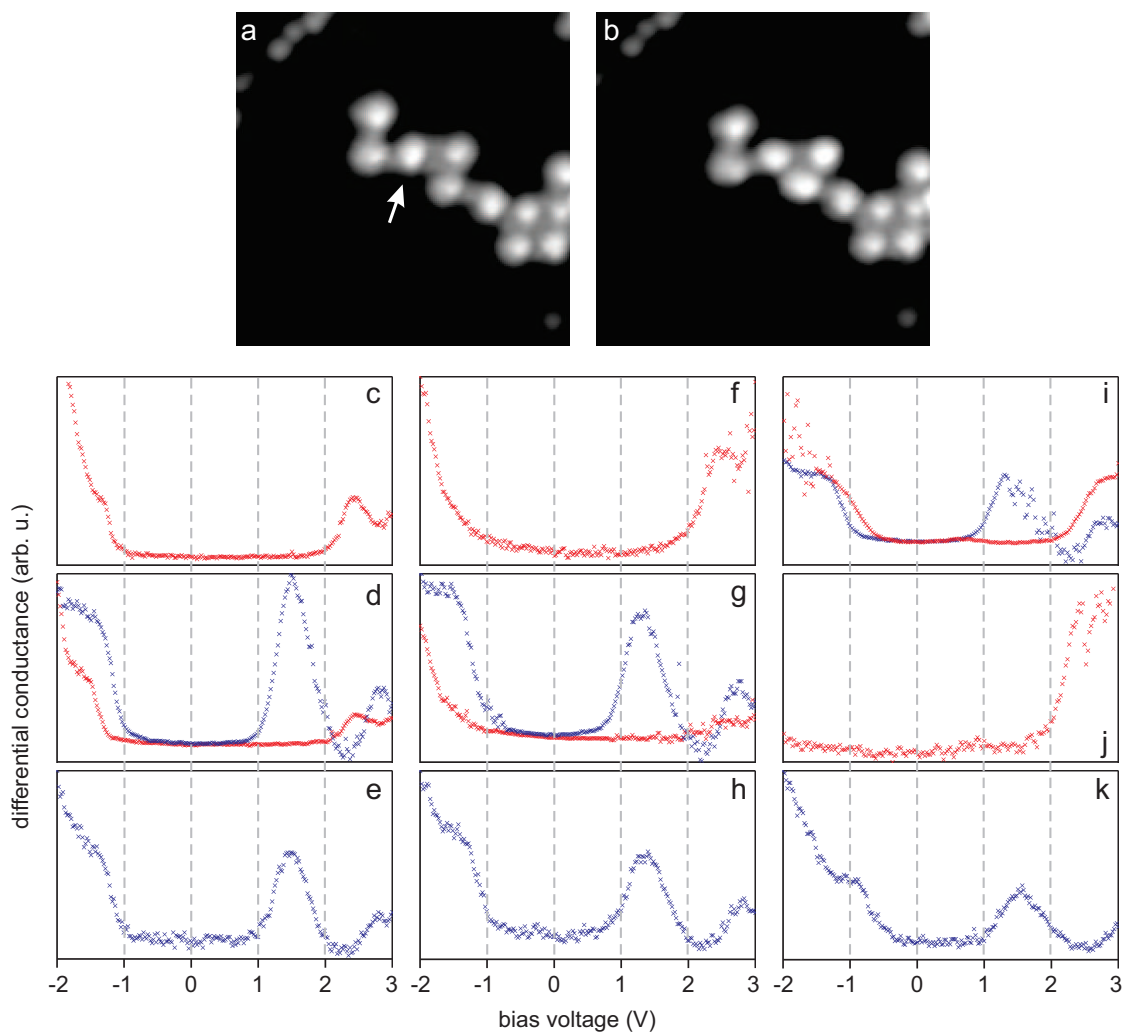


**Figure 4.29:** STM images of a chain of DTE before (a) and after (b) a series of 35 bias ramps performed on top of the linear unit indicated by the arrow. Image sizes  $12 \times 12 \text{ nm}^2$ ,  $-500 \text{ mV}$ ,  $0.1 \text{ nA}$ . Graphs (c) to (k) document the  $dI/dV$  signals of selected attempts.

of the unit as shown in Fig. 4.29 (b) is barely changed with respect to the starting point (a) and there is no sign of debris that could indicate damage inflicted on the molecule. Thus, while there are only a small number of similar switching cycles, the recorded spectra clearly show the reversibility of the process, albeit with a small yield under the applied conditions.

Fig. 4.25 demonstrated the unfolding of the chains by means of lateral manipulation. During several such procedures a temporary attachment of the polymer to the tip could be observed, usually accompanied by its lateral displacement and conformational change. In rare events the chain became permanently attached and basically required the formation of a new tip (by repeatedly bringing it into contact with the surface, cf. ch. 1.3.2). This behavior is analogous to the one of the oligo-terfluorene and thus provides the possibility of two-terminal measurements like the ones described in chapter 2.1.1. In the following I will describe attempts to apply this method to the investigation the oligo-DTE chains. The first objective is the determination of the inverse decay length  $\beta$  for both the open and closed isomers. They are expected to be

substantially different due to the difference in delocalization and the changed HOMO-LUMO gap. The second objective is to address the question of whether the switching can be induced by passing a current through the molecule contacted to electrodes on both sides. This would then render the molecule isomerizable as a unit integrated in a hypothetical circuit architecture.

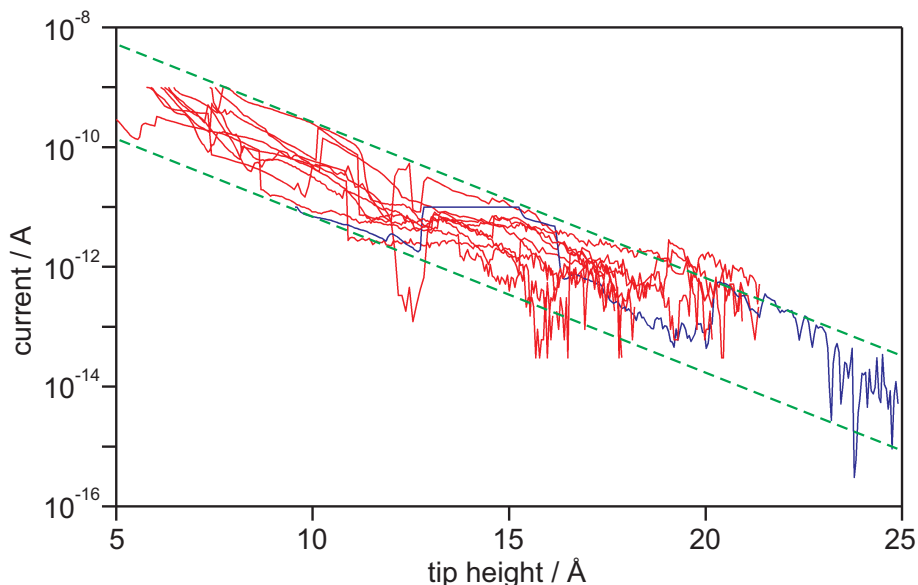


**Figure 4.30:** Ten current curves acquired during the retraction of the tip with an oligo-DTE chain bridging the gap. The bias is held constant at  $-200$  mV. Abscissa values denote the tip-sample distance above the gold surface. Green lines serve as guide to the eye. Different settings of the preamplifier gain allow the recording of the current in windows spanning different orders of magnitude. (red curves: gain 10, blue curve: gain 12).

Examination of the pulling current curves reveals that they are more noisy and characterized by more current jumps than is the case for oligo-TF. To diminish the influence of these fluctuations and to establish a general trend, ten such curves are plotted in Fig. 4.30. It can be seen that for chains made of the open-ring isomers, the current steeply drops and can barely be measured at a tip-sample distance of 3 nm (at greater heights the signal drops into the noise, not shown). Fitting an exponential decay to the curves, a mean inverse decay factor of  $\beta_{\text{open}} = (0.6 \pm 0.2) \text{ \AA}^{-1}$  is found. This factor reflects a much stronger attenuation than in the case of oligo-TF (characterized by  $\beta = (0.38 \pm 0.09) \text{ \AA}^{-1}$ , cf. ch. 2.1.1) and limits the measurable current to a narrow range of distances, which increases the influence of the fluctuations. Another reason for the jittery appearance of the current signal can be suspected in the larger conformational changes that these units undergo, turning the previously mostly angled conformers into the straightened form. As these units are supposed to represent the "OFF"-form of the switch, the strong attenuation is in accordance with the intended function.

The measurement of the decay factor of the closed-ring form and the ring-closure in the pulling geometry shall be treated together. These experiments proved to be complicated and while the amount of collected data is not sufficient for a reliable result, it should serve to demonstrate the proof of principle on both issues. Because the units are initially all observed in the open conformation and because of the low likelihood of tip-induced ring-closure, the above pulling

experiment is not identically reproducible, i.e. employing a chain consisting entirely of closed-isomer units. Instead, it was resorted to close a single unit in a chain and look for its signature in the chain's I-z curve. Even restricting the attempts to chains containing only a single closed unit the pulling turned out to be challenging, as the probability of successful lifting of the chain appeared to be negatively affected. The reason for this might be suspected in the reduced flexibility of the closed-ring unit due to the introduction of a bond linking the two thieno groups. Furthermore, to still being able to detect the signal associated with a unit at small bias, this unit has to be in one of the initial positions of a chain segment that can facilitate a measurable tunneling current. Another important issue is the state of the tip that has to be in a suitable shape for the pulling and the subsequent spectroscopy. Optimally meeting these requirements is not necessarily simultaneously possible, similar to performing high-res scanning and spectroscopy. Fig. 4.31 (a) shows the starting point of a noteworthy example of a pulling attempt aimed at the end of an oligo-DTE chain. The units are all in the open state as is visible from their (angled) conformation. The tip is brought into contact with the apex of the chain (position indicated by the arrow) and subsequently retracted while increasing the bias voltage. The recorded current signal displayed in Fig. 4.31 (b) indicates that the chain was successfully attached. It detached at a height of around 21 Å at a bias voltage of 2020 mV, visible as the sudden drop into the noise level. This means that before the breaking off the tip, the first unit was completely detached from the surface, forming a junction between the two electrodes. The same area is subsequently scanned again to reveal changes in the switches' appearance. Indeed, the last unit is changed into a linear conformer while the contrast is more homogeneous and slightly brighter than the attached units. While this is in agreement with the ring-closing process as discussed above, these modifications could simply be caused by the manipulation, as shown in Fig. 4.25. Fortunately, the above spectroscopic results allow to unambiguously assign a state to the unit.  $dI/dV$  curves recorded on top of the last switch (indicated by the  $\times$  in (c)) are shown in (d). While the curve is slightly noisy, the states are found at the energies of  $E_{\text{HOMO}} = -1370$  meV and  $E_{\text{LUMO}} = 1020$  meV (Gaussian fit added for visibility).

Thus, acknowledging a slight shift in energy towards the occupied side, these features are in agreement with the values observed for the ring-closed species above. This is especially true for the gap of  $\approx 2.4$  eV which is close to the 2.3 eV (on average) reported above and is distinctly smaller than the one of the open-ring form (3.5 eV). The signature was stable and recorded several times. Thus, it is possible to conclude that switching could indeed be induced in a junction geometry, i.e. with a chain of switches spanning the gap between the electrodes. Note that the pulse-induced isomerization on the molecules adsorbed back to the surface can be excluded, because switching has not been observed for such large tip-heights and in the absence of measurable tunneling current. Because the current in a pulling experiment decreases rapidly with the number of chain segments, the closed switch in the first position constitutes a convenient configuration. Thus, the chain apex is targeted again (position denoted by the dashed arrow in (c)) in a pulling experiment, to highlight the difference in the conductance with regard to the open segment examined before. The corresponding current signal is shown in (e). A signal is detected up to 17 Å, again indicating a successful attempt. Fitting an exponential decay to the curve is not so easy, however and the blue dashed line represents a tentative attempt with an

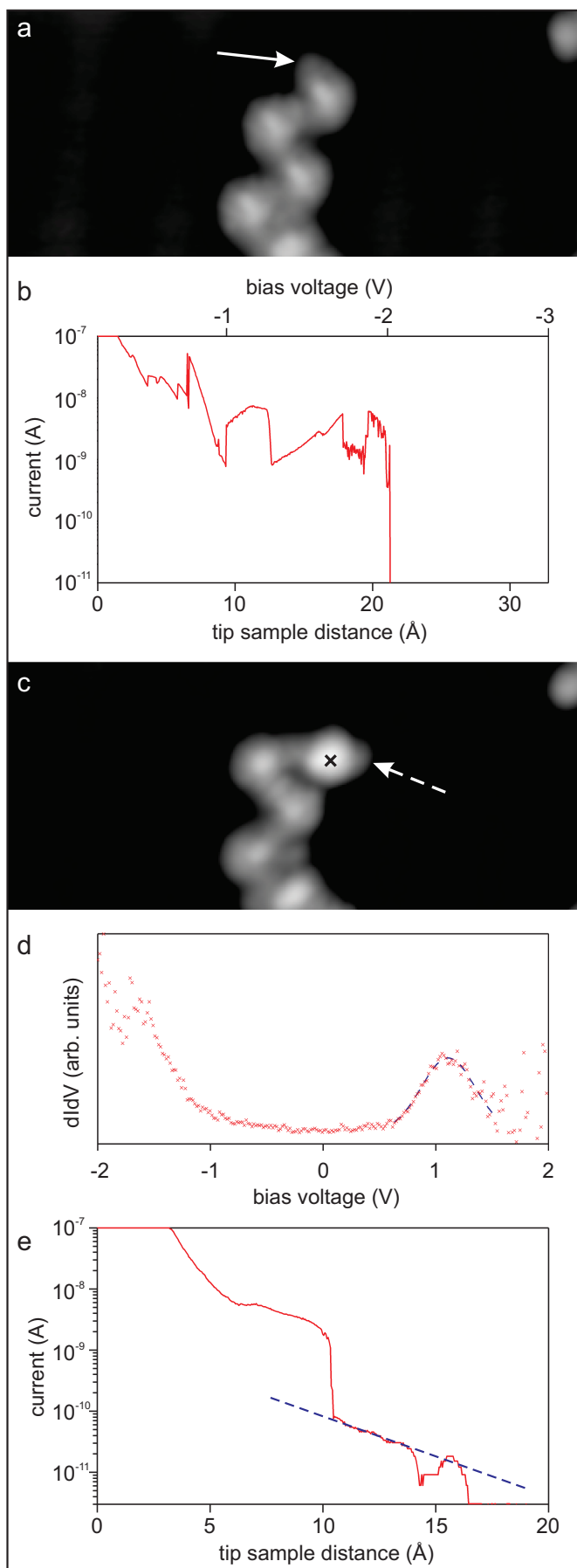


**Figure 4.31:** STM images of the end of an oligo-DTE chain before (a) and after (c) a pulling experiment (tip aimed at the position indicated by the solid arrow). (b) shows the current recorded as the tip-sample distance and the bias voltage are increased simultaneously. (d)  $dI/dV$ -spectrum taken on the terminal unit indicated by the x in (c). STM images  $6 \times 14 \text{ nm}^2$ ,  $-500 \text{ mV}$ ,  $0.1 \text{ nA}$ . A subsequent pulling attempt (position indicated by the dashed arrow in (c)) is displayed in (e), during the pulling, the bias was held constant at  $-200 \text{ mV}$ .

associated decay factor of  $\beta_{\text{closed}} = 0.35 \text{ \AA}^{-1}$ . A restriction to the second part of the curve is justified by the assumption that the first half is associated with the progressing detachment of the first segment from the surface with a developing tunneling pathway, analogous to what was experimentally observed and corroborated by calculation for oligo-TF chains on the first few angstroms [56]. The latter part of the curve on the other hand is guided through the closed DTE unit and displays a more even signal. Thus, while the distance over which the signal was recorded is shorter than in the other examples, nonetheless the measurement was shown to be feasible. Furthermore, the change of the value of the decay factor with regard to one measured for the open-ring species is in agreement with the predicted influence of the ring-closure on conductance, i.e. the open unit attenuates the tunneling current more strongly than the closed one.

## 4.5 Conclusion

In conclusion, the ring-opening/closing switch dithienylethene has been studied on a Au(111) surface. Differently substituted monomers were characterized with STM imaging, manipulation and local dI/dV-spectroscopy. The investigation of individual molecules directly adsorbed to the metal provided novel insight into the switch molecules, as previous studies were mostly conducted in solution and break-junction type setups. In the present study, it was found that the molecules can be applied to the Au(111) surface by thermal evaporation, which they reach mostly intact and in the ring-open state. Rotation around the sigma bonds connecting the thienyl groups with the cyclopentene results in different conformations which could be identified on the surface. After thorough characterization, the monomers were employed in polymerization experiments in which both homopolymers and also copolymers in combination with terfluorene units could successfully be produced, thus realizing the goal of connecting functional molecular components in a controlled fashion into robust, i.e. covalent structures. Most importantly, it was found that the molecules' capability of isomerization was retained upon adsorption to the metal and coupling into oligomers. Ring-closure of dithienylethene was demonstrated for the first time by resonant tunneling, which adds a new modality to the previously employed isomerization by light irradiation and redox reaction in solution. Furthermore, due to the possibility of applying the STM current with submolecular resolution the switching could be facilitated with single-unit addressability. Despite the small efficiency of the process its reversibility was demonstrated as evidenced by the recurring spectroscopic signature of the ring-open species, thus showing the proof of principle of the functionality of the covalently connected dithienylethene. The considerable change in the HOMO-LUMO gap upon isomerization (1.1 eV on average) is accompanied by a change in molecular conductance, which was investigated by two-terminal current measurements applying the pulling technique devised for the poly-terfluorene molecular wires to the chains made of dithienylethene. Finally, results were presented that indicate that the switching is feasible in this contacted geometry passing a current along such a molecular wire, which opens the exciting prospect of employing dithienylethene as units to regulate the flow of electrical signal through a molecular circuit.

## Conclusion and outlook

In conclusion, organic molecules have been investigated using scanning tunneling microscopy at gold surfaces under UHV conditions and mainly at cryogenic temperature with the intention to gain a deeper understanding of their conductance, polymerization and isomerization. These three themes appear intertwined in this work. Thus, while the conductance experiments build on the molecular structures formed by on-surface-synthesis, the study focussing on isomerization is facilitated by insights of both the polymerization and conductance experiments. Interesting science is always based on the discovery and investigation of new systems. In this vein, the on-surface synthesis technique developed in my diploma thesis at the Freie Universität constitutes the corner stone of the present work. The resulting networks at metal surfaces are promising systems for the study of molecular properties and processes. Three different types of building blocks have been successfully utilized in this manner during the course of this work, namely fluorene, porphyrin and dithienylethene, highlighting the generality of the technique.

Chapter 2 describes efforts for the formation of a setup featuring molecular wires in a horizontal geometry, facilitating the simultaneous measurement of single-molecule conductance and image recording. This was intended to complement previous experiments which employed a vertical arrangement with a molecular chain suspended between the tip and the sample and which therefore did not permit simultaneous imaging. The molecules chosen for investigation were linear oligo-fluorene chains. Because STM requires a conductive sample surface, thin insulating films made of sodium chloride were employed to decouple the wires from the gold substrate underneath. The sequential preparation of the polymeric chains and NaCl islands (mostly single and double layers), although challenging, was successfully performed on the same Au(111) sample. Metallic areas were left uncovered of sodium chloride to act as electrical contacts for the molecular wires. Due to the small diffusion barrier of the insulator, the chains were found exclusively on these metallic areas, whereas adsorption on top of the sodium chloride did not take place. Because sufficient mobility is required for the covalent coupling of the monomers it precludes their deposition onto a cold sample, which is the usual method to facilitate adsorption on top of insulating films. Therefore, a different approach had to be conceived to arrive at the desired configuration.

Two methods were devised and successfully employed, one based on manipulation with the STM tip and another on a preparative route. In the former, chains are peeled off the surface continuously using the STM pulling technique developed for the oligo-terfluorene. Molecular segments are detached from the sample surface and readsorb subsequently, often in a different position, upon detachment from the tip. As this procedure is performed at low temperature (10 K), it permits a stable adsorption configuration on top of the insulator. Performing this manipulation in the vicinity of the NaCl islands, the transfer of chain segments several nanometers in length on top of the insulator has been observed, while the rest of the molecule remained adsorbed to the adjacent gold surface. Thus, the successful realization of the intended configuration could be demonstrated. However, the method is characterized by the stochastic nature of the readsorption rendering the process difficult to control and the chain end adsorbed on top of the NaCl often proved labile during subsequent scanning. Therefore, a different technique was developed which relies on the observation that the resumption of the deposition of sodium chloride facilitates the

continued growth of the salt islands in a lateral and crystalline fashion, surprisingly even in the presence of the polymeric chains. As a consequence, the weakly adsorbed oligo-fluorene wires are displaced until they are forced to adsorb on top of the insulating film. In this way, the intended arrangement is routinely produced, while in this case the chain is pinned on both sides by the adsorption to the bare metal surface, which stabilizes the middle segment on the salt island. Local tunneling spectroscopy performed along these wires revealed the electronic decoupling of the chain segments lying on top of the insulator. It showed the re-emergence of a HOMO level at 1.5 eV below the Fermi energy, which was not observed for the segments belonging to the same chain that are adsorbed directly to the gold surface. Thus, the fabrication of a novel configuration comprising the simultaneous adsorption of one and the same molecular chain to metallic and insulating areas has been demonstrated.

While this setup in principle allows the investigation of the injection and transmission of electrical current along the decoupled segments of the chains, it was found in the present case that the conductance of the oligo-fluorenes cannot compete with the tunneling pathway through the NaCl. However, this issue should be amendable by the utilization of a better conducting molecular wire or the introduction of additional layers of insulating material.

In chapter 3, the focus is on the on-surface synthesis process. The potential of the 2D-confined polymerization has been shown through the realization of a number of stable, i.e. covalently connected molecular structures of predetermined shape, such as the oligo-fluorene chains employed in chapter 2. However, all of these experiments so far have been based on a single coupling step, limiting the level of control of the process and leading to rather simple architectures. Thus, with an eye to the fabrication of more sophisticated structures, it was attempted to realize a hierarchical synthesis procedure in which the coupling takes place in a stepwise and selective manner. To that end, specially designed monomers were employed ( $\text{Br}_2\text{I}_2\text{TPP}$ ), consisting of a porphyrin core substituted with bromo- and iodophenyl side groups in a *trans* configuration. Two types of halogen atoms, characterized by different binding energies, are utilized to separate the activation of the reactive sites into different steps. Performing variable-temperature STM, the existence of two temperature thresholds was revealed, associated with the activation of the functional side groups. The identification of the halogen substituents from their appearance in STM images led to the conclusion that the catalytically induced dissociation of iodine is taking place already at room temperature. Therefore, the observation of the intact monomers required their deposition onto a cooled sample. The subsequent application of the first heating step (120 °C) led to the efficient formation of chains reflecting the arrangement of the functional groups. The covalent character of the newly formed bonds has been asserted by means of local spectroscopy and manipulation with the STM tip. At this stage only the iodine is dissociated while the bromophenyl is left intact entirely. The brominated sites were only activated by a heating step to at least 200 °C resulting in the efficient formation of two-dimensional networks. Thus, the activation stages of  $\text{Br}_2\text{I}_2\text{TPP}$  on Au(111) are comfortably separated in temperature, which allowed to follow the polymerization through the individual steps, starting with the intact monomers, via the one-dimensional intermediates to the final network products.

The potential of the hierarchical approach was demonstrated by the fabrication of copolymers from DBTF and  $\text{Br}_2\text{I}_2\text{TPP}$  monomers. It was shown that the formation of oligo-porphyrin chains takes place undisturbed by the presence of the yet unreactive DBTF monomers. The ac-

tivation of the latter happens only after the conclusion of the first step and simultaneously with the provision of connection points along the sides of the previously formed porphyrin chains. Performing the polymerization in a stepwise fashion allowed to direct the binding of 96 % of terfluorene chains to one specific type of porphyrin sites. Thus, the hierarchical approach allows the coupling with a high degree of selectivity. The resulting structures are unobtainable via a one-step process, which highlights the increased level of control of the procedure. Moreover, it proved applicable to address another challenge regarding the on-surface synthesis, which lies in the enhancement of their regularity. Because the irreversibility of the bonding precludes error correction, the reduction of defects has to be asserted during the coupling. The networks consisting only of porphyrins have been employed as a testing case in this regard, as they allow the direct comparison of structures formed by a hierarchical and a non-hierarchical process. The stepwise procedure was found to hold a considerable advantage over the one-step polymerization in terms of network size and regularity. This was ascribed to the one-dimensional and virtually defect-free chain intermediates and their interaction prior to the second coupling step. Furthermore, the adsorbate-surface interaction could be employed to exert a guiding influence on the intermediates by utilizing a corrugated Au(100) surface, which was found to have a directing effect on the diffusion and arrangement of the chains, leading to a further improvement of the produced networks.

Chapter 4 describes the investigation of molecular isomerization, more specifically the ring-opening and -closing reactions of dithienylethenes, with the ultimate goal to employ the on-surface synthesis approach to fabricate covalent networks containing both single-molecule wires and switches. Unlike e.g. the *cis-trans* isomerization of azobenzene, the cyclization of dithienylethenes is associated with only a small conformational change, which renders their incorporation into a rigid structure compatible with their switching functionality. As previous studies on this type of molecule at surfaces are rare, a thorough examination was conducted first on the monomers, detailing their conformation, aggregation and electronic properties adsorbed on Au(111). Judging from these properties, it was concluded that the molecules are encountered exclusively in the ring-open form, which is likely the consequence of cycloreversion induced during the evaporation procedure. With the characterization gleaned on the individual building blocks, their coupling into stable structures was pursued. However, attempting the polymerization of the brominated switches it had to be concluded that the dithienylethene molecules do not sustain the heating step required for their activation. Therefore, the functional groups were exchanged for iodophenyl, a step motivated by the results of the coupling of Br<sub>2</sub>I<sub>2</sub>TPP, leading to the successful formation of covalently coupled structures. Thus, polymeric chains were produced consisting exclusively of switches and additionally copolymers intermixing the dithienylethene building blocks with terfluorene wire units. Isomerization of dithienylethenes has been shown previously by light irradiation and by redox reactions in solution. Furthermore, previous studies showed that the isomerizability of molecular switches oftentimes suffers upon adsorption to a metal surface. In the present case, the switching units are furthermore rigidly connected into a covalent structure. Nonetheless, successful cyclization of individual dithienylethene units was observed upon application of bias pulses from the STM tip. While changes in the conformation of the molecule are – as anticipated – rather small, the ring-closure could be identified in single units by a pronounced change of its electronic properties, i.e. the reduction of the HOMO-LUMO

gap by approximately 1.1 eV. The polarity dependence and the coincidence of the LUMO with the energy required for the ring-closure indicate that resonant tunneling is responsible for the switching. This mechanism has not been observed so far for this type of molecule and therefore adds a new modality of isomerization. All dithienylethene units, the monomers as well as the ones coupled in oligomeric chains, are initially encountered in the ring-open form and electron pulses constitute the only means of producing the ring-closed species on the surface. As this method is characterized by a small probability – cyclization was observed in approx. 6 % of attempts – the cycloreversion reaction posed a challenge due to the small number of closed-ring isomers. Despite this fact, the reappearance of the open-ring spectroscopic signature could be observed upon continued application of bias pulses, demonstrating the reversibility of the process. Finally, as dithienylethene is supposed to act as a conductance switch, the chains made of DTE were suspended between the tip and sample to perform two-terminal measurements. While these experiments turned out to be very challenging, results corroborate the expected dependence of the conductance on the state of the molecules and moreover provide hints at the isomerizability in the contacted geometry.

The investigations described in this work open several promising perspectives for further experiments. The application of an insulating layer has been shown to result in the local electronic decoupling and promises to facilitate the length dependent measurement of molecular conductance in a horizontal geometry. It would be highly interesting to employ the method with a more efficient conductor to spatially resolve electrical transport along the wire. Furthermore, the incorporation into polymer chains conceivably constitutes an approach towards the stabilization of functional units on top of thin films. This would be especially interesting with regard to molecular switches, as they generally have been found to be very sensitive to the interaction with a metal substrate, in many cases leading to the loss of isomerizability. The reduced electronic coupling of the switch with the metal substrate and the enhanced life times of its excited states would likely lead to a considerable enhancement of the switching yield.

Finally, the hierarchical on-surface-synthesis method developed in this work holds a lot of promise. With the growing ability to guide the coupling process, better and more complex structures become available that will allow to tailor molecular networks to the requirements of a particular experiment and model systems for molecular electronics. Furthermore, a process based on self-organization could conceivably constitute a route to connecting the nano-structures with the outside world, an issue that poses a main challenge on the way to employing molecules in devices.

## List of presentations

### Publications resulting from this thesis

- C. Bombis, F. Ample, L. Lafferentz, H. Yu, S. Hecht, C. Joachim and L. Grill, Single molecular wires connecting metallic and insulating surface areas, *Ang. Chem. Int. Ed.* **48**, 9966 (2009)
- L. Lafferentz, V. Eberhardt, C. Dri, C. Africh, G. Comelli, F. Esch, S. Hecht and L. Grill, Controlling on-surface polymerization by hierarchical and substrate-directed growth, *Nat. Chem.* **4**, 215 (2012)
- L. Lafferentz, M. Pätzelt, M. Grisolia, C. Joachim, M. Wolf, S. Hecht and L. Grill, Covalent linking and switching of single molecules in polymer chains, *in preparation*

### Additional publications

- L. Grill, M. Dyer, L. Lafferentz, M. Persson, M. V. Peters and S. Hecht, Nano-architectures by covalent assembly of molecular building blocks, *Nat. Nanotechnol.* **2**, 687 (2007)
- L. Lafferentz, F. Ample, H. Yu, S. Hecht, C. Joachim and L. Grill, Conductance of a single conjugated polymer as a continuous function of its length, *Science* **323**, 1193 (2009)

### Oral presentations

- Covalent connection of organic molecules on Au(111), Seminar at Laboratorio TASC, Trieste, Italy (2008)
- Formation of covalently bound chains from dibromoterfluorene molecules on Au(111), Spring meeting of the Deutsche Physikalische Gesellschaft (DPG), Berlin (2008)
- Conductance of a single conjugated polymer as a continuous function of its length, Spring meeting of the DPG, Dresden (2009)
- Measurement of the conductance of a single molecular chain as a continuous function of its length, International conference on molecular electronics, Emmetten, Switzerland (2010)
- **(1)** Measurement of the conductance of a single molecular chain as a continuous function of its length, **(2)** Covalent assembly of molecular building blocks by 'on-surface-synthesis', March meeting of the American physical society (APS), Portland, USA (2010)
- Controlling on-surface polymerization by hierarchical and substrate-directed growth, Spring meeting of the DPG, Berlin (2012)
- Hierarchical on-surface polymerization studied with STM, International conference on nanoscience and technology, Paris, France (2012)

## List of abbreviations

Br <sub>4</sub> TPP	porphyrin with four bromophenyl legs in the meso position
Br <sub>2</sub> I <sub>2</sub> TPP	porphyrin with two bromophenyl and two iodophenyl legs at opposite meso positions
DAE	diarylethene
DBTF	dibromoterfluorene
DITF	diiodoterfluorene
DTE	dithienylethene
ESQC	elastic scattering quantum chemistry
fcc	face centered cubic
hcp	hexagonally close packed
LDOS	local density of states
LT	low temperature
MBJ	mechanical break junction
MPD	most probable distribution
MSA	molecular self-assembly
QMS	quadrupole mass spectrometer
RT	room temperature
SAM	self-assembled monolayer
STM	scanning tunneling microscope / microscopy
TF	terfluorene
TPP	tetraphenyl-porphyrin
VdW	van der Waals
VT	variable temperature

## Acknowledgements

I am indebted to many people for their help and encouragement which was instrumental for the successful completion of this work.

First and foremost I would like to express my sincere gratitude to Leonhard Grill for the opportunity to perform this thesis in his group and his outstanding support and guidance.

I would also like to thank my former and present colleagues at the Freie Universität and the Fritz-Haber-Institut, which have made the work in the lab always a pleasant experience: Sofia, Micol, Michael, Christian B., Christian R., Carlos, Johannes, Matthias, Alex, Christophe, Takashi, Simon and furthermore all members of the PC department and also of Nacho Pascual's group.

Special thanks go to Giovanni Comelli and his group in Trieste, with whom I was allowed to perform a fruitful collaboration; Friedrich Esch, Christina Africh and Carlo Dri have made my work and stay most enjoyable.

Moreover, I would like to thank Stefan Hecht and his group at the Humboldt Universität for the creative supply of molecules and Christian Joachim and his group in Toulouse for theoretical support.

I am grateful to Martin Wolf for the possibility to work in his department and the DFG for financial support through SFB 658 "Molecular Switches".

Finally, I would like to thank my parents and my wife Sabine for their great moral support and patience at all times.

## References

- [1] Binnig, G. & Rohrer, H. Scanning tunneling microscopy. *Helv. Phys. Acta* **55**, 726–735 (1982).
- [2] Binnig, G. & Rohrer, H. Nobel lecture: "Scanning tunneling microscopy, from birth to adolescence" (1986).
- [3] Oppenheimer, J. R. Three notes on the quantum theory of aperiodic effects. *Phys. Rev.* **31**, 66–81 (1928).
- [4] Fowler, R. H. & Nordheim, L. Electron emission in intense electric fields. *Proc. Roy. Soc.* **119**, 173 – 181 (1928).
- [5] Duke, C. B. *Tunneling in solids* (Academic Press Inc., 1969).
- [6] Wiesendanger, R. *Scanning probe microscopy and spectroscopy* (Cambridge University Press, 1994).
- [7] Fisher, J. C. & Giaever, I. Tunneling through thin insulating layers. *J. Appl. Phys.* **32**, 172 (1961).
- [8] Simmons, J. G. Generalized formula for electric tunnel effect between similar electrodes separated by a thin insulating film. *J. Appl. Phys.* **34**, 1793 (1963).
- [9] Tersoff, J. & Hamann, D. R. Theory and application for the scanning tunneling microscope. *Phys. Rev. Lett.* **50**, 1998–2001 (1983).
- [10] Tersoff, J. & Hamann, D. R. Theory of the scanning tunneling microscope. *Phys. Rev. B* **31**, 805–813 (1985).
- [11] Bardeen, J. Tunneling from a many-particle point of view. *Phys. Rev. Lett.* **6**, 57 (1961).
- [12] Hamers, R. J. Atomic-resolution surface spectroscopy with the scanning tunneling microscope. *Annu. Rev. Phys. Chem.* **40**, 531–559 (1989).
- [13] Binnig, G. *et al.* Tunneling spectroscopy and inverse photoemission - image and field states. *Phys. Rev. Lett.* **55**, 991–994 (1985).
- [14] Mueller, P., Alvarado, S., Rossi, L. & Riess, W. STM-based charge-injection spectroscopy at the organic/metal interface. *Mater. Phys. Mech.* **4**, 76 – 80 (2001).
- [15] Alemani, M. *et al.* Electric field-induced isomerization of azobenzene by STM. *J. Am. Chem. Soc.* **128**, 14446–14447 (2006).
- [16] Shen, T. C. *et al.* Atomic-scale desorption through electronic and vibrational excitation mechanisms. *Science* **268**, 1590–1592 (1995).
- [17] Stokbro, K. *et al.* STM-induced hydrogen desorption via a hole resonance. *Phys. Rev. Lett.* **80**, 2618–2621 (1998).

- [18] Stipe, B. C., Rezaei, M. A. & Ho, W. Inducing and viewing the rotational motion of a single molecule. *Science* **279**, 1907–1909 (1998).
- [19] Komeda, T., Kim, Y., Kawai, M., Persson, B. N. J. & Ueba, H. Lateral hopping of molecules induced by excitation of internal vibration mode. *Science* **295**, 2055–2058 (2002).
- [20] Sonnleitner, T., Swart, I., Pavlicek, N., Poellmann, A. & Repp, J. Molecular symmetry governs surface diffusion. *Phys. Rev. Lett.* **107**, 186103 (2011).
- [21] Tierney, H. L. *et al.* Experimental demonstration of a single-molecule electric motor. *Nat. Nanotechnol.* **6**, 625–629 (2011).
- [22] Eigler, D. M. & Schweizer, E. K. Positioning single atoms with the scanning tunneling microscope. *Nature* **344**, 524–526 (1990).
- [23] Meyer, G. & Rieder, K. H. Controlled manipulation of single atoms and small molecules with the scanning tunneling microscope. *Surf. Sci.* **377**, 1087–1093 (1997).
- [24] Meyer, G. *et al.* Controlled manipulation of atoms and small molecules with a low temperature scanning tunneling microscope. *Single Mol.* **1**, 79–86 (2000).
- [25] Moresco, F. *et al.* Low temperature manipulation of big molecules in constant height mode. *Appl. Phys. Lett.* **78**, 306–308 (2001).
- [26] Grill, L. *et al.* Rolling a single molecular wheel at the atomic scale. *Nat. Nanotechnol.* **2**, 95–98 (2007).
- [27] Manzano, C. *et al.* Step-by-step rotation of a molecule-gear mounted on an atomic-scale axis. *Nat. Mater.* **8**, 576–579 (2009).
- [28] Ohara, M., Kim, Y. & Kawai, M. Electric field response of a vibrationally excited molecule in an STM junction. *Phys. Rev. B* **78**, 201405 (2008).
- [29] Lauhon, L. J. & Ho, W. Direct observation of the quantum tunneling of single hydrogen atoms with a scanning tunneling microscope. *Phys. Rev. Lett.* **85**, 4566–4569 (2000).
- [30] Zambelli, T., Trost, J., Wintterlin, J. & Ertl, G. Diffusion and atomic hopping of N atoms on Ru(0001) studied by scanning tunneling microscopy. *Phys. Rev. Lett.* **76**, 795–798 (1996).
- [31] Schunack, M. *et al.* Long jumps in the surface diffusion of large molecules. *Phys. Rev. Lett.* **88**, 156102 (2002).
- [32] Kühnle, A., Meyer, G., Hla, S. W. & Rieder, K. H. Understanding atom movement during lateral manipulation with the STM tip using a simple simulation method. *Surf. Sci.* **499**, 15–23 (2002).
- [33] Hla, S. W., Braun, K. F. & Rieder, K. H. Single-atom manipulation mechanisms during a quantum corral construction. *Phys. Rev. B* **67**, 201402 (2003).
- [34] Stroscio, J. A. & Eigler, D. M. Atomic and molecular manipulation with the scanning tunneling microscope. *Science* **254**, 1319–1326 (1991).

- [35] Eigler, D. M., Lutz, C. P. & Rudge, W. E. An atomic switch realized with the scanning tunneling microscope. *Nature* **352**, 600–603 (1991).
- [36] Bartels, L., Meyer, G. & Rieder, K. H. Controlled vertical manipulation of single CO molecules with the scanning tunneling microscope: A route to chemical contrast. *Appl. Phys. Lett.* **71**, 213–215 (1997).
- [37] Gross, L. *et al.* High-resolution molecular orbital imaging using a p-wave STM tip. *Phys. Rev. Lett.* **107**, 086101 (2011).
- [38] Chen, C. J. *Introduction to Scanning Tunneling Microscopy* (Oxford University Press, 1993).
- [39] Stipe, B. C. *et al.* Single-molecule dissociation by tunneling electrons. *Phys. Rev. Lett.* **78**, 4410–4413 (1997).
- [40] Lee, H. J. & Ho, W. Single-bond formation and characterization with a scanning tunneling microscope. *Science* **286**, 1719–1722 (1999).
- [41] Hla, S. W., Bartels, L., Meyer, G. & Rieder, K. H. Inducing all steps of a chemical reaction with the scanning tunneling microscope tip: Towards single molecule engineering. *Phys. Rev. Lett.* **85**, 2777–2780 (2000).
- [42] Hahn, J. R. & Ho, W. Oxidation of a single carbon monoxide molecule manipulated and induced with a scanning tunneling microscope. *Phys. Rev. Lett.* **87**, 166102 (2001).
- [43] Ho, W. Single-molecule chemistry. *J. Chem. Phys.* **117**, 11033–11061 (2002).
- [44] Hla, S. W., Meyer, G. & Rieder, K. H. Selective bond breaking of single iodobenzene molecules with a scanning tunneling microscope tip. *Chem. Phys. Lett.* **370**, 431–436 (2003).
- [45] Besocke, K. An easily operable scanning tunneling microscope. *Surf. Sci.* **181**, 145–153 (1987).
- [46] Meyer, G. A simple low-temperature ultrahigh-vacuum scanning tunneling microscope capable of atomic manipulation. *Rev. Sci. Instrum.* **67**, 2960 (1996).
- [47] Schaeffer, K. *Aufbau eines Tieftemperatur-Rastertunnelmikroskops*. Master’s thesis, Freie Universität Berlin (1997).
- [48] Zöphel, S. *Der Aufbau eines Tieftemperatur-Rastertunnelmikroskops und Strukturuntersuchungen auf vicinalen Kupferoberflächen*. Ph.D. thesis, Freie Universität Berlin (2000).
- [49] Kittel, C. *Introduction to solid state physics* (John Wiley & Sons, Inc., 1996), 7. edn.
- [50] Barth, J. V., Brune, H., Ertl, G. & Behm, R. J. Scanning tunneling microscopy observations on the reconstructed Au(111) surface: Atomic structure, long-range superstructure, rotational domains, and surface defects. *Phys. Rev. B* **42**, 9307–9318 (1990).

- [51] Chen, W., Madhavan, V., Jamneala, T. & Crommie, M. F. Scanning tunneling microscopy observation of an electronic superlattice at the surface of clean gold. *Phys. Rev. Lett.* **80**, 1469–1472 (1998).
- [52] Lafferentz, L. *Bottom-up Construction of Covalently Bound Molecular Nano-Structures on Surfaces: A Low-Temperature STM Study*. Master’s thesis, Freie Universität Berlin (2008).
- [53] Binnig, G., Rohrer, H., Gerber, C. & Stoll, E. Real-space observation of the reconstruction of Au(100). *Surf. Sci.* **144**, 321–335 (1984).
- [54] Havu, P., Blum, V., Havu, V., Rinke, P. & Scheffler, M. Large-scale surface reconstruction energetics of Pt(100) and Au(100) by all-electron density functional theory. *Phys. Rev. B* **82**, 161418 (2010).
- [55] Grill, L. *et al.* Nano-architectures by covalent assembly of molecular building blocks. *Nat. Nanotechnol.* **2**, 687–691 (2007).
- [56] Lafferentz, L. *et al.* Conductance of a single conjugated polymer as a continuous function of its length. *Science* **323**, 1193–1197 (2009).
- [57] Barth, J. V., Costantini, G. & Kern, K. Engineering atomic and molecular nanostructures at surfaces. *Nature* **437**, 671–679 (2005).
- [58] Milgrom, L. R. *The colours of life* (Oxford university press, 1997).
- [59] Yokoyama, T., Yokoyama, S., Kamikado, T. & Mashiko, S. Nonplanar adsorption and orientational ordering of porphyrin molecules on Au(111). *J. Chem. Phys.* **115**, 3814–3818 (2001).
- [60] Jentzen, W. *et al.* Planar and nonplanar conformations of (meso-tetraphenylporphinato)nickel(II) in solution as inferred from solution and solid-state Raman spectroscopy. *J. Phys. Chem. A* **101**, 5789–5798 (1997).
- [61] Qiu, X. H., Nazin, G. V. & Ho, W. Mechanisms of reversible conformational transitions in a single molecule. *Phys. Rev. Lett.* **93**, 196806 (2004).
- [62] Iancu, V., Deshpande, A. & Hla, S. W. Manipulation of the Kondo effect via two-dimensional molecular assembly. *Phys. Rev. Lett.* **97**, 266603 (2006).
- [63] Kraft, A., Grimsdale, A. C. & Holmes, A. B. Electroluminescent conjugated polymers - seeing polymers in a new light. *Ang. Chem. Int. Ed.* **37**, 402–428 (1998).
- [64] Venkataraman, L., Klare, J. E., Nuckolls, C., Hybertsen, M. S. & Steigerwald, M. L. Dependence of single-molecule junction conductance on molecular conformation. *Nature* **442**, 904–907 (2006).
- [65] Ample, F. & Joachim, C. A semi-empirical study of polyacene molecules adsorbed on a Cu(110) surface. *Surf. Sci.* **600**, 3243–3251 (2006).
- [66] Hansma, P. K. (ed.) *Tunneling spectroscopy* (Plenum Press, New York, 1982).

- [67] Pascual, J. I. *et al.* Properties of metallic nanowires - from conductance quantization to localization. *Science* **267**, 1793–1795 (1995).
- [68] Landauer, R. Spatial variation of currents and fields due to localized scatterers in metallic conduction. *IBM J. Res. Dev.* **1**, 223–231 (1957).
- [69] Aviram, A. & Ratner, M. A. Molecular rectifiers. *Chem. Phys. Lett.* **29**, 277–283 (1974).
- [70] Xiao, X. Y., Xu, B. Q. & Tao, N. J. Changes in the conductance of single peptide molecules upon metal-ion binding. *Ang. Chem. Int. Ed.* **43**, 6148–6152 (2004).
- [71] Patolsky, F. & Lieber, C. M. Nanowire nanosensors. *Mater. Today* **8**, 20 – 28 (2005).
- [72] Mann, B. & Kuhn, H. Tunneling through fatty acid salt monolayers. *J. Appl. Phys.* **42**, 4398 (1971).
- [73] Choi, S. H., Kim, B. & Frisbie, C. D. Electrical resistance of long conjugated molecular wires. *Science* **320**, 1482–1486 (2008).
- [74] Mativetsky, J. M. *et al.* Azobenzenes as light-controlled molecular electronic switches in nanoscale metal-molecule-metal junctions. *J. Am. Chem. Soc.* **130**, 9192 (2008).
- [75] Ferri, V. *et al.* Light-powered electrical switch based on cargo-lifting azobenzene monolayers. *Ang. Chem. Int. Ed.* **47**, 3407–3409 (2008).
- [76] Cui, X. D. *et al.* Reproducible measurement of single-molecule conductivity. *Science* **294**, 571–574 (2001).
- [77] Davis, W. B., Svec, W. A., Ratner, M. A. & Wasielewski, M. R. Molecular-wire behaviour in p-phenylenevinylene oligomers. *Nature* **396**, 60–63 (1998).
- [78] Blum, A. S. *et al.* Molecularly inherent voltage-controlled conductance switching. *Nat. Mater.* **4**, 167–172 (2005).
- [79] Fink, H. W. & Schonberger, C. Electrical conduction through DNA molecules. *Nature* **398**, 407–410 (1999).
- [80] Reed, M. A., Zhou, C., Muller, C. J., Burgin, T. P. & Tour, J. M. Conductance of a molecular junction. *Science* **278**, 252–254 (1997).
- [81] Loertscher, E., Ciszek, J. W., Tour, J. & Riel, H. Reversible and controllable switching of a single-molecule junction. *Small* **2**, 973–977 (2006).
- [82] Guo, X. F. *et al.* Covalently bridging gaps in single-walled carbon nanotubes with conducting molecules. *Science* **311**, 356–359 (2006).
- [83] Whalley, A. C., Steigerwald, M. L., Guo, X. & Nuckolls, C. Reversible switching in molecular electronic devices. *J. Am. Chem. Soc.* **129**, 12590 (2007).
- [84] Joachim, C., Gimzewski, J. K., Schlittler, R. R. & Chavy, C. Electronic transparency of a single C-60 molecule. *Phys. Rev. Lett.* **74**, 2102–2105 (1995).

- [85] Ramachandran, G. K. *et al.* A bond-fluctuation mechanism for stochastic switching in wired molecules. *Science* **300**, 1413–1416 (2003).
- [86] Lotze, C., Corso, M., Franke, K. J., von Oppen, F. & Pascual, J. I. Driving a macroscopic oscillator with the stochastic motion of a hydrogen molecule. *Science* **338**, 779–782 (2012).
- [87] Bruot, C., Hihath, J. & Tao, N. Mechanically controlled molecular orbital alignment in single molecule junctions. *Nat. Nanotechnol.* **7**, 35–40 (2012).
- [88] Magoga, M. & Joachim, C. Conductance of molecular wires connected or bonded in parallel. *Phys. Rev. B* **59**, 16011–16021 (1999).
- [89] Sedghi, G. *et al.* Long-range electron tunnelling in oligo-porphyrin molecular wires. *Nat. Nanotechnol.* **6**, 517–523 (2011).
- [90] Li, X. L. *et al.* Conductance of single alkanedithiols: Conduction mechanism and effect of molecule-electrode contacts. *J. Am. Chem. Soc.* **128**, 2135–2141 (2006).
- [91] Xiao, X. Y., Xu, B. Q. & Tao, N. J. Conductance titration of single-peptide molecules. *J. Am. Chem. Soc.* **126**, 5370–5371 (2004).
- [92] He, J. *et al.* Electronic decay constant of carotenoid polyenes from single-molecule measurements. *J. Am. Chem. Soc.* **127**, 1384–1385 (2005).
- [93] Temirov, R., Lassise, A., Anders, F. B. & Tautz, F. S. Kondo effect by controlled cleavage of a single-molecule contact. *Nanotechnology* **19**, 065401 (2008).
- [94] Bieri, M. *et al.* Two-dimensional polymer formation on surfaces: Insight into the roles of precursor mobility and reactivity. *J. Am. Chem. Soc.* **132**, 16669–16676 (2010).
- [95] He, J., Chen, F., Liddell, P. A., Andreasson, J. & Straight, S. D. Switching of a photochromic molecule on gold electrodes: single-molecule measurements. *Nanotechnology* **16**, 695–702 (2005).
- [96] Koch, M., Ample, F., Joachim, C. & Grill, L. Voltage-dependent conductance of a single graphene nanoribbon. *Nat. Nanotechnol.* **7**, 713–717 (2012).
- [97] Chen, W. *et al.* Highly conducting pi-conjugated molecular junctions covalently bonded to gold electrodes. *J. Am. Chem. Soc.* **133**, 17160–17163 (2011).
- [98] Joachim, C. *et al.* Multiple atomic scale solid surface interconnects for atom circuits and molecule logic gates. *J. Phys. Condens. Mat.* **22**, 084025 (2010).
- [99] Gourdon, A. Synthesis of molecular landers. *Eur. J. Org. Chem.* **12**, 2797–2801 (1998).
- [100] Moresco, F. *et al.* Probing the different stages in contacting a single molecular wire. *Phys. Rev. Lett.* **91**, 036601 (2003).
- [101] Grill, L. *et al.* Controlled manipulation of a single molecular wire along a copper atomic nanostructure. *Phys. Rev. B* **69**, 035416 (2004).

- [102] Ramoino, L. *et al.* Layer-selective epitaxial self-assembly of porphyrins on ultrathin insulators. *Chem. Phys. Lett.* **417**, 22–27 (2006).
- [103] Schintke, S. & Schneider, W. D. Insulators at the ultrathin limit: electronic structure studied by scanning tunnelling microscopy and scanning tunnelling spectroscopy. *J. Phys. Condens. Mat.* **16**, R49–R81 (2004).
- [104] Repp, J. *Rastertunnelmikroskopie und -spektroskopie and ultradünnen NaCl -Filmen auf hochinduzierten Cu-Substratflächen.* Master’s thesis, Freie Universität Berlin (1999).
- [105] Repp, J., Foelsch, S., Meyer, G. & Rieder, K. H. Ionic films on vicinal metal surfaces: Enhanced binding due to charge modulation. *Phys. Rev. Lett.* **86**, 252–255 (2001).
- [106] Repp, J. *Rastertunnelmikroskopie und -Spektroskopie an Adsorbaten auf Metall- und Isolatoroberflächen.* Ph.D. thesis, Freie Universität Berlin (2002).
- [107] Repp, J. & Meyer, G. Scanning tunneling microscopy of adsorbates on insulating films. from the imaging of individual molecular orbitals to the manipulation of the charge state. *Appl. Phys. A-Mater. Sci. Process.* **85**, 399–406 (2006).
- [108] Hebenstreit, W. *et al.* Atomic resolution by stm on ultra-thin films of alkali halides: experiment and local density calculations. *Surf. Sci.* **424**, L321–L328 (1999).
- [109] Pivetta, M., Patthey, F., Stengel, M., Baldereschi, A. & Schneider, W. D. Local work function Moire pattern on ultrathin ionic films: NaCl on Ag(100). *Phys. Rev. B* **72**, 115404 (2005).
- [110] Sun, X., Felicissimo, M. P., Rudolf, P. & Silly, F. NaCl multi-layer islands grown on Au(111)-(22 ×  $\sqrt{3}$ ) probed by scanning tunneling microscopy. *Nanotechnology* **19**, 495307 (2008).
- [111] Bombis, C. *et al.* Hydrogen-bonded molecular networks of melamine and cyanuric acid on thin films of NaCl on Au(111). *Small* **5**, 2177–2182 (2009).
- [112] Fölsch, S. *Elektronenspektroskopische Untersuchungen zur H<sub>2</sub>O-Adsorption auf der NaCl(100)-Oberfläche.* Ph.D. thesis, Universität Hannover (1991).
- [113] Schwennicke, C., Schimmelpfennig, J. & Pfnuer, H. Morphology of thin NaCl films grown epitaxially on Ge(100). *Surf. Sci.* **293**, 57 – 66 (1993).
- [114] Bombis, C. *et al.* Single molecular wires connecting metallic and insulating surface areas. *Ang. Chem. Int. Ed.* **48**, 9966–9970 (2009).
- [115] Lastapis, M. *et al.* Picometer-scale electronic control of molecular dynamics inside a single molecule. *Science* **308**, 1000–1003 (2005).
- [116] Saywell, A., Schwarz, J., Hecht, S. & Grill, L. Polymerization on stepped surfaces: Alignment of polymers and identification of catalytic sites. *Ang. Chem. Int. Ed.* **51**, 5096–5100 (2012).

- [117] Zhong, D. *et al.* Linear alkane polymerization on a gold surface. *Science* **334**, 213–216 (2011).
- [118] Linden, S. *et al.* Electronic structure of spatially aligned graphene nanoribbons on Au(788). *Phys. Rev. Lett.* **108**, 216801 (2012).
- [119] Flory, P. *Principles of polymer chemistry* (Cornell University Press, New York, 1953).
- [120] Bieri, M. *et al.* Surface-supported 2D heterotriangulene polymers. *Chem. Commun.* **47**, 10239 (2011).
- [121] Crommie, M. F., Lutz, C. P. & Eigler, D. M. Confinement of electrons to quantum corrals on a metal surface. *Science* **262**, 218–220 (1993).
- [122] Vettiger, P. *et al.* The "millipede" - nanotechnology entering data storage. *IEEE Transactions on Nanotechnology* **1**, 39–55 (2002).
- [123] Whitesides, G. M. & Grzybowski, B. Self-assembly at all scales. *Science* **295**, 2418–2421 (2002).
- [124] Lehn, J. M. Toward complex matter: Supramolecular chemistry and self-organization. *P. Natl. Acad. Sci.* **99**, 4763–4768 (2002).
- [125] Barth, J. V. Molecular architectonic on metal surfaces. *Annu. Rev. Phys. Chem.* **58**, 375–407 (2007).
- [126] Poirier, G. E. Characterization of organosulfur molecular monolayers on Au(111) using scanning tunneling microscopy. *Chem. Rev.* **97**, 1117–1127 (1997).
- [127] Love, J. C., Estroff, L. A., Kriebel, J. K., Nuzzo, R. G. & Whitesides, G. M. Self-assembled monolayers of thiolates on metals as a form of nanotechnology. *Chem. Rev.* **105**, 1103–1169 (2005).
- [128] Bartels, L. Tailoring molecular layers at metal surfaces. *Nat. Chem.* **2**, 87–95 (2010).
- [129] Jung, T. A., Schlittler, R. R. & Gimzewski, J. K. Conformational identification of individual adsorbed molecules with the STM. *Nature* **386**, 696–698 (1997).
- [130] Gross, L. *et al.* Tailoring molecular self-organization by chemical synthesis: Hexaphenylbenzene, hexa-*peri*-hexabenzocoronene, and derivatives on Cu (111). *Phys. Rev. B* **71**, 165428 (2005).
- [131] Yokoyama, T., Yokoyama, S., Kamikado, T., Okuno, Y. & Mashiko, S. Selective assembly on a surface of supramolecular aggregates with controlled size and shape. *Nature* **413**, 619–621 (2001).
- [132] Wong, K., Kwon, K. Y., Rao, B. V., Liu, A. W. & Bartels, L. Effect of halo substitution on the geometry of arenethiol films on Cu(111). *J. Am. Chem. Soc.* **126**, 7762–7763 (2004).
- [133] Yokoyama, T., Takahashi, T., Shinozaki, K. & Okamoto, M. Quantitative analysis of long-range interactions between adsorbed dipolar molecules on Cu(111). *Phys. Rev. Lett.* **98**, 206102 (2007).

- [134] Wang, Y., Kroeger, J., Berndt, R. & Hofer, W. Structural and electronic properties of ultrathin tin-phthalocyanine films on Ag(111) at the single-molecule level. *Ang. Chem. Int. Ed.* **48**, 1261–1265 (2009).
- [135] Riedel, E. *Anorganische Chemie* (de Gruyter, 2007), 7th edn.
- [136] Aradhya, S. V., Frei, M., Hybertsen, M. S. & Venkataraman, L. Van der Waals interactions at metal/organic interfaces at the single-molecule level. *Nat. Mater.* **11**, 872 – 876 (2012).
- [137] Tao, N. J., DeRose, J. A. & Lindsay, S. M. Self-assembly of molecular superstructures studied by in situ scanning tunneling microscopy: DNA bases on gold (111). *J. Phys. Chem.* **97**, 910–919 (1993).
- [138] Barth, J. V. *et al.* Building supramolecular nanostructures at surfaces by hydrogen bonding. *Ang. Chem. Int. Ed.* **39**, 1230 (2000).
- [139] Furukawa, M., Tanaka, H. & Kawai, T. Formation mechanism of low-dimensional superstructure of adenine molecules and its control by chemical modification: a low-temperature scanning tunneling microscopy study. *Surf. Sci.* **445**, 1–10 (2000).
- [140] Theobald, J. A., Oxtoby, N. S., Phillips, M. A., Champness, N. R. & Beton, P. H. Controlling molecular deposition and layer structure with supramolecular surface assemblies. *Nature* **424**, 1029–1031 (2003).
- [141] Stöhr, M. *et al.* Controlling molecular assembly in two dimensions: The concentration dependence of thermally induced 2D aggregation of molecules on a metal surface. *Ang. Chem. Int. Ed.* **44**, 7394–7398 (2005).
- [142] Pawin, G., Wong, K. L., Kwon, K. Y. & Bartels, L. A homomolecular porous network at a Cu(111) surface. *Science* **313**, 961–962 (2006).
- [143] Otero, R. *et al.* Elementary structural motifs in a random network of cytosine adsorbed on a gold(111) surface. *Science* **319**, 312–315 (2008).
- [144] Krull, C., Valencia, S., Pascual, J. I. & Theis, W. Formation of extended straight molecular chains by pairing of thymine molecules on the Ag-Si(111) surface. *Appl. Phys. A Mater.* **95**, 297–301 (2009).
- [145] Lobo-Checa, J. *et al.* Band formation from coupled quantum dots formed by a nanoporous network on a copper surface. *Science* **325**, 300–303 (2009).
- [146] Wang, Y., Kroeger, J., Berndt, R. & Hofer, W. A. Pushing and pulling a Sn ion through an adsorbed phthalocyanine molecule. *J. Am. Chem. Soc.* **131**, 3639–3643 (2009).
- [147] Nacci, C., Kanisawa, K. & Fölsch, S. Reversible switching of single tin phthalocyanine molecules on the InAs(111)A surface. *J. Phys. Condens. Mat.* **24**, 394004 (2012).
- [148] Gottfried, J. M., Flechtner, K., Kretschmann, A., Lukasczyk, T. & Steinruck, H. P. Direct synthesis of a metalloporphyrin complex on a surface. *J. Am. Chem. Soc.* **128**, 5644–5645 (2006).

- [149] Yoshimoto, S. & Kobayashi, N. Supramolecular nanostructures of phthalocyanines and porphyrins at surfaces based on the "Bottom-Up assembly". In *Functional Phthalocyanine Molecular Materials*, vol. 135, 137–167 (Springer-Verlag Berlin, 2010).
- [150] Langner, A. *et al.* Self-recognition and self-selection in multicomponent supramolecular coordination networks on surfaces. *P. Natl. Acad. Sci.* **104**, 17927–17930 (2007).
- [151] Kley, C. S. *et al.* Highly adaptable two-dimensional Metal-Organic coordination networks on metal surfaces. *J. Am. Chem. Soc.* **134**, 6072–6075 (2012).
- [152] Villagomez, C., Sasaki, T., Tour, J. M. & Grill, L. Bottom-up assembly of molecular wagons on a surface. *J. Am. Chem. Soc.* **132**, 16848–16854 (2010).
- [153] Haq, S. *et al.* Clean coupling of unfunctionalized porphyrins at surfaces to give highly oriented organometallic oligomers. *J. Am. Chem. Soc.* **133**, 12031–12039 (2011).
- [154] Adisojoso, J., Li, Y., Liu, J., Liu, P. N. & Lin, N. Two-dimensional metallo-supramolecular polymerization: Toward size-controlled multi-strand polymers. *J. Am. Chem. Soc.* **134**, 18526–18529 (2012).
- [155] Han, M. Y., Ozyilmaz, B., Zhang, Y. & Kim, P. Energy band-gap engineering of graphene nanoribbons. *Phys. Rev. Lett.* **98**, 206805 (2007).
- [156] Ullmann, F. & Bielecki, J. Synthesis in the biphenyl series. (I. announcement). *Berichte Der Deutschen Chemischen Gesellschaft* **34**, 2174–2185 (1901).
- [157] Bent, B. E. Mimicking aspects of heterogeneous catalysis: Generating, isolating, and reacting proposed surface intermediates on single crystals in vacuum. *Chem. Rev.* **96**, 1361–1390 (1996).
- [158] Krasnikov, S. A. *et al.* Formation of extended covalently bonded Ni porphyrin networks on the Au(111) surface. *Nano Research* **4**, 376–384 (2011).
- [159] Gourdon, A. On-surface covalent coupling in ultrahigh vacuum. *Ang. Chem. Int. Ed.* **47**, 6950–6953 (2008).
- [160] Franc, G. & Gourdon, A. Covalent networks through on-surface chemistry in ultra-high vacuum: state-of-the-art and recent developments. *Phys. Chem. Chem. Phys.* **13**, 14283–14292 (2011).
- [161] Lackinger, M. & Heckl, W. M. A STM perspective on covalent intermolecular coupling reactions on surfaces. *J. Phys. D Appl. Phys.* **44**, 464011 (2011).
- [162] Gutzler, R. *et al.* Surface mediated synthesis of 2D covalent organic frameworks: 1,3,5-tris(4-bromophenyl)benzene on graphite(001), Cu(111), and Ag(110). *Chem. Commun.* **29**, 4456–4458 (2009).
- [163] Bieri, M. *et al.* Porous graphenes: two-dimensional polymer synthesis with atomic precision. *Chem. Commun.* **45**, 6919 (2009).

- [164] Lipton-Duffin, J. A., Ivasenko, O., Perepichka, D. F. & Rosei, F. Synthesis of polyphenylene molecular wires by surface-confined polymerization. *Small* **5**, 592–597 (2009).
- [165] Lipton-Duffin, J. A. *et al.* Step-by-step growth of epitaxially aligned polythiophene by surface-confined reaction. *P. Natl. Acad. Sci.* **107**, 11200–11204 (2010).
- [166] Wang, W., Shi, X., Wang, S., Van Hove, M. A. & Lin, N. Single-molecule resolution of an organometallic intermediate in a surface-supported Ullmann coupling reaction. *J. Am. Chem. Soc.* **133**, 13264–13267 (2011).
- [167] Schloegl, S., Heckl, W. M. & Lackinger, M. On-surface radical addition of triply iodinated monomers on Au(111)- the influence of monomer size and thermal post-processing. *Surf. Sci.* **606**, 999–1004 (2012).
- [168] McCarty, G. S. & Weiss, P. S. Formation and manipulation of protopolymer chains. *J. Am. Chem. Soc.* **126**, 16772–16776 (2004).
- [169] Cai, J. *et al.* Atomically precise bottom-up fabrication of graphene nanoribbons. *Nature* **466**, 470–473 (2010).
- [170] Blunt, M. O., Russell, J. C., Champness, N. R. & Beton, P. H. Templating molecular adsorption using a covalent organic framework. *Chem. Commun.* **46**, 7157 (2010).
- [171] Kittelmann, M. *et al.* On-surface covalent linking of organic building blocks on a bulk insulator. *ACS Nano* **5**, 8420–8425 (2011).
- [172] In't Veld, M., Iavicoli, P., Haq, S., Amabilino, D. B. & Raval, R. Unique intermolecular reaction of simple porphyrins at a metal surface gives covalent nanostructures. *Chem. Commun.* **13**, 1536 (2008).
- [173] Matena, M., Riehm, T., Stöhr, M., Jung, T. A. & Gade, L. H. Transforming surface coordination polymers into covalent surface polymers: Linked polycondensed aromatics through oligomerization of n-heterocyclic carbene intermediates. *Ang. Chem. Int. Ed.* **47**, 2414 – 2417 (2008).
- [174] Weigelt, S. *et al.* Surface synthesis of 2D branched polymer nanostructures. *Ang. Chem. Int. Ed.* **47**, 4406 – 4410 (2008).
- [175] Abel, M., Clair, S., Ourdjini, O., Mossoyan, M. & Porte, L. Single layer of polymeric Fe-phthalocyanine: An organometallic sheet on metal and thin insulating film. *J. Am. Chem. Soc.* **133**, 1203–1205 (2011).
- [176] Zwaneveld, N. A. A. *et al.* Organized formation of 2D extended covalent organic frameworks at surfaces. *J. Am. Chem. Soc.* **130**, 6678–6679 (2008).
- [177] Dienstmaier, J. F. *et al.* Synthesis of well-ordered COF monolayers: Surface growth of nanocrystalline precursors versus direct on-surface polycondensation. *ACS Nano* **5**, 9737–9745 (2011).
- [178] Rowan, S. J., Cantrill, S. J., Cousins, G. R. L., Sanders, J. K. M. & Stoddart, J. F. Dynamic covalent chemistry. *Ang. Chem. Int. Ed.* **41**, 898–952 (2002).

- [179] Lafferentz, L. *et al.* Controlling on-surface polymerization by hierarchical and substrate-directed growth. *Nat. Chem.* **4**, 215–220 (2012).
- [180] Kanuru, V. K. *et al.* Sonogashira coupling on an extended gold surface in vacuo: Reaction of phenylacetylene with iodobenzene on Au(111). *J. Am. Chem. Soc.* **132**, 8081–8086 (2010).
- [181] Mielke, J. & Grill, L. in preparation.
- [182] Faury, T. *et al.* Sequential linking to control growth of a surface covalent organic framework. *J. Phys. Chem. C* **116**, 4819 – 4823 (2012).
- [183] Baber, A. E., Tierney, H. L. & Sykes, E. C. H. A quantitative single-molecule study of thioether molecular rotors. *ACS Nano* **2**, 2385–2391 (2008).
- [184] Lu, G., Linsebigler, A. L. & Yates, J. T. Elimination of serious artifacts in temperature-programmed desorption spectroscopy. *J. Vac. Sci. Technol. A* **12**, 384–387 (1994).
- [185] Ourdjini, O. *et al.* Substrate-mediated ordering and defect analysis of a surface covalent organic framework. *Phys. Rev. B* **84**, 125421 (2011).
- [186] Zambelli, T. *et al.* Deposition of large organic molecules in UHV: a comparison between thermal sublimation and pulse-injection. *Int. J. Nanosci.* **3**, 331–341 (2004).
- [187] Mattera, A., Goodman, R. & Somorjai, G. Low energy electron diffraction study of the (100) face of silver, gold, and palladium. *Surf. Sci.* **7**, 26–40 (1967).
- [188] Sweetman, A. *et al.* Toggling bistable atoms via mechanical switching of bond angle. *Phys. Rev. Lett.* **106**, 136101 (2011).
- [189] Yang, J., Erwin, S. C., Kanisawa, K., Nacci, C. & Fölsch, S. Emergent multistability in assembled nanostructures. *Nano Lett.* **11**, 2486–2489 (2011).
- [190] Feringa, B. L. & Browne, W. B. (eds.) *Molecular Switches* (Wiley-VCH, Weinheim, 2011), 2nd edn.
- [191] Rando, R. The chemistry of vitamin-A and vision. *Ang. Chem. Int. Ed.* **29**, 461–480 (1990).
- [192] Comstock, M. J. *et al.* Reversible photomechanical switching of individual engineered molecules at a metallic surface. *Phys. Rev. Lett.* **99**, 038301 (2007).
- [193] Alemani, M. *et al.* Adsorption and switching properties of azobenzene derivatives on different noble metal surfaces: Au(111), Cu(111), and Au(100). *J. Phys. Chem C* **112**, 10509–10514 (2008).
- [194] Selvanathan, S., Peters, M. V., Schwarz, J., Hecht, S. & Grill, L. Formation and manipulation of discrete supramolecular azobenzene assemblies. *Appl. Phys. A Mater.* **93**, 247–252 (2008).
- [195] Selvanathan, S., Peters, M. V., Hecht, S. & Grill, L. Island formation and manipulation of prochiral azobenzene derivatives on Au(111). *J. Phys. Condens. Mat.* **24**, 354013 (2012).

- [196] Leyssner, F. *et al.* Photoisomerization ability of molecular switches adsorbed on Au(111): Comparison between azobenzene and stilbene derivatives. *J. Phys. Chem. C* **114**, 1231–1239 (2010).
- [197] Moresco, F. *et al.* Conformational changes of single molecules induced by scanning tunneling microscopy manipulation: A route to molecular switching. *Phys. Rev. Lett.* **86**, 672–675 (2001).
- [198] Feringa, B. (ed.) *Molecular Switches* (Wiley-VCH, Weinheim, 2001).
- [199] Hugel, T. *et al.* Single-molecule optomechanical cycle. *Science* **296**, 1103–1106 (2002).
- [200] Henzl, J., Mehlhorn, M., Gawronski, H., Rieder, K. H. & Morgenstern, K. Reversible cis-trans isomerization of a single azobenzene molecule. *Ang. Chem. Int. Ed.* **45**, 603–606 (2006).
- [201] Choi, B. Y. *et al.* Conformational molecular switch of the azobenzene molecule: A scanning tunneling microscopy study. *Phys. Rev. Lett.* **96**, 156106 (2006).
- [202] Dri, C., Peters, M. V., Schwarz, J., Hecht, S. & Grill, L. Spatial periodicity in molecular switching. *Nat. Nanotechnol.* **3**, 649–653 (2008).
- [203] Wolf, M. & Tegeder, P. Reversible molecular switching at a metal surface: A case study of tetra-tert-butyl-azobenzene on Au(111). *Surf. Sci.* **603**, 1506–1517 (2009).
- [204] Tamai, N. & Miyasaka, H. Ultrafast dynamics of photochromic systems. *Chem. Rev.* **100**, 1875–1890 (2000).
- [205] Auwaerter, W. *et al.* A surface-anchored molecular four-level conductance switch based on single proton transfer. *Nat. Nanotechnol.* **7**, 41–46 (2012).
- [206] Hagen, S. *et al.* Excitation mechanism in the photoisomerization of a surface-bound azobenzene derivative: Role of the metallic substrate. *J. Chem. Phys.* **129**, 164102 (2008).
- [207] Saalfrank, P. Manipulation of adsorbates with electric fields. *J. Chem. Phys.* **113**, 3780–3791 (2000).
- [208] Kudernac, T. *et al.* Electrically driven directional motion of a four-wheeled molecule on a metal surface. *Nature* **479**, 208–211 (2011).
- [209] Liljeroth, P., Repp, J. & Meyer, G. Current-induced hydrogen tautomerization and conductance switching of naphthalocyanine molecules. *Science* **317**, 1203–1206 (2007).
- [210] Nacci, C., Erwin, S. C., Kanisawa, K. & Fölsch, S. Controlled switching within an organic molecule deliberately pinned to a semiconductor surface. *ACS Nano* **6**, 4190–4195 (2012).
- [211] Schulze, G. *Elementary Processes in Single Molecule Devices: Electronic Transport and Molecular Isomerization*. Ph.D. thesis, Freie Universität Berlin (2009).
- [212] Hirshberg, Y. Reversible formation and eradication of colors by irradiation at low temperatures. a photochemical memory model. *J. Am. Chem. Soc.* **78**, 2304–2312 (1956).

- [213] Raymo, F. M. Digital processing and communication with molecular switches. *Adv. Mater.* **14**, 401 (2002).
- [214] Irie, M. & Mohri, M. Thermally irreversible photochromic systems - reversible photocyclization of diarylethene derivatives. *J. Org. Chem.* **53**, 803–808 (1988).
- [215] Irie, M. Photochromic diarylethenes for photonic devices. *Pure Appl. Chem.* **68**, 1367–1371 (1996).
- [216] Waldeck, D. H. Photoisomerization dynamics of stilbenes. *Chem. Rev.* **91**, 415–436 (1991).
- [217] Nakamura, S. & Irie, M. Thermally irreversible photochromic systems - a theoretical-study. *J. Org. Chem.* **53**, 6136–6138 (1988).
- [218] Irie, M., Uchida, K., Eriguchi, T. & Tsuzuki, H. Photochromism of single-crystalline diarylethenes. *Chem. Lett.* **10**, 899–900 (1995).
- [219] Morimoto, M. & Irie, M. A diarylethene cocrystal that converts light into mechanical work. *J. Am. Chem. Soc.* **132**, 14172–14178 (2010).
- [220] Browne, W. R. *et al.* Oxidative electrochemical switching in dithienylcyclopentenes, part 1: Effect of electronic perturbation on the efficiency and direction of molecular switching. *Chem. Eur. J.* **11**, 6414–6429 (2005).
- [221] Dulic, D. *et al.* One-way optoelectronic switching of photochromic molecules on gold. *Phys. Rev. Lett.* **91**, 207402 (2003).
- [222] Kudernac, T., van der Molen, S. J., van Wees, B. J. & Feringa, B. L. Uni- and bi-directional light-induced switching of diarylethenes on gold nanoparticles. *Chem. Commun.* **34**, 3597–3599 (2006).
- [223] van der Molen, S. J. *et al.* Stochastic and photochromic switching of diarylethenes studied by scanning tunnelling microscopy. *Nanotechnology* **17**, 310–314 (2006).
- [224] Katsonis, N. *et al.* Reversible conductance switching of single diarylethenes on a gold surface. *Adv. Mater.* **18**, 1397 (2006).
- [225] Ikeda, M., Tanifuji, N., Yamaguchi, H., Irie, M. & Matsuda, K. Photoswitching of conductance of diarylethene-Au nanoparticle network. *Chem. Commun.* **13**, 1355–1357 (2007).
- [226] Arai, R., Uemura, S., Irie, M. & Matsuda, K. Reversible photoinduced change in molecular ordering of diarylethene derivatives at a solution-HOPG interface. *J. Am. Chem. Soc.* **130**, 9371–9379 (2008).
- [227] Wang, D., Chen, Q. & Wan, L. Structural transition of molecular assembly under photoirradiation: an STM study. *Phys. Chem. Chem. Phys.* **10**, 6467–6478 (2008).
- [228] Coudret, C., Guirado, G., Estrampes, N. & Coratger, R. Adsorption of a single molecule of a diarylethene photochromic dye on Cu(111). *Phys. Chem. Chem. Phys.* **13**, 20946–20953 (2011).

- [229] Uchida, K., Yamanoi, Y., Yonezawa, T. & Nishihara, H. Reversible On/Off conductance switching of single diarylethene immobilized on a silicon surface. *J. Am. Chem. Soc.* **133**, 9239–9241 (2011).
- [230] Arramel, A. *et al.* Electronic properties of individual diarylethene molecules studied using scanning tunneling spectroscopy. *J. Appl. Phys.* **111** (2012).
- [231] Briechle, B. M. *et al.* Current-voltage characteristics of single-molecule diarylethene junctions measured with adjustable gold electrodes in solution. *Beilstein J. Nanotechnol.* **3**, 798–808 (2012).
- [232] Calculations were performed at the ASED+ level of theory by M. Grisolia and C. Joachim, CEMES-CNRS, Toulouse.
- [233] Politzer, P., Murray, J. S. & Clark, T. Halogen bonding: an electrostatically-driven highly directional noncovalent interaction. *Phys. Chem. Chem. Phys.* **12**, 7748 (2010).
- [234] Hypercube Inc. HyperChem 7, Molecular mechanics optimizations were performed with the MM+ force field and the Polak-Ribiere algorithm.
- [235] Higashiguchi, K., Matsuda, K., Tanifuji, N. & Irie, M. Full-color photochromism of a fused dithienylethene trimer. *J. Am. Chem. Soc.* **127**, 8922–8923 (2005).
- [236] Perrier, A., Maurel, F. & Jacquemin, D. Single molecule multiphotochromism with diarylethenes. *Acc. Chem. Res.* **45**, 1173–1182 (2012).
- [237] Heimann, P. & Neddermeyer, H. Ultraviolet photoemission from single-crystals and band-structure of gold. *J. Phys. F Met. Phys.* **7**, L37–L42 (1977).

## Erklärung gemäß §7 der Promotionsordnung

Sämtliche verwendete Hilfsmittel, Hilfen und Quellen sind an der entsprechenden Stelle angegeben. Ich versichere, daß ich auf dieser Grundlage diese Arbeit selbstständig verfasst habe.

Berlin, 06.05.2013

Leif Lafferentz